Agglomeration during Fluidized Bed Combustion and Gasification of Biomass

Zhao, Liyan

Publication date:
2021

Document Version
Publisher's PDF, also known as Version of record

Agglomeration during Fluidized Bed Combustion and Gasification of Biomass

Liyan Zhao

PhD thesis

May 2021

Supervisors Hao Wu (DTU, Chemical and Biochemical Engineering)

Weigang Lin (DTU, Chemical and Biochemical Engineering)

Kim Dam-Johansen (DTU, Chemical and Biochemical Engineering)

DTU Chemical Engineering
Department of Chemical and Biochemical Engineering

Preface and Acknowledgments

This dissertation is the results of three years of research, from May 15th 2018 to May 14th 2021, carried out in the Combustion and Harmful Emission Control (CHEC) research center, at the Department of Chemical & Biochemical Engineering (KT), Technical University of Denmark (DTU). This work was performed under the supervision of Associate Professor Hao Wu, Associate Professor Weigang Lin, and Professor Kim Dam-Johansen from KT-DTU.

I would like to sincerely thank my supervisors for their patient guidance and great support throughout the project. Thanks to Hao Wu for giving me valuable suggestions and comprehensive comments on the project. Thanks to Weigang Lin for the practical help on my experimental work, as well as for a lot discussion and constructive suggestions on the project at any time. Thanks to Kim Dam-Johansen for the continuous support and fruitful discussion. I want to express my gratitude to Ulrik Birk Henriksen and Jesper Ahrenfeldt for providing the two batches of wheat straw used in this work.

I would like to thank all CHEC technicians and the technicians from the workshop. Thanks to Søren Post, Anders Kjersgaard, and Nikolaj Vinterberg Nissen for their technical support on the fluidized bed rector. Thanks to Malene Hessellund Dinesen for helping to order the laboratory supplies. I would like to thank Lilian Beenfeldt Holgersen and Brian Brun Hansen for their assistance on TGA experiments. Thanks to Lars Møller for helping to solve various electric related issues. Thanks to IT Helpdesk team in KT for their assistance on the computer and software related issues. Thanks to Hanne Mikkelsen for answering all kinds of questions in the work.

I would like to thank all of my colleagues at KT who make the three years so wonderful. Thanks to Burak Ulusoy and Božidar Aničić for their guidance and assistance on the fluidized bed experiments. I also would like to thank Burak for his help on translation of the abstract to Danish. Thanks to my Chinese friends for bringing so much fun to my life in Denmark. A special thanks goes to my friend Yu Zhang for being with me and sharing my happiness and sadness, as well as the discussions about the project in the past three years.

Lastly, I would like to thank my families for their supporting and encouraging, as well as the understanding and caring during these three years.

Liyan Zhao

May 2021

Summary

Biomass is considered as a renewable and carbon-neutral energy source, and has been utilized as a substitute for fossil fuels. Fluidized bed combustion and gasification are promising technologies for biomass utilization. However, agglomeration in fluidized bed combustion and gasification of biomass, caused by the presence of molten phase originated from biomass, affects the operation of the reactors, and may eventually lead to defluidization and unscheduled shut down of the plant. Therefore, an in-depth understanding of agglomeration in fluidized bed combustion and gasification of biomass and the development of countermeasures for minimizing the operational problems caused by agglomeration are important.

Systematic experiments on agglomeration during combustion and gasification of biomass were carried in a lab-scale bubbling fluidized bed reactor. The experiments focused on the influence of equivalence ratio (ER) in air blown, air/steam and air/carbon dioxide gasification. The influence of biomass type on agglomeration was studied in the same way. Different techniques, such as scanning electron microscopy with energy-dispersive X-ray spectroscopy (SEM-EDX), X-ray diffraction (XRD), and thermogravimetric analysis (TGA), were applied for characterization of agglomerates, biomass ash, and char. The fusion behaviors of the ash were investigated a fixed bed reactor under combustion and gasification conditions to further understand the influence of gas atmosphere on agglomeration. The thermodynamic equilibrium calculations were carried out to shed light upon the distribution of potassium in the ash under the experimental conditions. A pulsed flow was applied to explore the possibility of mitigating the agglomeration in fluidized bed combustion/gasification of biomass and its effect on the conversion process.

Combustion and gasification of wheat straw at different ERs in the fluidized bed reveal a trend that the agglomeration tendency first increases gradually with decreasing ER. When ER reaches a critical value, the agglomeration tendency decreases with further decreasing ER. It has been observed that the amount of unconverted carbon in the bed increases as ER decreases. By adding a high concentration of steam to the fluidized bed, the agglomeration is promoted. However, when carbon dioxide is added, slightly lower agglomeration tendency is observed. The visual examination of the fusion behaviors of wheat straw ash in the fixed bed indicates that the ash obtained from gasification with steam has the highest fusion tendency followed by the ash from combustion with presence of steam and lastly the ash from normal combustion. The experimental results indicate that an enhanced reducing atmosphere may result in a slightly higher agglomeration tendency, probably due to an increased melting of ash. The inhibition effect of residual carbon on the agglomeration is probably attributed to a reduced fusion tendency and melting flow behavior of ash and a retarded interaction between ash and bed material. The competition between an enhanced reducing atmosphere and an

increased amount of unconverted carbon by lowering ER results in the occurrence of a maximal agglomeration tendency at a critical ER. The presence of high concentration of steam accelerates the agglomeration probably due to an increased carbon conversion and a lowered ash viscosity, which also leads to a lower critical ER value.

Combustion and gasification of sunflower husk in the fluidized bed indicate that a reducing atmosphere, a high concentration of steam, and the residual carbon show consistent influences on the agglomeration of sunflower husk and wheat straw, although the agglomeration tendency of sunflower husk ash is higher than that of wheat straw ash in both combustion and gasification. In the air blown system, the critical ERs of sunflower husk and wheat straw are 0.04 and 0.36, respectively. The differences in agglomeration characteristics of these two types of biomass may be attributed to their different char reactivity and different molar ratios of silicon to potassium, which are 1.56 and 0.04, respectively, for wheat straw and sunflower husk. Different with wheat straw, the accelerated agglomeration of sunflower husk under a reducing atmosphere and a high concentration of steam may be attributed to their promotive effect on the interaction between sunflower husk ash and bed material. The results of TGA experiments indicate that sunflower husk has a higher char reactivity than wheat straw, leading to a less amount of residual carbon during gasification of biomass, and thereby causing a reduced inhibition effect of residual carbon. Compared to wheat straw, the lower critical ER of sunflower husk may be attributed to a higher char reactivity and a different mechanism of reducing atmosphere on agglomeration results from a lower molar ratio of silicon to potassium in sunflower husk. Gasification of two batches of wheat straw show that the straw with a lower char reactivity has a lower agglomeration tendency in gasification at low ERs due to a more pronounced inhibition effect caused by a higher amount of residual carbon.

The results of pulsed fluidized bed experiments suggest that the introducing of a pulsed flow in the primary gas mitigates the agglomeration in fluidized bed combustor and gasifier, and the pulsed flow shows a minor effect on the combustion behaviors. Among the parameters that have been studied, the pulsation duty cycle shows the most significant effect on the agglomeration tendency, while the pulsation frequency shows the least impact. Under the combination of pulsation flow rate ratio of 0.4, pulsation frequency of 1.5 Hz and pulsation duty cycle of 25/75, the amounts of straw fed for inducing defluidization are 151.7% and 137.5% of that at the condition with the continuous flow for combustion and gasification, respectively.

The results of this work reveal that the agglomeration in fluidized bed combustion and gasification of biomass can be promoted by a reducing atmosphere and mitigated by the residual carbon. A decrease in ER results in an enhanced reducing atmosphere and an increased amount of residual carbon, and the competition between two factors results in the occurrence of a maximal agglomeration tendency at a critical ER. The presence of high concentration of steam accelerates the agglomeration tendency of biomass. A higher char reactivity leads to a reduced inhibition effect of residual carbon, thus causing a promoted agglomeration. An increase in steam concentration and char reactivity will

result in a decreased critical ER. The different molar ratios of silicon to potassium for different types of biomass may result in different agglomeration tendency and mechanisms. The observed results indicate that the application of pulsed fluidized bed of promising to mitigate the agglomeration during combustion and gasification of biomass and shows insignificant effect on conversion behaviors.

Dansk resumé

Biomasse betragtes som en vedvarende og kulstofneutral energikilde og er blevet brugt som erstatning for fossile brændstoffer. Forbrænding of forgasning i fluid bed reaktorer er lovende teknologier til anvendelse af biomasse. Imidlertid forårsager tilstedeværelsen af smeltet fase fra biomasseaske agglomerering under forbrænding og forgasning, hvilket i værste fald kan føre til defluidisering og uønsket lukning af anlægget. Det er derfor yderst vigtigt at opnå en dybtgående forståelse af agglomerering under fluid bed forbrænding og forgasning af biomasse for dermed at kunne udvikle modforanstaltninger for at minimere de operationelle problemer forårsaget af agglomerering.

Systematiske eksperimenter med agglomerering under forbrænding og forgasning af biomasse blev udført i en boblende fluid bed-reaktor i laboratorieskala. Eksperimenterne fokuserede på indflydelsen af ækvivalensforholdet (ER) under luft, luft/damp og luft/carbondioxid -forgasning. Indflydelsen af biomassetype på agglomereringen blev undersøgt på samme måde. Forskellige teknikker, såsom scanningelektronmikroskopi med energidispersiv røntgenspektroskopi (SEM-EDX), røntgendiffraktion (XRD) og termogravimetrisk analyse (TGA) blev anvendt til karakterisering af agglomerater, biomasseaske og kul. Askens smelteadfærd blev undersøgt i en fixed bed reaktor under forbrændings- og forgasningsbetingelser for yderligere at forstå indflydelsen af gasatmosfære på agglomerering. Termodynamiske ligevægtsberegninger blev udført for at belyse fordelingen af kalium i asken under de eksperimentelle betingelser. En pulserende strøm blev anvendt for at undersøge muligheden for at reducere agglomerering i fluid bed forbrænding/forgasning af biomasse og dens virkning på omdannelsesprocessen.

Fluid bed forbrænding og forgasning af hvedehalm ved forskellige ER afslører, at agglomereringstendensen først øges gradvist med faldende ER. Når ER når en kritisk værdi, begynder agglomereringstendensen at falde med yderligere faldende ER. Det blev observeret, at mængden af ureageret kulstof i beden stiger, når ER falder. Ved at tilføje en høj koncentration af damp til fluid beden fremmes agglomerering. Når carbondioxid tilsættes, observeres der dog en lidt lavere agglomereringstendens. Den visuelle undersøgelse af smelteadfærden af hvedehalmaske i beden indikerer, at asken opnået ved forgasning med damp har den højeste fusionstendens efterfulgt af asken fra forbrænding med tilstedeværelse af damp og sidst af asken fra normal forbrænding. De eksperimentelle resultater indikerer, at en i høj grad reducerende atmosfære kan resultere i en lidt højere agglomereringstendens sandsynligvis på grund af en øget smeltning af asken. Inhiberingseffekten af resterende kulstof på agglomerationen tilskrives sandsynligvis en reduceret fusionstendens og askensmeltens strømningsadfærd og en forsinket interaktion mellem aske og bedmaterialet. Konkurrencen mellem en meget reducerende atmosfære og en øget mængde ikke-omdannet kulstof ved at sænke ER resulterer i forekomsten af en maksimal agglomereringstendens

ved en kritisk ER. Tilstedeværelsen af en høj dampkoncentration fremskynder agglomereringen sandsynligvis på grund af en øget kulstofomdannelse og en sænket askeviskositet, hvilket også fører til en lavere kritisk ER-værdi.

Fluid bed forbrænding og forgasning af solsikkefrøskal indikerer, at en reducerende atmosfære, en høj koncentration af damp og det resterende kulstof viser ensartet indflydelse på agglomereringen af solsikkefrøskal og hvedehalm, skønt agglomereringstendensen for solsikkefrøskal er højere end af hvedehalmaske i både forbrænding og forgasning. I det luftblæste system er de kritiske ER værdier af solsikkefrøskal og hvedehalm henholdsvis 0,04 og 0,36. Forskellene i agglomereringskarakteristika for disse to typer af biomasse kan tilskrives deres forskellige silicium til kalium molforhold og koks-reaktivitet. De signifikant forskellige molforhold mellem silicium til kalium, som henholdsvis er 1,56 og 0,04 for hvedehalm og solsikkefrøskal. Forskellig fra hvedehalm kan den accelererede agglomerering af solsikkefrøskal under en reducerende atmosfære og en høj koncentration af damp tilskrives deres promoverende virkning på interaktionen mellem solsikkefrøskal og bedmateriale. Resultaterne af TGA-eksperimenter indikerer, at solsikkefrøskal har en højere koks-reaktivitet end hvedehalm, hvilket fører til en mindre mængde resterende kulstof under forgasning af biomasse og derved forårsager en reduceret inhiberingseffekt af resterende kulstof. Sammenlignet med hvedehalm kan den lavere kritiske ER værdi for solsikkefrøskal tilskrives en højere koks-reaktivitet, og en alternativ mekanisme for agglomereringen, der er relevant ved reducerende betingelser forårsaget af et lavere molforhold mellem silicium til kalium i solsikkefrøskal. Forgasning af to batch hvedehalm viser, at halmen med en lavere koksreaktivitet har en lavere agglomereringstendens i forgasning ved lave ER værdier på grund af en mere udtalt inhiberingseffekt forårsaget af en større mængde restkulstof.

Resultaterne af puls-forsøg i fluid bed reaktoren antyder, at indførelsen af en pulserende strøm i den primære gas dæmper agglomerationen under fluid bed forbrænding og gasificering, og det pulserende flow har en mindre effekt på forbrænding. Blandt de parametre, der er blevet undersøgt, viser pulseringscyklus sig at være den mest signifikante på agglomereringstendensen, mens pulsationsfrekvensen udviser mindst påvirkning. Ved at benytte et pulseringsflowhastighedsforhold på 0,4, pulsationsfrekvens på 1,5 Hz og pulsationscyklus på 25/75 er mængderne af halm, der tilføres før af defluidisering, 151,7% og 137,5% højere sammenlignet med forholdene uden pulsering dvs. med en kontinuerlig strøm under forbrænding henholdsvis forgasning.

Resultaterne af dette arbejde viser, at agglomerering i fluid bed forbrænding og forgasning af biomasse kan fremmes ved en reducerende atmosfære og mindskes af tilstedeværelsen af resterende kulstof. En reduktion i ER forårsager en øget reducerende atmosfære og en øget mængde ikke-omdannet kulstof, og konkurrencen mellem disse to faktorer resulterer i forekomsten af en maksimal agglomereringstendens ved en kritisk ER. Tilstedeværelsen af en høj koncentration af damp fremskynder biomassens agglomereringstendens. En højere koks-reaktivitet fører til en reduceret inhiberingseffekt af resterende carbon, hvilket forårsager en fremmet agglomerering. En stigning i

dampkoncentration og kulreaktivitet vil resultere i en nedsat kritisk ER. De forskellige molforhold mellem silicium til kalium for forskellige typer biomasse kan resultere i forskellige agglomereringstendenser og mekanismer. De observerede resultater indikerer, at anvendelsen af en pulserende fluid bed udviser potentiale til at mindske agglomerering under forbrænding og forgasning af biomasse med en ubetydelig effekt på forbrændingen.

List of Figures

List of Tables

Abbreviations and Symbols

Abbreviations

AFT	Standard Ash Fusion Temperatures
atom%	Atom percent
AGG	Agglomerates
BFB	Bubbling Fluidized Bed
CFB	Circulating Fluidized Bed
Def.	Defluidization
DEM	Discrete Element Method
Exp.	Experiment
ER	Equivalence Ratio
HTA	High Temperature Ash (prepared at 850 °C)
ICP-OES	Inductively Coupled Plasma - Optical Emission Spectrometry
IDT	Initial Deformation Temperature
LTA	Low Temperature Ash (prepared at 550 °C)
LTCFB	Low-Temperature Circulating Fluidized Bed
MFC	Mass Flow Controller
mol.%	Molar percent
No.	Number
ODA	Optical Dilatometry Analysis
Ref.	Reference
SFH	Sunflower Husk
SFR	Steam To Fuel Ratio
SEM-EDX	Scanning Electron Microscopy with Energy-Dispersive X-ray spectroscopy
TMA	Thermal Mechanical Analysis
TGA	Thermogravimetric Analysis
TG/DSC	Thermo-Gravimetric/Differential Scanning Calorimetry
TG/DTA	Thermogravimetry/Differential Thermal Analysis
TG/DTG	Thermogravimetry/Derivative Thermogravimetry
vol.%	Volume percent
WS	Wheat Straw
wt.%	Weight percent
XRD	X-Ray Diffraction

Symbols

d_{p10}	µm	The portion of particles with diameters smaller than this value is 10%.
d_{p90}	µm	The portion of particles with diameters below this value is 90%.
H_{mf}	m	Static bed height
g	$m \cdot s^{-2}$	Gravitational acceleration
$T_{Def.}$	°C	Defluidization temperature
$T_{melting}$	°C	Melting temperature
U_{mf}	m/s	Minimum fluidization velocity
U_g	m/s	Superficial gas velocity
U_t	m/s	Total flow rat of primary gas
U_p	m/s	Flow rate of pulsed flow
U_c	m/s	Flow rate of continuous flow
T_{ON}	ms	Time of “flow-ON” period
T_{OFF}	ms	Time of “flow-OFF” period
DTG_{max}	$\% \cdot min^{-1}$	Maximum weight loss rates
T_p	°C	Temperature of maximum weight loss rates

Greek letters

f	Hz	Pulsation frequency
f_N	Hz	Natural frequency of fluidized bed

Contents

1. Introduction

1.1 Background

Biomass is a renewable and carbon neutral energy resource, and it is considered as a good substitute to fossil fuels. More than 35% of Denmark's energy consumption comes from renewable in 2018[1], and Denmark is striving to be 100% independent of fossil fuels by 2050[2]. Biomass is one of important renewable energy sources in Denmark, especially woody biomass and straw. In 2018, woody biomass and straw account for 48% and 7% of the consumption of renewable energy in Denmark[1]. More than 50% of the demand of woody biomass in Denmark depends on import, while straw is produced domestically[1].

Fluidized bed combustor and gasifier are widely applied to biomass combustion and gasification owing to their characteristics of homogeneous temperature and high fuel flexibility. However, the utilization of biomass in fluidized bed faces the challenge of agglomeration, which can strongly influence the performance of the reactors and may eventually lead to defluidization and unscheduled plant shutdown[3–6]. The agglomeration in a fluidized bed is mainly caused by the presence of molten phase, i.e. the alkali containing compounds, from biomass ash and/or the interaction between biomass ash and bed materials. Because of the high content of potassium, the herbaceous biomass is especially problematic regarding the agglomeration. For example, the agglomeration was observed at as low as 700 °C in a straw fired fluidized bed[7]. The agglomeration in fluidized bed conversion of biomass at high temperatures is a complex process[4,8]. The occurrence and the degree of agglomeration depend on biomass properties (such as ash content and ash-forming composition), bed material properties (such as size and material type), operation parameters (such as temperature and gas velocity), and reaction environment (such as combustion and gasification)[8–10].

Although the agglomeration in biomass combustion and gasification are extensively studied in the past decades, the detailed agglomeration tendency and mechanisms in gasification are still not fully understood. In particular, the effect of equivalence ratio (ER), which one of the most important parameter for the yield and quality of the producer gas[11], on the agglomeration is unclear. Moreover, steam is introduced to a gasifier alone or together with air/O_2, depending on the gasification is allothermal or autothermal. The effect of a high concentration of steam on agglomeration in fluidized bed gasification of biomass is unknown. A systematically investigation on the influence of these two factors on agglomeration could provide more knowledge for design and operation of biomass gasifiers.

At the beginning of this project, a low-temperature circulating fluidized bed (LTCFB) gasifier at CHEC in Risø campus experienced an unscheduled shutdown in gasification of a batch of wheat

straw due to the defluidization after operating for two days. However, no such problem was observed in gasification of another batch of wheat straw with similar composition after running for more than two weeks under the same operation conditions. In order to understand the different agglomeration behaviors of two batches of wheat straw, the bed materials from two cases were examined in term of defluidization temperature[12]. As shown in Figure 1-1, the results show that the defluidization temperatures of the two bed samples under combustion condition are both around 770 °C. However, the carbon content contained in the bed sample that taken from case without defluidization is almost five times of that in the bed sample that taken from case with defluidization. It would be of interest to study the mechanisms behind the different agglomeration behaviors in gasification of two batches of wheat straws.

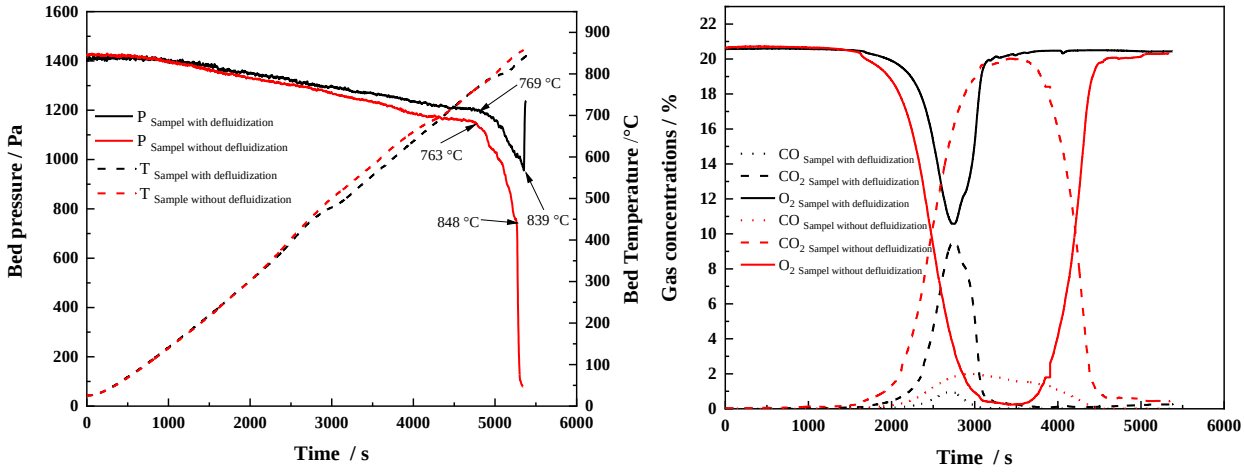

Figure 1-1 Bed temperature & pressure (left) and concentrations of CO, CO_2 and O_2 (right) as a function of time during the combustion of bed samples that taken from gasification of two batches of wheat straw in LTCFB gasifier.

Most proposed countermeasures for reducing agglomeration during biomass utilization have been focused on changing the ash chemistry in the bed, such as pretreatment of biomass, co-combustion of K-lean fuels, addition of additive, and utilization of alternative bed materials[13–15]. However, all of these countermeasures are associated with an additional cost or environmental problems. The pulsed flow was applied as a measure to fluidize the sticky particles, e.g., sub-micro size particle[16–18], due to its positive effects on the fluidization quality in fluidized bed. However, its effect on agglomeration in fluidized bed combustion and gasification of biomass is not reported.

1.2 Project objectives

This PhD project aims at having an improved understanding of the agglomeration in fluidized bed combustion and gasification of biomass, with a special emphasis on the influence of the equivalence ratio (ER), the gasification agents (such as air, steam and carbon dioxide), and the biomass types on agglomeration. The objectives are to:

- Investigate the tendency and mechanism of agglomeration in combustion/gasification of wheat straw, focusing on the impacts of varying ER, as well as addition of steam and carbon dioxide in the bed on agglomeration.
- Explore the fusion behavior of ashes from wheat straw under combustion and gasification conditions to further understand the agglomeration in biomass gasification, highlighting the influence of gas atmosphere on the melting of wheat straw ash.
- Study the agglomeration of different types of biomass in combustion/gasification, underlining the influences of ash-forming elements and char reactivity of different biomasses on agglomeration characteristics. Investigate the agglomeration of different batches of same type of biomass (two batches of wheat straw described in Section 1.1) to understand the mechanism of their different agglomeration behaviors during gasification.
- Evaluate the pulsed flow as a potential economic countermeasure for mitigating agglomeration in combustion and gasification of biomass.

1.3 Structure of this thesis

This thesis is divided into seven chapters, including introduction. The content of each chapter is listed below:

Chapter 2: Literature Survey

This chapter provides an overview of agglomeration in fluidized bed combustion and gasification of biomass. Two extensively reported mechanisms of agglomeration in biomass combustion and gasification are introduced. The factors that influencing agglomeration, including operating conditions, fuel property, bed material property, and gas atmosphere, are reviewed. In addition, the countermeasures for retarding agglomeration are discussed.

Chapter 3: Agglomeration in Fluidized Bed Gasification of Wheat Straw

This chapter presents the investigations on the agglomeration during combustion and gasification of a wheat straw (the wheat straw that caused defluidization in LTCFB gasifier, as described in Section 1.1) in a lab-scale fluidized bed reactor, with an emphasis on the influence of equivalence ratio (ER) on agglomeration in gasification air blown, air/steam and air/carbon dioxide gasification. The influence of gasification agents, such as steam and carbon dioxide, on agglomeration tendency are discussed.

Chapter 4: Fusion Behavior of Wheat Straw Ash under Combustion and Gasification Conditions

In this chapter, the fusion behaviors of the ashes from wheat straw (the straw used in Chapter 3), straw char and mixture of straw and silica sand under combustion conditions (100% air, and a mixture

of 50 vol.% steam and 50 vol.% air) and gasification condition (a mixture of 50 vol.% steam and 50 vol.% N_2) are investigated in a fixed bed reactor at 850 °C. The influences of a high concentration of steam and a reducing atmosphere on the fusion tendency of wheat straw ash are studied to further understand of the agglomeration tendency in gasification of wheat straw described in Chapter 3.

Chapter 5: Influence of Biomass Types on Agglomeration during Combustion and Gasification

In this chapter, the tendencies and mechanisms of agglomeration during combustion and gasification of two types of biomass, including two batches of wheat straw used in LTCFB gasifier and one sunflower husk, are studied in a lab-scale fluidized bed. The influence of ash-forming elements of biomass, especially the molar ratio of silicon to potassium, on the distribution of potassium during combustion and gasification, as well as their further effect on the tendency and mechanism of agglomeration are discussed. In addition, the effect of char reactivity of biomass on agglomeration are investigated, providing an improved understanding for the different agglomeration behaviors of two wheat straws in LTCFB gasifier that has been described in Section 1.1.

Chapter 6: Application of Pulse Flow to a Fluidized Bed for Combustion and Gasification of Wheat Straw

The experimental results of application of a pulsed flow to the fluidized bed combustion and gasification of wheat straw (the one used in Chapter 3) are summarized in this chapter. The potential of pulsed fluidized bed on mitigating agglomeration is presented. The effects of important operating parameters, such as flow rate ratio of pulsation, pulsation frequency, and pulsation duty cycle on agglomeration tendency, are investigated.

Chapter 7: Conclusions and future work

In this chapter, the main conclusions obtained in this PhD project are summarized. Some suggestions for the future work are put forward based on the findings of this work.

Appendix

Appendix A-C contain supporting information for Chapters 3, 4, and 5.

Reference

(1) Danish Energy Agency. *Energy Statistics 2018*; Copenhagen, Denmark, 2020.

(2) Gregg, J. S.; Bolwig, S.; Ola, S.; Vejlgaard, L.; Gundersen, S. H.; Grohnheit, P. E. *Experiences with Biomass in Denmark*; Herrmann, I. T., Karlsson, K. B., Eds.; DTU Management Engineering, 2014.

(3) Anicic, B.; Lin, W.; Dam-Johansen, K.; Wu, H. Agglomeration Mechanism in Biomass Fluidized Bed Combustion – Reaction between Potassium Carbonate and Silica Sand. *Fuel Process. Technol.* **2018**, *173*, 182–190.

(4) Michel, R.; Kaknics, J.; De Bilbao, E.; Poirier, J. The Mechanism of Agglomeration of the Refractory Materials in a Fluidized-Bed Reactor. *Ceram. Int.* **2016**, *42* (2), 2570–2581.

(5) Gatternig, B.; Karl, J. Investigations on the Mechanisms of Ash-Induced Agglomeration in Fluidized-Bed Combustion of Biomass. *Energy & Fuels* **2015**, *29*, 931–941.

(6) Grimm, A.; Skoglund, N.; Boström, D.; Öhman, M.; Bostr, D.; Ohman, M.; Boström, D.; Öhman, M.; Bostr, D.; Ohman, M. Bed Agglomeration Characteristics in Fluidized Quartz Bed Combustion of Phosphorus-Rich Biomass Fuels. *Energy & Fuels* **2011**, *25* (3), 937–947.

(7) Grubor, B.D.; Oka, S.N.; Ilic, M.S.; Dakic, D.V.; Arsic, B. .; Grubor, B. D.; Oka, S. N.; Ilic, M. S.; Dakic, D. V.; Arsic, B. T. Biomass FBC Combustion - Bed Agglomeration Problems. In *Proceedings of the 13th International Conference on Fluidized Bed Combustion*; American Society of Mechanical Engineers: United States, 1995; Vol. 1, pp 515–522.

(8) Scala, F.; Chirone, R.; Consiglio, C.; Tecchio, P. V.; July, R. V; Re, V.; Recei, M.; October, V. Characterization and Early Detection of Bed Agglomeration during the Fluidized Bed Combustion of Olive Husk. *Energy & Fuels* **2006**, *20* (10), 120–132.

(9) Lin, W.; Dam-Johansen, K.; Frandsen, F. Agglomeration in Bio-Fuel Fired Fluidized Bed Combustors. *Chem. Eng. J.* **2003**, *96* (1–3), 171–185.

(10) Öhman, M.; Pommer, L.; Nordin, A. Bed Agglomeration Characteristics and Mechanisms during Gasification and Combustion of Biomass Fuels. *Energy & Fuels* **2005**, *19* (4), 1742–1748.

(11) Alauddin, Z. A. B. Z.; Lahijani, P.; Mohammadi, M.; Mohamed, A. R. Gasification of Lignocellulosic Biomass in Fluidized Beds for Renewable Energy Development: A Review. *Renew. Sustain. Energy Rev.* **2010**, *14*, 2852–2862.

(12) Aničić, B. Agglomeration Mechanisms during Fluidized Bed Combustion of Biomass, Technical University of Denmark, 2018.

(13) Niu, Y.; Tan, H. Ash-Related Issues during Biomass Combustion : Alkali-Induced Slagging , Silicate Melt-Induced Slagging (Ash Fusion), Agglomeration , Corrosion , Ash Utilization , and Related Countermeasures. *Prog. Energy Combust. Sci.* **2016**, *52*, 1–61.

(14) Scala, F. Particle Agglomeration during Fluidized Bed Combustion: Mechanisms, Early

Detection and Possible Countermeasures. *Fuel Process. Technol.* **2018**, *171*, 31–38.

(15) Bartels, M.; Lin, W.; Nijenhuis, J.; Kapteijn, F.; van Ommen, J. R. Agglomeration in Fluidized Beds at High Temperatures: Mechanisms, Detection and Prevention. *Prog. Energy Combust. Sci.* **2008**, *34* (5), 633–666.

(16) Guo, Q.; Wang, M.; Li, Y.; Yang, C. Fluidization of Ultrafine Particles in a Bubbling Fluidized Bed with Sound Assistance. *Chem. Eng. Technol.* **2005**, *28* (10), 1117–1124.

(17) Ali, S. S.; Asif, M. Fluidization of Nano-Powders: Effect of Flow Pulsation. *Powder Technol.* **2012**, *225*, 86–92.

(18) Akhavan, A.; Rahman, F.; Wang, S.; Rhodes, M. Enhanced Fluidization of Nanoparticles with Gas Phase Pulsation Assistance. *Powder Technol.* **2015**, *284*, 521–529.

2. Literature Survey

Abstract

This chapter provides an overview of the agglomeration in fluidized bed combustion and gasification of biomass. The agglomeration mechanisms, factors influencing agglomeration, and countermeasures for mitigating agglomeration are reviewed. It has been shown that the agglomeration in fluidized bed combustion and gasification is aggravated by a high bed temperature, a small ratio of superficial gas velocity to the minimum fluidization velocity (U_g/U_{mf}), and a high alkali content in biomass. The different gas atmospheres in the bed, such as the concentrations of H_2, CO, steam, CO_2, and O_2, may be responsible for the different agglomeration characteristics in combustion and gasification. The influence of gas atmosphere on the agglomeration tendency of model compounds (alkali chloride, carbonate, and sulfate and biomass ashes) has been investigated, showing that a reducing atmosphere and a high concentration of steam in the bed accelerate the agglomeration of these alkali salts and biomass ashes. However, the agglomeration tendency and mechanism in biomass gasification with different gasification agents and equivalence ratios are unclear. Some countermeasures, such as utilization of alternative bed materials, application of additives, pretreatment of biomass, and co-combustion/gasification with alkali-lean fuels, have been proposed for retarding agglomeration in fluidized bed combustion and gasification by altering of ash chemistry to reduce the formation of low-melting temperature compounds. However, most of these countermeasures lead to an additional operation cost. An effective and economic countermeasure for the agglomeration shows great practical implication for the utilization of biomass fluidized bed. Due to the improvement of fluidization quality in the bed by imposing of a pulsed flow in a conventional fluidized bed, the application of pulsed fluidized bed has great potential on mitigating agglomeration in biomass combustion and gasification.

2.1 Introduction

2.1.1 Biomass fuels

Biomass is a kind of biogenic solid product generated by natural and anthropogenic processes. It is a mixture of organic matters (mainly cellulose, hemicellulose and lignin) and inorganic matters (such as silicates, oxides, hydroxides, sulphates, phosphates, carbonates and chlorides etc.)[1,2]. According to their biological diversity, source and origin, biomass can be categorized into several groups listed below[1].

- Wood and woody biomass, e.g., soft and hard wood, bark, and sawdust
- Herbaceous and agricultural biomass, e.g., grasses and flowers, straws, and husks
- Aquatic biomass, e.g., algae and seaweed
- Animal and human biomass wastes, e.g., meat-bone meal and chicken litter
- Contaminated biomass and industrial biomass wastes, e.g., refuse derived fuel and sewage sludge

Table 2-1 Compositions of representative biomass fuels from each category[1]

		Spruce wood	Spruce bark	Wheat straw	Coffee husk	Micro-algae	Chicken litter	Sewage sludge
Ash content /wt.% db*		0.5	3.2	7.1	2.5	23.6	37.8	46.3
Ultimate analysis /wt.% daf‡	C	52.3	53.6	49.4	45.4	43.2	60.5	50.9
	O	41.2	40.0	43.6	48.3	45.8	25.3	33.4
	H	6.10	6.20	6.10	4.9	6.20	6.80	7.30
	N	0.30	0.10	0.70	1.1	2.20	6.20	6.10
	S	0.10	0.10	0.17	0.35	2.6	1.20	2.33
	Cl	0.01	0.03	0.61	-	3.34	0.50	0.04
Chemical ash composition (normalized to 100%) / wt.%	SiO_2	49.30	6.13	50.35	14.65	1.65	5.77	33.28
	CaO	17.20	72.39	8.21	13.05	12.39	56.85	13.04
	K_2O	9.60	7.22	24.89	52.45	15.35	12.19	1.60
	P_2O_5	1.90	2.69	3.54	4.94	9.76	15.40	15.88
	Al_2O_3	9.40	0.68	1.54	7.07	0.85	1.01	12.91
	MgO	1.10	4.97	2.74	4.32	12.50	4.11	2.49
	Fe_2O_3	8.30	1.90	0.88	2.06	1.87	0.45	15.70
	SO_3	2.60	1.88	4.24	0.53	25.74	3.59	2.05
	Na_2O	0.50	2.02	3.52	0.66	19.88	0.60	2.25
	TiO_2	0.10	0.12	0.09	0.27	-	0.03	0.80

* db: dry basis

‡ daf: dry ash free basis

-: no data

The typical compositions of representative biomass from each category are summarized in Table 2-1. The organic composition (C, H, O, N) are similar for various group of biomass. However, the ash

content and ash-forming composition of biomass are highly variable. Generally, woody biomass has a relatively low ash content and the ash is dominated by Ca and Si. Straw is rich in K and Si, and husk is rich in K and Ca[3].

2.1.2 Biomass combustion and gasification in fluidized bed

Gasification and combustion are extensively applied technologies for the conversion of biomass[4,5]. Combustion is a process that converts biomass into gaseous products (e.g., H_2O and CO_2) to provide heat and other forms of energy in the presence of sufficient oxygen or air[6]. Gasification transforms biomass to combustible gases (e.g., H_2, CO, and CH_4) with a limited amount of oxidant supply, which can be carbon dioxide, steam or oxygen[7]. Therefore, when the oxygen or air is used as an oxidant, gasification process can be considered as a partial combustion process. In industry, the primary gasification agents are CO_2 and steam, and the dominate product gases are CO and H_2[8]. Steam gasification attracts increasing attention due to the formation of H_2-rich products[9], and CO_2 gasification will convert CO_2 and carbon in biomass into CO, which could further be processed to valuable synthetic fuels[10]. However, the reactions that occurs during steam and CO_2 gasification are the endothermic reactions. In order to make the process self-sufficient in heat, air or oxygen is introduced to provide the necessary heat by partially oxidizing of biomass[11].

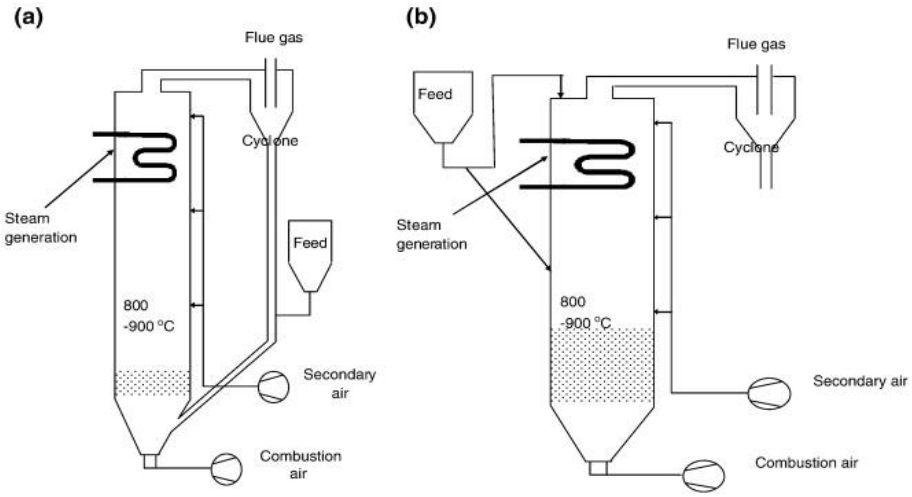

Figure 2-1 Schematic of (a) typical circulating fluidized reactor and (b) typical bubbling fluidized bed reactor[12]

The types of combustors and gasifiers can be distinguished into fixed bed, fluidized bed, and entrained flow according to the gas velocity[13]. Compared to fixed beds, fluidized beds have a better temperature distribution, a higher fuel flexibility, a superior conversion efficiency, and a lower investment and maintenance cost[14]. Therefore, fluidized beds are applied in large scale operations extensively. The fluidized bed reactors are divided into bubbling fluidized beds (BFBs) and circulating fluidized beds (CFBs) according to the fluidizing gas velocity[15], as presented in Figure 2-1. BFB is a classical approach in which the gas velocity is slightly higher than the minimum fluidization velocity (U_{mf}) of bed particles. Compared to BFB, the superficial gas velocity in CFB is much higher. For CFB, a high

reactor (riser) and a recirculation loop are used to ensure that the particles circulate around the loop multiple times before leaving the system, while the gas passes through only once. Usually, the operational temperatures of CFB combustor and BFB combustor are 800-900°C and 760-870°C[16] ,and the operating temperature of fluidized bed gasifier is maintained at 700-900°C[6]. Generally, non-combustible materials, such as silica sand, lime stone, dolomite, are used as bed materials[12,17].

2.1.3 Challenges in fluidized bed combustion and gasification of biomass

Biomass combustion and gasification in fluidized bed face many challenging problems, such as agglomeration, slagging, corrosion[18]. Agglomeration of bed materials affects the performance of a reactor. Defluidization is observed when the bed particles no longer behave as a fluid in response to the fluidizing gas, resulting from an increased mean bed particle size caused by agglomeration[19]. Agglomeration phenomena is observed even at 650 °C during agricultural biomass combustion[20]. Agglomeration at high temperature is mainly attributed to the presence of molten phase, i.e. the low-melting temperature alkali containing compounds originated from biomass[21,22]. Agglomeration and defluidization phenomena are illustrated in Figure 2-2.

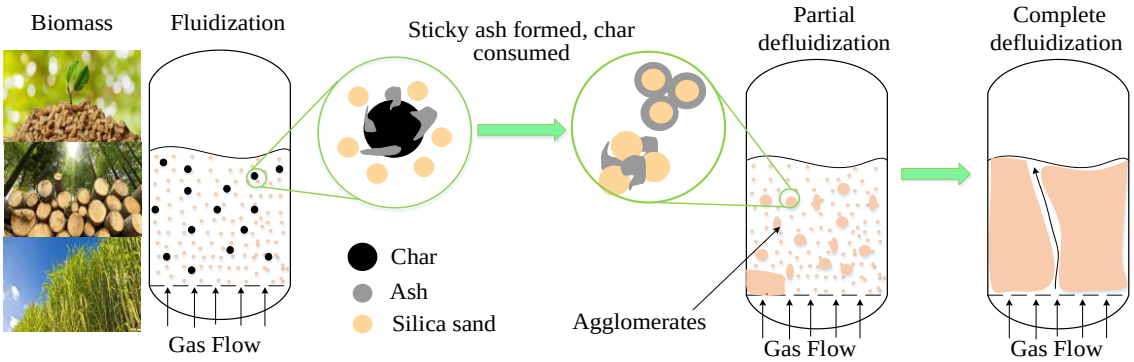

Figure 2-2 Illustration of agglomeration and bed defluidization, redrawn from[23]

2.1.4 Outline of review

In the past decades, the agglomeration in biomass combustion are extensively investigated to reveal the agglomeration mechanisms, the influencing factors of agglomeration, and the countermeasures for reducing agglomeration, as discussed in a few review papers[24–27]. However, the agglomeration phenomena in biomass gasification are less studied. This chapter reviews the agglomeration during fluidized bed combustion and gasification of biomass, with a special focus on the agglomeration in biomass gasification. This chapter is divided into three sections:

- Section 2.2: the mechanisms of agglomeration in fluidized bed combustion and gasification of biomass
- Section 2.3: the influencing factors of agglomeration in biomass combustion and gasification
- Section 2.4: the countermeasures for agglomeration

2.2 Mechanisms of agglomeration

Agglomeration in a fluidized bed combustor or gasifier is a self-promoting process. Two types of agglomeration mechanisms, "melt-induced" agglomeration and "coating-induced" agglomeration, are extensively studied[28–33]. The illustrations of "melt-induced" agglomeration and "coating induced" agglomeration are shown in Figure 2-3.

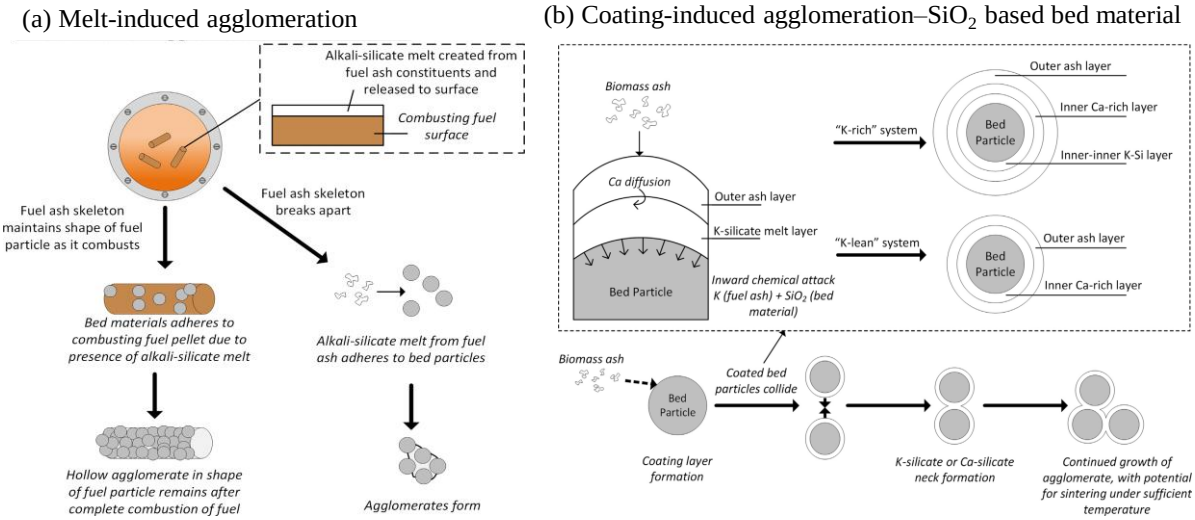

Figure 2-3 (a) "Melt-induced" agglomeration mechanism and (b) "coating-induced" agglomeration mechanism in a system with a SiO_2-based bed material, adopted from[26]

2.2.1 "Melt-induced" agglomeration

"Melt-induced" agglomeration refers to that the bed particles are directly bonded by a molten compound[34]. The binder, e.g., alkali-salts, is already sticky (i.e., molten) before it deposits on the bed particles, with a sufficient surface tension for wetting the bed particles and a viscosity low enough to be shaped into a liquid bridge[24,35]. "Melt-induced" agglomeration is mainly induced by the occurrence of (local) peak temperatures, e.g., "hot-spots", which are higher than the targeted operating temperature. A "hot-spot", that resulting from uneven fuel feeding or temporary defluidization of one area of the bed, causes a local temperature rise, resulting in the melting of ash[36]. Gatternig & Karl[35] found that the less dense fuels, e.g., straws, are observed to "float" on top of the fluidized bed during combustion, instead of being submerged within the bed. Olofsson *et al.*[36] suggested that the temperature "hot-spots" during less dense fuels combustion perhaps is attributed to this "floating" behavior.

Lin *et al.*[19,37–40] suggested that the agglomerates are already formed in a couple of minutes after the straw is fed during fluidized bed combustion. These agglomerates have a similar shape with the straw granules and a blackish ash core. They believed that these agglomerates are formed due the transformation of potassium-rich ash from the burning char particles to the sand through collisions. The transformation of potassium and the subsequent fusion are further accelerated by the high

temperature of burning char particles. Scala *et al.*[21,41–44] investigated the role of fine char particles on agglomeration during biomass combustion. They found that a large fraction of char particles are converted to fine particles due to the attrition/percolative fragmentation process in the bed during biomass combustion even when coarsely grained fuel is used[41,42]. The conversion of fixed carbon takes place essentially along two competitive pathways: (1) direct coarse char combustion and (2) generation of elutriable carbon fines by attrition of the coarse char, followed by their post-combustion. The second pathway is negligible for low-volatile solid fuels (such as Snibston coal), while is important for high-volatile biomass fuels (such as Robinia Pseudoacacia). About half of the fixed carbon burns along the second pathway, and the remainder is burnt directly as coarse char carbon[41]. The attrited char may experience, upon further burn-off, peak temperatures that largely exceeding the bed temperature, whilst coarse particles burn at temperatures only slightly above the bed temperature. The combination of attrition-induced generation of fines particles and combustion-induced overheating of char particles is responsible for the formation of ash-layered bed material, eventually leading to bed agglomeration and defluidization[43]. It is suggested that the combustion mechanism of char fines is that the formation of a "captive" solid carbon phase by adhesion of char fines onto bed solids[42], implying that the burning char particles could cause a "hot-spot" and could act as a platform for agglomerates to grow[19]. The ash on the char fragment are molten at around 900 °C and attached on the sands in the collisions with bed materials. Eventually, the char fragment fully combusts, typically leaving an agglomerate with a hollow center in the shape of the initial fuel fragment[45].

2.2.2 "Coating-induced" agglomeration

"Coating-induced" agglomeration is caused by a coating layer on the sand surface, which is formed via continuous deposition of gaseous phase inorganic compounds or solid phase ash on the bed materials[34]. The agglomeration is initiated with the bonding of coated particles when the coating thickness or temperature is achieved[34]. Therefore, "coating-induced" agglomeration is often observed under the condition with long operating time[29]. In addition, the agglomerates formed by "coating-induced" mechanism usually are easily crushed or fall apart, meaning that the mechanical strength between agglomerates is very limited[29]. Öhman *et al.*[30,46] proposed that a multiple-layers (two- or three-layers) coating is formed during agglomeration in fluidized bed combustion and gasification. The illustrations of typical cross sections of bed particles are shown in Figure 2-4[46,47].

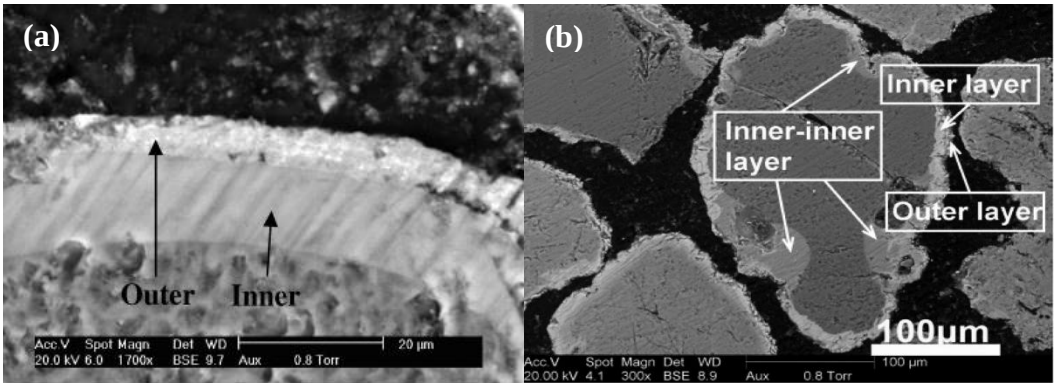

Figure 2-4 Illustration of typical cross sections of bed particles (a) taken after 40 hour of operation in the bench-scale rig during the combustion of olive residue[46] and (b) taken from CFB at 122 MWth versus operation times of 4 days during the combustion of 40% bark and 60% sawdust & logging residues[47]

A homogeneous inner layer is formed by the interaction between multi-components fuel ash and bed particles, which is consisted of Ca-rich silicates with slightly amount of K[46]. For K-rich biomass, K-Ca silicates are the mainly compositions of the inner layer[48]. An additional "inner-inner" layer consisted of K silicates is observed for the K-rich fuel at long operation time[47]. Potassium or other alkali silicates are dominated at the locations where calcium is not as available, such as cracks in sand particles, or when the fuel ash contains less calcium[30,46]. A heterogeneous and powdery outer layer is formed when the small ash particles (<10 μm) are attached on the bed particles during collision. Then these small ash particles gradually melt and immerse in the homogeneous inner layer from the inside[46]. During collision, the particles of the outer layer in the contact area are submerged, enabling the melt of both colliding bed particles to contact and form a liquid bridge[35]. The composition of the porous, inhomogeneous outer layer is similar with the composition of ash, which largely depended on the used fuels. Therefore, the composition of outer layer is more complex.

The inner layer is found to grow inward through the interaction of ash particles and quartz[46]. According to the second law of thermodynamics, the overall entropy of the system keeps increasing. In order to increase the total entropy, ash components interact with the bed material by invading the highly ordered SiO_2 lattice (Figure 2-5)[35]. The elements such as Al and Ca incline to replace the positions of silicon atoms in tetrahedral grid, and in the meanwhile Na and K occupy the interstitial spaces within the crystal lattice. This transformation results in an additional stress on the Si−O−Si bonds and reduces the thermal energy required for bond breakage. As a result, the melting point of the layer is effectively lowered. Once sufficient amount of silicate melt is produced, continuous layers are created on the particle surface. Increased adhesive forces caused by these layers promote further adhesion of fresh ash particles, providing additional material to penetrate the remaining SiO_2 crystal lattice[49].

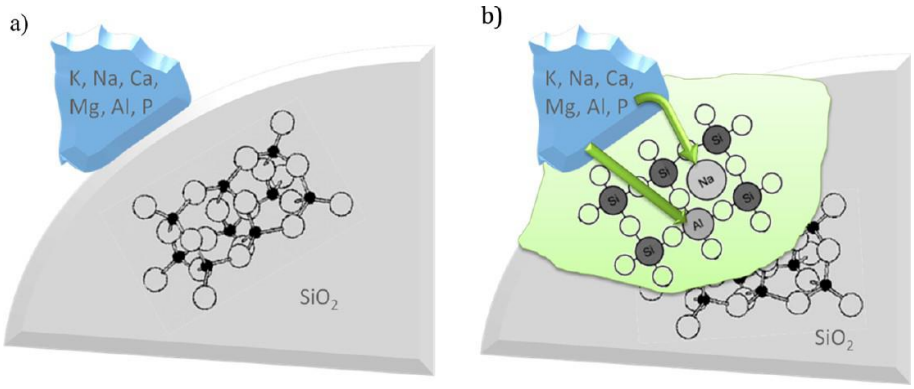

Figure 2-5 Silicate melt formation in ash coatings[35]

A three-step mechanism for the formation of two-layer coating is suggested as shown in Figure 2-6[50]. Firstly, ash deposits on the sand surfaces via three paths: a) attachment of the small ash particles; b) condensation of the gaseous alkali species (KCl, KOH, and K_2SO_4); c) reaction of the gaseous alkali species with SiO_2. Secondly, the inner coating layer become homogenized through sintering as incessant ash deposition on the bed particles proceeds, and thereby forming a homogeneous layer. Last, the molten homogeneous silicate layer, which has a strong impact on the adhesive forces, leads to the collision of bed particles, and eventually to the agglomeration.

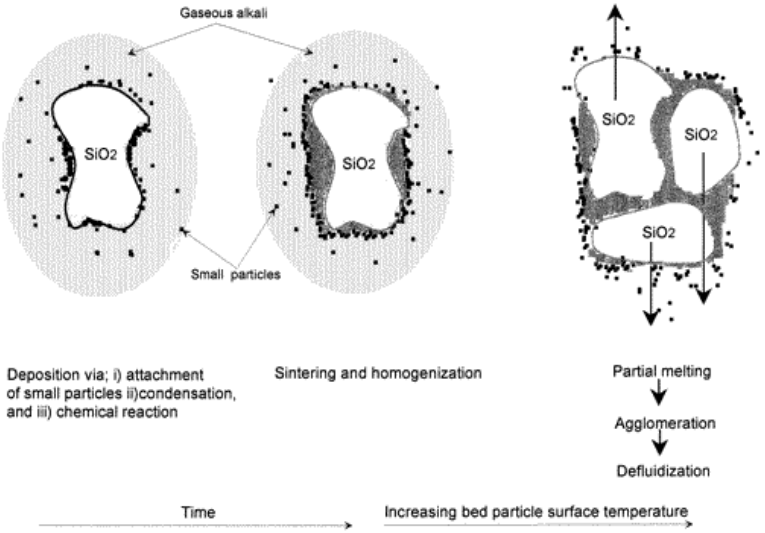

Figure 2-6 Illustration of the important chemical sub-processes of the bed agglomeration mechanism[50].

2.3 Agglomeration in combustion and gasification

As mentioned above, the presence of molten phase, including the soften ash particles and the fused eutectics formed by the interactions between ash and bed materials, is responsible for agglomeration both in fluidized combustor and gasifier. Agglomeration in fluidized bed combustion or gasification of biomass is a complex process influenced by a number of factors, such as bed temperature, the ratio of superficial gas velocity to the minimum fluidization velocity (U_g/U_{mf}), bed materials properties, types of biomass, as well as gas environment.

2.3.1 Influencing parameters on agglomeration in combustion

Morris *et al*.[26] reviewed the impacts of operational variables on agglomeration in biomass combustion and found that the bed temperature, the ratio of U_g/U_{mf}, the compositions of bed materials and fuels are the major influence parameters.

2.3.1.1 Bed temperature

Bed agglomeration shows a significantly intensifying tendency with increasing bed temperature[19]. Chaivatamaset *et al.*[51] noted that the defluidization time, which defined as the time interval between the starting of the fuel feeding and the occurrence of defluidization, is reduced to around one third when bed temperature is increased from 850 °C to 950 °C during combustion of eucalyptus bark. In addition, the defluidization in fluidized bed is accelerated by a high local temperature, which could be caused by char particles burning[52], fluctuations in feeding, and other momentary disturbances[36]. It is shown that the temperature of char particles is approximately 50-80 °C higher than the bed temperature[52]. With increasing bed temperatures, the fraction of molten ash increases and the viscosity of the molten layer decreases[53], both accelerating the agglomeration during combustion[19].

2.3.1.2 Ratio of U_g/U_{mf}

Bed agglomeration can be mitigated by increasing the ratio of U_g/U_{mf}, i.e. increasing gas velocity[51,54] and utilizing smaller bed materials[19,55]. Lin *et al*.[19] found that the defluidization time is about 30% longer when the gas velocity is doubled. Chaivatamaset *et al.*[51] found that the influence of gas velocity on defluidization time is more pronounced at higher bed temperatures. They attribute the good performance of a high U_g/U_{mf} ratio on prolonging defluidization time to a good mixing of bed particles. With a higher gas velocity, the agglomerates are more easily broken due to the larger force acting on agglomerates.

2.3.1.3 Bed materials

Agglomeration is often observed in fluidized bed combustion and gasification of biomass using silica sand as bed material[29], due the formation of low-melting compounds via the interaction between biomass ash and SiO_2-based bed material[56,57]. Ghaly *et al*.[57] investigated the behaviors of the mixtures of straw ash and silica sand at 620, 740, 850 and 1000 ℃ in a muffle furnace. The results reveal that a eutectic layer with low-melting temperature is formed on the silica sand surface at the temperatures of 850 and 1000 ℃, resulting from the interaction between straw ash and silica sand. Some bed materials, such as Al_2O_3[58], Fe_2O_3[36], dolomite[59], and limestone[50], have been reported that effectively mitigate the agglomeration by reducing the formation of low-melting point eutectics. The details of influence of bed materials on agglomeration are reviewed in Section 2.4.1.1.

2.3.1.4 Types of biomass

As mentioned above, agglomeration during biomass conversion is mainly ascribed to the alkali (K/Na) containing compounds originated from biomass[60]. The agglomeration tendency of K/Na-rich biomass, therefore, could be high[60]. The formation of Ca/Mg silicates and K-Ca/Mg phosphates with high-melting temperatures[61] inhibit the agglomeration in combustion of Ca- and Mg-rich biomass[62,63]. Generally, the biomass that has a high fraction of K/Na and a lower fraction of Ca/Mg favors agglomeration[21,64].

In addition to the alkali (K and Na) and alkaline earth metals (Mg and Ca), other inorganic elements, such as Si, Al, Fe, P, and S, also affect the agglomeration during biomass combustion. A biomass with an initial fuel ash composition that is close to the low-melting point eutectic composition appears to enhance agglomeration[64]. The softening of wheat straw ash, which is originally rich in both alkali and silicon, may start before the ash encounters the sand particles[35,65]. The presence of a high phosphorous content in biomass influences the ash chemistry, resulting in the formed ash is dominated by phosphates instead of silicates, and thereby affecting the agglomeration phenomenon in combustion of biomass. Piotrowska *et al.*[66] found that the defluidization temperature of bark is lowered by co-combustion with rapeseed cake, which is rich in K and P. The low defluidization temperature of rapeseed cake is attributed to the formation of sticky ash, which is dominated by K-Ca/Mg phosphates. Boström *et al.*[67] observed that the co-combustion of bark and rapeseed meal causes a low initial defluidization temperature than the pure fuels, implying that an interaction between the phosphates and the silicates probably exists that reduces the melting temperature of the ash during co-combustion. Billen *et al.*[28] studied the combustion of poultry litter, which is a P-rich fuel. It is suggested that the agglomerates found at the walls of freeboard above the fluidized bed are caused by K-silicates, while the agglomerates in the bed are caused by a solid bridge of $Ca_3(PO_4)_2$ between bed materials formed via the interaction between CaO or Ca and molten $HPO4_2^-$ or $H_2PO_4^-$ salts. The impact of sulfur on agglomeration in biomass combustion are limitedly reported. Some studies[68,69] showed that co-combustion of high-sulfur coals and biomass could prevented agglomeration. Varol *et al.*[69] suggested that the sulfur in the coal may react with alkali oxides forming alkali sulfates. Therefore, sulfur is an alternative reactant for alkali metals, generating a competitive reaction to the reactions of Si and alkali oxides or salts. In addition, the existence of iron and aluminum content will slow down the agglomeration due to the formation of eutectic with high-melting point[36].

2.3.2 Influencing parameters on agglomeration in gasification

The number of studies on agglomeration in fluidized bed gasification appears lower compared to combustion, although the studies started earlier for gasification of coal[70] and biomass[71]. In addition to the factors that have been discussed for the combustion process, the equivalence ratio (ER, also

called air ratio), which will affect the yield and composition of the producer gas in gasification[72], is an important operational parameter.

2.3.2.1 Bed temperature, ratio of U_g/U_{mf}, bed materials, and types of biomass

In biomass gasification, the influences of bed temperature[33,71], ratio of U_g/U_{mf}[73], bed material types[74,75], and biomass types[74,76–80] have been investigated. Nisamaneenate *et al.*[33] observed that the defluidization time extends to 3 - 6 times by decreasing the bed temperature from 900 °C to 700 °C in gasification of rice straw. Lin *et al.* [73] found that the defluidization time can be prolonged at a larger ratio of U_g/U_{mf}, resulting from either decreasing particle size of bed material or increasing gas velocity. Ergudenler *et al.*[71,81] reported that the agglomeration temperature of alumina sand in gasification of wheat straw is higher than that of silica sand. Although alumina sand could mitigate agglomeration, it is difficult to fluidize due to its high density[82]. The alkali-rich fuels often show high agglomeration tendency. The defluidization is observed at temperatures of 750 °C[76] and 780 °C[77] during gasification of palm empty fruit bunches and cardoon, whose K content in the ash are 50.8 wt.% and 30.6 wt.% respectively. Kittivech *et al.*[76] found that the defluidization time of rubber wood sawdust is more than 5 times of palm empty fruit bunch, although the ash content of rubber wood sawdust is only three tenths of palm empty fruit bunch. This may be attributed to the high Ca and Mg content contained in the rubber wood sawdust. Lin *et al.*[73] investigated the effect of Na concentration on the agglomeration in gasification of the mixture of sawdust and polyethylene by adding $NaNO_3$ solution. The results reveal that the addition of $NaNO_3$ sharply reduces the defluidization time of the mixture, and this effect becomes less pronounced with increasing Na concentration in the range of 0.2% - 3%. The addition of $Mg(NO_3)_2$ and $Ca(NO_3)_2$ could prolong the defluidization time at the Na concentration below 1%, whilst the addition of Mg and Ca shows insignificant effect on the defluidization time at Na concentration of 3%.

In general, the bed temperature, the ratio of U_g/U_{mf}, the fuel composition, and bed material type show consistent effects on the agglomeration tendency in biomass gasification and combustion. Therefore, the countermeasures that effective for retarding agglomeration in combustion usually also are effective for the gasification process[76,83,84], such as co-gasification of alkali-lean fuel and utilization of alternative bed materials.

2.3.2.2 Equivalence Ratio (ER)

The influence of ER on agglomeration in gasification is limitedly studied. Ergudenler and Ghaly[71,81] investigated the impact of ER on the agglomeration in wheat straw gasification using silica sand or alumina sand as bed material. It is found that a severe agglomeration is observed in silica sand bed as long as the temperature is above 800 °C, thus influence of ER on the agglomeration characteristics is hardly to observe at the ER in a range of 0.26 - 0.76. In addition, no agglomeration is found for alumina sand at ER in the range of 0.18 - 0.26. In their works, the ER is varied by adjusting the fuel

feeding rate with a constant gas flow rate or changing gas flow rate at a same fuel feeding rate. Therefore, the bed temperature or the ratio of U_g/U_{mf} seems to be difficult to keep at the same level in investigation. Nisamaneenate *et al.*[33] studied the influence of ER on defluidization time of rice straw using bed materials with different alumina sand to silica sand ratios at temperature between 700 and 900 °C. They found that the influence of ER on agglomeration is related to the bed material composition and bed temperature. For the pure silica sand or alumina sand, the ER shows negligible effect on the defluidization time at 700 and 800 °C. However, the defluidization time is prolonged at 900 °C by increasing the ER from 0.2 to 0.4. For the mixture of alumina sand and silica sand in different proportions, the influence of ER on agglomeration tendency is different.

2.3.3 Comparison of agglomeration in combustion and gasification

Different with the oxidizing atmosphere produced in combustion process, the gas environment formed during gasification is mainly composed of CO, H_2, CH_4, H_2O, and CO_2, and the content of each composition strongly depends on the ER and the gasify agent, e.g., air, oxygen, steam and carbon dioxide[10,85–87]. The agglomeration tendencies and mechanisms in biomass gasification and combustion may be different, resulting from the different gas environment in the two processes.

The comparison of agglomeration tendency in biomass combustion and gasification is limitedly explored in the literatures. The agglomeration behaviors of several biomasses under gasification and combustion atmospheres are compared in fluidized bed using silica sand as bed material by Öhman *et al.*[30,88]. In their work, the ashes from combustion and gasification are firstly produced with 1.06 and 0.3/0.35 stoichiometric air, respectively. Then the initial agglomeration temperature of biomass ash is determined at the point that the occurrence of agglomeration during heating process under combustion and gasification atmospheres. The combustion atmosphere is simulated by the combustion products of propane-air mixture, and the gasification atmosphere is simulated by the products of a gas mixture containing CO, CO_2, H_2 and N_2 that passes through the preheater and platinum catalyst. The initial agglomeration temperatures of bark, olive flesh, and cane trash under gasification atmosphere are tens of degrees lower than that under combustion atmosphere. However, the reed cancan grass shows the opposite trend. It is suggested that no major difference in the agglomeration mechanisms of these fuels is observed between the two different operational modes, and the reason for the differences in their agglomeration temperatures under two gas atmospheres is not investigated. It is noticed that the agglomeration temperature of Lucerne, which riches in S but lean in Si, under gasification condition is much higher (180 °C) than that of combustion. They attribute this to the formation of low-melting point KCl and K_2SO_4 eutectic under combustion condition, whilst K_2SO_4 is unstable at reducing atmospheres. The eutectic mixture of KCl and K_2SO_4 is as low as 690 °C[89]. However, it is noteworthy that the inner layers of agglomerates from combustion and gasification of Lucerne are dominated by K and Si, although Lucerne is a Si-lean fuel. The K silicates may be produced by the interaction between Lucerne ash and bed material.

Ma *et al.*[90] investigated the defluidization temperatures of several straw ashes (wheat straw, rice straw and corn straw) in fluidized bed under air, CO_2, H_2 and steam atmospheres, which was used for simulation of combustion and gasification conditions. It is found that the defluidization temperatures of the ash samples, which were prepared at 550 °C under air condition, in four atmospheres decrease in the order of: air ≈ CO_2 > H_2 > steam, indicating that the reducing gas and steam promote the agglomeration tendency of the straw ashes. The low defluidization temperatures of the straw ashes under H_2 atmosphere may be attributed to the transformation of K_2SO_4 into K silicates by interacting with bed materials. However, the mechanism of the influence of steam on agglomeration is unclear. In addition, these studies were carried out under the simulated gas atmospheres using the biomass ashes as material, and the difference in agglomeration characteristics in a continuously feeding combustion and gasification system is still unclear.

2.3.4 Influence of gas environment on ash transformation

Agglomeration in fluidized bed during thermal conversion process is an ash-related problem, especially relates to the molten alkali (K and Na) containing compounds in biomass ash. Compared to sodium, potassium plays a more crucial role in agglomeration due to its significant amount in biomass[91]. K may be both organically and inorganically associated in biomass[92–98]. The chemical forms of potassium in woody biomass and wheat straw have been investigated using chemical fractionation analysis method[99,100]. It is suggested that the mainly water-soluble salts contained in woody biomass may be KCl, K_2SO_4, K_2HPO_4 and KH_2PO_4[99], and the potassium in wheat straw may present in the forms of KCl, K_2SO_4 and K silicates[100]. During biomass conversion, the potassium in biomass can be transformed into gaseous phase (such as KCl and KOH vapor) and/or into condensed phase (such as K_2SO_4 aerosols and K silicates particles)[101–105], and then interacts with the bed materials, resulting in agglomeration[35]. Although the comparison of agglomeration tendency in combustion and gasification of biomass is limitedly studied, the influence of gas atmospheres, such as oxidizing atmosphere, reducing atmosphere (i.e. CO and H_2), high concentration of steam, and high concentration of CO_2, on transformation of K, e.g., the release of K and the reactions of K-species and SiO_2, and the ash behaviors, e.g., melting temperature and viscosity of the ashes, are extensively investigated.

2.3.4.1 Release of K

Oxidizing atmospheres

During combustion, the release of potassium mainly takes place at two main stages: devolatilization stage and char burnout stage[92,106], as shown in Figure 2-7. In the devolatilization stage, the biomass bonded potassium, for example, K-carboxylates and K-phenols, can be decomposed at temperature below 700 ℃ to release atomic potassium. During the char oxidation stage, the residual char bonded potassium is favored to be transformed to K_2CO_3 and K_2SO_4. K_2CO_3 starts to decompose at

temperature above 800 ℃[107], the potassium will be further released in the form of K (g) or KOH (g). The remaining potassium is likely to transform into K silicates at temperature exceeding 800 ℃[92]. In addition, the potassium could be released as KCl (g), and it is suggested that KCl is the dominate form of potassium released[108].

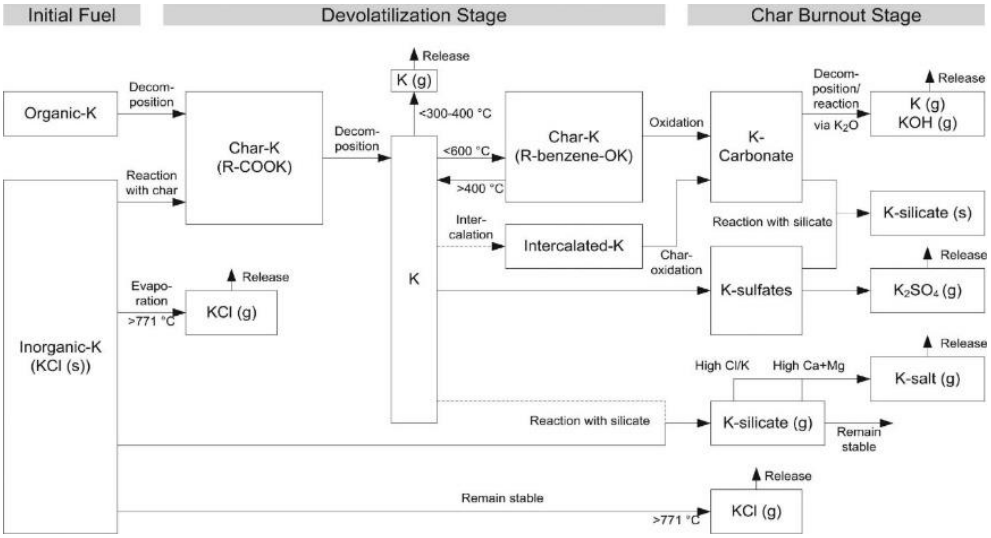

Figure 2-7 Possible reaction paths and release mechanism of potassium in biomass during combustion[92]

van Lith *et al.*[107] investigated the release of potassium during combustion of woody biomass in a laboratory-scale tube reactor at temperature in the range of 500 - 1050 °C. 30g of biomass was devolatilized in N_2 for 60 min, and then was combusted in the atmosphere with the O_2 concentration stepwise increased from 1 vol.% to 20 vol.%. The experiments were stopped after the total combustion stage of 140 min or when the CO and CO_2 concentrations in flue gas was below 50 ppm. Knudsen *et al.*[109] studied the release of potassium in annual biomass combustion using similar method. 4 g of biomass was heated in N_2 for 5 - 15 min, depending on the reactor temperature, until biomass was completely devolatilized. Subsequently, the gas atmosphere was shifted to the O_2 containing gas with the O_2 concentration stepwise increased from 2 vol.% to ambient air concentration to combust the char samples until the CO and CO_2 concentrations in flue gas below 5 ppm. The amount of potassium remained in the ashes after combustion are summarized in Figure 2-8. Around 20% of initial potassium is released at temperature below 700 ℃, and more than half of potassium is released at 1050. It is suggested that most potassium can be released when temperature reach 1300 ℃[110,111].

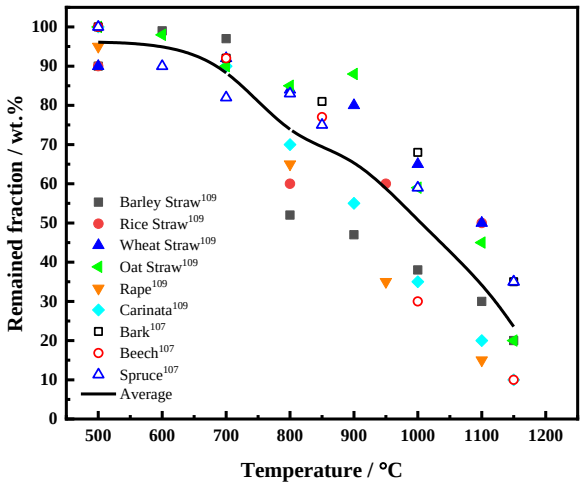

Figure 2-8 Remained potassium in ash at different combustion temperatures. Redraw based on data from[107,109]

Steam

The release of potassium in air gasification are seldom reported, and this may be attributed to the release are usually investigated in batch experiments. Dayton *et al.*[108] suggested that the oxygen concertation in the gas flow has little effect on the K release during Switchgrass combustion in an oven. The amount of potassium release is related to the carbon conversion. Tchoffor *et al.*[112] investigated the potassium release of wheat straw pellets in a laboratory-scale bubbling fluidized bed reactor at 800 and 900 °C. Two wheat straw char samples are prepared by a 6 min gasification in steam (86 vol.% in N_2) and a 3 min gasification in steam followed by a 3 min combustion in O_2 (6 vol.% in N_2), and the samples are named as G6 and GC3. It is found that the potassium release amount in GC3 is around 10% higher than G6, resulting from the higher char conversion and less compact char formed. The addition of steam shifts a part of K release from KCl (g) to KOH (g)[108,113].

2.3.4.2 Reactivity of various K-species towards SiO_2

Oxidizing atmospheres

The presentences of KOH, KCl, K_2CO_3, K_2SO_4, K- phosphates and various K-silicates are suggested in biomass combustion process[65,110,114–117]. The global thermodynamic equilibrium distribution of potassium species during wheat straw combustion have been calculated by Factsage with the compositions of H, C, O, Si, N, K, Cl, Ca, Mg, Na, S, and P are included[92]. The calculation predict that the dominated K-species formed during wheat straw combustion in the temperature range of 800 - 900 °C are KCl (g), K_2SO_4 (s) and K silicates (s), as shown in Figure 2-9[92].

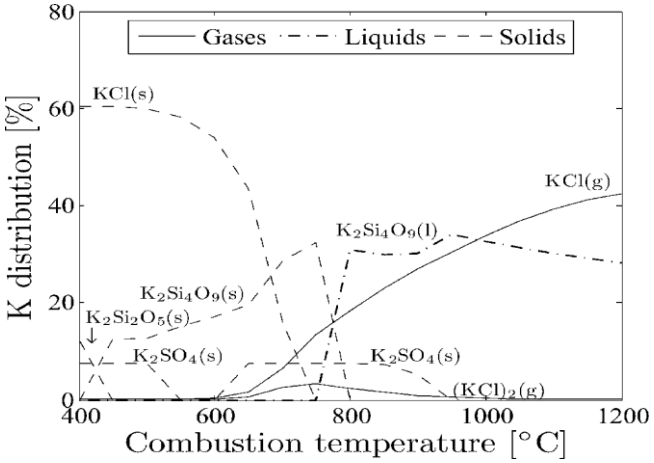

Figure 2-9 Calculated potassium distribution of biomass combustion. Calculation composition (wt.% on dry basis) and condition: H-5.9%, C-47.5%, N-0.7%, Si-0.8%, K-1.0, Cl-0.4%,Ca-0.4%, Mg-0.07%, Na-0.05%, S-0.15%, and P-0.08% at the excess air ratio of 1.4[92].

The actual forms of K compounds presented in the ash are more complex and difficult to detect. One possible analysis technique is X-ray powder diffraction (XRD), which can be used to identify the crystalline phase of biomass ash. The typical crystalline phase species detected in wheat straw ashes from combustion at different temperatures are summarized in Table 2-2. At fluidized bed temperatures (800 - 900 °C), KCl and K_2SO_4 are the dominated crystalline phase K-species. Although K_2CO_3 is not detected in the ash samples, it is believed that it also plays an important role during biomass combustion[107]. It is reported that the formation of amorphous silicate or glass starts at temperatures as low as 400°C[118], and the amount of amorphous matters could up to 50% by weight[119]. However, the amorphous silicates cannot be determined by XRD.

Table 2-2 Typical crystalline phase species detected by XRD in wheat straw ashes from combustion

Species	Ashing Temperature/°C	Reference
KCl, K_2SO_4, $KCaPO_4$, SiO_2	550	120
KCl, K_2SO_4, $K_2Ca(CO_3)_2$, SiO_2, $CaCO_3$	550	121
KCl, K_2SO_4, $CaCO_3$	500	122
KCl, K_2SO_4, SiO_2	550	90
KCl, K_2SO_4	900	90
KCl, K_2SO_4, SiO_2	700-800	123
K_2SO_4,$Ca(Mg,Fe)Si_2O_6$, $CaAl_2Si_2O_8$, SiO_2	900	123

Various K-species have different melting temperatures and show diverse reaction activities towards bed materials, resulting in the different agglomeration tendency and mechanisms. The melting temperatures of typical K-species are presented in Table 2-3. The melting temperatures of KCl, KOH, and KPO_3 are in the range of operational temperatures of fluidized bed, whilst the melting temperature of K_2SO_4 and $KCaPO_4$ are higher than the operational temperatures. K_2CO_3 is prone to be decomposed during combustion and gasification[124] (Equation 2-1), and subsequently reacts with other compounds due K_2O is not stable.

$$K_2CO_{3(s,l)} \rightarrow CO_{2(g)} + K_2O_{(s,l)}$$ Equation 2-1

Table 2-3 Melting temperature of typical K-species

K-species	Melting temperature (°C)	K-species	Melting temperature (°C)
KCl	770	K_2SO_4	1069
KOH	360	KPO_3	810[125]
K_2CO_3	891(Decomposes)	$KCaPO_4$	1560[125]

The agglomeration of typical K-species and their mixture under air condition (oxidizing atmosphere) are summarized in Table 2-4. The defluidization mechanisms of these K-salts can be categorized into two groups: direct melting of K-salts (e.g., KCl and KCl/K_2SO_4 eutectic mixture) and formation of K silicates by interaction between K-salts (e.g., K_2CO_3) and SiO_2-based bed materials (Equation 2-2). The agglomeration temperatures of the salts that cause defluidization by direct melting are close to their melting temperatures. For the salts that cause agglomeration by the interaction between slats and bed material, the agglomeration temperatures of the salts depend on the operation conditions of experiments, such as heating rate, salts amount, and ratio of U_g/U_{mf}. It is noteworthy to highlight that no defluidization is observed when around 10 wt.% of $K_2Si_4O_9$ is added in fluidized bed at 850 °C due to the high viscosity of $K_2Si_4O_9$. Some agglomerates are formed in the bed, being attributed to the soften $K_2Si_4O_9$ could acts a binder for silica sand[89].

$$K_2CO_{3(s)} + \mathrm{nSiO_{2(s)}} \rightarrow K_2O \cdot \mathrm{nSiO_{2(l)}} + 3CO_{2(g)} \quad (n = 1, 2\ and\ 4)$$ Equation 2-2

Table 2-4 Agglomeration tendency and mechanisms of K-species under air condition (oxidizing condition)

Salts	Def.	$T_{Def.}$ (°C)	$T_{melting}$ (°C)	Fed Salts (wt.%)	Defluidization Mechanism	Ref.
KCl	Yes	-[ɬ]	770	3.0	KCl melting	[126]
K_2CO_3	Yes	-[ɬ]	891	0.97	K_2CO_3 interact with SiO_2	[126]
K_2SO_4	No	-[ɬ]	1069	3.60	-	[126]
KCl	Yes	750	770	1.2	KCl melting	[127]
K_2CO_3	Yes	670	891	2.85	K_2CO_3 interact with SiO_2	[127]
K_2SO_4	No	n/a	1069	2.25	-	[127]
KCl	Yes	773	770	0.94	KCl melting	[89]
KCl/K_2SO_4=54/46 wt.%[*]	Yes	675	690	1.53	Salts melting	[89]
KCl/K_2SO_4=11/89 wt.%	Yes	713	960	5.78	Salts melting	[89]
K_2CO_3	Yes	802	891	1.44	K_2CO_3 interact with SiO_2	[89]
KCl/K_2CO_3=49/51 wt.%	Yes	771	629	1.37	Both KCl melting and K_2CO_3 interact with SiO_2, KCl melting dominant	[89]
$K_2Si_4O_9$	No	n/a	764	9.68	-	[89]

[ɬ] The defluidization tendency are investigated at 800, 850 and 900 °C

[*] The eutectic composition is corrected from KCl/K_2SO_4=46/54 wt.%

Reducing atmospheres

The agglomeration mechanisms and tendencies of KCl, K_2SO_4, and K_2CO_3 under reducing and oxidizing atmospheres are compared by Ma *et al.*[127], as shown in Table 2-5. The reducing atmosphere promotes the agglomeration of K_2SO_4 and K_2CO_3 due to the improvement of their reactivity towards silica sand. The interaction between K_2CO_3 and SiO_2 is promoted in reducing atmosphere. K_2SO_4 may transform into K silicates by reacting with silica sand according to Equation 2-3 under a reducing atmosphere[124].

$$K_2SO_{4(s)} + \mathrm{nSiO_{2(s)}} + 4H_{2(g)} \rightarrow K_2O \cdot \mathrm{nSiO_{2(l)}} + H_2S_{(g)} + 3H_2O_{(g)} \quad (n = 2\ and\ 4) \qquad \text{Equation 2-3}$$

Table 2-5 Impact of reducing atmospheres (H_2) on agglomeration temperature and mechanisms of K slats[127]

K -species	Agglomeration temperatures compared to oxidizing atmosphere	Agglomeration mechanisms
KCl	Almost same	Melting of KCl
K_2CO_3	Lower	Faster the formation of alkali silicates and alkali-hydroxide is formed
K_2SO_4	Lower	Formation of $K_2Si_4O_9$

Steam

The agglomeration tendency and mechanism of pure K/Na slats[124,126–128] and K/Na slats-doped wood[129] under steam atmosphere are compared to oxidizing atmosphere, and the results are summarized in Table 2-6. The presence of steam accelerates the agglomeration tendency of the K/Na-chloride and K/Na-carbonate. Zhao *et al.*[124] found that the KCl in the mixture of KCl and SiO_2 is almost released to gas phase at the temperatures in the range from 800 to 1000 °C under an inert gas environment (pure N_2). With addition of 10 vol.% of steam in N_2, significant amount of insoluble K-species, which is believed to be K-silicates, is produced. The amount of insoluble K-species decrease with the increasing temperature. The addition of steam shifts a part of released K from KCl (g) to KOH (g)[108,113] (Equation 2-4), and K-silicates are produced through interaction between KCl and bed materials according to Equation 2-5[127]. Agglomeration of KCl under steam condition may be caused by the molten KOH and K-silicates[127].

$$\mathrm{KCl_{(g)}} + H_2O_{(g)} \rightarrow KOH_{(g)} + \mathrm{HCl_{(g)}} \qquad \text{Equation 2-4}$$

$$2\mathrm{KCl_{(g)}} + \mathrm{nSiO_{2(s)}} + H_2O_{(g)} \rightarrow K_2O \cdot \mathrm{nSiO_{2(l)}} + 2\mathrm{HCl_{(g)}} \quad (n = 1, 2\ and\ 4) \qquad \text{Equation 2-5}$$

The K_2CO_3 is active and can react with SiO_2 even in oxidizing or inert atmosphere[124]. Under the steam condition, these reactions will be significantly accelerated by the presentence of steam, and KOH is formed during process (Equation 2-6)[109].

$$K_2O_{(s,l)} + H_2O_{(g)} \rightarrow 2KOH_{(g)} \qquad \text{Equation 2-6}$$

The impact of steam on agglomeration of wood that doped with K/Na-salts (chloride, carbonate, sulfate and phosphate) are investigated under gasification (50 vol.% steam in N_2) and combustion (5 vol.% O_2 in N_2) in a horizontal tube furnace[129]. The size of agglomerates and amount of alkali silicates are used to evaluate the agglomeration tendency. It is found that the agglomeration of the K/Na-salts-doped wood except K/Na-phosphate-doped wood is promoted under steam gasification. The agglomeration of K/Na-phosphate-doped wood under both atmosphere is caused by the melting of the K/Na-phosphate, while the agglomeration of other K/Na-salts-doped wood under steam gasification is attributed to the formation of alkali silicates. Compared to combustion, the larger agglomerates are formed during steam gasification of K/Na-chloride/carbonate/sulfate-doped wood due to the formation of more alkali silicates with a lower melting temperature. For the K/Na-chloride-doped wood, significantly increased amount of alkali silicates are produced via the interaction of KCl and SiO_2 in steam gasification.

Table 2-6 Influence of steam atmosphere on agglomeration tendency and mechanisms of K/Na salts and K/Na doped wood

K/Na-species	Agglomeration tendency and mechanisms
Alkali-chloride	Increase the formation of alkali silicates by interact with alkali-chloride, thus lower the amount of salts needed to reach defluidization under moist condition[124]
Alkali-carbonate	Faster the formation of alkali silicates and alkali-hydroxide is formed under moist condition[126,128]. Melting temperature is reduced, wettability increased a lot after melting due to the formation of alkali-hydroxides[130,131]
Alkali-sulfate	No defluidization under both dry and moist conditions[126,128].
Alkali-chloride-doped wood	Larger agglomerates and increases the melting and the formation of alkali silicates. The gas-solid reactions is important under steam condition. Coating-induced mechanism is dominate[129].
Alkali-carbonate-doped wood	Larger agglomerates but similar amount of alkali silicates with combustion. Faster formation of agglomerates during steam gasification[129].
Alkali-sulfate-doped wood	Larger agglomerates but similar amount of alkali silicates[129]
Alkali-phosphate-doped wood	Not influenced by steam. Melting-induced mechanism due to melting of partially molten alkali-phosphate[129]

CO_2

The impact of high concentration of CO_2 in the system on the agglomeration are limitedly discussed in the literatures. Anicic *et. al.*[132] found that the reaction reactivity of K_2CO_3 towards silica sand decreases with increasing CO_2 concentration in TGA experiments, because the conversion of K_2CO_3 is less favorable in the presence of CO_2.

2.3.4.3 Melting temperature and viscosity of ash

Oxidizing atmospheres

Agglomeration occurs when a critical layer thickness and viscosity are reached[50]. As is obvious, a low-melting temperature ash, which would result in a high amount of liquid phase in the bed, will promote agglomeration. In addition, it is suggested that the liquid with low viscosity is likely to migrate to the surface of the agglomerates[133,134], and thus easier forming a coating layer on the bed particles. The chemical compositions in ashes can be divided into three categories: network formers, network modifiers and amphoteric according to the network theory of molten slag at high temperature[49]. The network formers (e.g., Si^{4+} and Ti^{4+}), which become the polymers, increase the slag viscosity; the network modifiers (e.g., Na^+, K^+, Mg^{2+}, Ca^{2+} and Fe^{2+}), which destroy the polymers, decrease the slag viscosity; and the amphoteric cation (e.g., Al^{3+} and Fe^{3+}) can play as network formers or network modifiers in different system[135]. An increase in Al^{3+} concentration increases the viscosity of silicate glass at $Al_2O_3/(M_2O+MeO)$ ratio below 1, whilst reduce the viscosity of silicate glass when the $Al_2O_3/(M_2O+MeO)$ ratio higher than 1 (where M could be Na^+, K^+, and Me could be Mg^{2+}, Ca^{2+}). Mostly studies with respect to the ash viscosity are performed based on the coal ashes. It is found that the viscosity of coal ashes is strongly affected by the ash compositions and temperature[136–139].

Reducing atmospheres

The reduction of Fe^{3+} to Fe^{2+} under reducing atmosphere at high temperature results in an decrease in the viscosity of slag[140,141]. As mentioned above, in a system with high contents of alkali and alkane earth metals, Fe^{3+} tends to enhance the three-dimensional structure of the melt and increases the slag viscosity. Fe^{2+} is likely to disrupt the connectivity of network by providing non-bridging oxygen (NBO), thus lowering the slag viscosity[140].

The melting temperature of coal ash under reducing atmosphere is lower than that under oxidizing atmosphere[142–145]. Similar with ash viscosity, the decreasing of sintering temperature of coal ash is related to the states of the iron ion. A part of Fe^{3+} will be converted to Fe^{2+}, which may react with other ash constituents, leading to the formation of the eutectics with low-melting point[146,147]. Wei *et al.*[148] found that a more pronounced decreased is observed for the coal with high Fe content under

reducing atmosphere. However, these studies focus on the coal ashes, which usually contain higher iron content than biomass ashes[149].

The investigations on the melting of biomass ashes under gasification atmosphere are not as extensively as coal ashes. Niu *et al.*[150] investigated the melting tendency of the gasified ash of a mixture of straw, waste carton, plastic and spent mushroom compost, which is papered in an air blown fluidized bed reactor at 800 °C with an equivalence ratio of 0.2, under different gas atmospheres. It is found that the melting tendency of gasified ash under reducing condition (a mixture of 50 vol.% N_2, 30 vol.% CO and 20 vol.% CO_2) is higher than that under oxidizing condition (100% air). In addition to the reduction of Fe^{3+} to Fe^{2+}, the conversion of $CaSO_4$ to CaO and the subsequent formation of low melting eutectics via interaction between CaO with other compounds are considered to be one of the reasons that responsible for the high melting tendency of the mixture under reducing atmosphere.

Steam

The viscosity of ash relates to the polymerization degree and network structure of ash[141,151]. Folkedahl *et al.*[141] reported that for the viscous and glassy slag contains high silica, who is expected to have a three-dimensional network silicate structure, the addition of water vapor could lower its viscosity. It is attributed to the cleavage of Si-O-Si bonds by the water molecules according to the following reaction:

$$-\mathrm{Si}-\mathrm{O}-\mathrm{Si}-\ +H_2O\ \ \rightarrow 2-\mathrm{SiOH} \qquad \text{Equation 2-7}$$

The depolymerization of the melt caused by water could reduce the viscosity of slag at a given temperature. This result agrees what have been found by Cao *et al.*[151]. In addition, the addition of water vapor also influence the structure of Al-O bonds. Cao *et al.*[151] found that the ratio of $[AlO_4]^{5-}$ /$[AlO_4]^{5-}$+$[AlO_6]^{9-}$ in the slag structure decreases with increasing steam concentration, indicating that the presence of water vapor weakens the polymerization degree of the slag, thus decreasing the viscosity of slag.

The impact of steam on the melting of ashes is not widely investigated. Mao *et al.*[152,153] suggested that the addition of water vapor lowered the sintering temperature of coal ash significantly. It is attributed to that the presence of water vapor promotes the formation of low-melting point eutectics by the interaction between K species and bed materials, thus lowering sintering temperature. The impact of high steam concentration on the viscosity and melting of biomass ash is still unclear.

2.4 Countermeasures of agglomeration

Based on the mechanisms of agglomeration and the factors influencing agglomeration discussed above, some effective and applicable countermeasures are put forward to decelerate the agglomeration in combustion and gasification of biomass[18,24,25]. These countermeasures can be categorized into two groups according to their basic mechanisms: reducing the formation of compounds with low-melting point via altering the ash chemistry and improving of hydrodynamics in the bed.

2.4.1 Altering ash chemistry

The agglomeration during fluidized bed combustion and gasification of biomass is primarily attributed to the formation of low-melting point compounds. Therefore, the techniques that avoid or lessen the production of low-melting point compounds by altering ash chemistry, such as utilizing alternative bed materials, applying additives, pretreatment of biomass, and co-combustion with alkali-lean fuels are effective for reducing agglomeration in fluidized bed.

2.4.1.1 Alternative bed materials

The interaction between biomass ash and SiO_2-based bed material is one of main origins of low-melting point eutectics. The replacement of SiO_2-based bed material by alternative bed materials, aluminum (Al), calcium (Ca), magnesium (Mg), and iron (Fe) containing compounds, could retard the agglomeration tendency in fluidized bed.

Aluminum compounds

Al-containing compounds are widely applied as the bed materials to substitute the SiO_2-based bed material in fluidized bed combustion and gasification, such as Al_2O_3[58,71], mullite ($3Al_2O_3{\cdot}2SiO_2$ and $2Al_2O_3{\cdot}SiO_2$)[36], sillimanite (Al_2SiO_5) and Bauxite ($Al(OH)_3$)[61,154,155]. Ghaly *et al.*[71] found that the agglomeration temperature of alumina sand (85-90% Al_2O_3 and 8-10% SiO_2) during wheat straw gasification, which is 920 °C, is significant higher than that of silica sand, which is 800 °C. It is proposed that the agglomeration is caused by the alumina sands are bonded by the sticky molten straw ash[58,71]. Both sillimanite (Al_2SiO_5) and Bauxite ($Al(OH)_3$) could extend the defluidization time during coal combustion compared to silica sand[61,155]. The addition of Al_2O_3 in K_2O-SiO_2 system results in an increased melting temperature. The liquidus temperatures of $K_2O{\cdot}4SiO_2$ and $K_2O{\cdot}Al_2O_3{\cdot}SiO_2$ are around 770 and 990 °C, respectively[58].

Calcium/Magnesium compounds

During biomass combustion and gasification, calcium and magnesium show consistent influence on the agglomeration behaviors due to their similar properties. Ca-containing compounds, such as limestone ($CaCO_3$)[55,88,156,157], dolomite ($CaCO_3{\cdot}MgCO_3$)[55], bone ash (45% CaO, 29% P_2O_3, 8% SiO_2, 5% Fe_2O_3, and rest others)[36] and blast furnace slag (32% CaO, 18% MgO, 34% SiO_2, 12% Al_2O_3)[48],

as well as Mg-containing compounds, such as magnesium oxide (MgO)[158], magnesite ($MgCO_3$)[36,61,78,156], and Olivine ($(MgFe)_2SiO_4$)[74,78,159,160], have been utilized as alternative bed materials in fluidized bed combustion of biomass. The limestone and magnesite are likely to be in the calcined state, lime and magnesium oxide, at the typical operating temperature of fluidized bed combustor and gasifier. When calcite ($CaCO_3$) and magnesite are used as bed materials, the defluidization times are prolonged to 8-12 times of that using silica bed material during coal combustion at 800 °C[156], due to the formation of eutectics with a higher melting point[156].

Iron compounds

Ferric oxide (Fe_2O_3)[20,161] can be used as alternative bed material in fluidized bed combustion. The agglomerates are observed when the mixture of $KNaC_4H_4O_6{\cdot}4H_2O$ and silica sand was heated in a laboratory furnace at 700 °C, whereas no agglomerate are observed during the heating of the mixture of $KNaC_4H_4O_6{\cdot}4H_2O$ and Fe_2O_3 at 900 °C. It is attributed to the formation of high-melting temperature eutectics ($K_2Fe_2O_4$ and $Na_2Fe_2O_4$) through the interaction between Fe_2O_3 and the alkali (K or Na) compounds in biomass ash[161].

2.4.1.2 Additives

Bed additives can be applied to fluidized bed combustion and gasification to reduce or avoid agglomeration. Similar with alternative bed materials, the basic underlying mechanism of influence of bed additives on agglomeration is to prevent the formation of low-melting point compounds by changing the ash chemistry. Generally, the effective additives can be grouped into Al-Si-based, Ca-based, P-based, and S-based additives.

Al-Si-based additives

Kaolin, a clay mineral consisting of alumina silicate ($Al_2Si_2O_5(OH)_4$), is the most common tested Al-Si-based additive[121,162–165]. It is found that the addition of kaolin increases the defluidization temperature of wheat straw from 739 °C to 886 °C[162]. It is attributed to the fact that the released potassium is effectively captured by kaolin via the interaction between kaolin and potassium[163], according to Equation 2-8[164]. The formation of K-Al silicates with a high-melting temperature reduces the agglomeration. In attrition to kaolin, pulverized coal ash[166] is also used as additive due to it high Al and Si content.

$$Al_2O_3 \cdot 2SiO_{2(s)} + 2KCl_{(g)} + H_2O_{(g)} \rightarrow K_2O \cdot Al_2O_3 \cdot 2SiO_{2(s)} + 2\,HCl_{(g)} \qquad \text{Equation 2-8}$$

Ca/Mg-based additives

Ca/Mg-based additives, such as CaO[167], Ca $(NO_3)_2$[167], $CaCO_3$[167,168], $MgCO_3$[89], and marble sludge (95.47% CaO and rest others)[169], are used during fluidized bed combustion/gasification to reduce the agglomeration tendency. Ca-based additives effectively prolong defluidization time due to the formation of high-melting temperature Ca silicates and K-Ca phosphates[168]. Chou *et al*.[167] found that the aqueous-phase $Ca(NO_3)_2$ is more effective than powder-phase CaO on reducing the agglomeration risk in the fluidized bed combustion, which may be attributed to the lager contact area between bed particles and aqueous-phase additives.

P-based additives

Grimm *et al*.[65,170] investigated the influence of P-based additive, H_3PO_4, on agglomeration tendency in bench scale fluidized bed combustion of logging residue and wheat straw. The results reveal that the addition of a certain amount of phosphorus could significantly reduce the formation of volatilized deposits and fine particles, whose mainly composition is KCl, for both fuels. For the fuel contains relatively high fraction of Ca in comparison to K, such as logging residue, the agglomeration necks are mainly composed of Ca-K silicates. The P-based additives will accelerate agglomeration by lowering the Ca/K ratio of the Ca-K silicates, since a part of Ca is associated by P. For the K- and Si-rich wheat straw, increasing amount of potassium presents as K-Ca/Mg phosphates, such as $KMgPO_4$, CaK_2P_2O, and $CaKPO_4$, with addition of P-based additive. The melting temperature of ash is therefore increased, thus reducing the agglomeration tendency. However, an excessive amount of phosphorus additives will promote the formation of alkali-rich phosphates with low-melting point and leads to the risk of bed agglomeration.

S-based additives

S-based additives, S[165] and $(NH_4)_2SO_4$[89], are reported that could decrease agglomeration tendency during combustion of straw and wood pellets, resulting from the formation of K_2SO_4 with high-melting point. Ulusoy[171] studied the influence of a series of S-based additives, including $(NH_4)_2Fe(SO_4)_2$, $NH_4Fe(SO_4)_2$, and $AlNH_4(SO_4)_2$, on agglomeration during wheat straw combustion, and found that these additives effectively mitigate the agglomeration during combustion of straw.

2.4.1.3 Biomass pretreatment

Pretreatment of biomass is a potential way to prolong the defluidization time. Leaching and fractionation are two potential methods reported.

Leaching

Leaching, a pretreatment method by removing water-soluble and ion exchangeable inorganic elements in biomass using water before combustion, is a possible way to slow down the agglomeration tendency[172–175]. It is found that both the ash content and the contents of alkali species

(Na and K), chlorine, and sulfur in washed biomass are much lower than the untreated biomass[176–179]. Said *et al*.[180] suggested that the decrease in ash content of straw could be as high as around 20% after washing. The removal ratios of chlorine and potassium in washed straw reach to about 87% and 50%, respectively. Consequently, the washed straw shows no ash sintering tendency at the temperature in the range of 900 - 1000 ℃, where the untreated straw is strongly sintered. However, leaching largely increases the cost of process, especially on the drying.

Fractionation

Fractionation is a method that splitting of the fuels into two fractions: a "coarse" fraction that particle size is larger than the average grain width size and a "meal" fraction that particle size is smaller than the average grain width size[181]. Although the ash content significantly decreases (up to 50 wt.% for olive residue) with increasing fuel particles size, the potassium content in the ash increases a lot and other elements (Ca, Mg, Al etc.) decreases[174,175,181,182]. Therefore, the fractionation should be used with care. In order to overcome the disadvantages of fractionation, the combination of the two pretreatment techniques, fractionation and leaching, are applied to prolong the defluidization time during biomass combustion.

2.4.1.4 Co-combustion

Co-combust the alkali-rich fuels with an alkali-lean one is an effective way to reduce the agglomeration tendency during biomass combustion. Coal, woody biomass and sewage sludge are suitable co-combustion fuels due to their low potassium content.

Coal

Co-combustion biomass and coal is an effective way to reduce the risk of agglomeration[183–185]. Lin and Dam-Johansen[37,38] found that the defluidization time of straw is largely prolonged when wheat straw is co-combusted with a fraction of 20 - 30 wt.% coal at temperature below 900 ℃. The coal ash, which is mainly consisted of silicon, aluminum and calcium, has a much higher melting point than the straw ash, which is mainly composed of silicon and potassium. The K-Al silicates are formed by the interaction of coal ash and straw ash during co-combustion process, and thereby reducing the agglomeration tendency.

Woody biomass

Compared to the herbaceous and agricultural biomass (e.g., straw), woody biomass (e.g., bark) usually has lower ash yield and potassium content in the ash[3]. Therefore, some woody biomass is co-combusted with herbaceous biomass to reduce the agglomeration risk[66,76,186,187]. Nordgren *et al.* [186] found that the defluidization time of co-combustion of a mixture of straw and woody biomass (bark and wood) is longer than that of pure straw combustion. Two reasons can explain this tendency: a)

the ash forming elements of straw (K, Si, Cl etc.) are diluted by the woody biomass; b) the change of ash composition (decrease in K, Si and increase in Ca) leads to a higher melting point of ash.

Sewage sludge

The agglomeration tendency is significantly reduced when the sewage sludge is added during potassium-rich fuel combustion[123,188,189]. The high content of P and S in the sewage sludge causes the ash of mixture of sewage sludge and straw is dominated by phosphates and sulfates[188]. In addition, increased amounts of hematite and aluminosilicates are formed during co-combustion of sewage sludge and straw compared to pure straw combustion due to the high content of aluminum, calcium, and iron in the sewage sludge[189]. Therefore, the ash with high-melting temperature, which is dominated by alkali phosphates (e.g., $Ca_9MgK(PO_4)_7$) and potassium aluminosilicates (e.g., $KAlSi_2O_6$ and $KAlSi_3O_8$)[123], is formed during co-combustion of sewage sludge and straw, thus reducing the agglomeration tendency.

2.4.2 Improving fluidization quality in the bed

2.4.2.1 Controlling of operational conditions

The fluidization quality in bed can be improved by raising the ratio of superficial gas velocity to minimum fluidization velocity (U_g/U_{mf}), such as selecting small bed particles[38] and applying high fluidizing gas velocity[190]. However, these methods will result in a higher bed particles entrainment during operation[190].

2.4.2.2 Pulsed fluidized bed

In past decades, the pulsed flow gas, as an external assistant, has been reported that could improve the fluidization quality of the Geldart Group A/B/C particles[191,192]. Pulsed fluidization is a method that using an on-and-off fluidizing gas to fluidize the bed particles. The pulsed flow fluidization has shown the potential for enhancing the heating transfer in fluidized bed[193–196], accelerating the drying of biomass and pharmaceutical products[197–199], improving the mixing of particles[200], and reducing the agglomerates size of nanoparticles[201]. The influences of some key parameters of pulsation, such as frequency, duty cycle, and flow rate, are extensively discussed.

Frequency of pulsation is one of most extensively investigated parameters for the pulsed flow gas, and its effects on the hydrodynamics in the fluidized bed, mixing of particles, heating transfer and drying rate has been reported. A series of studies investigated the effects of pulsed flow on the hydrodynamics characteristics in the bed[202–205], covering the minimum fluidization velocity (U_{mf}), bubble sizes, bubble velocity, and bed expansion. Pulsed fluidized beds are frequently reported in reducing the minimum fluidization velocity (U_{mf}) of particles, especially for the nanoparticles, which

are difficult to fluidize[204,206,207]. The bubble properties, such as size and velocity, in the bed are used as the indicators of bed behavior[204]. The bed expansion may be used as an indicator of particles displacement in the fluidized bed[193]. The minimum fluidization velocity decreases with the increasing pulsation frequency[208]. It is suggested that the minimum fluidization velocity of Group B particles can be reduced by up to a third of the minimum fluidization velocity required in continuous flow at a frequency of 10 Hz[204]. Generally, the reduction of bubble size by imposing pulsed flow in the conventional fluidized bed is closely related to the pulsation frequency[204,207]. The bubble size decreases with increasing pulsation frequency, and it may be attributed to the reduction of air amount that enters in each cycle[204]. It is found that the size of bubbles formed at a frequency of 10 Hz is same as the bubbles formed in the continuous flow at the halfway height point of the bed, but bubbles are smaller at positions above this[204], indicating that the bubbles formed under continuous flow are easily to coalesce at greater distance from the distributor, while are likely to remain scattered and coalesce less under the pulsed fluidization[204,207]. Consistent with the bubble size, the bubble velocity is reduced at high pulsation frequency[204]. It has been found both in experimental work and numerical simulation that increasing particles displacement is found at low pulsation frequencies[204,209]. Bizhaem & Tabrizi[204] suggests that the great particle displacement is related to the high pressure build up during "OFF" period. Zhang &Koksal[193] attributes the larger bed expansion at lower frequencies to the larger amount of gas that goes into the bed during each "ON" period and the greater extent bed collapses during the longer "OFF" periods. Generally, the fluidization quality of the bed particles can be improved by increasing the pulsation frequency[204].

Hadi *et al.*[200] investigate the effect of the pulsation on the mixing of the particles with a wide particle size distribution (d_{p10} =42 μm and d_{p90} =650 μm) at a pulsation frequency in the range of 0.5 - 5 Hz. The static bed height is 200 mm. It is found that the introducing of pulsed flow could improve the mixing of the particles, and the optimal mixing behaviors is observed at the pulsation frequency of 3 Hz due to the formation of the maximum bubble size and highest bubble frequency.

The influence of pulsation frequency on heat transfer and drying process are also investigated. Jia *et al.*[194,195,197] studied the heat transfer coefficient and drying rate of various biomass particles in a pulsed fluidized bed at a pulsation frequency in the range of 0.5 Hz - 6 Hz. They suggested that the heat transfer coefficient and drying rate are strongly affected the pulsation frequency. It is found that the optimum frequency are close to the natural frequency of the system (f_N), which is calculated according to the theory proposed by Hao and Bi[205]:

$$f_N = \frac{1}{2\pi}\sqrt{\frac{g}{H_{mf}}} \qquad \text{Equation 2-9}$$

where H_{mf} (m) is the static bed height. For a bed with a static bed height of 150 mm, the natural frequency is 1.28 Hz. They attribute the good performance of the frequency closed to natural frequency to the occurrence of resonance effect could enhance the motion of particles and mass transfer. Although a better fluidization is achieved at a higher pulsation frequency, the optimum performance of a pulsed flow for biomass drying and particles mixing in fluidized bed is usually observed at a frequency in the range of 1 to 3 Hz. Jia *et al.*[210] proposed that the fluidized bed appears only will be fluidized intermittently at the frequencies below 3 Hz, resulting in the formation of slugs above the distributer and formation of the gas channels in the bed. The larger bubbles instead of gas channel are formed at the frequency of 3 Hz, and the bubble sizes will be reduced by increasing pulsation frequency. At an even higher frequency, the behaviors of the pulsed fluidized bed are similar to a conventional one.

The effect of flow rate on the biomass drying and heat transfer coefficient are less reported in the literatures. It is found that an increase in gas flow rate results in a higher heat transfer coefficient and drying rate[197,210] due to the better fluidization at a high total flow rate.

The influence of pulsation duty cycle, which is defined as the time of "flow-ON" period divided by the "flow-OFF" period, on heat transfer has been investigated. Kobayashi *et al.*[211] investigated the heat transfer of the glass beads with a static bed height of 300 mm. They found that the highest heat transfer coefficient for the glass beads with an average diameter of 138 μm is observed at a pulsation duty cycle of 50/50 (a combination of "ON" and "OFF" period of 0.5s and 0.5 s), while for the glass beads with an average diameter of 301 μm, the optimum pulsation duty cycle is 25/75 (a combination of "ON" and "OFF" period of 0.25 s and 0.75 s). Nishimura *et al.*[212] studied the heat transfer of glass beads bed with a static bed height of 700 mm. For the glass beads with an average diameter of 90 and 340 μm, the optimum heat transfer is observed at the combination of a "OFF" period of 2 s and 3 s and an "ON" period of 1 s, namely the duty cycle of 33/66 and 25/75, respectively. It is attributed to the formation of larger bubbles at longer "OFF" period. In addition, it is addressed the increasing pressure build-up at longer "OFF" period will result in a higher instantaneous gas velocity. The instantaneous gas velocity is reduced by increasing duty cycle, since the same amount of gas enters in the bed over a longer "ON" period. However, the excessive increase in "OFF" period brings a disadvantage for heat transfer, since the bed will be in a static condition in the latter stage of "OFF" period. Jia *et al.*[194] investigated the effect of duty cycle on heat transfer of Douglas fir sawdust in the range of 10/90 to 90/10 at various frequency with different gas velocity. It is found that the optimum duty cycle are related to the pulsation frequency and gas velocity. By decreasing the pulsation frequency or increasing the gas velocity, the optimum duty cycle is increased. This may be attributed to the air amount introducing into the bed are together decided by the pulsation frequency, the gas flow rate and duty cycle.

The pulsed fluidized bed reactor may be a potential countermeasure for mitigating agglomeration tendency during biomass combustion and gasification. The potential of pulsed flow on tackling

defluidization of Group B particles has been proved by the discrete element method (DEM) simulation[213]. However, the effect of pulsed flow on the agglomeration is not clearly.

2.5 Summary

Biomass is a renewable energy resource and is considered as a substitute for fossil fuels. In Denmark, wheat straw is one of the main biomass resources. However, the utilization of wheat straw in fluidized bed combustion and gasification is challenging due to the high content of potassium and silicon in wheat straw. Agglomeration, which influences the operation of a fluidized bed reactor, can be observed even at temperature below 700 °C in a straw fired fluidized bed. Although the agglomeration behaviors in fluidized bed combustion of wheat straw has been investigated extensively, the agglomeration tendency and mechanisms during wheat straw gasification are limitedly studied. A reducing atmosphere and a high concentration of steam could promote the agglomeration of straw ashes, due to their influences on the ash chemistry and physical properties. However, the agglomeration behaviors during continuous wheat straw gasification is still unclear, especially the influences of gasification agents and equivalence ratio on agglomeration behaviors.

Agglomeration tendency is closely related to biomass composition. Different biomass types result in different agglomeration tendency. The contents of other inorganic elements, such as Si, S, P, and Cl, in biomass also have different effects on agglomeration during combustion. The difference in the agglomeration temperatures of an S-rich but Si-lean fuel, Lucerne, under combustion and gasification atmospheres is more pronounced compared to other fuel. The agglomeration behaviors during gasification of different types of biomass are unclear.

A series of countermeasures have been evaluated based on the mechanism of reducing the formation of compounds with low-melting point via utilizing alternative bed materials, applying additives, pretreatment of biomass, and co-combustion with alkali-lean fuels. Most of these countermeasures lead to an additional operation cost. An effective and economic countermeasure for the agglomeration is lacking. The imposing of pulsed flow in the fluidized bed improves the fluidization quality in the bed, indicating that pulsed fluidized bed may be a potential countermeasure for mitigating the agglomeration in fluidized bed combustion and gasification.

Reference

(1) Vassilev, S. V.; Baxter, D.; Andersen, L. K.; Vassileva, C. G. An Overview of the Chemical Composition of Biomass. *Fuel* **2010**, *89* (5), 913–933.

(2) Vassilev, S. V.; Baxter, D.; Andersen, L. K.; Vassileva, C. G.; Morgan, T. J. An Overview of the Organic and Inorganic Phase Composition of Biomass. *Fuel* **2012**, *94*, 1–33.

(3) Vassilev, S. V.; Vassileva, C. G.; Song, Y. C.; Li, W. Y.; Feng, J. Ash Contents and Ash-Forming Elements of Biomass and Their Significance for Solid Biofuel Combustion. *Fuel* **2017**, *208*, 377–409.

(4) Bridgwater, A. V.; Peacocke, G. V. C. Fast Pyrolysis Processes for Biomass. *Renew. Sustain. energy Rev.* **2000**, *4* (1), 1–73.

(5) Bridgwater, A. V. Renewable Fuels and Chemicals by Thermal Processing of Biomass. *Chem. Eng. J.* **2003**, *91* (2–3), 87–102.

(6) Zhang, L.; Xu, C. (Charles); Champagne, P. Overview of Recent Advances in Thermo-Chemical Conversion of Biomass. *Energy Convers. Manag.* **2010**, *51* (5), 969–982.

(7) McKendry, P. Energy Production from Biomass (Part 2): Conversion Technologies. *Bioresour. Technol.* **2002**, *83* (1), 47–54.

(8) Wang, Y.; Bell, D. A. Competition between H_2O and CO_2 during the Gasification of Powder River Basin Coal. *Fuel* **2017**, *187*, 94–102.

(9) Dong, J.; Nzihou, A.; Chi, Y.; Weiss-Hortala, E.; Ni, M.; Lyczko, N.; Tang, Y.; Ducousso, M. Hydrogen-Rich Gas Production from Steam Gasification of Bio-Char in the Presence of CaO. *Waste and Biomass Valorization* **2017**, *8* (8), 2735–2746.

(10) Mauerhofer, A. M.; Fuchs, J.; Müller, S.; Benedikt, F.; Schmid, J. C.; Hofbauer, H. CO_2 Gasification in a Dual Fluidized Bed Reactor System: Impact on the Product Gas Composition. *Fuel* **2019**, *253*, 1605–1616.

(11) Campoy, M.; Gómez-Barea, A.; Vidal, F. B.; Ollero, P. Air-Steam Gasification of Biomass in a Fluidised Bed: Process Optimisation by Enriched Air. *Fuel Process. Technol.* **2009**, *90* (5), 677–685.

(12) Khan, A. A.; de Jong, W.; Jansens, P. J.; Spliethoff, H. Biomass Combustion in Fluidized Bed Boilers: Potential Problems and Remedies. *Fuel Process. Technol.* **2009**, *90* (1), 21–50.

(13) Nussbaumer, T. Combustion and Co-Combustion of Biomass: Fundamentals, Technologies, and Primary Measures for Emission Reduction. *Energy & Fuels* **2003**, *17* (6), 1510–1521.

(14) Wiltsee, G. A. J.; McGowin, C. R.; Hughes, E. E. Biomass Combustion Technologies for Power Generation; National Renewable Energy Lab., Golden, CO: Burlington, Vermont, United States, 1993.

(15) Yang, W.-C. *Handbook of Fluidization and Fluid-Particles Systems*; CRC Press, 2003.

(16) Koornneef, J.; Junginger, M.; Faaij, A. Development of Fluidized Bed Combustion-An Overview of Trends, Performance and Cost. *Prog. Energy Combust. Sci.* **2007**, *33* (1), 19–55.

(17) Romeo, L. M.; Díez, L. I.; Guedea, I.; Bolea, I.; Lupiáñez, C.; González, A.; Pallarés, J.; Teruel, E. Design and Operation Assessment of an Oxyfuel Fluidized Bed Combustor. *Exp. Therm. Fluid Sci.* **2011**, *35* (3), 477–484.

(18) Niu, Y.; Tan, H. Ash-Related Issues during Biomass Combustion : Alkali-Induced Slagging , Silicate Melt-Induced Slagging (Ash Fusion), Agglomeration , Corrosion , Ash Utilization , and Related Countermeasures. *Prog. Energy Combust. Sci.* **2016**, *52*, 1–61.

(19) Lin, W.; Dam-Johansen, K.; Frandsen, F. Agglomeration in Bio-Fuel Fired Fluidized Bed Combustors. *Chem. Eng. J.* **2003**, *96* (1–3), 171–185.

(20) Grubor, B.D.; Oka, S.N.; Ilic, M.S.; Dakic, D.V.; Arsic, B. .; Grubor, B. D.; Oka, S. N.; Ilic, M. S.; Dakic, D. V.; Arsic, B. T. Biomass FBC Combustion - Bed Agglomeration Problems. In *Proceedings of the 13th International Conference on Fluidized Bed Combustion*; American Society of Mechanical Engineers: United States, 1995; Vol. 1, pp 515–522.

(21) Scala, F.; Chirone, R.; Consiglio, C.; Tecchio, P. V.; July, R. V; Re, V.; Recei, M.; October, V. Characterization and Early Detection of Bed Agglomeration during the Fluidized Bed Combustion of Olive Husk. *Energy & Fuels* **2006**, *20* (10), 120–132.

(22) Michel, R.; Kaknics, J.; De Bilbao, E.; Poirier, J. The Mechanism of Agglomeration of the Refractory Materials in a Fluidized-Bed Reactor. *Ceram. Int.* **2016**, *42* (2), 2570–2581.

(23) Balland, M.; Froment, K.; Ratel, G.; Valin, S.; Roussely, J.; Michel, R.; Poirier, J.; Kara, Y.; Galnares, A. Biomass Ash Fluidised-Bed Agglomeration: Hydrodynamic Investigations. *Waste and Biomass Valorization* **2017**, *8* (8), 2823–2841.

(24) Scala, F. Particle Agglomeration during Fluidized Bed Combustion: Mechanisms, Early Detection and Possible Countermeasures. *Fuel Process. Technol.* **2018**, *171*, 31–38.

(25) Bartels, M.; Lin, W.; Nijenhuis, J.; Kapteijn, F.; van Ommen, J. R. Agglomeration in Fluidized Beds at High Temperatures: Mechanisms, Detection and Prevention. *Prog. Energy Combust. Sci.* **2008**, *34* (5), 633–666.

(26) Morris, J. D.; Sheraz, S.; Chilton, S.; Nimmo, W. Mechanisms and Mitigation of Agglomeration during Fluidize Bed Combustion of Biomass : A Review. *Fuel* **2018**, *230*, 452–473.

(27) Mettanant, V.; Basu, P.; Butler, J. Agglomeration of Biomass Fired Fluidized Bed Gasifier and Combustor. *Can. J. Chem. Eng.* **2009**, *87* (5), 656–684.

(28) Billen, P.; Creemers, B.; Costa, J.; Van Caneghem, J.; Vandecasteele, C. Coating and Melt Induced Agglomeration in a Poultry Litter Fired Fluidized Bed Combustor. *Biomass and Bioenergy* **2014**, *69*, 71–79.

(29) Visser, H. J. M.; Hofmans, H.; Huijnen, H.; Kastelein, R.; Kiel, J. H. A. Biomass Ash - Bed Material Interactions Leading to Agglomeration in Fluidised Bed Combustion and Gasification.

Prog. Thermochem. Biomass Convers. **2008**, 272–286.

(30) Öhman, M.; Pommer, L.; Nordin, A. Bed Agglomeration Characteristics and Mechanisms during Gasification and Combustion of Biomass Fuels. *Energy & Fuels* **2005**, *19* (4), 1742–1748.

(31) Mac an Bhaird, S. T.; Walsh, E.; Hemmingway, P.; Maglinao, A. L.; Capareda, S. C.; McDonnell, K. P. Analysis of Bed Agglomeration during Gasification of Wheat Straw in a Bubbling Fluidised Bed Gasifier Using Mullite as Bed Material. *Powder Technol.* **2014**, *254*, 448–459.

(32) Visser, H. J. M. H. J. M. The Influence of Fuel Composition on Agglomeration Behaviour in Fluidised-Bed Combustion. *ECN Rep. ECN-C–04-054* **2004**.

(33) Nisamaneenate, J.; Atong, D.; Seemen, A.; Sricharoenchaikul, V. Mitigating Bed Agglomeration in a Fluidized Bed Gasifier Operating on Rice Straw. *Energy Reports* **2020**, *6*, 275–285.

(34) Visser, H. J. M. M.; van Lith, S. C.; Kiel, J. H. A. a. Biomass Ash-Bed Material Interactions Leading to Agglomeration in FBC. *J. Energy Resour. Technol.* **2008**, *130* (1), 1–6.

(35) Gatternig, B.; Karl, J. Investigations on the Mechanisms of Ash-Induced Agglomeration in Fluidized-Bed Combustion of Biomass. *Energy & Fuels* **2015**, *29*, 931–941.

(36) Olofsson, G. G.; Ye, Z.; Bjerle, I.; Andersson, A. Bed Agglomeration Problems in Fluidized-Bed Biomass Combustion. *Ind. Eng. Chem. Res.* **2002**, *41* (12), 2888–2894.

(37) Lin, W.; Jensen, A. D.; Johnsson, J. E.; Dam-Johansen, K. Combustion of Biomass in Fluidized Beds: Problems and Some Solutions Based on Danish Experiences. In *Proceedings of the 17th International Conference on Fluidized Bed Combustion*; American Society of Mechanical Engineers: Jacksonville, Florida USA, 2003; pp 945–953.

(38) Lin, W.; Dam-Johansen, K. Agglomeration in Fluidized Bed Combustion of Biomass--Mechanisms and Co-Firing with Coal. In *Proceedings of the 15h International Conference on Fluidized Bed Combustion*; American Society of Mechanical Engineers: Savannah, Georgia, 1999; pp 1188–1191.

(39) Lin, W.; Dam-Johansen, K. Modelling of Agglomeration in Straw Fired Fluidized Bed Combustors. In *Proceedings of the 16th International Conference on Fluidized Bed Combustion*; American Society of Mechanical Engineers: United States, 2001; pp 1–13.

(40) Lin, W.; Krusholm, G.; Dam-Johansen, K.; Musahl, E.; Bank, L. Agglomeration Phenomena in Fluidized Bed Combustion of Straw. In *Proceedings of the 14h International Conference on Fluidized Bed Combustion*; American Society of Mechanical Engineers: Canada, 1997; Vol. 2, pp 831–837.

(41) Salatino, P.; Scala, F.; Chirone, R. Fluidized-Bed Combustion of A Biomass Char: The Influence of Carbon Attrition and Fines Postcombustion on Fixed Carbon Conversion. In *Proceedings of Twenty-Seventh Symposium (International) on Combustion*; United States, 1998; pp 3103–3110.

(42) Scala, F.; Salatino, P.; Chirone, R. Fluidized Bed Combustion of a Biomass Char (Robinia Pseudoacacia). *Energy & Fuels* **2000**, *14* (4), 781–790.

(43) Chirone, R.; Salatino, P.; Scala, F. The Relevance of Attrition to The Fate of Ashes During Fluidized-Bed Combustion of A Biomass. *Proc. Combust. Inst.* **2000**, *28*, 2279–2286.

(44) Scala, F.; Chirone, R.; Salatino, P. The Influence of Fine Char Particles Burnout on Bed Agglomeration during the Fluidized Bed Combustion of a Biomass Fuel. *Fuel Process. Technol.* **2003**, *84* (1–3), 229–241.

(45) Chirone, R.; Salatino, P.; Scala, F.; Solimene, R.; Urciuolo, M. Fluidized Bed Combustion of Pelletized Biomass and Waste-Derived Fuels. *Combust. Flame* **2008**, *155* (1–2), 21–36.

(46) Brus, E.; Öhman, M.; Nordin, A. Mechanisms of Bed Agglomeration during Fluidized-Bed Combustion of Biomass Fuels. *Energy & Fuels* **2005**, *19* (3), 825–832.

(47) He, H.; Bostro, D.; Marcus, O. Time Dependence of Bed Particle Layer Formation in Fluidized Quartz Bed Combustion of Wood-Derived Fuels. *Energy & Fuels* **2014**, *28*, 3841–3848.

(48) Brus, E.; Öhman, M.; Nordin, A.; Boström, D.; Hedman, H.; Eklund, A. Bed Agglomeration Characteristics of Biomass Fuels Using Blast-Furnace Slag as Bed Material. *Energy & Fuels* **2004**, *18* (4), 1187–1193.

(49) Vargas, S.; Frandsen, F. J.; Dam-Johansen, K. Rheological Properties of High-Temperature Melts of Coal Ashes and Other Silicates. *Prog. Energy Combust. Sci.* **2001**, *27* (3), 237–429.

(50) Öhman, M.; Nordin, A.; Skrifvars, B. J.; Backman, R.; Hupa, M. Bed Agglomeration Characteristics during Fluidized Bed Combustion of Biomass Fuels. *Energy & Fuels* **2000**, *14* (1), 169–178.

(51) Chaivatamaset, P.; Tia, S. The Characteristics of Bed Agglomeration during Fluidized Bed Combustion of Eucalyptus Bark. *Appl. Therm. Eng.* **2015**, *75*, 1134–1146.

(52) Park, D. Estimation of Temperature Difference between Char Particles and the Fluidized Bed in Char Combustion. *Fuel* **1989**, *68* (10), 1320–1324.

(53) Senior, C. L.; Srinivasachar, S. Viscosity of Ash Particles in Combustion Systems for Prediction of Particle Sticking. *Energy & Fuels* **1995**, *9* (2), 277–283.

(54) Chirone, R.; Miccio, F.; Scala, F. Mechanism and Prediction of Bed Agglomeration during Fluidized Bed Combustion of a Biomass Fuel: Effect of the Reactor Scale. *Chem. Eng. J.* **2006**, *123* (3), 71–80.

(55) Resjdues, C. Agglomeration of Turkish Lignites in Fluidised-Bed Combustion. *Jouof Inst. Energy* **1989**, *March*, 56–61.

(56) Hupa, M. Ash-Related Issues in Fluidized-Bed Combustion of Biomasses : Recent Research Highlights. *Energy & Fuels* **2012**, *26*, 4–14.

(57) Ghaly, A. E.; Ergüdenler, A.; Laufer, E. Study of Agglomeration Characteristics of Silica

Sand-Straw Ash Mixtures Using Scanning Electronic Microscopy and Energy Dispersion X-Ray Techniques. *Bioresour. Technol.* **1994**, *48* (2), 127–134.

(58) Ghaly, A. E.; Ergüdenler, A.; Laufer, E. Agglomeration Characteristics of Alumina Sand-Straw Ash Mixtures at Elevated Temperatures. *Biomass and Bioenergy* **1993**, *5* (6), 467–480.

(59) van der Drift, A.; Olsen, A. Conversion of Biomass, Prediction and Solution Methods for Ash Agglomeration and Related Problems. *ECN (Energy Res. Cent. Netherlands) Rep. ECN-C–99-090* **1999**.

(60) Olofsson, G.; Ye, Z.; Bjerle, I.; Andersson, A. Bed Agglomeration Problems in Fluidized-Bed Biomass Combustion. *Ind. Eng. Chem. Res.* **2002**, *41*, 2888–2894.

(61) Vuthaluru, H. B.; Zhang, D. K. Remediation of Ash Problems in Fluidized-Bed Combustors. *Fuel* **2001**, *80* (4), 583–598.

(62) Liu, Z.; Peng, T.; Lin, C. Impact of CaO and $CaCO_3$ Addition on Agglomeration / Defluidization and Heavy Metal Emission during Waste Combustion in Fluidized-Bed. *Fuel Process. Technol.* **2014**, *118*, 171–179.

(63) Lin, C.; Kuo, J.; Wey, M.; Chang, S.; Wang, K. Inhibition and Promotion : The Effect of Earth Alkali Metals and Operating Temperature on Particle Agglomeration/Defluidization during Incineration in Fluidized Bed. *Powder Technol.* **2009**, *189* (1), 57–63.

(64) Scala, F.; Chirone, R. An SEM / EDX Study of Bed Agglomerates Formed during Fluidized Bed Combustion of Three Biomass Fuels. *Biomass and Bioenergy* **2008**, *32*, 252–266.

(65) Grimm, A.; Skoglund, N.; Boström, D.; Öhman, M.; Bostr, D.; Ohman, M.; Boström, D.; Öhman, M.; Bostr, D.; Ohman, M. Bed Agglomeration Characteristics in Fluidized Quartz Bed Combustion of Phosphorus-Rich Biomass Fuels. *Energy & Fuels* **2011**, *25* (3), 937–947.

(66) Piotrowska, P.; Grimm, A.; Skoglund, N.; Boman, C.; Öhman, M.; Zevenhoven, M.; Boström, D.; Hupa, M. Fluidized-Bed Combustion of Mixtures of Rapeseed Cake and Bark: The Resulting Bed Agglomeration Characteristics. *Energy & Fuels* **2012**, *26* (4), 2028–2037.

(67) Boström, D.; Eriksson, G.; Boman, C.; Öhman, M. Ash Transformations in Fluidized-Bed Combustion of Rapeseed Meal. *Energy & Fuels* **2009**, *23*, 2700–2706.

(68) Yang, T.; Kai, X.; Sun, Y.; He, Y.; Li, R. The Effect of Coal Sulfur on the Behavior of Alkali Metals during Co-Firing Biomass and Coal. *Fuel* **2011**, *90* (7), 2454–2460.

(69) Varol, M.; Atimtay, A. T. Bioresource Technology Effect of Biomass-Sulfur Interaction on Ash Composition and Agglomeration for the Co-Combustion of High-Sulfur Lignite Coals and Olive Cake in a Circulating Fluidized Bed Combustor. *Bioresour. Technol.* **2015**, *198*, 325–331.

(70) Yerushalmi, J.; Kolodney, M.; Graff, R. A.; Squires, A. M.; Harvey, R. D. Agglomeration of Ash in Fluidized Beds Gasifying Coal: The Godel Phenomenon. *Science (80-.).* **1975**, *187* (4177), 646–648.

(71) Ergudenler, A.; Ghaly, A. E. Agglomeration of Alumina Sand in a Fluidized Bed Straw Gasifier at Elevated Temperatures. *Bioresour. Technol.* **1993**, *43* (3), 259–268.

(72) Alauddin, Z. A. B. Z.; Lahijani, P.; Mohammadi, M.; Mohamed, A. R. Gasification of Lignocellulosic Biomass in Fluidized Beds for Renewable Energy Development: A Review. *Renew. Sustain. Energy Rev.* **2010**, *14*, 2852–2862.

(73) Lin, C. L.; Wey, M. Y. The Effect of Mineral Compositions of Waste and Operating Conditions on Particle Agglomeration/Defluidization during Incineration. *Fuel* **2004**, *83* (17–18), 2335–2343.

(74) Fryda, L. E.; Panopoulos, K. D.; Kakaras, E. Agglomeration in Fluidised Bed Gasification of Biomass. *Powder Technol.* **2008**, *181* (3), 307–320.

(75) Seemen, A.; Atong, D.; Sricharoenchaikul, V. Effect of Silica and Alumina Ratio on Bed Agglomeration during Fluidized Bed Gasification of Rice Straw. *Proc. - 2018 2nd Int. Conf. Green Energy Appl. ICGEA 2018* **2018**, 268–272.

(76) Kittivech, T.; Fukuda, S. Investigating Agglomeration Tendency of Co-Gasification between High Alkali Biomass and Woody Biomass in a Bubbling Fluidized Bed System. *Energies* **2020**, *13* (56), 1–15.

(77) Process, C.; Hellas, T.; Plants, T. Agglomeration Problems During Cardoon Fluidized Bed Gasification. *Therm. Sci.* **2014**, *18* (2), 645–656.

(78) Liliedahl, T.; Sjöström, K.; Engvall, K.; Rosén, C. Defluidisation of Fluidised Beds during Gasification of Biomass. *Biomass and Bioenergy* **2011**, *35* (SUPPL. 1), 3–10.

(79) Zevenhoven-Onderwater, M.; Backman, R.; Skrifvars, B. J.; Hupa, M.; Liliendahl, T.; Rosén, C.; Sjöström, K.; Engvall, K.; Hallgren, A. The Ash Chemistry in Fluidised Bed Gasification of Biomass Fuels. Part I: Predicting the Chemistry of Melting Ashes and Ash-Bed Material Interaction. *Fuel* **2001**, *80* (10), 1489–1502.

(80) Zevenhoven-Onderwater, M.; Backman, R.; Skrifvars, B. J.; Hupa, M. The Ash Chemistry in Fluidised Bed Gasification of Biomass Fuels. Part II: Ash Behaviour Prediction versus Bench Scale Agglomeration Tests. *Fuel* **2001**, *80* (10), 1503–1512.

(81) Ergudenler, A.; Ghaly, A. E. Agglomeration of Silica Sand in a Fluidized Bed Gasifier Operating on Wheat Straw. *Biomass and Bioenergy* **1993**, *4* (2), 135–147.

(82) Kittivech, T.; Fukuda, S. Effect of Bed Material on Bed Agglomeration for Palm Empty Fruit Bunch (EFB) Gasification in a Bubbling Fluidised Bed System. *Energies* **2019**, *12*, 4336–4352.

(83) George, J.; Arun, P.; Muraleedharan, C. Experimental Investigation on Co-Gasification of Coffee Husk and Sawdust in a Bubbling Fluidised Bed Gasifier. *J. Energy Inst.* **2019**, *92* (6), 1977–1986.

(84) Zhang, H.; Hao, Z.; Li, J.; Yang, X.; Wang, Z.; Liu, Z.; Huang, J.; Zhang, Y.; Fang, Y. Effect of Coal Ash Additive on Potassium Fixation and Melting Behaviors of the Mixture under Simulated Biomass Gasification Condition. *Renew. Energy* **2021**, *168*, 806–814.

(85) Parthasarathy, P.; Narayanan, K. S. Hydrogen Production from Steam Gasification of Biomass: Influence of Process Parameters on Hydrogen Yield - A Review. *Renew. Energy* **2014**, *66*, 570–579.

(86) Meng, F.; Ma, Q.; Wang, H.; Liu, Y.; Wang, D. Effect of Gasifying Agents on Sawdust Gasification in a Novel Pilot Scale Bubbling Fluidized Bed System. *Fuel* **2019**, *249* (March), 112–118.

(87) James, A. K.; Helle, S. S.; Thring, R. W.; Rutherford, P. M.; Masnadi, M. S. Investigation of Air and Air-Steam Gasification of High Carbon Wood Ash in a Fluidized Bed Reactor. *Energy Environ. Res.* **2014**, *4* (1).

(88) Abra, M. G.; Ordin, A. N.; Iliedahl, T. L.; Ao, A. N. R. Experimental Determination of Bed Agglomeration Tendencies of Some Common Agricultural Residues in Fluidized Bed Combustion and Gasification. *Biomass and Bioenergy* **1998**, *15* (2), 163–169.

(89) Aničić, B. Agglomeration Mechanisms during Fluidized Bed Combustion of Biomass, Technical University of Denmark, 2018.

(90) Ma, T.; Fan, C.; Hao, L.; Li, S.; Song, W.; Lin, W. Biomass-Ash-Induced Agglomeration in a Fluidized Bed. Part 1: Experimental Study on the Effects of a Gas Atmosphere. *Energy & Fuels* **2016**, *30* (8), 6395–6404.

(91) Vassilev, S. V.; Baxter, D.; Andersen, L. K.; Vassileva, C. G. An Overview of the Composition and Application of Biomass Ash. Part 1. Phase-Mineral and Chemical Composition and Classification. *Fuel* **2013**, *105*, 40–76.

(92) Johansen, J. M.; Jakobsen, J. G.; Frandsen, F. J.; Glarborg, P. Release of K, Cl, and S during Pyrolysis and Combustion of High-Chlorine Biomass. *Energy & Fuels* **2011**, *25* (11), 4961–4971.

(93) Frandsen, F. J.; van Lith, S. C.; Korbee, R.; Yrjas, P.; Backman, R.; Obernberger, I.; Brunner, T.; Jöller, M. Quantification of the Release of Inorganic Elements from Biofuels. *Fuel Process. Technol.* **2007**, *88* (11–12), 1118–1128.

(94) van Lith, S. C.; Alonso-Ramirez, V.; Jensen, P. A.; Frandsen, F. J.; Glarborg, P. Release to the Gas Phase of Inorganic Elements during Wood Combustion. Part 1: Development and Evaluation of Quantification Methods. *Energy & Fuels* **2006**, *20* (3), 964–978.

(95) Wu, H.; Castro, M.; Jensen, P. A.; Frandsen, F. J.; Glarborg, P.; Dam-Johansen, K.; Røkke, M.; Lundtorp, K. Release and Transformation of Inorganic Elements in Combustion of a High-Phosphorus Fuel. *Energy & Fuels* **2011**, *25* (7), 2874–2886.

(96) Khalil, R. A.; Seljeskog, M.; Hustad, J. E. Sulfur Abatement in Pyrolysis of Straw Pellets. *Energy & Fuels* **2008**, *22* (4), 2789–2795.

(97) Tortosa Masiá, A. A.; Buhre, B. J. P.; Gupta, R. P.; Wall, T. F. Characterising Ash of Biomass and Waste. *Fuel Process. Technol.* **2007**, *88* (11–12), 1071–1081.

(98) Wang, X.; Si, J.; Tan, H.; Ma, L.; Pourkashanian, M.; Xu, T. Nitrogen, Sulfur, and Chlorine

Transformations during the Pyrolysis of Straw. *Energy & Fuels* **2010**, *24* (9), 5215–5221.

(99) Werkelin, J.; Skrifvars, B. J.; Zevenhoven, M.; Holmbom, B.; Hupa, M. Chemical Forms of Ash-Forming Elements in Woody Biomass Fuels. *Fuel* **2010**, *89* (2), 481–493.

(100) Zhang, Y.; Xie, X.; Zhao, J.; Wei, X. The Alkali Metal Occurrence Characteristics and Its Release and Conversion during Wheat Straw Pyrolysis. *Renew. Energy* **2019**.

(101) Haynes, B. S.; Neville, M.; Quann, R. J.; Sarofim, A. F. Factors Governing the Surface Enrichment of Fly Ash in Volatile Trace Species. *J. Colloid Interface Sci.* **1982**, *87* (1), 266–278.

(102) Wiinikka, H.; Gebart, R.; Boman, C.; Boström, D.; Öhman, M. Influence of Fuel Ash Composition on High Temperature Aerosol Formation in Fixed Bed Combustion of Woody Biomass Pellets. *Fuel* **2007**, *86* (1–2), 181–193.

(103) Korbee, R.; Shah, K. V.; Cieplik, M. K.; Betrand, C. I.; Vuthaluru, H. B.; Van De Kamp, W. L. First Line Ash Transformations of Coal and Biomass Fuels during PF Combustion. *Energy & Fuels* **2010**, *24* (2), 897–909.

(104) Frandsen, F. J. Ash Formation , Deposition and Corrosion When Utilizing Straw for Heat and Power Production, Technical University of Denmark, 2011.

(105) Damoe, A. J.; Jensen, P. A.; Frandsen, F. J.; Wu, H.; Glarborg, P. Fly Ash Formation during Suspension Firing of Biomass: Effects of Residence Time and Fuel Type. *Energy & Fuels* **2017**, *31* (1), 555–570.

(106) Knudsen, J. N. Volatilization of Inorganic Matter during Combustion of Annual Biomass, Technical University of Denmark, 2004.

(107) van Lith, S. C.; Jensen, P. A.; Frandsen, F.; Glarborg, P. Release to the Gas Phase of Inorganic Elements during Wood Combustion. Part 2: Influence of Fuel Composition. *Energy & Fuels* **2008**, *22* (6), 1598–1609.

(108) Dayton, D. C.; French, R. J.; Milne, T. A. Direct Observation of Alkali Vapor Release during Biomass Combustion and Gasification. 1. Application of Molecular Beam/Mass Spectrometry to Switchgrass Combustion. *Energy & Fuels* **1995**, *9* (5), 855–865.

(109) Knudsen, J. N.; Jensen, P. A.; Dam-johansen, K. Transformation and Release to the Gas Phase of Cl , K , and S during Combustion of Annual Biomass. *Energy & Fuels* **2004**, *18*, 1385–1399.

(110) Johansen, J. M.; Aho, M.; Paakkinen, K.; Taipale, R.; Egsgaard, H.; Jakobsen, J. G.; Frandsen, F. J.; Glarborg, P. Release of K, Cl, and S during Combustion and Co-Combustion with Wood of High-Chlorine Biomass in Bench and Pilot Scale Fuel Beds. *Proc. Combust. Inst.* **2013**, *34* (2), 2363–2372.

(111) Misra, M. K.; Ragland, K. W.; Baker, A. J. Wood Ash Composition as a Function of Furnace Temperature. *Biomass and Bioenergy* **1993**, *4* (2), 103–116.

(112) Tchoffor, P. A.; Davidsson, K. O.; Thunman, H. Effects of Steam on the Release of Potassium, Chlorine, and Sulfur during Char Conversion, Investigated under Dual-Fluidized-Bed Gasification Conditions. *Energy & Fuels* **2014**, *28* (11), 6953–6965.

(113) Bläsing, M.; Müller, M. Investigations on the Influence of Steam on the Release of Sodium, Potassium, Chlorine, and Sulphur Species during High Temperature Gasification of Coal. *Fuel* **2012**, *94*, 137–143.

(114) Mason, P. E.; Darvell, L. I.; Jones, J. M.; Williams, A. Observations on the Release of Gas-Phase Potassium during the Combustion of Single Particles of Biomass. *Fuel* **2016**, *182*, 110–117.

(115) Niu, Y.; Du, W.; Tan, H.; Xu, W.; Liu, Y.; Xiong, Y.; Hui, S. Further Study on Biomass Ash Characteristics at Elevated Ashing Temperatures: The Evolution of K, Cl, S and the Ash Fusion Characteristics. *Bioresour. Technol.* **2013**, *129*, 642–645.

(116) Jensen, P. A.; Frandsen, F. J.; Dam-Johansen, K.; Sander, B. Experimental Investigation of the Transformation and Release to Gas Phase of Potassium and Chlorine during Straw Pyrolysis. *Energy & Fuels* **2000**, *14* (6), 1280–1285.

(117) Boström, D.; Skoglund, N.; Grimm, A.; Boman, C.; Öhman, M.; Broström, M.; Backman, R. Ash Transformation Chemistry during Combustion of Biomass. *Energy & Fuels* **2012**, *26* (1), 85–93.

(118) Vassilev, S. V; Baxter, D.; Vassileva, C. G. An Overview of the Behaviour of Biomass during Combustion: Part I. Phase-Mineral Transformations of Organic and Inorganic Matter. *Fuel* **2013**, *112*, 391–449.

(119) Vassilev, S. V.; Baxter, D.; Vassileva, C. G. An Overview of the Behaviour of Biomass during Combustion: Part II. Ash Fusion and Ash Formation Mechanisms of Biomass Types. *Fuel* **2014**, *117*, 152–183.

(120) Čepauskiene, D.; Pedišius, N.; Milčius, D. Chemical Composition of Agromass Ash and Its Influence on Ash Melting Characteristics. *Agron. Res.* **2018**, *16* (2), 357–364.

(121) Steenari, B. M.; Lindqvist, O. High-Temperature Reactions of Straw Ash and the Anti-Sintering Additives Kaolin and Dolomite. *Biomass and Bioenergy* **1998**, *14* (1), 67–76.

(122) Dodson, J. R.; Hunt, A. J.; Budarin, V. L.; Matharu, A. S.; Clark, J. H. The Chemical Value of Wheat Straw Combustion Residues. *RSC Adv.* **2011**, *1* (3), 523–530.

(123) Li, L.; Ren, Q.; Li, S.; Lu, Q. Effect of Phosphorus on the Behavior of Potassium during the Co-Combustion of Wheat Straw with Municipal Sewage Sludge. *Energy & Fuels* **2013**, *27* (10), 5923–5930.

(124) Zhao, H.; Xu, W.; Song, Q.; Zhuo, J.; Yao, Q. Effect of Steam and SiO2 on the Release and Transformation of K_2CO_3 and KCl during Biomass Thermal Conversion. *Energy & Fuels* **2018**, *32* (9), 9633–9639.

(125) Novakovic, A.; Lith, S. C. Van; Frandsen, F. J.; Jensen, P. a; Holgersen, L. B. Release of

Potassium from the Systems K-Ca-Si and K-Ca-P. *Energy & Fuels* **2009**, No. 3, 3423–3428.

(126) Sevonius, C.; Yrjas, P.; Hupa, M. Defluidization of a Quartz Bed - Laboratory Experiments with Potassium Salts. *Fuel* **2014**, *127*, 161–168.

(127) Ma, T.; Fan, C.; Hao, L.; Li, S.; Jensen, P. A.; Song, W.; Lin, W.; Dam-Johansen, K. Biomass Ash Induced Agglomeration in Fluidized Bed. Part 2: Effect of Potassium Salts in Different Gas Composition. *Fuel Process. Technol.* **2018**, *180*, 130–139.

(128) Sevonius, C.; Yrjas, P.; Lindberg, D.; Hupa, L. Impact of Sodium Salts on Agglomeration in a Laboratory Fluidized Bed. *Fuel* **2019**, *245*, 305–315.

(129) He, Z.; Saw, W. L.; Eyk, P. J. Van; Nathan, G. J.; Ashman, P. J. Interactions between Quartz Sand and Wood Doped with Either K or Na Salts under Steam Gasification and Combustion Atmospheres. *Ind. Eng. Chem. Res.* **2020**, *59*, 1712–1722.

(130) Song, B. H.; Kim, S. D. Catalytic Activity of Alkali and Iron Salt Mixtures for Steam-Char Gasification. *Fuel* **1993**, *72* (6), 797–803.

(131) Huttinger, K. J.; Minges, R. Catalytic Carbon Water Vapour Gasification and Wetting. *Fuel* **1985**, *64*, 491–494.

(132) Anicic, B.; Lin, W.; Dam-Johansen, K.; Wu, H. Agglomeration Mechanism in Biomass Fluidized Bed Combustion – Reaction between Potassium Carbonate and Silica Sand. *Fuel Process. Technol.* **2018**, *173*, 182–190.

(133) Kumar, L.; Pougatch, K.; Salcudean, M.; Grace, J.; Grecov, D.; Mcmillan, J. Population Balance Modeling for the Growth of Agglomerates via Primary and Secondary Agglomeration in Gas-Fluidized Beds. *Powder Technol.* **2017**, *321*, 499–513.

(134) Yuksel, H.; Dirim, S. N. Agglomeration Process in the Fluidized Bed , the Effecting Parameters and Some Applications. *Croat. J. Food Technol. Biotechnol. Nutr.* **2018**, *13* (3–4), 159–163.

(135) Gao, J.; Wen, G.; Huang, T.; Tang, P.; Liu, Q. Effects of the Composition on the Structure and Viscosity of the CaO–SiO2-Based Mold Flux. *J. Non. Cryst. Solids* **2016**, *435*, 33–39.

(136) Ilyushechkin, A. Y.; Hla, S. S. Viscosity of High-Iron Slags from Australian Coals. *Energy & Fuels* **2013**, *27*, 3736–3742.

(137) Hsieh, P. Y.; Kwong, K.; Bennett, J. Correlation between the Critical Viscosity and Ash Fusion Temperatures of Coal Gasifier Ashes. *Fuel Process. Technol.* **2016**, *142*, 13–26.

(138) Xu, J.; Zhao, F.; Guo, Q.; Yu, G.; Liu, X.; Wang, F. Characterization of the Melting Behavior of High-Temperature and Low-Temperature Ashes. *Fuel Process. Technol.* **2015**, *134*, 441–448.

(139) Tsuruda, A.; Hakim, L.; Takebe, H. Viscosity Measurement and Prediction of Gasified and Synthesized Coal Slag Melts. *Fuel* **2017**, *200*, 521–528.

(140) Wu, X.; Zhang, Z.; Piao, G.; He, X.; Chen, Y.; Kobayashi, N.; Mori, S.; Itaya, Y. Behavior of Mineral Matters in Chinese Coal Ash Melting during Char-CO_2/H_2O Gasification Reaction. *Energy & Fuels* **2009**, *23*, 2420–2428.

(141) Folkedahl, B. C.; Schobert, H. H. Effects of Atmosphere on Viscosity of Selected Bituminous and Low-Rank Coal Ash Slags. *Energy & Fuels* **2005**, *19*, 208–215.

(142) Jing, N.; Wang, Q.; Luo, Z.; Cen, K. Effect of Different Reaction Atmospheres on the Sintering Temperature of Jincheng Coal Ash under Pressurized Conditions. *Fuel* **2011**, *90* (8), 2645–2651.

(143) Schimpke, R.; Klinger, M.; Krzack, S.; Meyer, B. Determination of the Initial Ash Sintering Temperature by Cold Compression Strength Tests with Regard to Mineral Transitions. *Fuel* **2017**, *194*, 157–165.

(144) Jing, N.; Wang, Q.; Yang, Y.; Cheng, L.; Luo, Z.; Cen, K. Influence of Ash Composition on the Sintering Behavior during Pressurized Combustion and Gasification Process. *J Zhejiang Univ-Sci A (Appl Phys Eng)* **2012**, *13* (3), 230–238.

(145) Bryant, G. W.; Browning, G. J.; Emanuel, H.; Gupta, S. K.; Gupta, R. P.; Lucas, J. A.; Wall, T. F. The Fusibility of Blended Coal Ash. **2000**, No. 5, 316–325.

(146) Song, W. J.; Tang, L. H.; Zhu, X. D.; Wu, Y. Q.; Zhu, Z. B. Prediction of Chinese Coal Ash Fusion Temperatures in Ar and H2 Atmospheres. *Energy & Fuels* **2009**, *23*, 1990–1997.

(147) Dyk, J. C. Van; Benson, S. A.; Laumb, M. L.; Waanders, B. Coal and Coal Ash Characteristics to Understand Mineral Transformations and Slag Formation. *Fuel* **2009**, *88* (6), 1057–1063.

(148) Wei, B.; Tan, H.; Wang, X.; Yang, T.; Wang, Y.; Ruan, R.; Wei, B.; Tan, H.; Wang, X.; Yang, T.; et al. Impact of Complex Reacting Atmosphere on Ash Fusion Characteristics and Minerals Conversion in Coal Combustion Process. *Combust. Sci. Technol.* **2018**, *190* (7), 1178–1193.

(149) Vassilev, S. V.; Vassileva, C. G.; Vassilev, V. S. Advantages and Disadvantages of Composition and Properties of Biomass in Comparison with Coal: An Overview. *Fuel* **2015**, *158*, 330–350.

(150) Miaomiao, N.; Dong, Q.; Huang, Y.; Jin, B.; Wang, H.; Gu, H. Characterization of Ash Melting Behaviour at High Temperatures under Conditions Simulating Combustible Solid Waste Gasification. *Waste Manag. Res.* **2018**, *36* (5), 415–425.

(151) Cao, X.; Kong, L.; Bai, J.; Ge, Z.; Li, H.; Bai, Z. Effect of Water Vapor on Coal Ash Slag Viscosity under Gasification Condition. *Fuel* **2019**, *237*, 18–27.

(152) Mao, Y.; Jin, Y.; Li, K.; Bi, J.; Li, J.; Xin, F. Sintering Characteristic in Catalytic Gasification of China Inner Mongolia Bituminous Coal Ash. *Energy & Fuels* **2016**, *30*, 3975–3985.

(153) Mao, Y.; Jin, Y.; Li, K.; Bi, J.; Li, J.; Xin, F. Analysis of Influencing Factors on Sintering Temperature of Inner Mongolia Wangjiata Bituminous Coal Ash during Catalytic Coal Gasification (in Chinese). *Huagong Xuebao/CIESC J.* **2015**, *66*, 1080–1087.

(154) Vuthaluru, H. B.; Linjewile, T. M.; Zhang, D. ke; Manzoori, A. R. Investigations into the Control of Agglomeration and Defluidisation during Fluidised-Bed Combustion of Low-Rank Coals. *Fuel* **1999**, *78* (4), 419–425.

(155) Vuthaluru, H. B.; Zhang, D. K. Control Methods for Remediation of Ash-Related Problems in Fluidised-Bed Combustors. *Fuel Process. Technol.* **1999**, *60* (2), 145–156.

(156) Vuthaluru, H. B.; Zhang, D. K. Effect of Ca- and Mg-Bearing Minerals on Particle Agglomeration Defluidization during Fluidized-Bed Combustion of a South Australian Lignite. *Fuel Process. Technol.* **2001**, *69* (1), 13–27.

(157) Fernández Llorente, M. J.; Escalada Cuadrado, R.; Murillo Laplaza, J. M.; Carrasco García, J. E. Combustion in Bubbling Fluidised Bed with Bed Material of Limestone to Reduce the Biomass Ash Agglomeration and Sintering. *Fuel* **2006**, *85* (14–15), 2081–2092.

(158) van Ommen, J. R.; Schouten, J. C.; Coppens, M.-O.; Lin, W.; Dam-Johansen, K.; van den Bleek, C. M. Timely Detection of Agglomeration in Biomass Fired Fluidized Beds. In *Proceedings of the 16th International Conference on Fluidized Bed Combustion*; American Society of Mechanical Engineers: United States, 2001; pp 1–14.

(159) Nuutinen, L. H.; Tiainen, M. S.; Virtanen, M. E.; Enestam, S. H.; Laitinen, R. S. Coating Layers on Bed Particles during Biomass Fuel Combustion in Fluidized-Bed Boilers. *Energy & Fuels* **2004**, *18* (1), 127–139.

(160) De Geyter, S.; Öhman, M.; Boström, D.; Eriksson, M.; Nordin, A. Effects of Non-Quartz Minerals in Natural Bed Sand on Agglomeration Characteristics during Fluidized Bed Combustion of Biomass Fuels. *Energy & Fuels* **2007**, *21* (5), 2663–2668.

(161) Werther, J.; Saenger, M.; Hartge, E. U.; Ogada, T.; Siagi, Z. Combustion of Agricultural Residues. *Prog. Energy Combust. Sci.* **2000**, *26* (1), 1–27.

(162) Öhman, M.; Nordin, A. The Role of Kaolin in Prevention of Bed Agglomeration during Fluidized Bed Combustion of Biomass Fuels. *Energy & Fuels* **2000**, *14* (3), 618–624.

(163) Öhman, M.; Nordin, A.; Lundholm, K.; Boström, D.; Hedman, H.; Lundberg, M. Ash Transformations during Combustion of Meat-, Bonemeal, and RDF in a (Bench-Scale) Fluidized Bed Combustor. *Energy & Fuels* **2003**, *17* (5), 1153–1159.

(164) Davidsson, K. O.; Steenari, B. M.; Eskilsson, D. Kaolin Addition during Biomass Combustion in a 35 MW Circulating Fluidized-Bed Boiler. *Energy & Fuels* **2007**, *21* (4), 1959–1966.

(165) Davidsson, K. O.; Åmand, L. E.; Steenari, B. M.; Elled, A. L.; Eskilsson, D.; Leckner, B. Countermeasures against Alkali-Related Problems during Combustion of Biomass in a Circulating Fluidized Bed Boiler. *Chem. Eng. Sci.* **2008**, *63* (21), 5314–5329.

(166) Barišić, V.; Peltola, K.; Coda Zabetta, E. Role of Pulverized Coal Ash against Agglomeration, Fouling, and Corrosion in Circulating Fluidized-Bed Boilers Firing Challenging Biomass. *Energy & Fuels* **2013**, *27* (10), 5706–5713.

(167) Chou, J. D.; Lin, C. L. Inhibition of Agglomeration/Defluidization by Different Calcium

Species during Fluidized Bed Incineration under Different Operating Conditions. *Powder Technol.* **2012**, *219*, 165–172.

(168) Billen, P.; Costa, J.; Van Der Aa, L.; Westdorp, L.; Van Caneghem, J.; Vandecasteele, C. An Agglomeration Index for CaO Addition (as $CaCO_3$) to Prevent Defluidization: Application to a Full-Scale Poultry Litter Fired FBC. *Energy & Fuels* **2014**, *28* (8), 5455–5462.

(169) Wang, L.; Skjevrak, G.; Hustad, J. E.; Skreiberg, Ø. Investigation of Biomass Ash Sintering Characteristics and the Effect of Additives. *Energy & Fuels* **2014**, *28* (1), 208–218.

(170) Grimm, A.; Skoglund, N.; Boström, D.; Boman, C.; Öhman, M. Influence of Phosphorus on Alkali Distribution during Combustion of Logging Residues and Wheat Straw in a Bench-Scale Fluidized Bed. *Energy & Fuels* **2012**, *26* (5), 3012–3023.

(171) Ulusoy, B. NOx Formation and Reduction in Fluidized Bed Combustion of Biomass, Technical University of Denmark, 2019.

(172) Jenkins, B. M.; Bakker, R. R.; Wei, J. B. On the Properties of Washed Straw. *Biomass and Bioenergy* **1996**, *10* (4), 177–200.

(173) Arvelakis, S.; Vourliotis, P.; Kakaras, E.; Koukios, E. G. Effect of Leaching on the Ash Behavior of Wheat Straw and Olive Residue during Uidized Bed Combustion. *Biomass and Bioenergy* **2001**, *20*, 459–470.

(174) Arvelakis, S.; Gehrmann, H.; Beckmann, M.; Koukios, E. G. Agglomeration Problems during Fluidized Bed Gasification of Olive-Oil Residue : Evaluation of Fractionation and Leaching as Pre-Treatments. *Fuel* **2003**, *82*, 1261–1270.

(175) Arvelakis, S.; Gehrmann, H.; Beckmann, M.; Koukios, E. G. Preliminary Results on the Ash Behavior of Peach Stones during Fluidized Bed Gasification : Evaluation of Fractionation and Leaching as Pre-Treatments. *Biomass and Bioenergy* **2005**, *28*, 331–338.

(176) Carrillo, M. A.; Staggenborg, S. A.; Pineda, J. A. Washing Sorghum Biomass with Water to Improve Its Quality for Combustion. *Fuel* **2014**, *116*, 427–431.

(177) Deng, L.; Zhang, T.; Che, D. Effect of Water Washing on Fuel Properties , Pyrolysis and Combustion Characteristics , and Ash Fusibility of Biomass. *Fuel Process. Technol.* **2013**, *106*, 712–720.

(178) Link, S.; Arvelakis, S.; Paist, A.; Liliedahl, T. Effect of Leaching Pretreatment on the Gasification of Wine and Vine (Residue) Biomass. *Renew. Energy* **2018**, *115*, 1–5.

(179) Yu, C.; Thy, P.; Wang, L.; Anderson, S. N.; Vandergheynst, J. S.; Upadhyaya, S. K.; Jenkins, B. M. Influence of Leaching Pretreatment on Fuel Properties of Biomass. *Fuel Process. Technol.* **2014**, *128*, 43–53.

(180) Said, N.; Bishara, T.; García-maraver, A.; Zamorano, M. Effect of Water Washing on the Thermal Behavior of Rice Straw. *Waste Manag.* **2013**, *33* (11), 2250–2256.

(181) Arvelakis, S.; Koukios, E. G. Physicochemical Upgrading of Agroresidues as Feedstocks for

Energy Production via Thermochemical Conversion Methods. *Biomass and Bioenergy* **2002**, *22*, 331–348.

(182) Taralas, G.; Kontominas, M. G. Thermochemical Treatment of Solid and Wastewater Effluents Originating from the Olive Oil Food Industry. *Energy & Fuels* **2005**, *19*, 1179–1185.

(183) Datta, S.; Chauhan, V.; Sahu, G.; Chavan, P. D.; Saha, S.; Gupta, P. K.; Dutta, P. Co-Gasification of High Ash Indian Coal-Biomass Blends in a Pilot-Scale Fluidized Bed Gasifier. *Biomass Convers. Biorefinery* **2020**, *10* (4), 831–838.

(184) Teixeira, P.; Lopes, H.; Gulyurtlu, I.; Lapa, N.; Abelha, P. Evaluation of Slagging and Fouling Tendency during Biomass Co-Firing with Coal in a Fluidized Bed. *Biomass and Bioenergy* **2012**, *39*, 192–203.

(185) Teixeira, P.; Lopes, H.; Gulyurtlu, I.; Lapa, N.; Abelha, P.; Ed, J. Slagging and Fouling during Coal and Biomass Co Fi Ring : Chemical Equilibrium Model Applied to FBC. *Energy & Fuels* **2014**.

(186) Nordgren, D.; Hedman, H.; Padban, N.; Boström, D.; Öhman, M. Ash Transformations in Pulverised Fuel Co-Combustion of Straw and Woody Biomass. *Fuel Process. Technol.* **2013**, *105*, 52–58.

(187) Thy, P.; Jenkins, B. M.; Williams, R. B.; Lesher, C. E.; Bakker, R. R. Bed Agglomeration in Fluidized Combustor Fueled by Wood and Rice Straw Blends. *Fuel Process. Technol.* **2010**, *91* (11), 1464–1485.

(188) Elled, A. L.; Davidsson, K. O.; Åmand, L. E. Sewage Sludge as a Deposit Inhibitor When Co-Fired with High Potassium Fuels. *Biomass and Bioenergy* **2010**, *34* (11), 1546–1554.

(189) Skoglund, N.; Grimm, A.; Öhman, M.; Boström, D. Effects on Ash Chemistry When Co-Firing Municipal Sewage Sludge and Wheat Straw in a Fluidized Bed: Influence on the Ash Chemistry by Fuel Mixing. *Energy & Fuels* **2013**, *27* (10), 5725–5732.

(190) Ryabov, G.; Litoun, D.; Dik, E. Agglomeration of Bed Material: Influence on Efficiency of Biofuel Fluidized Bed Boiler. *Therm. Sci.* **2003**, *7* (1), 5–16.

(191) Saidi, M.; Basirat Tabrizi, H.; Grace, J. R. A Review on Pulsed Flow in Gas-Solid Fluidized Beds and Spouted Beds: Recent Work and Future Outlook. *Adv. Powder Technol.* **2019**, *30* (6), 1121–1130.

(192) Ireland, E.; Pitt, K.; Smith, R. A Review of Pulsed Flow Fluidisation; the Effects of Intermittent Gas Flow on Fluidised Gas-Solid Bed Behaviour. *Powder Technol.* **2016**, *292*, 108–121.

(193) Zhang, D.; Koksal, M. Heat Transfer in a Pulsed Bubbling Fluidized Bed. *Powder Technol.* **2006**, *168* (1), 21–31.

(194) Jia, D.; Bi, X.; Lim, C. J.; Sokhansanj, S.; Tsutsumi, A. Heat Transfer in a Tapered Fluidized Bed of Biomass Particles with Pulsed Gas Flow. *Particuology* **2019**, *42*, 2–14.

(195) Jia, D.; Bi, X.; Lim, C. J.; Sokhansanj, S.; Tsutsumi, A. Heat Transfer in a Pulsed Fluidized

Bed of Biomass Particles. *Ind. Eng. Chem. Res.* **2017**, *56* (13), 3740–3756.

(196) Liu, Y.; Liu, Z.; Ohara, H. Heat Transfer and Fluidization Characteristics of Lignite in a Pulsation-Assisted Fluidized Bed. *Ind. Eng. Chem. Res.* **2017**, *56* (31), 8995–9005.

(197) Jia, D.; Bi, X.; Lim, C. J.; Sokhansanj, S.; Tsutsumi, A. Biomass Drying in a Pulsed Fluidized Bed without Inert Bed Particles. *Fuel* **2016**, *186*, 270–284.

(198) Akhavan, A.; Van Ommen, J. R.; Nijenhuis, J.; Wang, X. S.; Coppens, M. O.; Rhodes, M. J. Improved Drying in a Pulsation-Assisted Fluidized Bed. *Ind. Eng. Chem. Res.* **2009**, *48* (1), 302–309.

(199) Nitz, M.; Taranto, O. P. Drying of Beans in a Pulsed Fluid Bed Dryer: Drying Kinetics, Fluid-Dynamic Study and Comparisons with Conventional Fluidization. *J. Food Eng.* **2007**, *80* (1), 249–256.

(200) Hadi, B.; Van Ommen, J. R.; Coppens, M. O. Enhanced Particle Mixing in Pulsed Fluidized Beds and the Effect of Internals. *Ind. Eng. Chem. Res.* **2012**, *51* (4), 1713–1720.

(201) Ali, S. S.; Asif, M. Fluidization of Nano-Powders: Effect of Flow Pulsation. *Powder Technol.* **2012**, *225*, 86–92.

(202) Li, Z.; Su, W.; Wu, Z.; Wang, R.; Mujumdar, A. S. Investigation of Flow Behaviors and Bubble Characteristics of a Pulse Fluidized Bed via CFD Modeling. *Dry. Technol.* **2010**, *28* (1), 78–93.

(203) Khosravi Bizhaem, H.; Basirat Tabrizi, H. Investigating Effect of Pulsed Flow on Hydrodynamics of Gas-Solid Fluidized Bed Using Two-Fluid Model Simulation and Experiment. *Powder Technol.* **2017**, *311*, 328–340.

(204) Khosravi Bizhaem, H.; Basirat Tabrizi, H. Experimental Study on Hydrodynamic Characteristics of Gas-Solid Pulsed Fluidized Bed. *Powder Technol.* **2013**, *237*, 14–23.

(205) Hao, B.; Bi, H. T. Forced Bed Mass Oscillations in Gas-Solid Fluidized Beds. *Powder Technol.* **2005**, *149* (2–3), 51–60.

(206) Ali, S. S.; Asif, M.; Ajbar, A. Bed Collapse Behavior of Pulsed Fluidized Beds of Nano-Powder. *Adv. Powder Technol.* **2014**, *25* (1), 331–337.

(207) Akhavan, A.; Rahman, F.; Wang, S.; Rhodes, M. Enhanced Fluidization of Nanoparticles with Gas Phase Pulsation Assistance. *Powder Technol.* **2015**, *284*, 521–529.

(208) Sobrino, C.; Almendros-Ibañez, J. A.; Santana, D.; de Vega, M. Fluidization of Group B Particles with a Rotating Distributor. *Powder Technol.* **2008**, *181* (3), 273–280.

(209) Gui, N.; Fan, J. R. Numerical Simulation of Pulsed Fluidized Bed with Immersed Tubes Using DEM-LES Coupling Method. *Chem. Eng. Sci.* **2009**, *64* (11), 2590–2598.

(210) Jia, D.; Cathary, O.; Peng, J.; Bi, X.; Lim, C. J.; Sokhansanj, S.; Liu, Y.; Wang, R.; Tsutsumi, A. Fluidization and Drying of Biomass Particles in a Vibrating Fluidized Bed with Pulsed Gas

Flow. *Fuel Process. Technol.* **2015**, *138*, 471–482.

(211) Kobayashi, M.; Ramaswasi, D.; Brazelton, W. T. HEAT TRANSFER FROM AN INTERNAL SURFACE TO A PULSED BED. *Chem. Eng. Prog. Symp. Ser.* **1970**, *66* (105), 58–67.

(212) Nishimura, A.; Deguchi, S.; Matsuda, H.; Hasatani, M.; Mujumdar, A. S. Heat Transfer Characteristics in a Pulsating Fluidized Bed in Relation to Bubble Characteristics. *Heat Transf. - Asian Res.* **2002**, *31* (4), 307–319.

(213) Wang, X. S.; Rhodes, M. J. Using Pulsed Flow to Overcome Defluidization. *Chem. Eng. Sci.* **2005**, *60* (18), 5177–5181.

3. Agglomeration in Fluidized Bed Gasification of Wheat Straw

Abstract

In this chapter, the agglomeration during combustion and gasification of wheat straw in an air blown system at different equivalence ratios (ERs) was studied in a lab-scale fluidized bed reactor at 850 °C using silica sand as bed material. The influence of gasification agents, such as steam and carbon dioxide, on agglomeration was further investigated by varying the concentrations of steam and CO_2 in the primary gas. The results reveal that the agglomeration tendency in the fluidized bed increases first to a maximum tendency as ER decreases, and then decreases with a decrease of ER. By decreasing ER in the primary gas, the produced reducing atmosphere accelerates the agglomeration probably due to an increased melting tendency of ash. Meanwhile, an increased residual carbon amount in the bed results from a decreased ER will mitigate the agglomeration possibly by reducing the fusion tendency and the melting flow behaviors of the straw ash and by retarding the interaction between ash and bed material. The competition between an enhanced reducing atmosphere and an increased amount of residual carbon caused by lowering ER results in the occurrence of a maximal agglomeration tendency at a critical ER. The promoted agglomeration of wheat straw under the condition with a high concentration of steam may be attributed to a decreased residual carbon amount in the bed and a lowered viscosity of straw ash. However, the addition of CO_2 in primary gas slightly slows down the agglomeration. A mechanism for agglomeration in fluidized bed gasification of wheat straw with respect to the effect of ER and steam is proposed based on the results from this study.

This chapter has been written in a manuscript format. A slightly modified version of this chapter will be submitted to a peer-reviewed journal.

3.1 Introduction

Fluidized bed combustion and gasification of biomass are promising technologies for production of power and chemicals from renewable resources[1–3]. However, the occurrence of bed agglomeration can affect the stable and efficient operation of fluidized beds[4,5], and may lead to defluidization and unscheduled plant shutdown in severe cases [6]. In the past decades, the mechanisms of agglomeration in fluidized bed combustion of biomass have been investigated extensively from many aspects, covering the mechanisms of agglomerate formation at particle scale[5,7–9], the influence of biomass type[10–12] and operation parameters[13,14], and the methods for mitigating the problems caused by agglomeration[15–17]. It has been widely accepted that the agglomeration in biomass fired fluidized beds results from the interaction between bed material and ash in the presence of a molten phase, e.g., low melting temperature alkali containing compounds originated from biomass. Therefore, the herbaceous biomass with a high alkali (mainly potassium) content, such as straws and Miscanthus, is problematic in connection to agglomeration. The agglomeration phenomena in fluidized bed combustion of biomass have been extensively discussed in several review papers[18–22].

Compared to combustion, the study on agglomeration in fluidized bed gasification appears less extensive, although the agglomeration studies started earlier for gasification of coal[23] and biomass[24]. The studies on agglomeration in biomass gasification investigate the influence of biomass type and the operation parameters, such as temperature on the agglomeration tendency[24–26], and propose the countermeasures for mitigating agglomeration[27–29]. The methodologies applied for gasification studies are normally similar to those for combustion studies, which can be categorized into the following groups: predicting the ash behavior via thermodynamic equilibrium calculations[30]; determining the defluidization tendency in trial tests and analyzing the formed agglomerates by scanning electron microscopy with energy-dispersive X-ray (SEM-EDX)[31,32]; the combination of the trial tests in fluidized bed and the thermodynamic equilibrium calculations[25]; estimating the agglomeration tendency of the agglomerates formed in fixed beds at designed temperatures[33]; and evaluating of defluidization temperatures of ashes at simulated gasification conditions[5,34].

In the gasification process, biomass converts at reducing conditions, which will result in a different ash chemistry from that under combustion. Therefore, the characteristics of biomass ash formed at gasification conditions may behave differently from that at combustion conditions with respect to fusion, which is strongly related to the agglomeration phenomena. It has been reported that the fusion temperature of the coal ash under reducing condition is lower than that under oxidizing condition[35–39], due to the reduction of iron(III) to iron(II) in coal ash. For biomass, the trend is not consistent, depending on the types of biomass from limited results[5,34,40]. Öhman *et al.*[5,40] reported that the agglomeration temperatures of bark, olive flesh, cane trash, and rice husk under gasification condition are slightly lower than that under combustion condition, while reed cancan grass and Lucerne show the opposite trend. Ma *et al.*[34] showed that the defluidization temperatures of three straw ashes (wheat,

rice and corn), prepared at 550 °C under air, CO_2, H_2 and steam atmospheres, which was used for simulation of combustion and gasification conditions. They found the decreased order of the defluidization temperatures of air ≈ CO_2 > H_2 >steam. However, the detailed mechanisms are not clear yet.

Moreover, the equivalence ratio (ER, also called air ratio) in gasification is an important operational parameter, which will affect the yield and composition of the producer gas[41]. The influence of ER on the agglomeration in fluidized bed gasification of biomass has not been thoroughly studied even though a few experimental studies had used the different values of ER[24,42,43], which were varied in the range of 0.18 to 0.38. Comprehensive studies on the influence of the important parameters, such as ER, steam to fuel ratio and CO_2 concentration, on the agglomeration tendency in fluidized bed gasification of biomass are not found in literature.

The aim of this work is to reveal the different behaviors of agglomeration of a typical problematic biomass, wheat straw, with different ERs, covering gasification and combustion region by a systematically experimental study in a lab-scale fluidized bed reactor with a continuously feeding system. The influence of the type of gasification agents on the agglomeration behaviors will be studied by introducing steam and CO_2 containing primary gases to the reactor. Based on the experimental results, the possible agglomeration mechanisms will be proposed.

3.2 Experimental section

3.2.1 Fuel and bed material

Wheat straw, the straw that caused defluidization in the low-temperature circulating fluidized bed (LTCFB) gasifier as described in Chapter 1, Section 1.1, with a size range of 2 - 4 mm was used as fuel in the experiments in order to minimize the elutriation of the fuel particles and to achieve a stable feeding. The proximate and ultimate analyses and the inorganic composition of the straw are shown in Table 3-1. Silica sand (SiO_2 > 97 wt.%) with a size range of 355 - 500 µm was used as bed material. The selection of bed particle size and fuel size are presented in Appendix A.

Table 3-1 Characteristics of wheat straw

Proximate analysis	Moisture		**Ash**		Volatile matter			Fixed carbon	
(wt.%, ar)	8.35		5.22		68.84			17.59	
Fuel elemental analysis	C		H		O (by difference)			N	
(wt.%, daf)	46.16		6.62		46.42			0.80	
Inorganic composition⸸	Cl	S	Al	Ca	Fe	**K**	Mg	Na	P	**Si**
(wt.%, db)	0.11	0.081	0.21	0.32	0.013	**0.98**	0.07	0.0086	0.11	**1.1**

ar: as received basis
daf: dry ash-free basis
db: dry basis
⸸ data obtained by inductively coupled plasma - optical emission spectrometry (ICP-OES)

3.2.2 Experimental apparatus

Experiments were conducted in a lab-scale bubbling fluidized bed reactor system, which consists of a gas supplying system, a fuel feeding system, a fluidized bed reactor, a gas sampling and analysis system and a data acquisition system, as illustrated in Figure 3-1. The flow rates of air, N_2, and CO_2 were controlled by a series of precision mass flow controllers (MFCs). The steam was generated by a steam generator (VEIT 2365) and its flow rate was controlled by a needle valve with pre-calibrated data. An electric heat trace with a setting temperature of 150 ˚C was applied to the steam line to the reactor to prevent the steam from condensation. Two streams of gas were introduced to the reactor, fluidizing gas (or primary gas), which is introduced at the bottom of the reactor, and feeding gas (or secondary gas), which is introduced with fuel particles. The reactor was made of high temperature stainless steel with a total height of 1400 mm. The reactor has three zones: preheating zone, bubbling bed and freeboard. The preheating zone is located below the gas distributor, above which is the bubbling fluidized bed reactor. The inner diameter of the bubbling bed is 62.5 mm. The reactor was externally heated by four independently controlled heating elements to achieve desired temperature profile in the reactor. A loss-in-weight gravimetric feeder with twin screws (K-ML-KT20, Coperion K-Tron) was used to feed the fuel particles to the reactor continuously. The feed position is located at 300 mm above the gas distributor. The inner diameter of the freeboard 500 mm above the dense bed is 100 mm to reduce elutriation of fine particles. After the exit of the flue gas at the reactor top, a cyclone was used to remove the fine particles in the gas stream. A small amount of flue gas was sampled from a port located in the downstream of the cyclone by a gas sampling system, consisting of a filter, a pump, and a cooler for water condensation. The concentrations of CO_2, CO, O_2, NO and SO_2 in the flue gas were continuously monitored by a series of gas analyzers (Emerson, NGA 2000 Analyser, FLSmidth A/S). The reactor was equipped with four thermocouples to measure the temperatures right below the gas distributor (T_1), right above the gas distributor (T_2), 7.5 cm above the distributor (T_3), and 5 cm above the distributor (T_4), and two pressure transducers for monitoring the pressure drop over the bed and pressure below the gas distributor. The signals from the thermocouples and pressure transducers, as well as from gas analyzers were continuously logged to a computer by a data acquisition system during experiments.

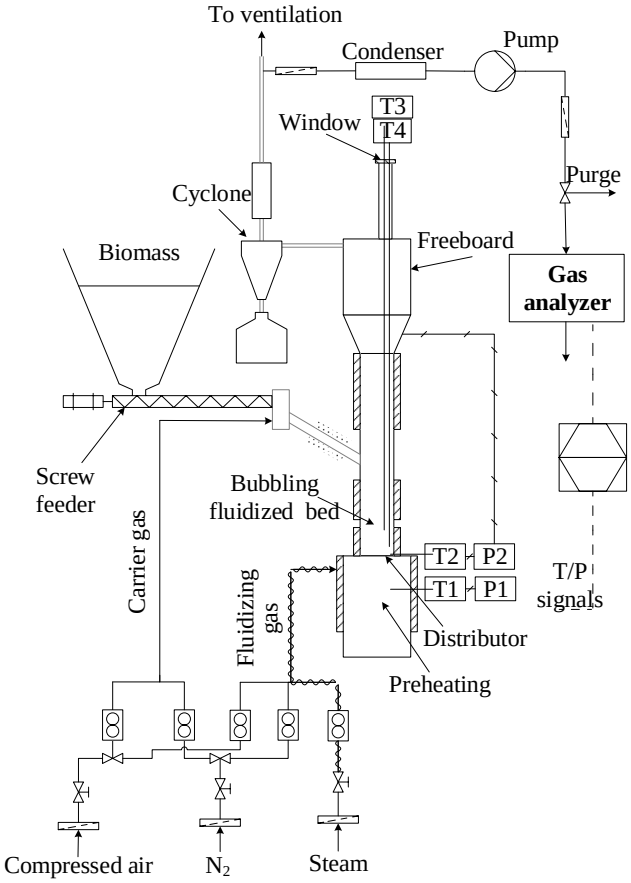

Figure 3-1 A schematic drawing of the lab-scale fluidized bed reactor

3.2.3 Experimental conditions and procedure

All experiments were performed at a bed temperature of 850°C with a fixed straw feeding rate of 0.11 kg/h (on a dry basis). The primary gas (fluidizing gas) flow rate was kept to a constant value of 11.5 Nl/min, corresponding to a U_g/U_{mf} ratio of 3 and 2.82 at the conditions with 100% of air and with a mixture of 50 vol.% steam and 50 vol.% N_2, respectively. The parameters with constant values in the experiments are given in Table 3-2. The values of ER in the bubbling bed were varied by changing the volume fraction of air, nitrogen and steam or carbon dioxide (in case of varying the gasification agents) in the primary gas flow. For the experiments with steam as the gasification agent, a parameter of steam to fuel ratio (SFR), defined as the weight ratio of steam to the fuel (g/g), is used. The feeding gas not only assists the stable feeding of fuel particles, but also functions as the secondary combustion air in order to burn the combustible gas in the freeboard for laboratory safety consideration. The composition of the feeding gas was varied in such a way that the total flow to the reactor was kept constant, and with a constant total combustion stoichiometric ratio of 1.45. The experimental matrix related to the operating parameters of gas feeding rates to the primary and secondary gas streams and in-bed ERs and SFRs are shown in Table 3-3. These experiments can be categorized into five groups: air blown (A-E), air blown with addition of steam (F-J), air blown with high concentration of steam (K-N), air blown with addition of CO_2 (O-R) and air blown with simultaneous addition of steam and

CO_2 (S-V). It should be mentioned here that the experiments were designed for studying the influence of ER on agglomeration. The heat balance for the auto-thermal air blown gasification is not considered.

Table 3-2 Typical operating parameters during experiments.

Parameters	Value
Bed temperature (T_4, °C)	850
Fuel feeding rate (kg/h, db)	0.11
Bed material loading (kg)	0.50
Primary gas flow rate (Nl/min, NTP)	11.5
Secondary gas flow rate (Nl/min, NTP)	15.5
Superficial fluidization velocity @850 °C (m/s)	0.24

Table 3-3 Gas compositions used in the experiments

Exp. Types	Exp. No.	Exp. Name	ER	SFR	Primary gas (vol.%)				Secondary gas (vol.%)	
					Air	Steam	CO_2	N_2	Air	N_2
Air blown combustion and gasification	A	2.5% air gasification	0.04	0	2.5%	0	0	97.5%	72%	28%
	B	9.5% air gasification	0.14	0	9.5%	0	0	90.5%	67%	33%
	C	25% air gasification	0.36	0	25%	0	0	75%	55.5%	44.5%
	D	75% air combustion	1.09	0	75%	0	0	25%	18.5%	81.5%
	E	100% air combustion	1.45	0	100%	0	0	0	0	100%
Air blown with addition of steam	F	25% steam gasification	0	0	0	25%	0	75%	74%	26%
	G	25% steam/2.5% air gasification	0.04	2.7	2.5%	25%	0	72.5%	72%	28%
	H	25% steam/9.5% air gasification	0.14	2.7	9.5%	25%	0	65.5%	67%	33%
	I	25% steam/25% air gasification	0.36	2.7	25%	25%	0	50%	55.5%	44.5%
	J	25% steam/75% air combustion	1.09	2.7	75%	25%	0	0	18.5%	81.5%
Air blown with high concentration of steam	K	50% steam gasification	0	5.4	0	50%	0	50%	74%	26%
	L	50% steam/2.5% air gasification	0.04	5.4	2.5%	50%	0	47.5%	72%	28%
	M	50% steam/9.5% air gasification	0.14	5.4	9.5%	50%	0	40.5%	67%	33%
	N	50% steam/25% air gasification	0.36	5.4	25%	50%	0	25%	55.5%	44.5%
Air blown with addition of CO_2	O	25% CO_2/2.5% air gasification	0.04	0	2.5%	0	25%	72.5%	72%	28%
	P	25% CO_2/9.5% air gasification	0.14	0	9.5%	0	25%	65.5%	67%	33%
	Q	25% CO_2/25% air gasification	0.36	0	25%	0	25%	50%	55.5%	44.5%
	R	25% CO_2/75% air gasification	1.09	0	75%	0	25%	0	18.5%	81.5%
Air blown with simultaneous addition of steam and CO_2	S	25% steam/25% CO_2 gasification	0	2.7	0	25%	25%	50%	74%	26%
	T	25% steam/25% CO_2/2.5% air gasification	0.04	2.7	2.5%	25%	25%	47.5%	72%	28%
	U	25% steam/25% CO_2/9.5% air gasification	0.14	2.7	9.5%	25%	25%	40.5%	67%	33%
	V	25% steam/25% CO_2/25% air gasification	0.36	2.7	25%	25%	25%	25%	55.5%	44.5%

The experiment started with loading the bed material (silica sand) of 500 g, corresponding to a static height of 100 mm, and with supplying the fluidizing gas. The reactor was then heated up at a heating rate of 10 ℃/min. The setting temperature is determined based on the preliminary tests that the bed temperature would be kept to a stable level of 850℃ after the straw particles feeding started. When the bed temperature reached a stable level, the feeder started with a set point of 0.11 kg/h (on a dry basis). The experiment would continuously proceed until defluidization occurred, which is indicated by a sudden decrease in pressure drop over the bed as illustrated in Figure 3-2. It is also shown that the temperature difference between the two thermocouples at different positions in the bed became significant when the bed approached the defluidization state, indicating a worsening mixing in the bed due to the formation of agglomerates. Previously, the agglomeration tendency was indicated in term of defluidization time[13], which is defined as the time when defluidization occurs after fuel feeding starts. In this work, the amount of fuel fed to the reactor until defluidization occurs is used to evaluate the agglomeration tendency for elimination of the errors caused by the fluctuation of the feeder. As soon as defluidization occurred, fuel feeding was stopped. The primary gas was shifted to N_2 in order to keep the remained carbon in the bed unreacted. The heating elements were switched off. After the reactor was cooled to the ambient temperature, the bed material was taken from the reactor for further analysis and characterization. Some of the experiments have been duplicated and Experiment A was repeated for four times. A good repeatability has been shown with a standard deviation of less than 3 g (see Figure A-4 in Appendix A).

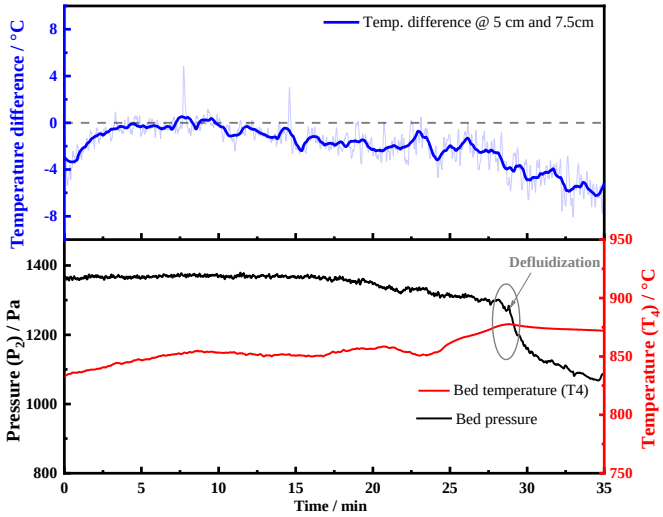

Figure 3-2 Diagram of determination of defluidization during gasification with an ER of 0.14 and a SFR of 1.15.

3.2.4 Characterization

Selected agglomerate samples taken from cold reactor were analyzed by Scanning Electron Microscopy (QUANTA FEG 250) with Energy X-ray (SEM-EDX) to obtain the information of the morphology and compositions. All samples were carbon-coated in the pretreatment to reduce the charging of samples.

3.2.5 Thermodynamic equilibrium calculations

For studying the influence of the atmosphere in the bed at various ERs, it is desirable to obtain the information of the gas compositions at different ERs. However, it is not possible to measure the gas composition inside the bubbling bed in the present setup due the overall stoichiometry for combustion is 1.45 by introducing the secondary gas in all experiments. Therefore, such information is unknown. Thermodynamic equilibrium calculations were performed with respect to the product distribution by using FACTSAGE 7.2 package, as estimations for the atmosphere in the bed. The K-species distribution in the bed was also carried out. The FToxid, FTsalt, FactPS, and FTpulp databases and FToxid-SLAGA solution phase were chosen for the calculations[44]. The input data was calculated based on the straw and primary gas compositions, as well as a dry basis feeding rate of 0.11 kg/h and a primary gas flow rate of 11.5 Nl/min. The silica sand amount is in a larger excess, corresponding to the molar ratio of SiO_2/K is 100. The calculations were performed at a temperature of 850 °C.

3.3 Results

The influence of the equivalence ratio (ER) on the agglomeration tendency was studied experimentally with and without addition of steam and CO_2. The results of experiments, equilibrium calculations and characterization of agglomerate samples are presented in this section.

3.3.1 Agglomeration tendency in an air blown system

Figure 3-3 shows the amount of fed fuel at occurrence of defluidization as a function of ER, covering the spectrum from gasification to combustion (Experiments A-E) in the air blown system. As previously described, the agglomeration tendency is indicated by the amount of straw fed until defluidization occurs. A high amount of straw fed to the reactor at the point of occurrence of defluidization indicates a low agglomeration tendency and vice versa. When the value of ER is higher than unity (right two points in Figure 3-3), the bubbling bed is operated in combustion region. The left three points are operated in gasification region. The results indicate that the agglomeration tendency is gradually increased when the reaction region shifts from combustion to gasification region to an ER value of around 0.35, which is within the typical range for auto-thermal air blown gasification[45]. When ER is further decreased, the agglomeration tendency would be decreased. Such phenomenon is new and has not been reported in literature from authors' knowledge. The existence of a maximum agglomeration tendency with respect to ER may be caused by two competing factors. The mechanisms behind the phenomenon will be explored and discussed in the discussion section of the paper.

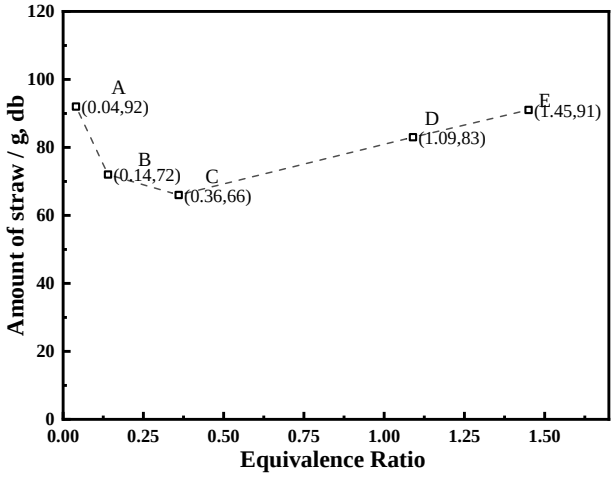

Figure 3-3 Amount of dry basis straw fed for inducing defluidization at various equivalence ratios in an air blown system.

3.3.2 Influence of steam on agglomeration tendency

The influence of the presence of steam was studied by replacing a part of N_2 flow with the same volume flow of steam in the primary gas with desired steam to fuel ratios (SFRs). The amount of straw fed at defluidization during gasification as a function of SFR with different ERs are presented in Figure 3-4. The results indicate that the agglomeration tendency is increased when steam is added to the bed. The results are in agreement with those reported by Ma *et al.*[34,46], who found that the defluidization temperatures are decreased in steam atmosphere for the ashes from different biomass and model compounds of potassium. It appears that a further increase of SFR from 1.15 to 2.3 will not affect the agglomeration tendency for the gasification with an ER of 0.14 and 0.36. However, the agglomeration tendency increases with a further increased SFR for very low ERs (0 and 0.04). At a high concentration of steam (SFR of 2.3, corresponding to an inlet steam concentration of 50 vol.%), the agglomeration tendency is very close for the ER in the range of 0.04 - 0.36.

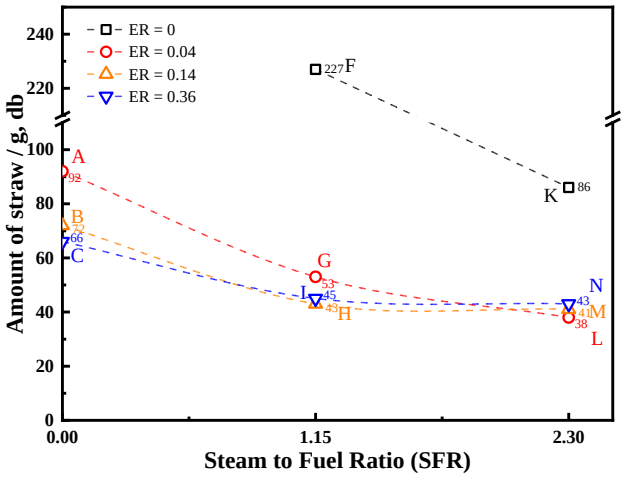

Figure 3-4 Amount of dry basis straw fed for inducing defluidization during gasification as a function of steam to fuel ratio at an equivalence ratio in the range of 0 - 0.36.

3.3.3 Influence of CO_2 on agglomeration tendency

The addition of CO_2 to the primary gas stream was done in the same way as the addition of steam. The influence of CO_2 was examined by two cases: 25 vol.% of CO_2 was added to the primary gas stream without addition of steam and with addition of 25 vol.% of steam (corresponding to an SFR of 1.15). The comparison of all cases is presented in Figure 3-5. It is shown that the effect of addition of CO_2 on the agglomeration tendency is insignificant although the agglomeration tendency appears slightly lower with addition of CO_2 than without CO_2 addition for both cases in the absence and the presence of steam.

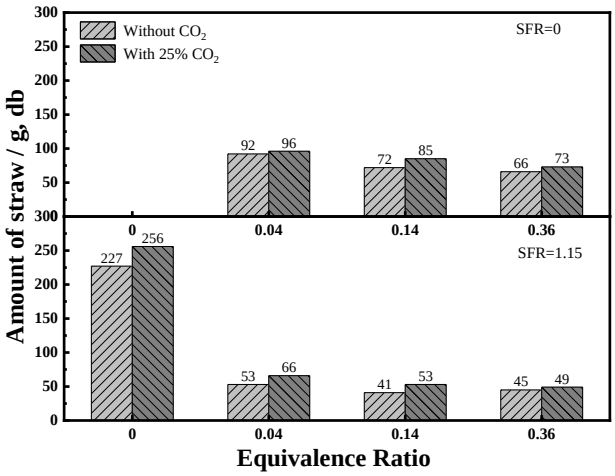

Figure 3-5 Impact of CO_2 on amount of dry basis straw fed for inducing defluidization during gasification with an equivalence ratio in the range of 0 – 0.36 (top: SFR = 0, bottom: SFR = 1.15).

3.3.4 Summary of all fluidized bed experiments

All the results from the experiments in the fluidized bed on the agglomeration tendency of wheat straw are summarized in Figure 3-6. The results show that the influence of ER on agglomeration tendency for all cases follows the same trend as the air blown system, i.e. the agglomeration tendency (indicated by the amount of fuel fed to the bed at defluidization) increases to a maximum value with decreasing ER and decreases with further decreasing ER. The values of ER, at which agglomeration tendency is the highest, are between 0.14 and 0.36 for the most of the cases except for the case with a high steam concentration (SFR of 2.3), at which the ER is 0.04. When CO_2 is added, the agglomeration tendency is slightly decreased comparing to that without addition of CO_2, for both with and without addition of steam. Such influence may be caused by the fact that the presence of high concentration of CO_2 will slow down the reaction between potassium carbonate and silicon oxide (e.g., quartz sand)[47], which may result in a reduced formation of low-melting temperature potassium silicates. The addition of steam results in an increased agglomeration tendency, and the impact of steam becomes more pronounced by lowering the ER.

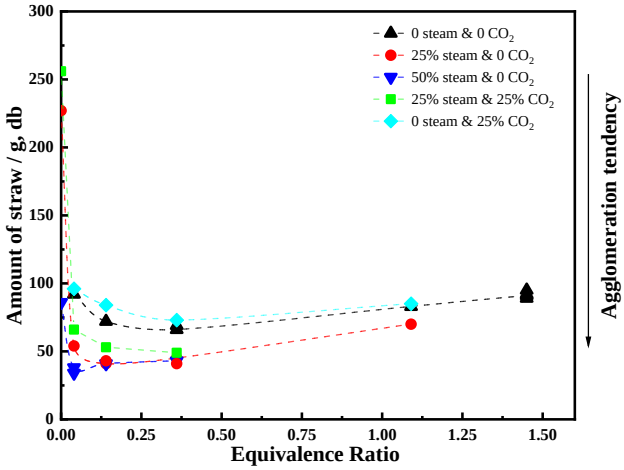

Figure 3-6 Amount of dry basis straw fed for inducing defluidization in the performed experiments.

3.3.5 Residual char in the bed

It was noticed that different amounts of residual char were present in the bed, when taking out the bed material after experiments. Figure 3-7 shows the appearances of three samples from the bed in combustion with an ER value (air ratio) of 1.45 (a), in gasification with an ER of 0.14 and a SFR of 1.15 (b), and in gasification with an ER of 0 and SFR of 1.15 (c). The visual observation of the samples seems to indicate that the amount of residual char in the bed increases with decreasing ER. The carbon content of selected bed samples was measured by heating the sample in a furnace at 550 °C under air condition for 3 hours, and the weight loss of sample after heated was considered as the carbon amount in the sample. The carbon conversion in each case was calculated by dividing the amount of unconverted carbon in the bed sample to the theoretical carbon amount in the fed straw. The calculated carbon conversion may be overestimated due to the elutriation of fine char particles during experiment and the loss of bed material during sampling. The results of the carbon content, the carbon conversion and the fed straw amount for these three cases are summarized in Table 3-4, which confirm the visual observation that a decrease in ER results in an increase in the amount of char residual, i.e. carbon content. The results in Table 3-4 also show that the highest carbon content corresponds to the highest amount of fed straw, i.e. the lowest agglomeration tendency, which indicates that the amount of carbon in the bed may affect the agglomeration tendency. In addition, it is noticed that the bed sample taken from the condition with an ER of 0 looks much darker than other two samples, implying that many soot particles may coated on the sand surface. The role of carbon in the bed will be discussed in Section 3.4.

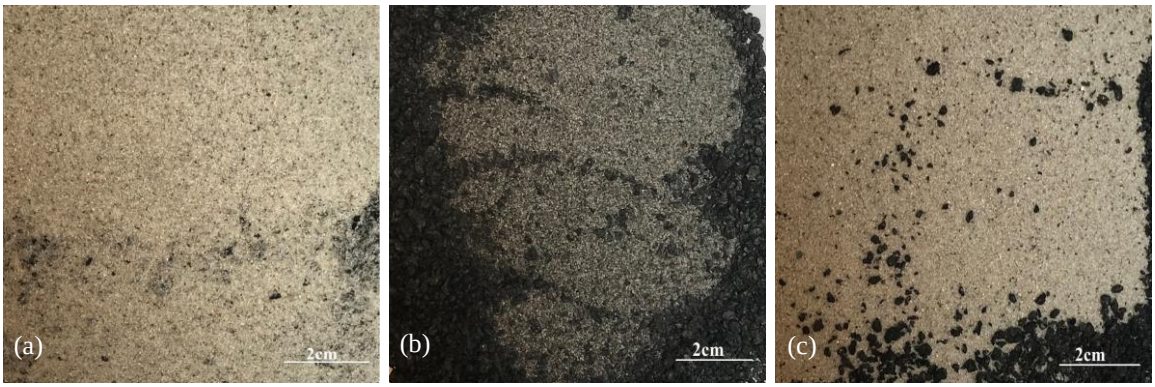

Figure 3-7 Bed samples taken from the cold reactor under condition of (a) ER = 1.45 & SFR = 0, (b) ER = 0 & SFR = 1.15, and (c) ER = 0.14 & SFR = 1.15.

Table 3-4 Carbon content, carbon conversion, and amount of fed straw for the cases shown in Figure 3-7

Exp. No.	ER = 1.45 & SFR = 0	ER = 0.14 & SFR = 1.15	ER = 0 & SFR = 1.15
Amount of unconverted carbon in the bed (g)	0.25	1.87	14.44
Carbon conversion (%)	99.34	89.39	85.13
Amount of fed straw (g, db)	91	43	227

3.3.6 Morphology and elemental composition of agglomerate samples

The morphology of silica sand, which was used as the bed material before experiments, and the agglomerates sampled from combustion with an ER of 1.45, from gasification with an ER of 0.14 and a SFR of 1.15, and from gasification with an ER of 0 and SFR of 1.15 are examined by SEM-EDX analysis. The results are shown in Figure 3-8 and Table 3-5. The EDX results are presented on a carbon and oxygen free basis, due to the fact that the samples are carbon coated for better images. The morphology of the raw silica sand particles (Figure 3-8-a) shows a smooth and clean surface that containing almost 100% Si (Spot A-1). The agglomerates sampled from gasification with an ER of 0.14 and a SFR of 1.15 (Figure 3-8-b) show a relatively homogeneous surface with unevenly coated ash. The EDX results of the spots on the smooth surface (Spot SA-1) and on the ash surface (Spot SA-2) indicate the similar compositions of mainly the melting potassium silicates. The morphologies and EDX analyses of the agglomerates sampled from combustion with an ER of 1.45 and gasification with an ER of 0 and SFR of 1.15 show a low potassium coated surface, with attached flocculent ash (Figure 3-8-c and 3-8-d). The main compositions of the flocculent ash (Spot C-2 and S-2) are Si, K, Ca, Mg and P, similar to those in Table 3-1. The K/Si molar ratio on the surfaces of the agglomerates (Spots SA-1, C-1 and S-1) decreases in the order of: gasification with an ER of 0.14 and SFR of 1.15 > combustion with an ER of 1.45 > gasification with an ER of 0 and SFR of 1.15, which is same as the decreasing trend of the agglomeration tendency observed in the defluidization experiments.

Humps are observed on the surface of samples taken from combustion with an ER of 1.45 and gasification with an ER of 0 and SFR of 1.15 when the magnification is further increased (Figure 3-8-e and 3-8-f). The humps (Spot C-3) formed during combustion with an ER of 1.45 may be the ash particles that immersed in the thin homogenous coating layer, suggested by its main compositions,

which is completely different with sand surface (Spot C-4). However, the humps (Spot S-3) show almost same compositions with the sand surface (Spot S-4) for the agglomerates from gasification with an ER of 0 and SFR of 1.15, leading to a speculation that these humps may be fine carbon particles. However, the speculation cannot be confirmed by the EDX analysis due to the carbon coating of samples.

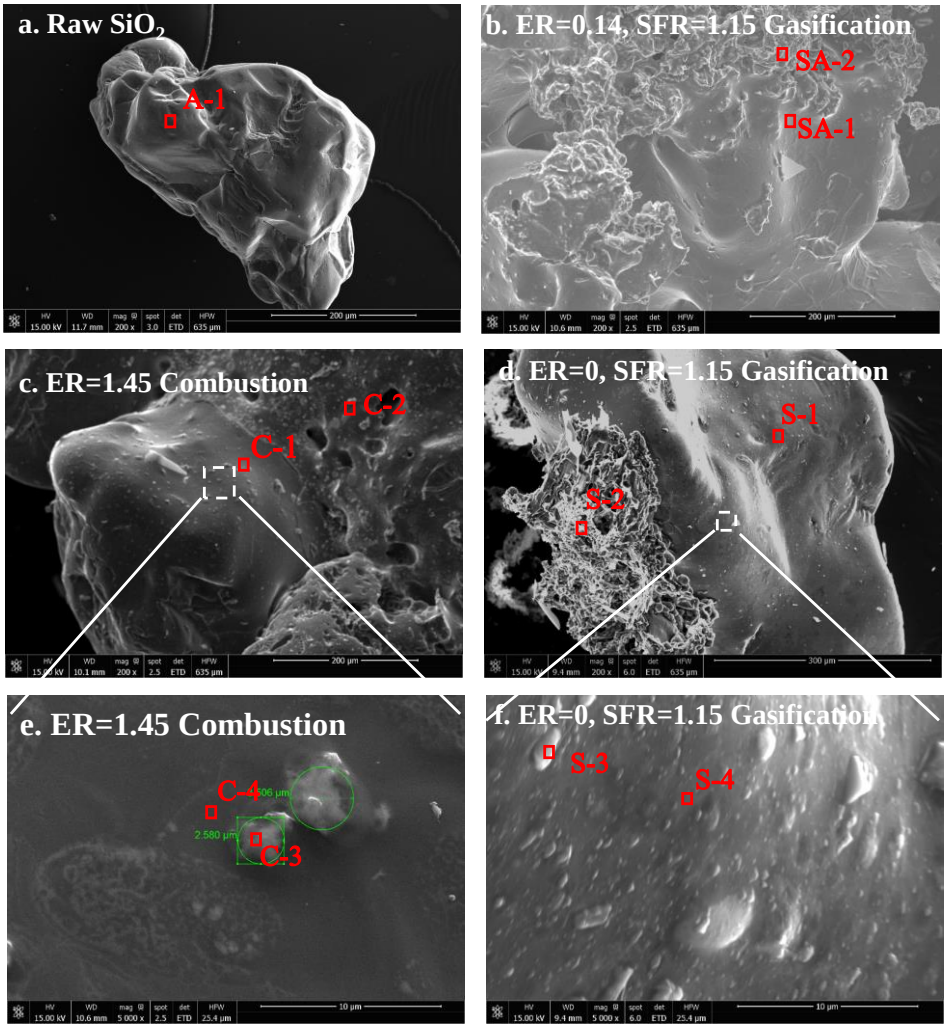

Figure 3-8 Morphology (SEM: SE mode) of (a) raw silica sand, and agglomerates sampled (b) from gasification with an ER of 0.14 and a SFR of 1.15, (c) and (e) from combustion with an ER of 1.45, as well as (d) and (f) from gasification with an ER of 0 and SFR of 1.15.

Table 3-5 EDX analysis of selected point of the agglomerates shown in Figure 3-8 (atom% on C-O-free basis)

	A-1	SA-1	SA-2	C-1	C-2	C-3	C-4	S-1	S-2	S-3	S-4
Si	99.51	41.61	51.02	85.53	36.95	66.22	88.59	91.27	6.88	89.58	90.46
K	0.00	41.61	33.37	12.02	26.8	16.07	8.44	7.67	52.80	7.64	6.44
Ca	0.00	8.07	10.60	1.12	17.4	8.86	1.58	0.00	22.05	0.63	0.59
Mg	0.00	3.01	1.33	0	4.56	2.09	0.30	0.00	5.97	0.27	0.33
P	0.00	3.32	2.05	0.49	8.81	6.01	0.30	0.00	9.56	0.27	0.17
K/Si	0.00	1.00	0.65	0.14	0.73	0.24	0.10	0.08	7.67	0.09	0.07

3.3.7 Thermodynamic equilibrium calculations

As explained in Section 3.2.5, the thermodynamic equilibrium calculations are used to estimate the distribution of products. Figure 3-9 shows the concentrations of the producer gas and carbon as a function of ER from the equilibrium calculations at 850 °C. The gaseous products are mainly comprised of O_2, CO_2, H_2O, and N_2 at ERs above 1 with an overall oxidizing condition. For the conditions with ER below 1, the gas environment is predominantly composed of H_2, CO, CO_2, H_2O, and N_2, implying a reducing atmosphere. A decrease in the ER value leads to an increased concentrations of CO and H_2, suggesting a stronger reducing atmosphere. When the ER is lower than 0.16, carbon is present in the products and will increase with a decrease of RE. Figure 3-10 shows that an increase in SFR results in an increase in formation of H_2 and CO_2, due to the water gas shift reaction. In addition, it is shown that the carbon will decrease with an increase of steam and carbon dioxide.

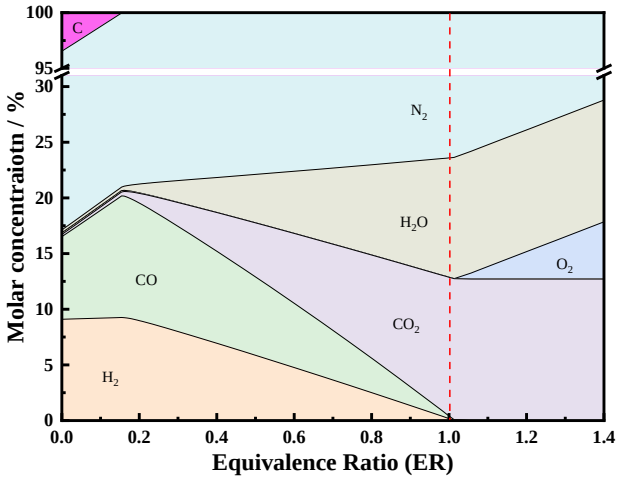

Figure 3-9 Impact of equivalence ratio on the thermodynamic equilibrium calculations of relative distribution of elemental C, CO, CO_2, H_2, O_2, H_2O, and N_2 at 850 °C.

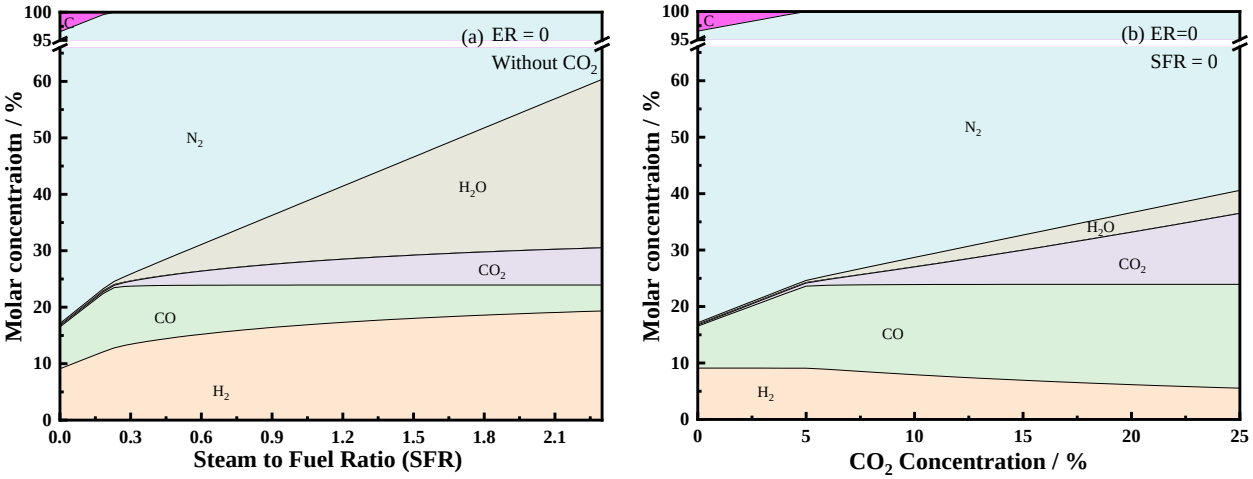

Figure 3-10 Impact of (a) steam to fuel ratio and (b) CO_2 concentration on the thermodynamic equilibrium calculations of relative distribution of elemental C, CO, CO_2, H_2, O_2, H_2O, and N_2 at 850 °C.

Figure 3-11 shows the influences of ER, SFR, and CO_2 concentrations on the K-species distribution at 850 °C by the equilibrium calculations. The results show that the amount of K_2O containing slag phase, which is K silicates indicated by the compositions of slag phase given in Figure A-5 in Appendix A, is increased when the condition is shifted from combustion to gasification due to the fact that K_2SO_4 is not stable at reducing atmosphere. A slight decrease of the slag phase with a decrease of ER is observed from the calculation due to the increased formation of gas phase KCl, which cannot explain the agglomeration tendency observed from the experiments. The steam and CO_2 show a minor effect on the amount of K_2O containing slag phase, which is indirectly influenced by the decreased amount of gas phase KCl.

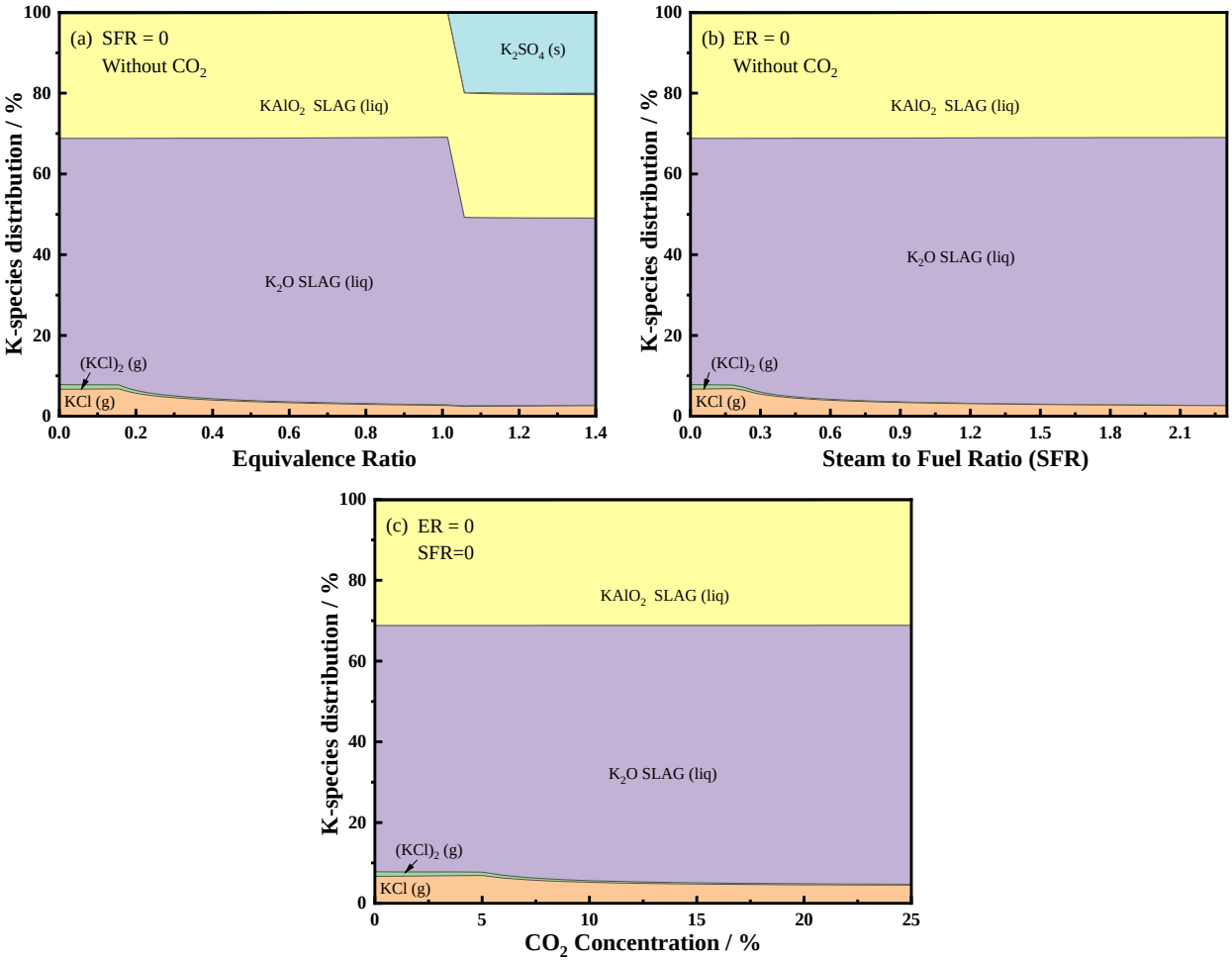

Figure 3-11 Impact of (a) equivalence ratio, (b) steam to fuel ratio and (c) CO_2 concentration on the thermodynamic equilibrium calculation of K-species distribution at 850 °C.

3.4 Discussion

The systematically experimental study reveals that the agglomeration tendency in gasification is higher than that in combustion for wheat straw in general. However, the agglomeration tendency will be significantly reduced at a very low ER. The agglomeration tendency is characterized by an increase as ER decreases first, reaching a maximum, followed by a decrease as ER increases. The ER, at which

the agglomeration tendency is maximal, will shift to the lower value when steam is added. These newly discovered phenomena are related to the reaction atmosphere, the presence of carbon (char) and the presence of steam, which will be discussed in the following sections.

3.4.1 Reducing atmosphere

The thermodynamic equilibrium calculations indicate that the amount of molten slag phase potassium silicates increases when the condition shifts from oxidizing to reducing, i.e. the potassium sulfate formed at oxidizing condition will be transformed to potassium silicate with low-melting temperature. This indication agrees with the experimental results by Ma *et al.*[46]. The high fusion of ash may be ascribed to the transformation of K_2SO_4 into K silicates and the increase in the reactivity of K_2CO_3, which is an important K-species during biomass gasification and combustion due to its significant amount[48], toward silica sand under reducing atmosphere[46]. However, the results from equilibrium calculation are not able to explain the fact that the agglomeration tendency gradually increases with decreasing ER. It is speculated that the fusion behavior of the ash may be correlated to the reducing degree that is related to the concentration of reducing agents, such as hydrogen and carbon monoxide, and is reaction rate controlled, though no evidence support it. Further studies are needed for more understanding.

3.4.2 Influence of char residuals (unconverted carbon) on the agglomeration

The visual observation of the bed materials and equilibrium calculations show the existence of unconverted carbon at low ERs, which is correlated to the significant reduction of the agglomeration tendency, shown in Figure 3-6. Intuitively, the presence of char particles may prevent the particles from sticking together. In order to examine the influence of char particles on agglomeration tendency, a few stepwise gasification experiments were performed. In the first step, around 50 g of straw was continuously fed into reactor using a mixture of 25 vol.% steam and 75 vol.% N_2 as primary gas, resulting in a certain amount of char accumulated in the bed. In the second step, straw feeding was stopped and the primary gas was either shifted to a nitrogen stream, or kept with the mixture of 25 vol.% steam and 75 vol.% N_2, or shifted to a mixture of 25 vol.% air and 75 vol.% N_2. The carbon converted in the second step were indicated by the outlet concentrations of CO or CO_2. The experiments were continued until the occurrence of defluidization or for about half hour if no defluidization was observed.

The results of these experiments are illustrated in Figure 3-12. The defluidization tendency is strongly affected by the type of the primary gas supplied in the second step. When the gas was shifted to nitrogen, the outlet concentrations of CO and CO_2 were quickly dropped to zero, indicating that no further conversion of the accumulated carbon. No defluidization was observed in 35.5 min in this case. When the mixture of 25 vol.% steam and 75 vol.% N_2 remains un-shifted, the outlet concentration of CO_2 was dropped to a low level and decreased slowly, indicating a slow conversion

of accumulated carbon. The defluidization occurred in 7 min when the carbon content in the bed is low in this case. Once the primary gas was shifted to a mixture of 25 vol.% air and 75 vol.% N_2, the defluidization occurred in 2 min accompanied by a fast conversion of the carbon in the bed. During the gas stream sifting, the bed temperature was kept unchanged, indicating that the occurrence of defluidization is caused by reduction of the carbon content in the bed. These results confirm that the accumulated char in the bed could inhibit the agglomeration process. It has been reported that the presence of residual carbon in the ash can significantly increase of the fusion temperatures and reduce the melting flow behaviors of biomass ash[49] and coal ash[50]. In addition, the occurrence of adhesion of carbon onto bed solids, indicated by the SEM image in Figure 3-8, may inhibit the formation of agglomerates upon the interaction between ash and bed material.

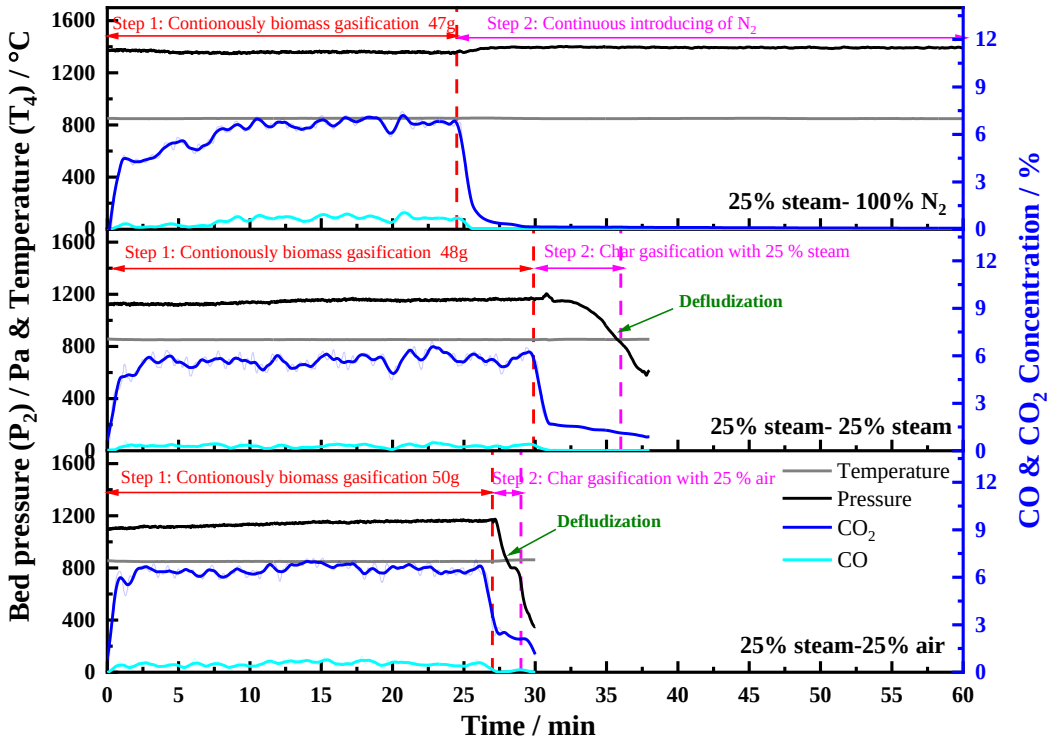

Figure 3-12 Bed temperature (T_4), bed pressure (P_2) and the concentrations of CO and CO_2 in flue gas during stepwise gasification.

3.4.3 Effect of steam

The experimental results in Figure 3-4 show that the presence of a high concentration of steam promotes the agglomeration tendency. This is partly due to the enhanced gasification rate at low ERs, leading to the low carbon content. Another reason may be caused by the effect of steam on the viscosity of the molten phase. It was reported that the presence of steam (water vapor) can significantly affect the viscosity of the coal ash slag from gasification[51–53]. The SEM-EDX analysis in Figure 3-8 shows the significant amount of potassium silicate melting on the surface sand from combustion and gasification. Experiments were performed to exam the effect of steam on the fusion behaviors of potassium silicates ($K_2Si_4O_9$). The $K_2Si_4O_9$ pellets with the mass of around 1 g were

placed in a crucible and heated in a fixed bed reactor under the conditions of 100% air and a mixture of 50 vol.% steam and 50 vol.% N_2 at 850 °C for 3 hours. The appearances of the pellets after heated are shown in Figure 3-13. Significant deformation of the $K_2Si_4O_9$ pellets after heating is observed, indicating that the pellets have been molten. It is noticed that the area of the pellets heated in the atmosphere with a high concentration of steam is larger than that in air condition, indicating a high fusion degree of the $K_2Si_4O_9$ pellets in steam or a low viscosity in molten phase. It is reported that for the viscous and glassy slag contains high silica content, which is expected to have a three-dimensional network silicate structure, the addition of water vapor could lower its viscosity due to the depolymerization of the melt[54–56]. It is attributed to the diffusion of water vapor into silica glass and the formation of Si-OH groups via reaction between water and the silicon-oxygen network, according to the following equation[57,58]:

$$-\mathrm{Si}-\mathrm{O}-\mathrm{Si}-\ +H_2O\ \ \rightarrow 2-\mathrm{SiOH}$$

This results provide one of the mechanisms of the influence of steam on the agglomeration tendency observed in the experiments.

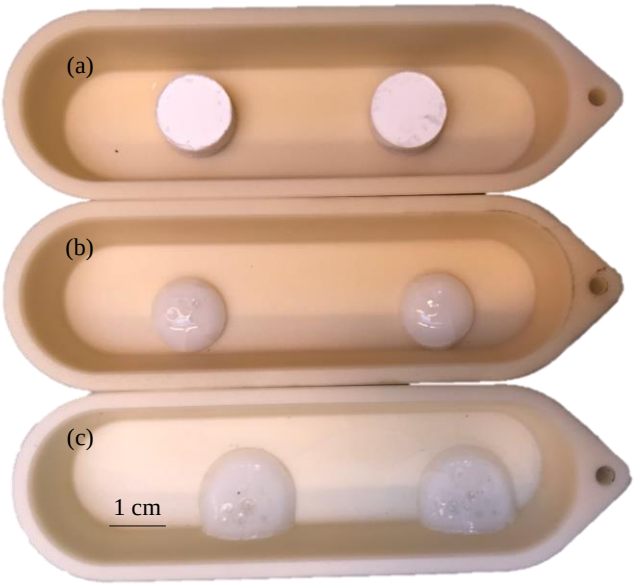

Figure 3-13 $K_2Si_4O_9$ pellets (a) before and after heating for 3 hours at 850 °C in a fixed bed reactor under (b) 100% air and (c) 50 vol.% steam and 50 vol.% N_2.

3.4.4 Role of in-bed high concentration CO_2

The addition of 25 vol.% of CO_2 in primary gas stream slightly slows down the agglomeration tendency when the ER and the steam concentration in the primary gas are constant (Figure 3-5). The reason is not clear, and may be partially attributed the slower reaction rate between K_2CO_3 and silica sand with presence of CO_2 [47]. The detailed mechanism need to be further studied.

3.4.5 Plausible mechanism for agglomeration in fluidized bed gasification of wheat straw

Based on the experimental results and discussion, a plausible mechanism for agglomeration in fluidized bed gasification of wheat straw with respect to the effect of ER and steam is proposed, as illustrated in Figure 3-14.

When ER is decreased, the amount of molten phase increases, leading to an increased agglomeration tendency, while the amount of residual char in the bed also increases, inhibiting the agglomeration tendency. These two competing factors result in the existence of a maximal agglomeration tendency, at which the ER can be defined as the critical ER. The influence of carbon is dominant at an ER lower than the critical ER, whilst the influence of reducing atmosphere is dominant at an ER higher than the critical ER. Such mechanism applies to all the experimental results in this work.

When steam is added, the critical ER value will shift to a lower value, which is due to the fact that the carbon content at the same ER will be lower than without addition of steam because of an enhanced carbon conversion. In addition, the increased steam concentration will result in a reduced viscosity of the molten potassium silicates, coated on the sand surfaces, which can increase the agglomeration tendency.

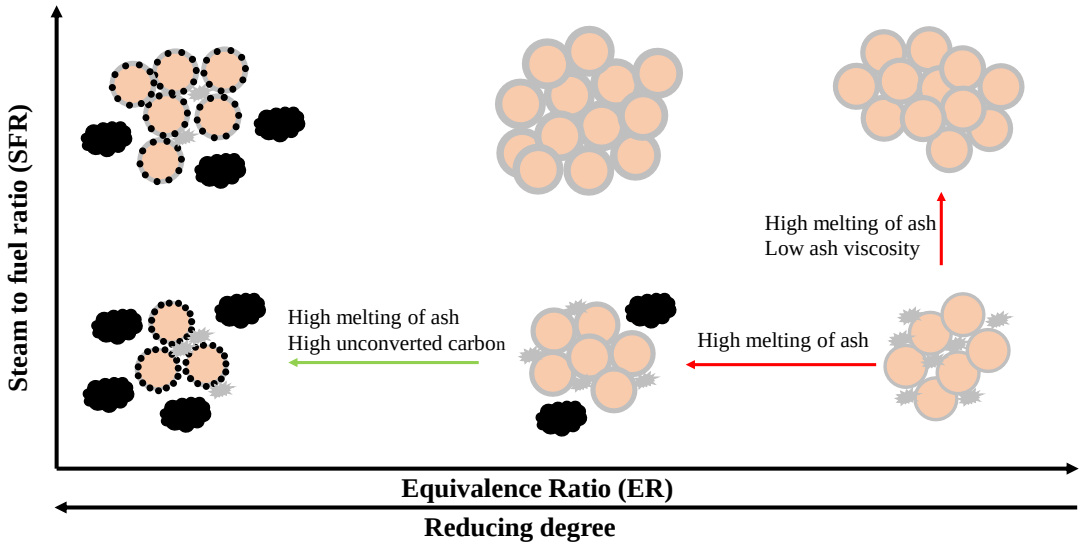

Figure 3-14 A plausible agglomeration mechanism of wheat straw during gasification in fluidized bed.

3.5 Conclusions

Systematic experiments have been conducted in a lab-scale fluidized bed reactor the study the agglomeration phenomena in biomass gasification with a focus on the effect ER and SFR. The following conclusions can be drawn from the study:

(1) The agglomeration tendency of wheat straw in fluidized bed is strongly influenced by the ER. The agglomeration tendency increases first to the maximal tendency with a decrease of ER, and then the agglomeration tendency decreases with the further deceasing ER. A decrease in ER will result in an increase both in the degree of reducing atmosphere and the amount of unconverted carbon, which will promote the agglomeration and mitigate the agglomeration, respectively. The competition between these two factors results in a maximal agglomeration tendency occurs at a critical ER. A reducing atmosphere formed during gasification could accelerate the agglomeration probably due to its promotive effect on the melting tendency of ash. The residual carbon may reduce the fusion tendency and the melting flow behaviors of the ash, and the carbon attached on the sand surface may inhibit the agglomeration by preventing the interaction between ash and bed material, thus mitigating the agglomeration tendency.

(2) The gasification agents affect the agglomeration tendency of wheat straw in the fluidized bed gasification. The presence of steam in primary gas significantly promotes the agglomeration. The promoted agglomeration under a high concentration of steam may be attributed to a higher carbon conversion, i.e. a lower amount of residual carbon, and a lowered ash viscosity induced by water vapor. An increase in steam concentration will result in a decrease in critical ER value due to a reduced inhibition effect of residual carbon resulting from a decreased amount of residual carbon. The addition of CO_2 in primary gas slightly mitigates the agglomeration. The detailed mechanism of influence of CO_2 on agglomeration need to be further studied.

Reference

(1) Anthony, E. J. Fluidized Bed Combustion of Alternative Solid Fuels; Status, Successes and Problems of the Technology. *Prog. Energy Combust. Sci.* **1995**, *21* (3), 239–268.

(2) Khan, A. A.; de Jong, W.; Jansens, P. J.; Spliethoff, H. Biomass Combustion in Fluidized Bed Boilers: Potential Problems and Remedies. *Fuel Process. Technol.* **2009**, *90* (1), 21–50.

(3) Motta, I. L.; Miranda, N. T.; Maciel Filho, R.; Wolf Maciel, M. R. Biomass Gasification in Fluidized Beds: A Review of Biomass Moisture Content and Operating Pressure Effects. *Renew. Sustain. Energy Rev.* **2018**, *94* (May), 998–1023.

(4) Visser, H. J. M.; Hofmans, H.; Huijnen, H.; Kastelein, R.; Kiel, J. H. A. Biomass Ash - Bed Material Interactions Leading to Agglomeration in Fluidised Bed Combustion and Gasification. *Prog. Thermochem. Biomass Convers.* **2008**, 272–286.

(5) Öhman, M.; Pommer, L.; Nordin, A. Bed Agglomeration Characteristics and Mechanisms during Gasification and Combustion of Biomass Fuels. *Energy & Fuels* **2005**, *19* (4), 1742–1748.

(6) Lin, W.; Jensen, A. D.; Johnsson, J. E.; Dam-Johansen, K. Combustion of Biomass in Fluidized Beds: Problems and Some Solutions Based on Danish Experiences. In *Proceedings of the 17th International Conference on Fluidized Bed Combustion*; American Society of Mechanical Engineers: Jacksonville, Florida USA, 2003; pp 945–953.

(7) Öhman, M.; Nordin, A.; Skrifvars, B. J.; Backman, R.; Hupa, M. Bed Agglomeration Characteristics during Fluidized Bed Combustion of Biomass Fuels. *Energy & Fuels* **2000**, *14* (1), 169–178.

(8) Brus, E.; Öhman, M.; Nordin, A. Mechanisms of Bed Agglomeration during Fluidized-Bed Combustion of Biomass Fuels. *Energy & Fuels* **2005**, *19* (3), 825–832.

(9) Visser, H. J. M. M.; van Lith, S. C.; Kiel, J. H. A. a. Biomass Ash-Bed Material Interactions Leading to Agglomeration in FBC. *J. Energy Resour. Technol.* **2008**, *130* (1), 1–6.

(10) Chirone, R.; Salatino, P.; Scala, F.; Solimene, R.; Urciuolo, M. Fluidized Bed Combustion of Pelletized Biomass and Waste-Derived Fuels. *Combust. Flame* **2008**, *155* (1–2), 21–36.

(11) Visser, H. J. M. H. J. M. The Influence of Fuel Composition on Agglomeration Behaviour in Fluidised-Bed Combustion. *ECN Rep. ECN-C–04-054* **2004**.

(12) Lin, W.; Krusholm, G.; Dam-Johansen, K.; Musahl, E.; Bank, L. Agglomeration Phenomena in Fluidized Bed Combustion of Straw. In *Proceedings of the 14h International Conference on Fluidized Bed Combustion*; American Society of Mechanical Engineers: Canada, 1997; Vol. 2, pp 831–837.

(13) Lin, W.; Dam-Johansen, K.; Frandsen, F. Agglomeration in Bio-Fuel Fired Fluidized Bed Combustors. *Chem. Eng. J.* **2003**, *96* (1–3), 171–185.

(14) Chaivatamaset, P.; Tia, S. The Characteristics of Bed Agglomeration during Fluidized Bed

Combustion of Eucalyptus Bark. *Appl. Therm. Eng.* **2015**, *75*, 1134–1146.

(15) Davidsson, K. O.; Åmand, L. E.; Steenari, B. M.; Elled, A. L.; Eskilsson, D.; Leckner, B. Countermeasures against Alkali-Related Problems during Combustion of Biomass in a Circulating Fluidized Bed Boiler. *Chem. Eng. Sci.* **2008**, *63* (21), 5314–5329.

(16) De Geyter, S.; Öhman, M.; Boström, D.; Eriksson, M.; Nordin, A. Effects of Non-Quartz Minerals in Natural Bed Sand on Agglomeration Characteristics during Fluidized Bed Combustion of Biomass Fuels. *Energy & Fuels* **2007**, *21* (5), 2663–2668.

(17) Davidsson, K. O.; Steenari, B. M.; Eskilsson, D. Kaolin Addition during Biomass Combustion in a 35 MW Circulating Fluidized-Bed Boiler. *Energy & Fuels* **2007**, *21* (4), 1959–1966.

(18) Morris, J. D.; Sheraz, S.; Chilton, S.; Nimmo, W. Mechanisms and Mitigation of Agglomeration during Fluidize Bed Combustion of Biomass : A Review. *Fuel* **2018**, *230*, 452–473.

(19) Scala, F. Particle Agglomeration during Fluidized Bed Combustion: Mechanisms, Early Detection and Possible Countermeasures. *Fuel Process. Technol.* **2018**, *171*, 31–38.

(20) Bartels, M.; Lin, W.; Nijenhuis, J.; Kapteijn, F.; van Ommen, J. R. Agglomeration in Fluidized Beds at High Temperatures: Mechanisms, Detection and Prevention. *Prog. Energy Combust. Sci.* **2008**, *34* (5), 633–666.

(21) Gatternig, B.; Karl, J. Investigations on the Mechanisms of Ash-Induced Agglomeration in Fluidized-Bed Combustion of Biomass. *Energy & Fuels* **2015**, *29*, 931–941.

(22) Hupa, M. Ash-Related Issues in Fluidized-Bed Combustion of Biomasses : Recent Research Highlights. *Energy & Fuels* **2012**, *26*, 4–14.

(23) Yerushalmi, J.; Kolodney, M.; Graff, R. A.; Squires, A. M.; Harvey, R. D. Agglomeration of Ash in Fluidized Beds Gasifying Coal: The Godel Phenomenon. *Science (80-.).* **1975**, *187* (4177), 646–648.

(24) Ergudenler, A.; Ghaly, A. E. Agglomeration of Alumina Sand in a Fluidized Bed Straw Gasifier at Elevated Temperatures. *Bioresour. Technol.* **1993**, *43* (3), 259–268.

(25) Fryda, L. E.; Panopoulos, K. D.; Kakaras, E. Agglomeration in Fluidised Bed Gasification of Biomass. *Powder Technol.* **2008**, *181* (3), 307–320.

(26) Seemen, A.; Atong, D.; Sricharoenchaikul, V. Effect of Silica and Alumina Ratio on Bed Agglomeration during Fluidized Bed Gasification of Rice Straw. *Proc. - 2018 2nd Int. Conf. Green Energy Appl. ICGEA 2018* **2018**, 268–272.

(27) George, J.; Arun, P.; Muraleedharan, C. Experimental Investigation on Co-Gasification of Coffee Husk and Sawdust in a Bubbling Fluidised Bed Gasifier. *J. Energy Inst.* **2019**, *92* (6), 1977–1986.

(28) Kittivech, T.; Fukuda, S. Investigating Agglomeration Tendency of Co-Gasification between High Alkali Biomass and Woody Biomass in a Bubbling Fluidized Bed System. *Energies* **2020**,

13 (56), 1–15.

(29) Zhang, H.; Hao, Z.; Li, J.; Yang, X.; Wang, Z.; Liu, Z.; Huang, J.; Zhang, Y.; Fang, Y. Effect of Coal Ash Additive on Potassium Fixation and Melting Behaviors of the Mixture under Simulated Biomass Gasification Condition. *Renew. Energy* **2021**, *168*, 806–814.

(30) Zevenhoven-Onderwater, M.; Backman, R.; Skrifvars, B. J.; Hupa, M.; Liliendahl, T.; Rosén, C.; Sjöström, K.; Engvall, K.; Hallgren, A. The Ash Chemistry in Fluidised Bed Gasification of Biomass Fuels. Part I: Predicting the Chemistry of Melting Ashes and Ash-Bed Material Interaction. *Fuel* **2001**, *80* (10), 1489–1502.

(31) Arvelakis, S.; Gehrmann, H.; Beckmann, M.; Koukios, E. G. Agglomeration Problems during Fluidized Bed Gasification of Olive-Oil Residue : Evaluation of Fractionation and Leaching as Pre-Treatments. *Fuel* **2003**, *82*, 1261–1270.

(32) Zevenhoven-Onderwater, M.; Backman, R.; Skrifvars, B. J.; Hupa, M. The Ash Chemistry in Fluidised Bed Gasification of Biomass Fuels. Part II: Ash Behaviour Prediction versus Bench Scale Agglomeration Tests. *Fuel* **2001**, *80* (10), 1503–1512.

(33) Ergudenler, A.; Ghaly, A. E. Agglomeration of Silica Sand in a Fluidized Bed Gasifier Operating on Wheat Straw. *Biomass and Bioenergy* **1993**, *4* (2), 135–147.

(34) Ma, T.; Fan, C.; Hao, L.; Li, S.; Song, W.; Lin, W. Biomass-Ash-Induced Agglomeration in a Fluidized Bed. Part 1: Experimental Study on the Effects of a Gas Atmosphere. *Energy & Fuels* **2016**, *30* (8), 6395–6404.

(35) Nowok, J. W.; Kalmanovitch, D. P.; Benson, A.; Jones, L. Sintering Behaviour and Strength Development in Various Coal Ashes. *Fuel* **1990**, *69*, 1020–1028.

(36) Huffman, G. P.; Huggins, F. E.; Dunmyre, G. R. Investigation of the High-Temperature Behaviour of Coal Ash in Reducing and Oxidizing Atmospheres. *Fuel* **1981**, *60* (7), 585–597.

(37) Backman, R. Sintering of FBC Ashes. *Fuel* **1994**, *73* (2), 171–176.

(38) Bryant, G. W.; Browning, G. J.; Emanuel, H.; Gupta, S. K.; Gupta, R. P.; Lucas, J. A.; Wall, T. F. The Fusibility of Blended Coal Ash. **2000**, No. 5, 316–325.

(39) Song, W. J.; Tang, L. H.; Zhu, X. D.; Wu, Y. Q.; Zhu, Z. B. Prediction of Chinese Coal Ash Fusion Temperatures in Ar and H2 Atmospheres. *Energy & Fuels* **2009**, *23*, 1990–1997.

(40) Abra, M. G.; Ordin, A. N.; Iliedahl, T. L.; Ao, A. N. R. Experimental Determination of Bed Agglomeration Tendencies of Some Common Agricultural Residues in Fluidized Bed Combustion and Gasification. *Biomass and Bioenergy* **1998**, *15* (2), 163–169.

(41) Alauddin, Z. A. B. Z.; Lahijani, P.; Mohammadi, M.; Mohamed, A. R. Gasification of Lignocellulosic Biomass in Fluidized Beds for Renewable Energy Development: A Review. *Renew. Sustain. Energy Rev.* **2010**, *14*, 2852–2862.

(42) Yao, X.; Hu, Y.; Ge, J.; Ma, X.; Mao, J.; Sun, L.; Xu, K. K.; Xu, K. K. A Comprehensive Study on Influence of Operating Parameters on Agglomeration of Ashes during Biomass

Gasification in a Laboratory-Scale Gasification System. *Fuel* **2020**, *276*, 118083.

(43) Xue, G.; Kwapinska, M.; Horvat, A.; Li, Z.; Dooley, S.; Kwapinski, W.; Leahy, J. J. Gasification of Miscanthus x Giganteus in an Air-Blown Bubbling Fluidized Bed: A Preliminary Study of Performance and Agglomeration. *Energy & Fuels* **2014**, *28* (2), 1121–1131.

(44) Aničić, B. Agglomeration Mechanisms during Fluidized Bed Combustion of Biomass, Technical University of Denmark, 2018.

(45) Arena, U. Fluidized Bed Gasification. In *Fluidized Bed Technologies for Near-Zero Emission Combustion and Gasification*; Elsevier Ltd., 2013; pp 765–812.

(46) Ma, T.; Fan, C.; Hao, L.; Li, S.; Jensen, P. A.; Song, W.; Lin, W.; Dam-Johansen, K. Biomass Ash Induced Agglomeration in Fluidized Bed. Part 2: Effect of Potassium Salts in Different Gas Composition. *Fuel Process. Technol.* **2018**, *180*, 130–139.

(47) Anicic, B.; Lin, W.; Dam-Johansen, K.; Wu, H. Agglomeration Mechanism in Biomass Fluidized Bed Combustion – Reaction between Potassium Carbonate and Silica Sand. *Fuel Process. Technol.* **2018**, *173*, 182–190.

(48) Tchoffor, P. A.; Davidsson, K. O.; Thunman, H. Transformation and Release of Potassium, Chlorine, and Sulfur from Wheat Straw under Conditions Relevant to Dual Fluidized Bed Gasification. *Energy & Fuels* **2013**, *27* (12), 7510–7520.

(49) Dai, X.; Jin, B.; Lu, P.; Wang, X.; Huang, Y. The Role of Residual Carbon on Fusibility and Flow Properties of Rice Straw Ash. *Fuel* **2019**, *253* (May), 1512–1520.

(50) CHEN, D. xia; TANG, L. hua; ZHOU, Y. ming; WANG, W. mei; WU, Y. qiang; ZHU, Z. bin. Effect of Char on the Melting Characteristics of Coal Ash. *Ranliao Huaxue Xuebao/Journal Fuel Chem. Technol.* **2007**, *35* (2), 136–140.

(51) Folkedahl, B. C.; Schobert, H. H. Effects of Atmosphere on Viscosity of Selected Bituminous and Low-Rank Coal Ash Slags. *Energy & Fuels* **2005**, *19*, 208–215.

(52) Cao, X.; Kong, L.; Bai, J.; Ge, Z.; Li, H.; Bai, Z. Effect of Water Vapor on Coal Ash Slag Viscosity under Gasification Condition. *Fuel* **2019**, *237*, 18–27.

(53) Kong, L.; Bai, J.; Li, W. Viscosity-Temperature Property of Coal Ash Slag at the Condition of Entrained Flow Gasification: A Review. *Fuel Process. Technol.* **2021**, *215* (November 2020), 106751.

(54) Buerger, M. J. The Role of Temperature in Mineralogy. *Am. Mineral.* **1948**, *33* (3–4), 101–121.

(55) Fisher, R. V.; Schmincke, H.-U. *Pyroclastic Rocks*; Springer-Verlag, 1984.

(56) Brown;, G. M. Melting Relations of Tertiary Granitic Rocks in Skye and Rhum. *Mineral. Mag. J. Mineral. Soc.* **1963**, *33* (262), 533–562.

(57) Shelby, J. E. *Handbook of Gas Diffusion in Solids and Melts*; ASM International, 1996.

(58) Doremus, R. H. Diffusion of Water in Silica Glass. *J. Mater. Res.* **1995**, *10* (9), 2379–2389.

4. Fusion Behavior of Wheat Straw Ash under Combustion and Gasification Conditions

Abstract

The fusion behavior of biomass ash affects the agglomeration tendency in fluidized bed combustion and gasification. In this chapter, the fusion behaviors of the ashes from wheat straw, as well as a mixture of wheat straw and silica sand, were investigated in a fixed bed reactor at 850 C under the atmospheres of 100% air, a mixture of 50 vol.% steam and 50 vol.% air, and a mixture 50 vol.% of steam and 50 vol.% N_2. Visual observation and scanning electron microscopy with energy-dispersive X-ray spectroscopy (SEM-EDX) analysis show that the fusion tendency of the ashes obtained from wheat straw under gasification conditions is higher than that under combustion conditions. In addition, the fusion tendency of the ash from combustion with presence of a high concentration of steam is higher than that from normal combustion. The results indicate that a reducing atmosphere and a high concentration of steam will promote the fusion behaviors of the wheat straw. The fusion tendency of ashes from a mixture of wheat straw and silica sand is consistent with the fusion tendency of ashes from wheat straw. The mixture that contains the ash with a highest fusion tendency shows a most severe agglomeration tendency. The fusion tendency of the wheat straw ash under combustion and gasification conditions is consistent with the agglomeration tendency that has been observed in fluidized bed combustion and gasification of wheat straw in Chapter 3.

4.1 Introduction

In Chapter 3, it is found that the agglomeration in fluidized bed gasification of wheat straw is accelerated by a reducing atmosphere and a high concentration of steam in the bed. Since the fusibility of ash has been considered as a key parameter affecting agglomeration tendency[1–3], evaluating the fusion behavior of wheat straw ash under combustion and gasification conditions may provide an improving understanding of agglomeration.

The fusibility of ash has been extensively investigated by various methods, such as standard ash fusion temperatures (AFTs) test[4,5], thermal mechanical analysis (TMA)[6,7], thermo-gravimetric and differential scanning calorimetry (TG/DSC) or differential thermal analysis (TG/DTA)[8–11], and optical dilatometry analysis (ODA)[12–14]. Huffman *et al.*[15] studied the fusibility of a series of coal ashes under reducing atmosphere (a mixture of 60 vol.% CO and 40 vol.% CO_2) and oxidizing atmosphere (air) by measuring their AFTs. It is found the AFTs of the ashes under the reducing atmosphere are 50 to 200 °C lower than that under the oxidizing atmosphere. And the partial melting of ash, which starts at a temperature 200 to 400 °C below the initial deformation temperature (IDT), is significantly increased under the reducing atmosphere compared to the oxidizing atmosphere[15]. Similar results have been observed by other researchers[2,5,16–18]. However, most of these investigations focus on coal ashes with a relative high Fe content. The increase in fusion tendency of ashes under the reducing condition is probably attributed to the reduction of Fe^{3+} to Fe^{2+}, which may subsequent react with other ash constituents to form the eutectics with low-melting temperature[19,20]. Mao *et al.*[21,22] suggested that the addition of water vapor significantly promotes the melting of coal ash due to the formation of K containing compounds with low-melting temperature, such as KOH, and the subsequently production of low-temperature eutectics via the interaction between K species in the ash and bed material.

The investigations on the fusion tendency of biomass ashes under different atmospheres are not as extensively as coal ashes. Niu *et al.*[23] investigated the melting tendency of the gasified ash of a mixture of straw, waste carton, plastic and spent mushroom compost in a fixed bed furnace under reducing condition (a mixture of 50 vol.% N_2, 30 vol.% CO and 20 vol.% CO_2) and oxidizing condition (air). The gasified ash was produced in an air blown fluidized bed gasifier at 800 °C with an equivalence ratio of 0.2. Based on SEM analysis, it is found that the melting tendency of gasified ash under the reducing condition is higher than that under the oxidizing condition. In addition to the reduction of Fe^{3+} to Fe^{2+}, the formation of CaO from $CaSO_4$ and afterwards the production of low-melting eutectics via interaction between CaO with other compounds are considered to be additional reason for the high melting tendency of the gasified ash under the reducing atmosphere. The fusion behaviors of wheat straw ash under combustion and gasification condition are still unclear.

In this chapter, the ashes will be produced from the wheat straw that used in Chapter 3 under combustion and gasification conditions in a lab-scale fixed bed reactor. The influence of a reducing

atmosphere and a high concentration of steam on the fusion behavior of wheat straw ash will be studied by a visual observation and the scanning electron microscopy with energy-dispersive X-ray spectroscopy (SEM-EDX) analysis of the formed ash. The fusion tendency of wheat straw ash will be compared with the agglomeration tendency during combustion and gasification of wheat straw in a fluidized bed discussed in Charter 3.

4.2 Experimental section

4.2.1 Materials

Wheat straw (the one used in Chapter 3) with a size range of 0 - 0.6 mm and silica sand (SiO_2 > 97 wt.%) with a size range of 355-500 µm were used in the experiments. The compositions of the straw are shown in Table 3-1 (Chapter 3, Section 3.2.1).

4.2.2 Experimental apparatus

Experiments were performed in a lab-scale fixed bed reactor, which consists of a gas supplying system, a horizontal ceramic tube reactor with water-cooled flanges at both ends in a furnace, a gas analysis system and a data acquisition system, as shown in Figure 4-1.

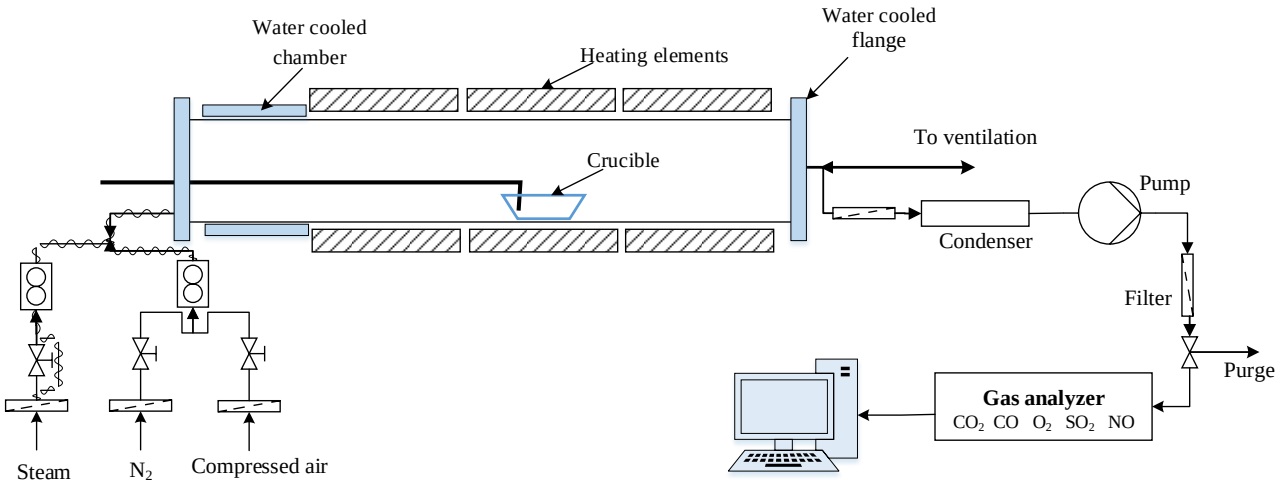

Figure 4-1 A schematic drawing of the lab-scale fixed bed reactor

The reactor with a length of 900 mm and an inner diameter of 60 mm was heated by three individually heating elements. A water cooled chamber was connected with the reactor at the gas supplying end. The temperature profile along with the reactor with a set temperature of 850°C is shown in Figure 4-2. The flow rate of compressed air and N_2 was controlled by the precision mass flow controllers (MFCs) and steam was provided by the steam generator described in Chapter 3, Section 3.2.2. The pre-mixed gas was heated by an electric heat tracing and was supplied at one end of the reactor. The flue gas was extracted at the opposite end of the reactor and sent to ventilation, creating a constant flow through the reactor. A stream of the flue gas was sent to a series of gas analyzers after removal

of steam by a condenser and fine particles by a filter to monitor the concentrations of CO_2, CO, O_2, NO and SO_2 in the flue gas. The signals of gas concentrations were continuously logged to a computer by a data acquisition system during experiments. The details of the gas supplying system, the gas analysis system and the data acquisition system are described in Chapter 3, Section 3.2.2.

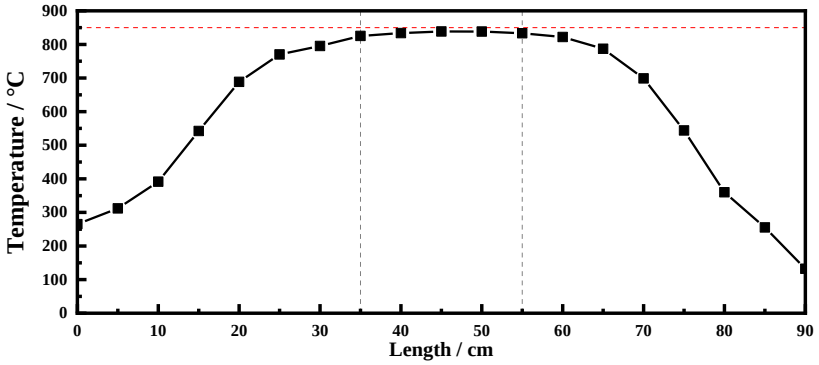

Figure 4-2 Temperature profile along with the reactor with a set temperature of 850 °C

4.2.3 Experimental conditions and procedures

Three sets of experiment were performed in this chapter.

Experiment Set 1 (wheat straw combustion/gasification): The crucible, which was filled lightly (without compaction) with 6 g of wheat straw, was placed at the water cooled chamber and the reactor was heated to 850°C with a purge of N_2 (3 Nl/min) was introduced. The crucible was inserted into the center of tube rector when the desired reactor temperature was achieved. The gas flow was immediately shifted to 100% air, a mixture of 50 vol.% steam and 50 vol.% air, or a mixture of 50 vol.% steam and 50 vol.% N_2 during experiment to combust/gasify the wheat straw. After a total conversion time of 3 h, the crucible was pulled out from the reactor and cooled to ambient temperature at the water cooled chamber under desired atmosphere. The ashes from experiments are named as high-temperature ashes (HTA), and the ash produced under three conditions are specified as HTA(100% air), HTA(50% steam/50% air) and HTA(50% steam/50% N_2). The ashes were stored in a desiccator and characterized by SEM-EDX and X-ray diffraction (XRD). The fusion behavior of HTA samples was analyzed by a visual observation and the SEM-EDX analysis.

Experiment Set 2 (wheat straw char combustion/gasification): In order to have a better understanding of the behavior of samples during char conversion stage and ash heating stage, the stepwise experiments were performed with the wheat straw char sample. The char sample was prepared from pyrolysis of wheat straw for 1 h at 550 °C under pure N_2 condition in the fixed bed reactor described above. In this set of experiments, the crucible was filled with around 1.6 g of char sample, which was obtained from around 6 g of straw, and inserted into the reactor when the reactor was heated to 850 °C. Similar with Experiment Set 1, the gas was shifted from 100% N_2 to 100% air, a mixture of 50 vol.% steam and 50 vol.% air, or a mixture of 50 vol.% steam and 50 vol.% N_2 once the crucible was in the

center of reactor. The temperature and CO and CO_2 concentrations in the flue gas was monitored during experiment. The sample was pulled out from reactor when the concentration CO and CO_2 in the flue gas was below 0.05 vol.%. After the total mass of crucible and ash was weighed by an analytical balance, the crucible was again inserted into the furnace and heated at desired atmosphere until the total conversion time reached 3 h. The total mass of crucible and ash was weighed again and the ash content after each step was calculated based on the dry basis straw.

Experiment Set 3 (wheat straw and silica sand mixture combustion/gasification): A mixture of 6 g of wheat straw and 1 g of SiO_2 was placed in a crucible and was combusted/gasified using the same procedure of Experiment Set 1. After a 3 h conversion, the crucible was pulled out from the reactor and cooled to ambient temperature at the water cooled chamber under desired atmosphere. Similar with the ashes, the agglomerates (AGGs) formed under three conditions are called as AGG(100% air), AGG(50% steam/50% air) and AGG(50% steam/50% N_2). The agglomerates were stored in a desiccator and characterized by SEM-EDX.

4.2.4 Characterization

The morphology and compositions of ashes and agglomerates samples were analyzed by Scanning Electron Microscopy (QUANTA FEG 250) with Energy X-ray (SEM-EDX). All samples were carbon-coated to reduce charging of samples.

The crystal phases in the ash samples were obtained by X-ray diffraction (XRD) analysis. The XRD spectra were determined with a Huber diffractometer with characteristic Cu Kα radiation and operation conditions of 40 kV and 40 mA. The wave length was 1.54056 Å. The identification of the main crystalline phase was performed with the JADE 6.0 software package (MDI Livermore, CA) and the diffraction database of PDF2-2004.

4.3 Results and discussion

4.3.1 Fusion behavior of high temperature ashes (HTA)

4.3.1.1 CO, CO_2 and O_2 concentrations in flue gas

The concentrations of CO, CO_2 and O_2 in the flue gas during wheat straw conversion under conditions of 100% air, 50% steam/50% air, and 50% steam/50% N_2 are shown in Figure 4-3. The CO, CO_2 and O_2 concentrations under the conditions with presence of 50 vol.% steam in supplying gas, i.e. 50% steam/50% air and 50% steam/50% N_2, are recalculated based on a total gas flow rate of 3 Nl/min due to fact that the steam in the flue gas has been removed before sending to analyzer. Under all conditions, large concentration peaks of CO and CO_2 are observed within 5 minutes after stating experiments, which may be attributed to the devolatilization of wheat straw. During devolatilization stage, the CO concentrations in the produced flue gas under three conditions are comparable, while

the CO_2 concentration decreases with a decrease of air concentration in the system. During carbon conversion stage, which follows after the devolatilization stage, the CO concentration in the flue gas produced under condition with 50% steam/50% N_2 is much higher than that under other two conditions with presence of air, which are almost zero. Therefore, HTA(100% air), HTA(50% steam/50% air), and HTA(50% steam/50% N_2) may represent the ash formed under the oxidizing atmosphere with a relative low steam concentration, the oxidizing atmosphere with a high steam concentration and the reducing atmosphere with a high steam concentration, respectively.

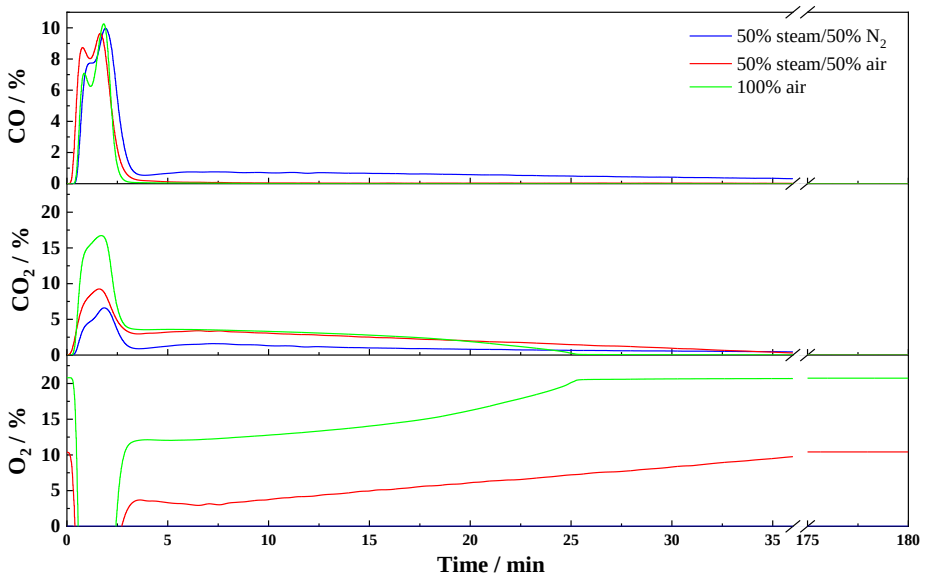

Figure 4-3 Concentrations of CO, CO_2 and O_2 in the flue gas during the formation of ash from wheat straw under conditions of 100% air, 50% steam/50% air, and 50% steam/50% N_2 at 850 °C.

4.3.1.2 Appearances of HTA samples

The raw wheat straw samples and the HTA samples from conversion of wheat straw under the atmospheres of 100% air, 50% steam/50% air, and 50% steam/50% N_2 are show in Figure 4-4. The appearances of the three HTA samples are obviously different. HTA(100% air) has a largest volume followed by HTA(50% steam/50% air) and lastly HTA(50% steam/50% N_2), indicating that the shrinking tendency of HTA from wheat straw is promoted by a high concentration of steam and a reducing atmosphere. HTA(100% air) is friable and less cohesive, while HTA(50% steam/50% air) and HTA(50% steam/50% N_2) are tight and compact.

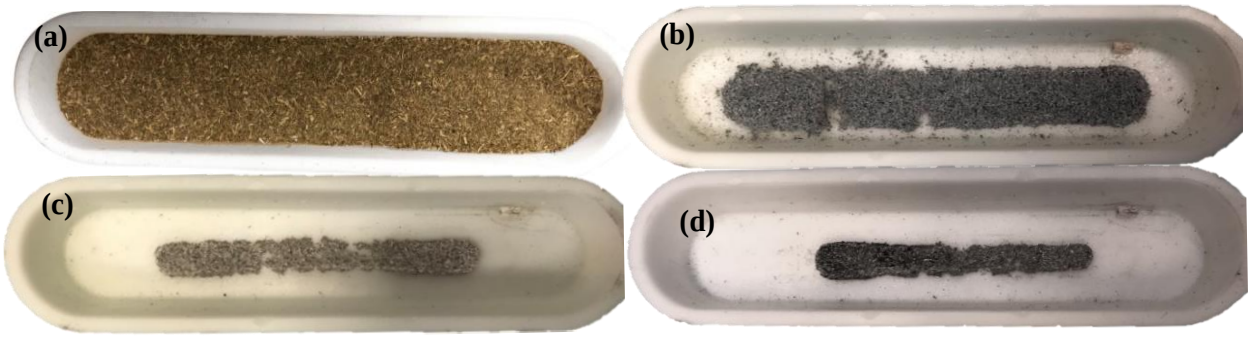

Figure 4-4 The appearances of (a) raw straw sample and HTA formed under (b) 100% air; (c) 50% steam/50% air; and (d) 50% steam/50% N_2.

4.3.1.3 XRD analysis of HTA samples

Figure 4-5 presents the crystalline phases detected by XRD analysis of HTA(100% air), HTA(50% steam/50% air), and HTA(50% steam/50% N_2). The main crystalline phase compounds in the three HTA samples are similar, except that K_2SO_4 is not found in HTA(50% steam/50% N_2), due to the fact that K_2SO_4 is unstable under a reducing atmosphere[24]. K_2SO_4 probably is transformed to K silicates as suggested by the results of thermodynamic equilibrium calculations shown in Chapter 3. The existence of K-silicates is difficult to be determined by XRD due to its characteristic of amorphous phase. The fusion tendency of HTA samples, therefore, may be increased by the presence of reducing atmosphere.

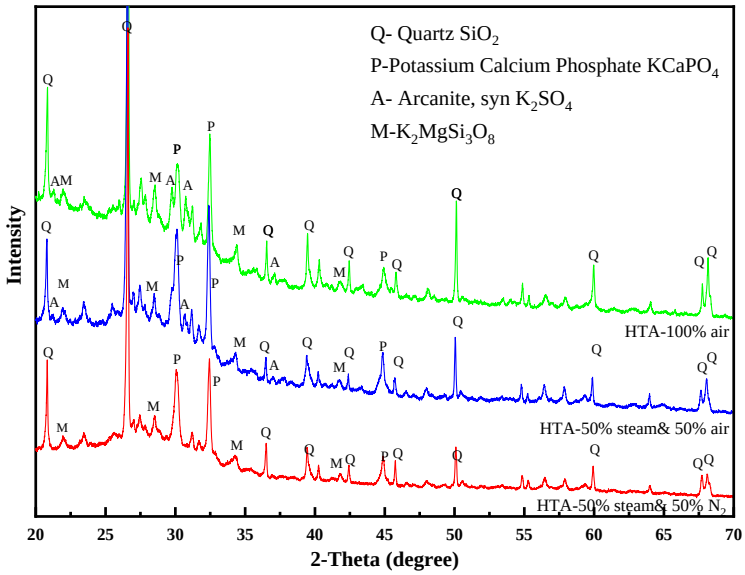

Figure 4-5 Crystalline phases in HTA(100% air), HTA(50% steam/50% air), and HTA(50% steam/50% N_2).

4.3.1.4 SEM-EDX of HTA samples

SEM-EDX was used to analyze the morphology and surface elemental compositions of the HTA samples, providing some indications for the fusion behavior of HTA samples. The results are given in Figure 4-6 and Table 4-1. Since HTA(100% air) is loose and friable, the particle sizes of HTA(100%

air) (Figure 4-6-a-1) are smaller than that of HTA(50% steam/50% air) and HTA(50% steam/50% N_2) (Figure 4-6-b-1 and c-1). Three types of morphology including floccules, smooth surface, and spherical particles are observed in the HTA samples from the three conditions. As shown in Figure 4-6-a-2, HTA(100% air) contains a larger amount of flocculent substances, and only some smooth surface and several spherical particles are found. The amount of flocculent substances is significantly reduced in HTA(50% steam/50% air) (Figure 4-6-b-2). However, the flocculent substances are hardly found in HTA(50% steam/50% N_2) (Figure 4-6-c-2), and the ash particles generally have a smooth surface.

The compositions of the selected points for each types of morphology are analyzed by EDX analysis, and the results are given on carbon and oxygen free basis due the samples are carbon coated. The compositions at the different measurement locations in HTA(100% air) are significantly different. The dark-colored spherical particle (Spot 1) and smooth surface (Spot 3) contain high contents of K, Si, and Ca, while the white-colored flocculent substance (Spot 2) are rich in K, Ca, P, and S. The flocculent substances may be the non-molten ash particles, and spherical particles and smooth surface probably indicate the molten ash particles. For HTA(50% steam/50% air), the dark-colored areas (Spot 4 and Spot 6) are rich in K, Ca and Si, being consistent with the dark-colored areas of HTA(100% air). The white-colored flocculent substances (Spot 5) in HTA(50% steam/50% air) is mainly composed of Si and Ca, as well as a low content of K. However, the difference in the compositions at different areas (Spot 7, 8, and 9) of HTA(50% steam/50% N_2) are small, indicating a relative homogenous surface caused by a high melting tendency. The morphology of ashes under the three conditions indicate that their melting tendency increases in the order of HTA(100% air) < HTA(50% steam/50% air) < HTA(50% steam/50% N_2), which is consistent with the observed shrinking tendency. The results reveal that a high concentration of steam and a reducing atmosphere promote the fusion tendency of HTA from wheat straw.

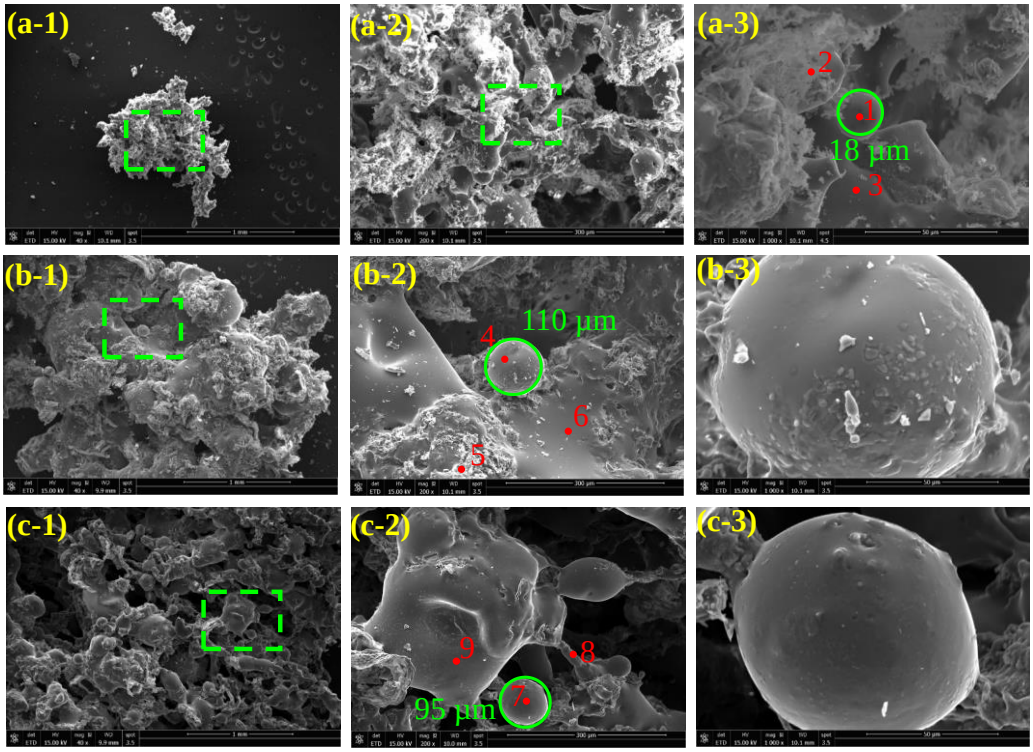

Figure 4-6 Morphology (SEM: SE mode) of ashes from wheat straw under (a) 100% air; (b) 50% steam/50% air; and (c) 50% steam/50% N_2.

Table 4-1 EDX analysis of selected point of the ashes shown in Figure 4-6 (atom% on C-O-free basis)

Spots	K	Si	Ca	Mg	P	S	Al	Na
Spot 1	21.64	52.27	15.45	3.65	4.78	0.18	1.72	0.31
Spot 2	30.26	4.86	26.69	5.22	19.62	12.71	0.36	0.28
Spot 3	22.52	58.82	9.12	5.09	3.17	0.09	0.43	0.71
Spot 4	24.34	57.27	8.22	3.19	3.69	1.93	0.70	0.57
Spot 5	10.26	44.14	35.90	2.71	3.71	2.18	0.50	0.50
Spot 6	48.46	32.62	10.28	1.87	3.15	1.45	1.33	0.75
Spot 7	21.28	59.26	9.03	6.86	2.75	0.08	0.26	0.50
Spot 8	25.26	53.47	12.69	3.27	3.99	0.00	0.98	0.30
Spot 9	20.99	69.74	5.97	2.13	0.55	0.02	0.24	0.29

4.3.1.5 Appearances of ashes from char after char conversion and ash heating stage

In Experiment Set 1, the conversion of wheat straw can be divided into three stages: devolatilization (char formation) stage, char conversion (ash formation) stage, and ash heating stage. The devolatilization stage during straw pyrolysis is finished in 5 minutes at 850 °C, indicated by the CO and CO_2 concentrations in the flue gas drop to below 0.05 vol.%, as given in Figure B-1 in Appendix B. Therefore, the fusion behavior of ash during char conversion stage and ash heating stage are investigated by combustion/gasification of wheat straw char. The ending of the char conversion stage and the beginning of the ash heating stage is determined at where the concentrations of CO and CO_2

in the flue gas below 0.05 vol.%. The reliability of this method can be proved by the fact that the ash ratios after two stages are very close, as shown in Table 4-2.

Table 4-2 Ash ratios at different stages under conditions of 100% air; 50% steam/50% air; and 50% steam/50% N_2.

	Ash formation stage/ wt.%	Ash heating stage / wt.%
100%air	18.7	18.7
50% steam/50% N_2	18.1	18.2
50% steam/50% air	19.1	18.5

Figure 4-7 shows the appearances of the char sample before heated, as well as the ashes from char samples after char conversion stage and ash heating stage under the conditions of 100% air, 50% steam/50% air, and 50% steam/50% N_2. The obtained char sample from pyrolysis (Figure 4-7-a-0) was collected, and was used to refill the crucible (Figure 4-7-a). The results show that the shrinking tendency of the ashes from straw char under three conditions is consistent with the ashes from wheat straw. The volumes of ash from both char conversion stage and ash heating stage under 100% air (Figure 4-7-b and 4-7-c) are obviously larger than the ashes from other two conditions. However, the mobility of ash from straw char seems to be lower than that from straw samples. It may be attributed to the porous structure of char samples, resulting in a large voidage of the straw char bed in the crucible. In addition, it is found that the shrinking both occurs during char conversion stage and ash heating stage. This is in agreement with the results has been reported by Wu *et.al*[25]. They found that the ash usually begins to melt when the carbon conversion is above 50% during coal char gasification under CO_2 or H_2O atmospheres.

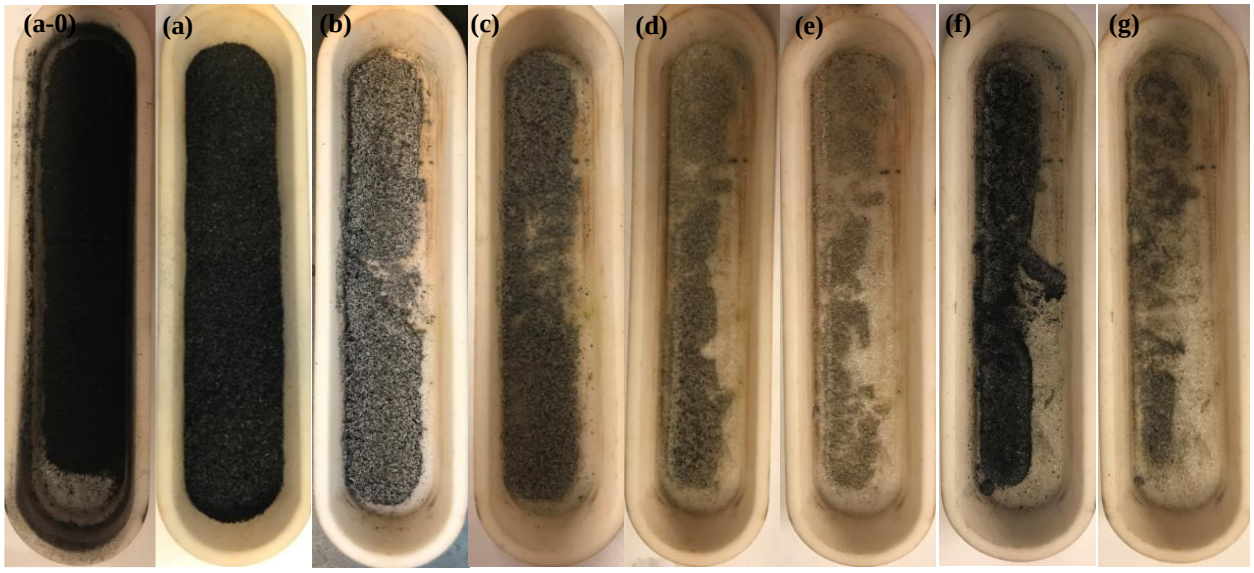

Figure 4-7 Appearances of (a-0) the obtained char samples from pyrolysis, (a) the char samples before heated and ash from char sample under (b) 100% air after char conversion stage; (c) 100% air after ash heating stage; (d) 50% steam/50% air after char conversion stage; (e) 50% steam/50% air after ash heating stage; (f) 50% steam/50% N_2 after char conversion stage; and (g) 50% steam/50% N_2 after ash heating stage.

4.3.2 Agglomerates of mixture of wheat straw and sand

The appearances of the mixture of wheat straw and sand before treatment, AGG(100% air), AGG(50% steam/50% air), and AGG(50% steam/50% N_2) are shown in Figure 4-8. Consistent with the ashes from wheat straw and straw char, the volumes of agglomerates under three conditions decrease in the order of: AGG(100% air) > AGG(50% steam/50% air) > AGG(50% steam/50% N_2). The mobility of agglomerates are less pronounced than the ash samples, probably due to the large density of sand particles. Similarly, AGG(100% air) are easily to be broken during collection, and therefore the sizes of AGG(100% air) are smaller than that of other two agglomerates.

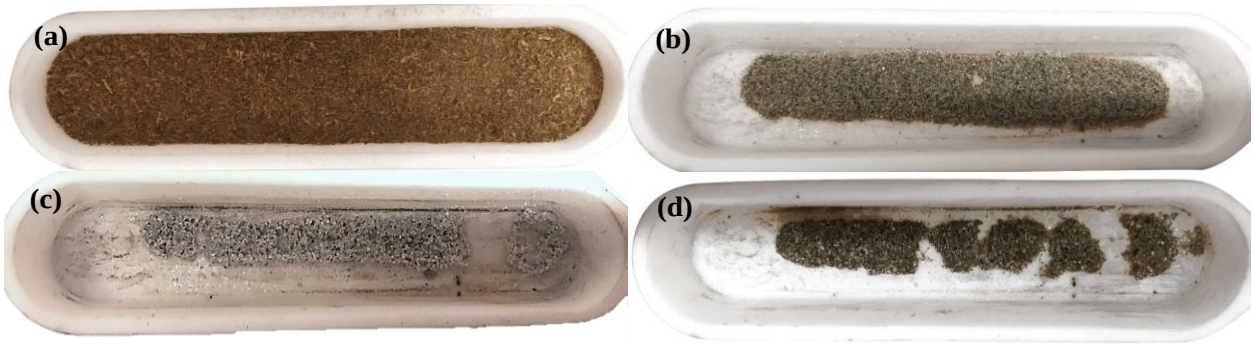

Figure 4-8 Mixture of straw and sand (a) before heated and agglomerates formed under (b) 100% air; (c) 50% steam/50% air; (d) 50% steam/50% N_2 in the fixed bed reactor.

The morphology of agglomerates formed under three conditions are shown in Figure 4-9. Consistent with the ash particles, the melting tendency of ash in AGG(50% steam/50% N_2) is highest followed by the ash in AGG(50% steam/50% air) and lastly the ash in AGG(100% air). The flocculent substances are only observed in AGG(100% air), while AGG(50% steam/50% air) and AGG(50% steam/50% N_2) have the relative homogeneous surfaces. Under all conditions, the formation of agglomerates seems to be attributed to the fact that the sand particles, which are covered by coating layer, are glued by a molten bridge. The EDX analyses of the selected locations in sand surfaces of agglomerates (Spot 2, 5 and 8) show that the coating layers is dominated by Si and K, indicating the sand particles are covered by the molten K silicates. For AGG(50% steam/50% N_2), slightly amount of Ca is also observed. The main compositions of the molten bridges (Spot 1, 4 and 7) are K, Si and Ca, suggesting that the agglomeration of wheat straw in combustion and gasification are probably caused by the molten K-Ca silicates. The SEM-EDX results reveal that the accelerated agglomeration under a reducing atmosphere and a high concentration of steam may be attributed to the high fusion tendency of ash.

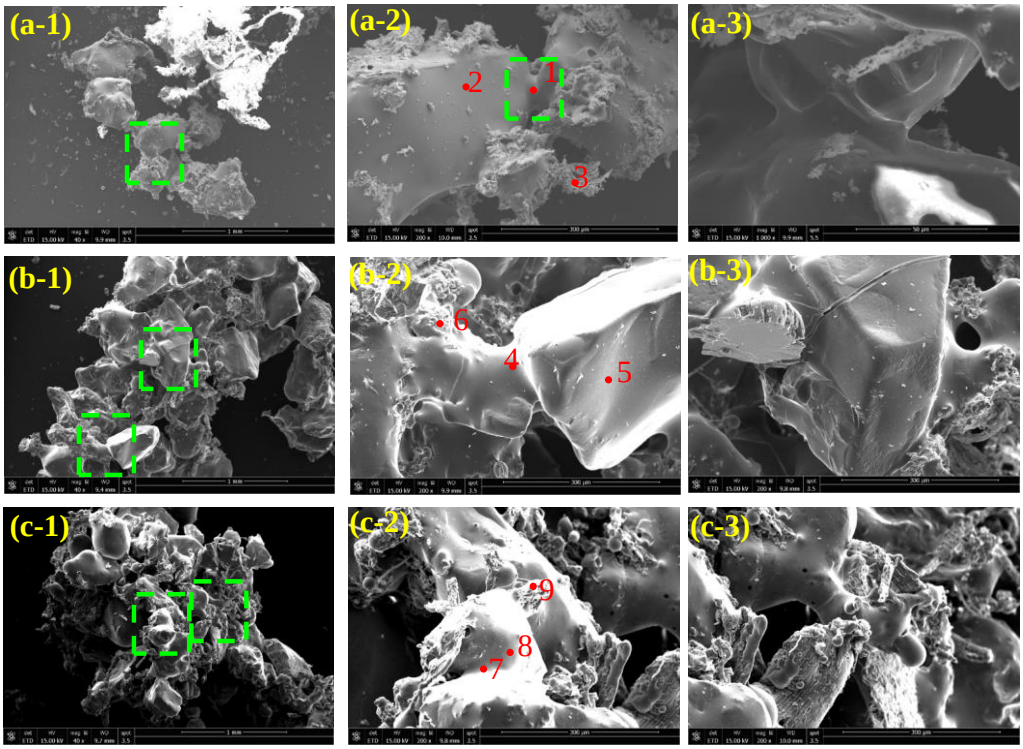

Figure 4-9 Morphology (SEM: SE mode) of agglomerates formed under (a) 100% air; (b) 50% steam/50% air; (c) 50% steam/50% N_2 for 3 h.

Table 4-3 EDX analysis of selected point of the agglomerates shown in Figure 4-9 (atom% on C-O-free basis)

Spot	K	Si	Ca	Mg	P	S	Al	Na
Spot 1	24.25	51.21	9.76	3.02	4.74	1.44	3.09	2.04
Spot 2	11.82	84.79	0.28	0.21	0.38	0.38	0.52	1.57
Spot 3	18.46	23.19	41.65	2.83	5.28	3.01	2.79	2.46
Spot 4	21.87	53.54	7.52	2.07	4.44	1.10	5.90	3.26
Spot 5	14.20	82.57	0.40	0.10	0.84	0.54	0.27	1.08
Spot 6	14.96	42.50	14.42	2.31	16.89	0.54	6.51	1.83
Spot 7	20.62	71.88	1.41	1.05	0.18	0.18	3.61	1.02
Spot 8	16.87	74.58	3.00	0.65	0.16	0.10	3.52	1.11
Spot 9	23.02	59.09	8.20	4.40	4.07	0.11	0.57	0.46

4.4 Conclusion

The fusion behavior of ashes from wheat straw, straw char, and mixture of wheat straw and silica sand under combustion and gasification conditions is investigated in a fixed bed reactor at 850 °C. The main conclusions are drawn as follows:

(1) The appearances of the wheat straw ash samples obtained from different conditions show that the ash from normal combustion (condition of 100% air) is friable and less cohesive, while the ashes from combustion with presence of steam (condition of a mixture of 50 vol.% steam and 50 vol.% air) and from gasification with steam (condition of a mixture of 50 vol.% steam and 50 vol.% N_2) are

tight and compact. The fusion tendency of three ash samples increase in the order: the ash from normal combustion < the ash from combustion with presence of steam < the ash from gasification with steam. The visual observation and SEM-EDX analyses of the ashes from wheat straw indicates that a high concentration of steam and a reducing atmosphere will promote the fusion tendency of wheat straw ash.

(2) The fusion tendency of ashes from the mixture of wheat straw and silica sand under the three conditions is consistent with the ashes from wheat straw. The ash in agglomerates from condition of a mixture of 50 vol.% steam and 50 vol.% N_2 shows the highest melting tendency, whist the ash in agglomerates from condition of 100% air shows the lowest melting tendency. The agglomerates formed under all conditions are caused by the presence of molten K-Ca silicates. A severer agglomeration is observed for the mixture that contains the ash with a higher fusion tendency. The fusion tendency of wheat straw ash is consistent with the agglomeration tendency of wheat straw in the fluidized bed descried in Chapter 3. The accelerated agglomeration under a reducing atmosphere and a high concentration of steam condition results from a promoted fusion tendency of ash.

Reference

(1) Ghaly, A. E.; Ergüdenler, A.; Laufer, E. Agglomeration Characteristics of Alumina Sand-Straw Ash Mixtures at Elevated Temperatures. *Biomass and Bioenergy* **1993**, *5* (6), 467–480.

(2) Backman, R. Sintering of FBC Ashes. *Fuel* **1994**, *73* (2), 171–176.

(3) Mac an Bhaird, S. T.; Walsh, E.; Hemmingway, P.; Maglinao, A. L.; Capareda, S. C.; McDonnell, K. P. Analysis of Bed Agglomeration during Gasification of Wheat Straw in a Bubbling Fluidised Bed Gasifier Using Mullite as Bed Material. *Powder Technol.* **2014**, *254*, 448–459.

(4) Liu, Y.; Gupta, R.; Elliott, L.; Wall, T.; Fujimori, T. Thermomechanical Analysis of Laboratory Ash, Combustion Ash and Deposits from Coal Combustion. *Fuel Process. Technol.* **2007**, *88* (11–12), 1099–1107.

(5) Chen, X.; Kong, L.; Bai, J.; Bai, Z.; Li, W. Study on Fusibility of Coal Ash Rich in Sodium and Sulfur by Synthetic Ash under Different Atmospheres. *Fuel* **2017**, *202*, 175–183.

(6) Ma, T.; Fan, C.; Hao, L.; Li, S.; Song, W.; Lin, W. Fusion Characterization of Biomass Ash. *Thermochim. Acta* **2016**, *638*, 1–9.

(7) Gupta, S. K.; Gupta, R. P.; Bryant, G. W.; Wall, T. F. The Effect of Potassium on the Fusibility of Coal Ashes with High Silica and Alumina Levels. *Fuel* **1998**, *77* (11), 1195–1201.

(8) Gilbe, C.; Lindström, E.; Backman, R.; Samuelsson, R.; Burvall, J.; Öhman, M. Predicting Slagging Tendencies for Biomass Pellets Fired in Residential Appliances: A Comparison of Different Prediction Methods. *Energy & Fuels* **2008**, *22* (6), 3680–3686.

(9) Schimpke, R.; Klinger, M.; Krzack, S.; Meyer, B. Determination of the Initial Ash Sintering Temperature by Cold Compression Strength Tests with Regard to Mineral Transitions. *Fuel* **2017**, *194*, 157–165.

(10) Nel, M. V; Strydom, C. A.; Schobert, H. H.; Beukes, J. P.; Bunt, J. R. Comparison of Sintering and Compressive Strength Tendencies of a Model Coal Mineral Mixture Heat-Treated in Inert and Oxidizing Atmospheres. *Fuel Process. Technol.* **2011**, *92* (5), 1042–1051.

(11) Du, S.; Yang, H.; Qian, K.; Wang, X.; Chen, H. Fusion and Transformation Properties of the Inorganic Components in Biomass Ash. *Fuel* **2014**, *117* (PARTB), 1281–1287.

(12) Adell, V.; Cheeseman, C. R.; Ferraris, M.; Salvo, M.; Smeacetto, F.; Boccaccini, A. R. Characterising the Sintering Behaviour of Pulverised Fuel Ash Using Heating Stage Microscopy. *Mater. Charact.* **2007**, *58* (10), 980–988.

(13) Xu, J.; Zhao, F.; Guo, Q.; Yu, G.; Liu, X.; Wang, F. Characterization of the Melting Behavior of High-Temperature and Low-Temperature Ashes. *Fuel Process. Technol.* **2015**, *134*, 441–448.

(14) Lawrence, A.; Ilayaperumal, V.; Dhandapani, K. P.; Srinivasan, S. V.; Muthukrishnan, M.; Sundararajan, S. A Novel Technique for Characterizing Sintering Propensity of Low Rank

Fuels for CFBC Boilers. *Fuel* **2013**, *109*, 211–216.

(15) Huffman, G. P.; Huggins, F. E.; Dunmyre, G. R. Investigation of the High-Temperature Behaviour of Coal Ash in Reducing and Oxidizing Atmospheres. *Fuel* **1981**, *60* (7), 585–597.

(16) Jing, N.; Wang, Q.; Luo, Z.; Cen, K. Effect of Different Reaction Atmospheres on the Sintering Temperature of Jincheng Coal Ash under Pressurized Conditions. *Fuel* **2011**, *90* (8), 2645–2651.

(17) Jing, N.; Wang, Q.; Yang, Y.; Cheng, L.; Luo, Z.; Cen, K. Influence of Ash Composition on the Sintering Behavior during Pressurized Combustion and Gasification Process. *J Zhejiang Univ-Sci A (Appl Phys Eng)* **2012**, *13* (3), 230–238.

(18) Bryant, G. W.; Browning, G. J.; Emanuel, H.; Gupta, S. K.; Gupta, R. P.; Lucas, J. A.; Wall, T. F. The Fusibility of Blended Coal Ash. **2000**, No. 5, 316–325.

(19) Song, W. J.; Tang, L. H.; Zhu, X. D.; Wu, Y. Q.; Zhu, Z. B. Prediction of Chinese Coal Ash Fusion Temperatures in Ar and H2 Atmospheres. *Energy & Fuels* **2009**, *23*, 1990–1997.

(20) Dyk, J. C. Van; Benson, S. A.; Laumb, M. L.; Waanders, B. Coal and Coal Ash Characteristics to Understand Mineral Transformations and Slag Formation. *Fuel* **2009**, *88* (6), 1057–1063.

(21) Mao, Y.; Jin, Y.; Li, K.; Bi, J.; Li, J.; Xin, F. Sintering Characteristic in Catalytic Gasification of China Inner Mongolia Bituminous Coal Ash. *Energy & Fuels* **2016**, *30*, 3975–3985.

(22) Mao, Y.; Jin, Y.; Li, K.; Bi, J.; Li, J.; Xin, F. Analysis of Influencing Factors on Sintering Temperature of Inner Mongolia Wangjiata Bituminous Coal Ash during Catalytic Coal Gasification (in Chinese). *Huagong Xuebao/CIESC J.* **2015**, *66*, 1080–1087.

(23) Miaomiao, N.; Dong, Q.; Huang, Y.; Jin, B.; Wang, H.; Gu, H. Characterization of Ash Melting Behaviour at High Temperatures under Conditions Simulating Combustible Solid Waste Gasification. *Waste Manag. Res.* **2018**, *36* (5), 415–425.

(24) Ma, T.; Fan, C.; Hao, L.; Li, S.; Song, W.; Lin, W. Biomass-Ash-Induced Agglomeration in a Fluidized Bed. Part 1: Experimental Study on the Effects of a Gas Atmosphere. *Energy & Fuels* **2016**, *30* (8), 6395–6404.

(25) Wu, X.; Zhang, Z.; Piao, G.; He, X.; Chen, Y.; Kobayashi, N.; Mori, S.; Itaya, Y. Behavior of Mineral Matters in Chinese Coal Ash Melting during Char-CO_2/H_2O Gasification Reaction. *Energy & Fuels* **2009**, *23*, 2420–2428.

5. Influence of Biomass Types on Agglomeration during Combustion and Gasification

Abstract

In this chapter, the agglomeration during combustion and gasification of two types of biomass, including two batches of wheat straw (WS, named as WS-1 and WS-2) and one sunflower husk (SFH), was studied in a lab-scale fluidized bed reactor at 850 °C using silica sand as bed material. The char reactivity of the biomasses was investigated by thermogravimetric analysis (TGA). Selected biomass residues and bed agglomerates were characterized by X-ray diffraction (XRD) and scanning electron microscopy with energy-dispersive X-ray spectroscopy (SEM-EDX). Thermodynamic equilibrium calculations were performed to explore the distribution of potassium during conversion of the three biomasses. Fluidized bed experiments show that the agglomeration tendency of SFH ash is higher than that of WS ashes under both combustion and gasification conditions. This may be attributed to their significantly different molar ratios of silicon to potassium (Si/K), which are 1.56, 2.60 and 0.04, respectively, for WS-1, WS-2 and SFH. During gasification, varying the ER and addition of a high concentration of steam in primary gas show consistent effects on the agglomeration of the three biomasses. A reducing atmosphere and a high concentration of steam promote the agglomeration of WS probably by increasing the melting of ashes. For SFH, the accelerated agglomeration under a reducing atmosphere and a high concentration of steam may be attributed to their promotive effect on the interaction between SFH ash and bed material. TGA experiments result show that SFH has the highest char reactivity followed by WS-2 and lastly WS-1. An increase in char reactivity leads to a decrease in the inhibition effect of accumulated carbon caused by decreasing ER during gasification of biomass. The critical ER of SFH, which is 0.04, is lower than that of WSs, which are 0.36. This may be attributed to a high char reactivity of SFH and the different mechanism of the influence of reducing atmosphere on the agglomeration results from a low Si/K molar ratio of SFH.

This chapter has been written in a manuscript format. A slightly modified version of this chapter will be submitted to a peer-reviewed journal.

5.1 Introduction

The agglomeration during combustion and gasification of biomass is mainly attributed to the presence of the low-melting temperature alkali containing compounds originated from biomass and/or interaction between biomass ash and bed materials[1,2]. Therefore, agglomeration tendencies and mechanisms in fluidized bed are closely related to the biomass types due to their diverse ash content and different ash-forming compositions[3–6].

Wheat straw, a biomass that both rich in potassium and silicon, is problematic during combustion and gasification in fluidized bed[7–9] due to the severe agglomeration problem. It is generally accepted that a K- and Si-rich ash may start melting before attaching to bed material, subsequently causing the agglomeration[3,4]. The Si-lean husks, such as coffee husk and sunflower husk, also show a high agglomeration tendency in combustion and gasification due to their high potassium content[10,11]. Chaivatamaset *et al.*[12] investigated the agglomeration in combustion of a Si-poor eucalyptus bark, whose ash is dominated by Ca followed by K. It is found that the dominant agglomeration mechanism is the presence of molten potassium silicates produced through the chemical reaction between the potassium and calcium of the bark and the silicon from the silica sand. Öhman *et al.*[5] found that the agglomeration temperature of olive flesh, a biomass rich in K, Ca, Mg and Si, is 270 °C higher than that of Lucerne, a biomass rich in K and Ca but lean in Si, during combustion. Chemical equilibrium calculations suggest that K in olive flesh is likely to be transformed into silicates and sulfates during combustion, while KCl, K_2CO_3, K_2SO_4, and K silicates are the dominant K compounds during Lucerne combustion. It is suggested by Öhman *et al.* that the agglomeration of Lucerne during combustion is caused by the melting of KCl and K_2SO_4 eutectic[5]. However, it is observed that the dominate elements of the inner layer around the bed particles from Lucerne combustion are K and Si, indicating that the interaction between Lucerne ash and bed material may be one important agglomeration mechanism.

In Chapter 3, it has been shown that the agglomeration tendency of wheat straw first increases with a decrease of ER to a maximal tendency, and then decreases with further decreasing ER. By decreasing ER, the produced reducing atmosphere promotes the agglomeration, while an increased amount of residual carbon in the bed will mitigate the agglomeration. The competition between these two factors results in the occurrence of the maximal agglomeration tendency at a critical ER. The promoted agglomeration by adding steam to the primary gas probably attributed to a decreased carbon amount in the bed and a lowered ash viscosity. However, whether such phenomena occur to other biomass is still unclear. In this chapter, the agglomeration behaviors of the wheat straw that without defluidization in the low-temperature circulating fluidized bed (LTCFB) gasifier (described in Chapter 1, Section 1.1) and a sunflower husk that rich in K but lean in Si will be investigated under combustion and gasification conditions, subsequently compared to the agglomeration behavior of wheat straw that used in Chapter 3. The influence of char reactivity and the molar ratio of Si/K on

agglomeration in biomass combustion and gasification will be studied to have an improved understanding of agglomeration in biomass gasification.

5.2 Methodology

5.2.1 Fuel and bed material

Two types of biomass, including two batches of wheat straw (WS, named as WS-1 and WS-2) and sunflower husk (SFH), were used as fuels in this chapter. WS-1 is the straw used in Chapter 3, and WS-2 is the straw that without defluidization problem in LTCFB gasifier as descried in Chapter 1, Section 1.1. The chemical compositions of the three fuels are shown in Table 5-1. Compared to WS-1, WS-2 has a relatively low K content but high contents of Al and Si. Although the K content in the three fuels is comparable, SFH contains a significantly lower Si content than WSs, causing a low Si/K molar ratio for SFH. The fuels were sieved to a size range of 0.6-4 mm in order to avoid feeding problem. Silica sand (SiO_2 > 97 wt.%) with a size range of 355-500 μm was used as materials in the experiments.

Table 5-1 Properties of the fuels used in the experiments

		WS-1	WS-2	SFH
Moisture (wt.%, ar)		8.35	8.52	9.10
Ash (wt.%, ar)		**5.22**	**6.64**	**2.91**
Fuel elemental analysis (wt.%, daf)	C	46.16	46.46	53.41
	H	6.62	5.72	5.89
	O(by difference)	46.42	46.90	39.87
	N	0.80	0.70	0.83
Inorganic composition[ɻ] (wt.%, db)	**Cl**	**0.11**	**0.12**	**0.04**
	S	**0.081**	**0.10**	**0.14**
	Al	**0.21**	**0.53**	**0.0055**
	Ca	0.32	0.34	0.37
	Fe	0.013	0.035	0.0094
	K	**0.98**	**0.75**	**0.96**
	Mg	0.07	0.073	0.21
	Na	0.0086	0.017	0.0021
	P	0.11	0.12	0.066
	Si	**1.1**	**1.4**	**0.029**
	Si/K (mol.%)	**1.56**	**2.60**	**0.04**

ar: as received basis

daf: dry ash-free basis

db: dry basis

[ɻ] data obtained by inductively coupled plasma - optical emission spectrometry (ICP-OES)

5.2.2 Experimental apparatus

The experiments on agglomeration were carried out in a lab-scale fluidized bed reactor, which consists of a gas supplying system, a fuel feeding system, a fluidized bed reactor, a gas sampling and analysis system and a data acquisition system. The details of experimental apparatus are described in Chapter 3, Section 3.2.2.

The char reactivity experiments were carried out in a thermogravimetric analyzer (TGA, Netzsch STA 449 F1 Jupiter ASC).

5.2.3 Experimental conditions and procedures

5.2.3.1 Fluidized bed combustion and gasification of biomass

All experiments were performed at a temperature of 850 °C with a constant primary gas (fluidizing gas) flow rate of 11.5 Nl/min, corresponding to a U/U_{mf} ratio of 3 and 2.82 at the conditions with 100% air and with a mixture of 50 vol.% steam and 50 vol.% N_2, respectively. The feeding rates of the biomasses were varied to keep a constant combustion stoichiometric ratio of 1.45. The flow rate of secondary gas was 15.5 Nl/min and the composition of the secondary gas was varied in such a way that the total amount of air to the reactor was kept constant to keep a total combustion stoichiometric ratio is constant. The procedures in this series of experiments are the same as those described in Chapter 3, Section 3.2.3. The experimental matrix with respect to the fuel types and in-bed equivalence ratios (ERs) and steam to fuel ratios (SFRs) are shown in Table 5-2. The experiment was stopped when the defluidization occurred or after 3 h if no defluidization was observed.

Table 5-2 Experiments matrix

Fuels	Exp. Types	Exp. Gas conditions	ER	SFR
SFH	Pyrolysis	100% N_2 pyrolysis	0	0
WS-1/WS-2/SFH	Combustion	100% air combustion	1.45	0
	Air blown gasification	2.5% air gasification	0.04	0
		25% air gasification	0.36	0
	Air blown gasification with steam	25% steam gasification	0	0
		25% steam/2.5% air gasification	0.04	1.15
		25% steam/25% air gasification	0.36	1.15
		50% steam gasification	0	2.3
		50% steam/2.5% air gasification	0.04	2.3
		50% steam/25% air gasification	0.36	2.3

5.2.3.2 Thermogravimetric analysis (TGA) of char samples

The char samples were prepared in a fixed bed reactor described in Chapter 4. The biomass was filled in a crucible and pyrolyzed at 850 °C under N_2 condition for 1 h. The char sample was collected after cooling to the ambient temperature and stored in a desiccator. Approximately 2 mg of char sample was heated from ambient temperature to 850 ºC at a heating rate of 5 °C/min and kept at 850°C for 30 min in the TGA setup. All experiments were performed with a total gas flow of 200 Nml/min. The char reactivity of the three biomass in combustion and gasification was investigated under the conditions of 4 vol.% O_2 in N_2 and 20 vol.% CO_2 in N_2, respectively.

5.2.3.3 Low-temperature ash (LTA) and high-temperature ash (HTA) preparation

The biomass was dried in the oven at 105 °C and weighed by an analytical balance, which is sensitive to 0.1 mg, several times until the mass of the sample varies by less than 0.3 mg from the previous weighing. Afterwards, the biomass was heated in a fixed bed reactor under an air atmosphere from ambient temperature to 250 °C at a rate of 10 °C/min and hold for 30 min. Following this, the sample was heated to 550 °C or 850 °C at a rate of 5 °C/min and hold for another 3 h. The ash sample was collected after cooling down and stored in a desiccator. The ashes obtained from 550 °C and 850 °C are defined as low-temperature ash (LTA) and high-temperature ash (HTA) respectively.

5.2.4 Characterization of ashes

The crystalline phases in the LTA and HTA samples obtained in the fixed bed reactor were detected by X-ray diffraction (XRD) analysis. The XRD spectra were determined with a Huber diffractometer with characteristic Cu Kα radiation and operation conditions of 40 kV and 40 mA. The wave length was 1.54056 Å. The identification of the main crystalline phase was performed with the JADE 6.0 software package (MDI Livermore, CA) and the diffraction database of PDF2-2004.

The morphology and compositions of selected residual samples from TGA experiments and agglomerates from fluidized bed experiments were analyzed by Scanning Electron Microscopy (QUANTA FEG 250) with Energy X-ray (SEM-EDX). All samples were Ag-coated to reduce charging of samples.

5.2.5 Thermodynamic equilibrium calculations

The distribution of potassium in combustion and gasification of the three fuels at various ERs were explored by the thermodynamic equilibrium calculations performed using FACTSAGE software version 7.2. The FToxid, FTsalt, FactPS, and FTpulp databases, as well as FToxid-SLAGA solution phase were chosen for the calculations[44]. The input data was calculated based on the primary gas compositions with a flow rate of 11.5Nl/min and biomasses composition with a dry basis feeding rate of 0.11 kg/h for WSs and 0.09 kg/h for SFH to maintain the stoichiometric ratio during combustion

at around 1.45. Two sets of calculations were performed. One set of calculations without inputting of silica sand were performed to predict the existence forms of K in the three ashes, and another set of calculations with addition of silica sand in input data were used to investigate the K transformation in fluidized bed reactor. The silica sand amount is in a larger excess, corresponding to the molar ratio of SiO_2/K is100.

5.3 Results

5.3.1 Agglomeration tendency during combustion

Figure 5-1 presents the agglomeration tendency of WS-1, WS-2 and SFH, indicated by both the amount of dry basis fuel fed and the amount of ash in the fed fuel for inducing defluidization, during combustion. The results based on dry fuel basis show that the agglomeration tendency of SFH during combustion is lower than that of WS-1 and WS-2. However, the results based on ash amount suggest that the agglomeration tendency of SFH ash is higher than that of WS ashes. The difference in agglomeration tendency evaluated based on two methods results from the low ash content of SFH. The amount of ash in the fed fuel is selected to evaluate the agglomeration tendency due to the fact that the agglomeration in fluidized bed is an ash-related problem. The agglomeration tendency of three ashes in combustion decrease in the order of: SFH > WS-1 > WS-2.

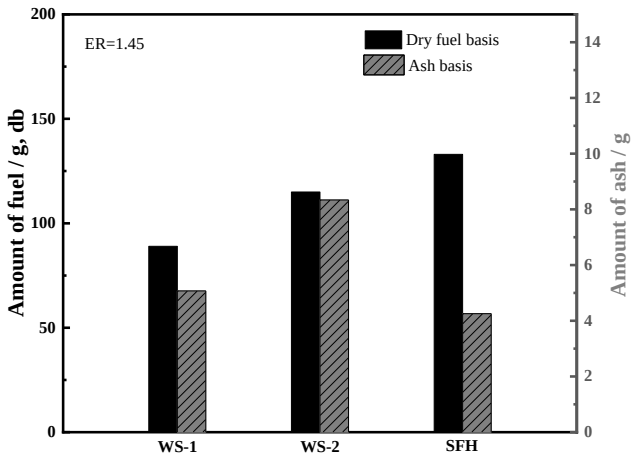

Figure 5-1 Amount of dry basis fuel fed and the amount of ash in the fed fuel for inducing defluidization during combustion with an ER of 1.45.

5.3.2 Agglomeration tendency during air blown gasification

Ash-based agglomeration tendencies of WS-1, WS-2 and SFH in air blown gasification/combustion at various ERs are given in Figure 5-2. The agglomeration tendencies of the two wheat straws are characterized by an initial increase followed by a decrease as ER decreases in the range of 0.04 - 1.45. By shifting the ER from 1.45 (combustion region) to 0.36 (gasification region), the amount of wheat straw ashes fed for inducing defluidization decreases, indicating that the agglomeration tendency of wheat straws is accelerated by a reducing atmosphere. It has been discussed in Chapter 3 and Chapter

4 that the reducing atmosphere could promote the melting of wheat straw ash. A further decrease in ER from 0.36 to 0.04 slows down the agglomeration of WSs in fluidized bed, most likely due to the high amount of residual carbon in the bed at a low ER. In addition, it is found that the decrease in ER from 0.36 to 0.04 shows a more pronounced inhibition effect on agglomeration for WS-2 compared to WS-1. Different from the WS ashes, the agglomeration tendency of SFH ash is continuously promoted by decreasing the ER from 1.45 to 0.04. It is found that no defluidization was observed during pyrolysis of SFH using N_2 as fluidizing gas when 365 g of dry SFH, corresponding to 11.65 g of SFH ash, was fed into the reactor, indicating that the agglomeration tendency of SFH ash is significantly mitigated due to the inhibition effect of unconverted carbon on agglomeration. Compared to the WSs, the critical ER of SFH, observed at 0.04, is lower. The possible reasons for the lower critical ER of SFH are the different char reactivity and different ash-forming elements of SFH and WSs, which will be evaluated through TGA experiments, ash characterization and thermodynamic equilibrium calculations.

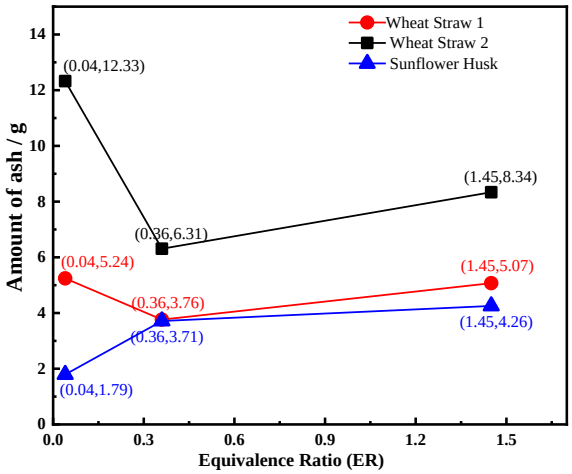

Figure 5-2 Amount of ash in the fed fuel for inducing defluidization at various equivalence ratio in air blown gasification and combustion.

5.3.3 Agglomeration tendency during steam gasification

Figure 5-3 shows the agglomeration tendencies of the three fuels during gasification at various SFRs with an ER in a range of 0 - 0.36. No defluidization was observed during SFH gasification with an ER of 0 and a SFR of 1.15 when 304 g dry SFH, corresponding to 9.73 g of SFH ash, was fed into the reactor. Under other conditions studied in this chapter, SFH ash shows the highest agglomeration tendency followed by WS-1 ash and lastly WS-2 ash, and this trend is consistent with the agglomeration tendency in air blown combustion/gasification. The steam shows a consistent influence on the agglomeration for the three biomasses. The agglomeration tendencies of the three ashes are promoted by increasing SFR in the primary gas at a constant ER in a range of 0 - 0.36. The influence of SFR becomes less pronounced at a higher ER. Consistent with combustion/gasification in the air blown system, the critical ERs in steam gasification are 0.36 and 0.04 for WS-2 and SFH, respectively, as shown in Figure C-1 in Appendix C. For WS-1, an increased steam concentration

results in a reduced critical ER due to an increased carbon conversion. The influence of steam concentration on the critical ERs of WS-2 and SFH may be covered by the large step size of ER, and the more accurate critical ERs of WS-2 and SFH in steam gasification needs to be further studied by decreasing the step size of ER.

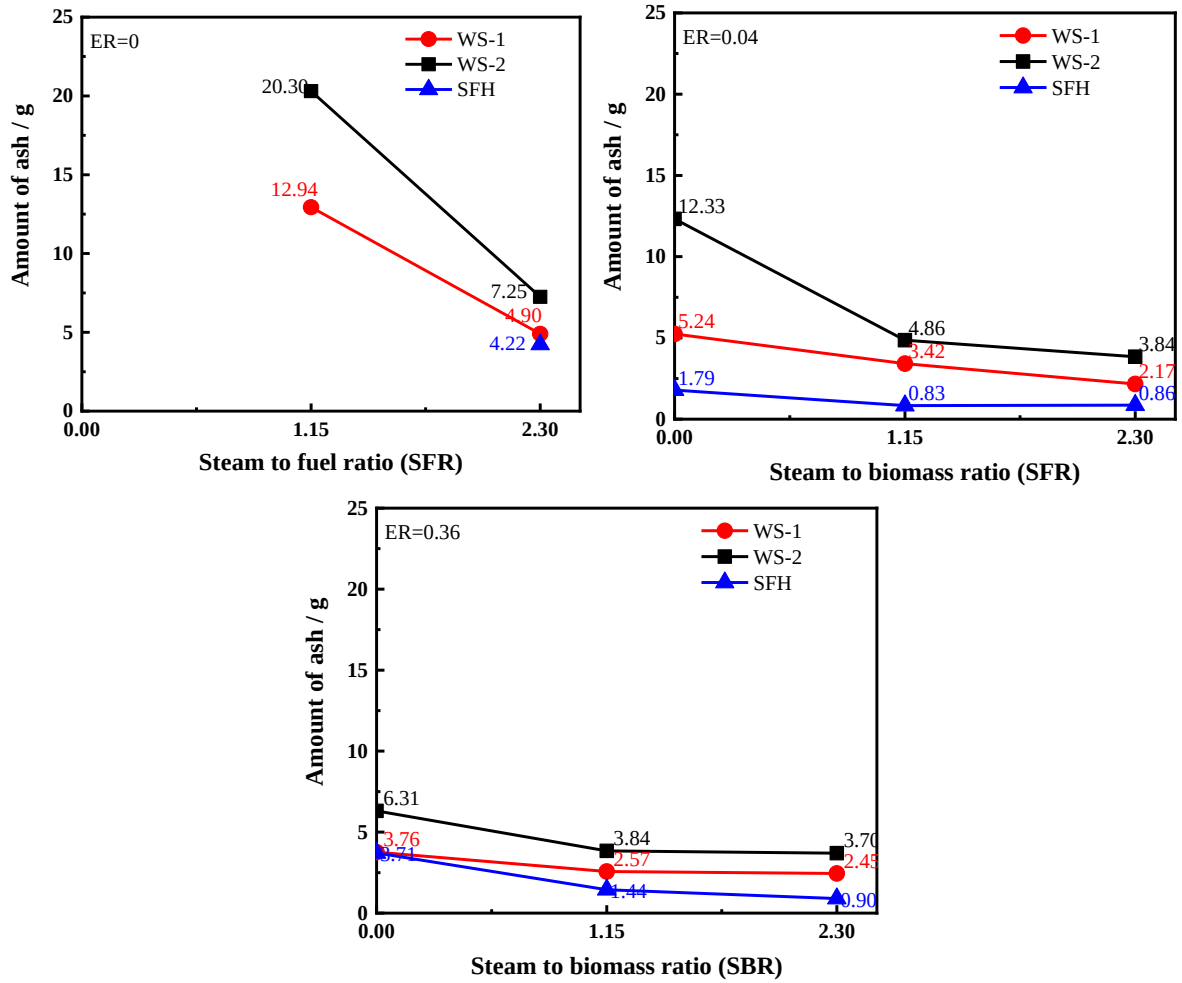

Figure 5-3 Influence of steam to fuel ratio on amount of ash in the fed fuel during gasification with an ER in the range of 0 – 0.36.

5.3.4 Reactivity of chars from WSs and SFH in combustion and CO_2 gasification

The char reactivity of the three char samples in combustion (4 vol.% O_2 in N_2) and CO_2 gasification (20 vol.% CO_2 in N_2) was investigated in TGA setup, and the results are given in Figure 5-4. The thermogravimetry/derivative thermogravimetry (TG/DTG) curves show the oxidization of three char samples starts from 300 °C. The maximum weight loss rates (DTG_{max}) of WS-1, WS-2, and SFH are respectively achieved at 423, 444, and 417 °C, as shown in Table 5-3. The reactivity of the three char samples during CO_2 gasification is much lower than that during char oxidation, and pronounced differences are observed among the reactivity of the three char samples under gasification condition. The char reactivity of SFH is higher than that of WSs. During SFH gasification, the weight loss starts at a temperature of 675 °C, and the weight loss rate reaches a maximum at 845 °C. SFH char is

completely converted when the sample is hold at 850 °C for 7 min. The char conversions of WS-1 and WS-2 are 82% and 65%, respectively, after the samples are hold at 850 °C for 30 min. The TG/DTG results of the three char samples reveal that their char reactivity under combustion and gasification conditions decreases in the order of: SFH > WS-1 > WS-2.

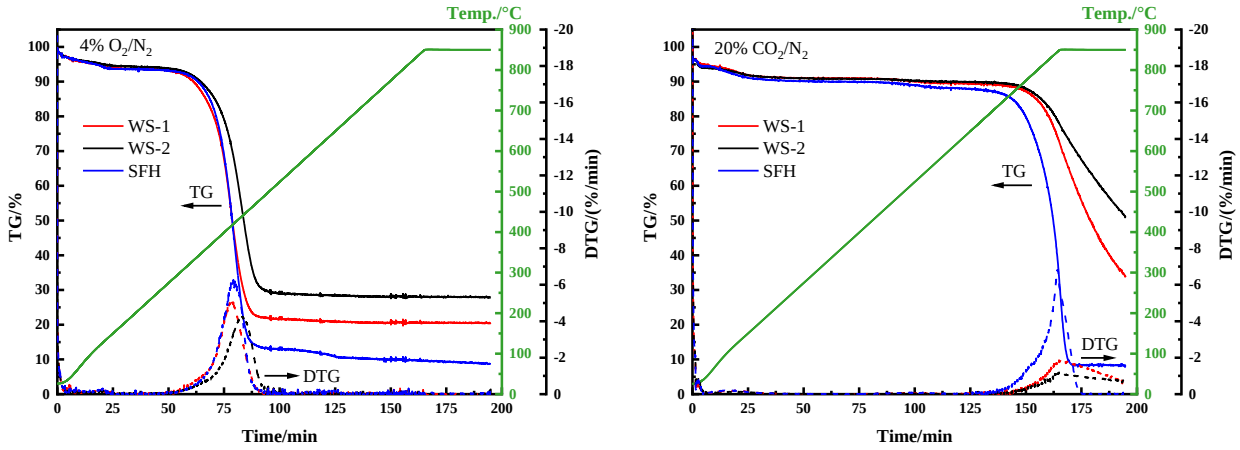

Figure 5-4 TG/DTG results of WS-1 char (red), WS-2 char (black) and SFH char (blue) under (a) 4 vol.% of O_2 in N_2 and (b) 20 vol.% of CO_2 in N_2 (TG: solid line and DTG: Dash line).

Table 5-3 Maximum weight loss rates (DTG_{max}) and temperature of maximum weight loss rates (T_p) of three char samples

	O_2 oxidization		CO_2 gasification	
	DTG_{max} / %·min^{-1}	T_p / °C	DTG_{max} / %·min^{-1}	T_p / °C
WS-1	5.01	423	1.86	850
WS-2	4.20	444	1.20	850
SFH	6.26	417	6.78	845

5.3.5 Characterization of ash and agglomerates

5.3.5.1 Crystalline phase in three ashes formed during combustion

The crystalline phases in the LTA and HTA samples were examined by XRD, and the results are presented in Figure 5-5. For WSs, in addition to quartz (SiO_2), which is an important crystalline compound in the ashes of WS-1 and WS-2, arcanite (K_2SO_4) is observed in both the LTA and HTA samples from combustion of the two wheat straws. The phosphates, which are $KCaPO_4$ and $Ca_9MgK(PO_4)_7$ for WS-1 and WS-2, respectively, are observed in the LTA samples, whilst silicates, which are $K_2MgSi_3O_8$ and $KAlSiO_4$, respectively, for WS-1 and WS-2, are detected in the HTA samples. In addition, Al phosphate ($AlPO_4$) is formed in the HTA of WS-2 due to the high Al content in WS-2. For the LTA of SFH, $K_2Ca(CO_3)_2$ and K_2SO_4 are the dominant crystalline compounds, and minor amounts of MgO and CaO are observed. However, $K_2Ca(CO_3)_2$ disappears in the HTA of SFH, probably being attributed to the decomposition of carbonates due to the fact that the ash is heated at high temperature (850 °C) for 3 hours. Increased amounts of MgO and CaO are found in the HTA of SFH.

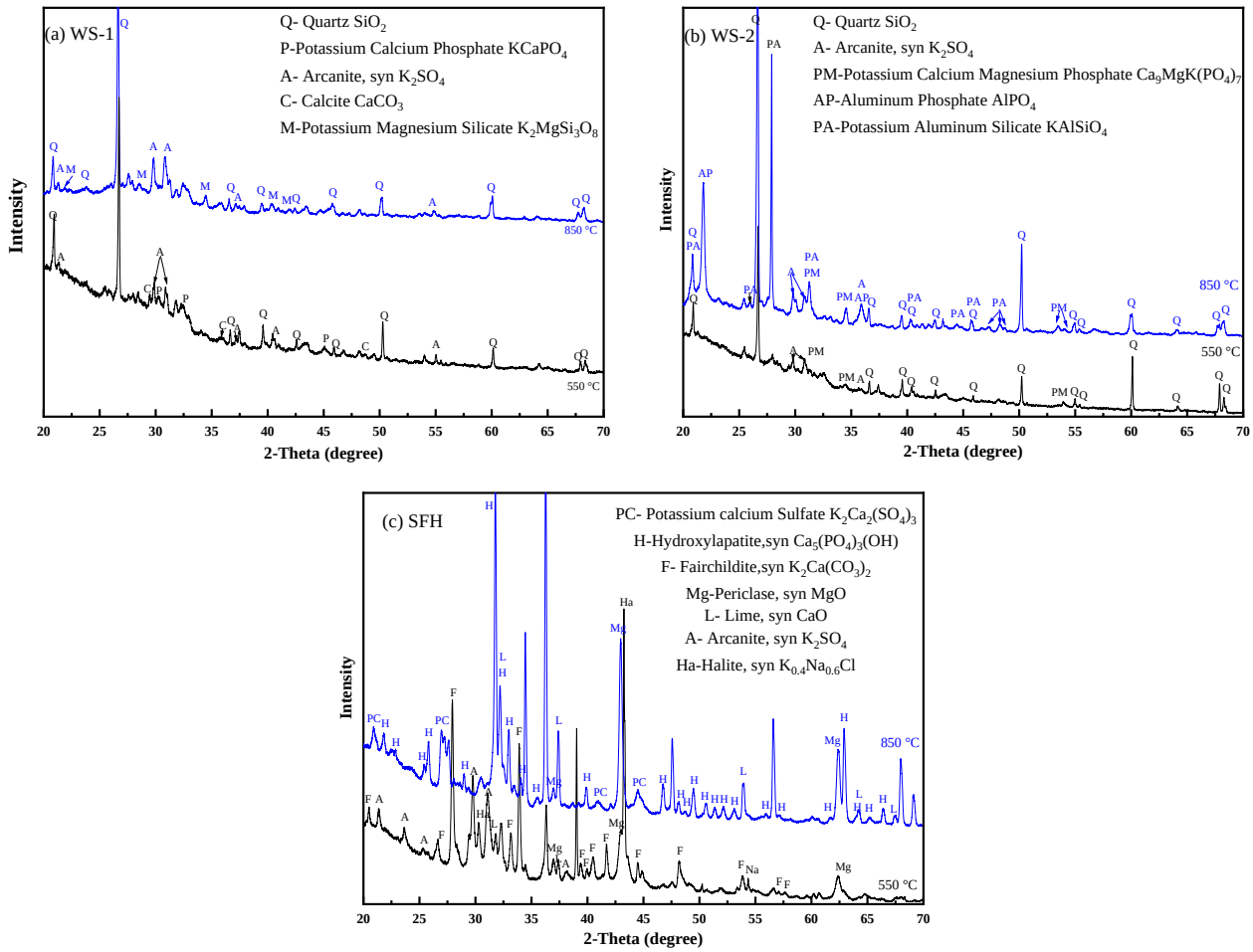

Figure 5-5 XRD results of the ash samples of (a) WS-1, (b) WS-2 and (c) SFH that prepared at 550 °C and 850 °C under air condition.

5.3.5.2 Surface elemental distribution of the resides of WS-1 and SFH

The morphology and mapping of the primary elements, including K, Ca, Mg, Si, P, S, C, and O, of WS-1 char and SFH ash produced under CO_2 gasification in TGA were examined by SEM-EDX, as given in Figure 5-6. The elemental compositions of the residues are shown on C-O-free basis. The results show that WS-1 char is dominated by K, Ca, and Si, and the main elements of SFH ash are K, Ca, and Mg. Generally, K is uniformly distributed in the two residues, whilst the distribution of Ca, Mg, Si, and P are not evenly. For WS-1 char sample, the Si-rich areas are consistent with K- and O-rich areas, indicating that Si may present as K-rich silicates. However, the Si-rich areas in SFH ash are in agreement with the Ca-rich area, suggesting that the slightly amount of Si in SFH probably exists in forms of Ca-rich silicates. The distribution of P in WS-1 char and SFH ash is consistent with the distribution of Mg and Ca, indicating that P may present as K-Ca/Mg phosphates.

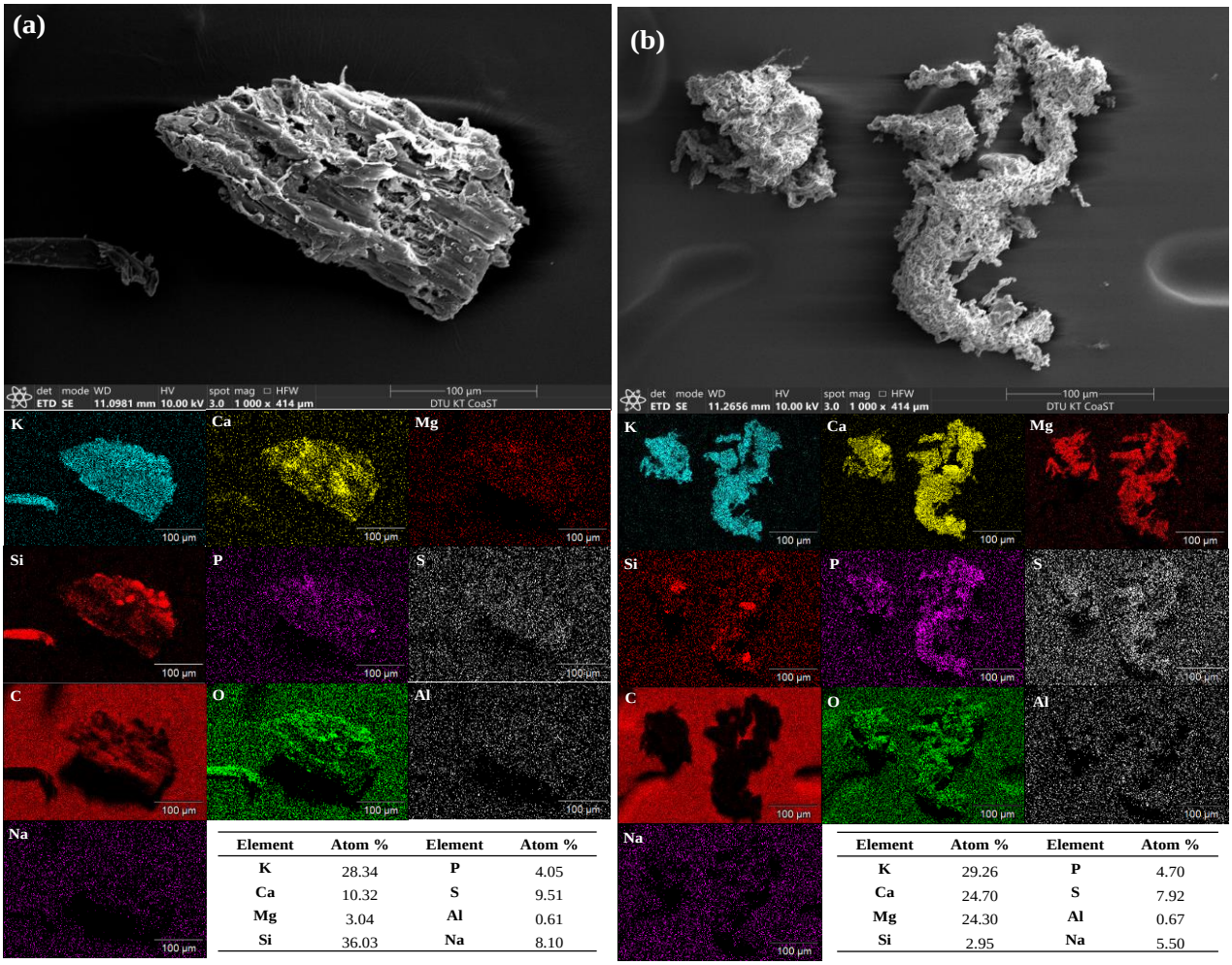

Element	Atom %	Element	Atom %
K	28.34	P	4.05
Ca	10.32	S	9.51
Mg	3.04	Al	0.61
Si	36.03	Na	8.10

Element	Atom %	Element	Atom %
K	29.26	P	4.70
Ca	24.70	S	7.92
Mg	24.30	Al	0.67
Si	2.95	Na	5.50

Figure 5-6 SEM-EDX elemental mapping of surfaces of (a) WS-1 char and (b) SFH ash produced during CO_2 gasification in TGA experiments (elemental analyses are presented as atom% on C-O-free basis).

To better illustrate the elemental compositions of the residues, the selected points of the two residues were analyzed by EDX, and the results are presented in Figure 5-7 and Table 5-4. The elemental compositions are shown on C-O-free basis, and the raw data is given in Table C-1 in Appendix C. As shown in Figure 5-7, three types of morphology can be observed in the WS-1 char, including light-colored flocculent substances, dark-colored smooth substances, and spherical particles. The light-colored areas (Point 1 and 2) contain a major amount of K, Ca, Si, and a small amount of Mg, P and S, indicating that the dominated compounds may be K-rich K-Ca/Mg silicates. The dark-colored areas are (Point 5 and 6) is dominated by K followed by Ca and S, and then Mg, P, and Si. The possible compounds may be K-Ca/Mg sulfates/phosphates/silicates. The partially molten spherical particles (Point 3 and 4) are mainly composed of K and Si, suggesting that they probably are K silicates. Two types of morphology are found in SFH ash. One is the light-colored flocculent substances, and the other is dark-colored smooth substances. The elements of the light-colored flocculent substances (Point 1 and 2) includes a significant amount of Mg, Ca and K, minor amount of P and S, as well as a slightly amount of Si. When the silicon, sulfur and phosphorous in the ash are assumed to be presented as K_2SiO_3, K_2SO_4, and KPO_3, respectively, the presence of K carbonates or K hydroxides

probably can be indicated by a molar ratio of K/(2Si+2S+P) higher than unity. The molar ratios of K/(2Si+2S+P) are 1.75 and 1.51, respectively, for Point 1 and 2, indicating that carbonates, hydroxides or oxides may exist in the SFH ash. The dominated elements of the dark-colored smooth substances (Point 3 and 4) are K, Ca and Si, revealing they may be Ca-rich K-Ca silicates. Around 10 atom% of carbon is detected in SFH ash (as shown in Table C-1 in Appendix C), which also indicates that the carbonates may be formed in SFH ash.

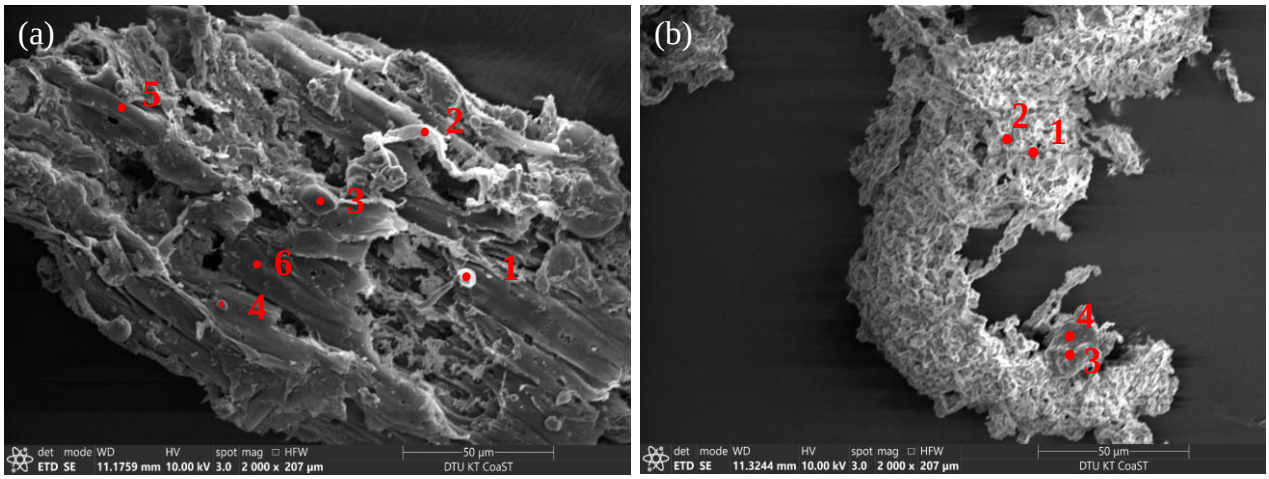

Figure 5-7 Morphology (SEM: SE mode) of (a) WS-1 char and (b) SFH ash produced during CO_2 gasification in TGA experiments.

Table 5-4 EDX analysis of selected point of the residues shown in Figure 5-7 (atom% on C-O-free basis)

	WS-1 Point 1	WS-1 Point 2	WS-1 Point 3	WS-1 Point 4	WS-1 Point 5	WS-1 Point 6	SFH Point 1	SFH Point 2	SFH Point 3	SFH Point 4
K	28.05	36.79	15.58	27.78	53.06	57.05	28.54	23.22	10.86	11.00
Ca	29.18	13.10	0.57	0.72	14.59	8.75	14.98	25.01	54.01	54.01
Mg	8.50	5.47	0.11	0.92	6.49	6.97	46.35	41.32	0.66	1.26
Al	0.47	0.46	0.20	0.13	0.18	0.32	0.28	1.15	0.28	0.33
Si	19.83	33.37	83.02	68.76	6.67	8.75	0.87	1.84	30.71	29.25
P	9.44	6.15	0.51	0.72	7.93	4.38	3.36	3.20	2.40	3.00
S	4.53	4.67	0.00	0.98	11.08	13.78	5.63	4.27	1.07	1.15
Si/K	0.71	0.91	5.33	2.48	0.13	0.15	0.03	0.08	2.83	2.66

5.3.5.3 Morphology of agglomerates from selected conditions

The morphology of the selected agglomerates from combustion of WS-1 and SFH are given in Figure 5-8. It is found that the bed particles from combustion of WS-1 and SFH are coated and glued by a molten phase, and some light-colored flocculent substances are attached on the sand surfaces. The elemental compositions of agglomerate necks, sand surfaces, and flocculent substances are examined by EDX analysis, and the results are summarized in Table 5-5. For WS-1, the necks between two bed particles from combustion (Point 1 and 2) are composed of Si, K and Ca, suggesting that the bed particles probably are agglomerated by the molten K silicates and K-Ca silicates. The sand surfaces (Point 3) have the similar elemental compositions with the necks. The light-colored flocculent

substances (Point 4) are consisted with Si, K, Ca, and P, indicating that they may be the unmelted wheat straw ash particles. The main elements of the neck of agglomerate from combustion of SFH (Point 1) are Si, K, Ca and Mg, suggesting that the sands possibly are glued by the molten K-Ca/Mg silicates, which may produce by the interaction between SFH ash and bed material (SiO_2) due SFH is a Si-lean fuel. The compositions of sand surfaces (Point 3) are similar with the agglomerate necks but with a relatively lower Mg and Ca content, suggesting that the coating layers may be K-silicates. The light-colored flocculent substances (Point 2) are composed of O, C, Mg, Ca, P, and a slightly amount of Si, indicating that they may be the SFH ash particles. Although the dominant K-species in WS-1 ash and SFH ash may be quite different, the agglomeration of WS-1 and SFH probably both are caused by the molten K containing silicates.

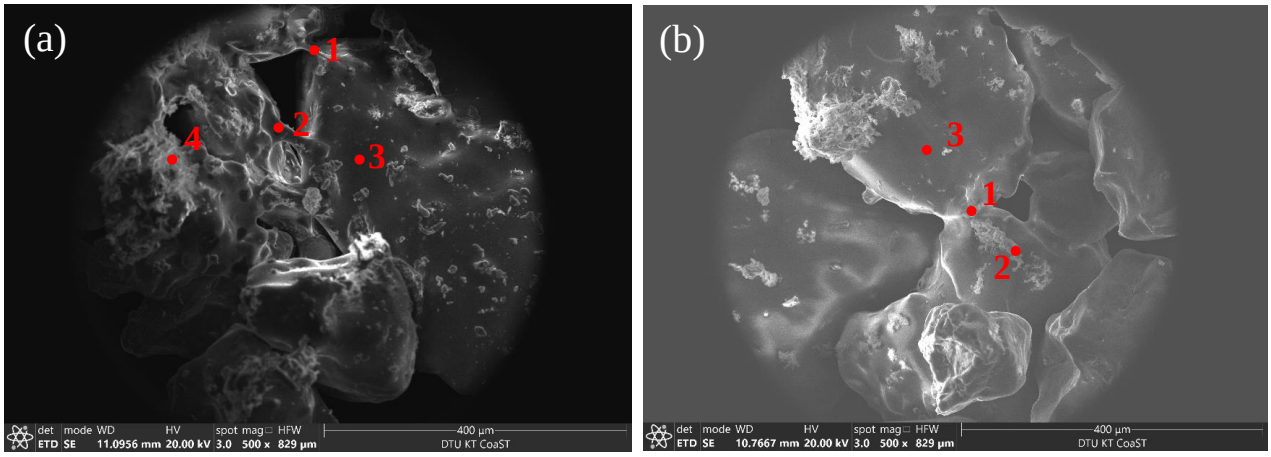

Figure 5-8 Morphology (SEM: SE mode) of agglomerates from (a) WS-1 and (b) SFH combustion with an ER of 1.45.

Table 5-5 EDX analysis of selected point of the agglomerates shown in Figure 5-8 (atom%)

	WS-1 Point 1	WS-1 Point 2	WS-1 Point 3	WS-1 Point 4	SFH Point 1	SFH Point 2	SFH Point 3
C	5.94	5.51	5.72	7.68	7.85	9.73	15.53
O	58.62	59.74	53.23	56.02	60.49	59.77	66.73
K	6.07	9.52	6.17	8.79	7.60	0.80	2.68
Ca	0.58	2.43	0.89	5.14	2.39	8.56	0.11
Mg	0.33	0.61	0.03	1.41	2.62	13.36	0.24
Al	0.41	0.24	0.09	2.40	1.21	0.63	0.21
Si	27.71	21.49	33.63	15.63	15.60	2.04	14.42
P	0.33	0.46	0.24	2.93	1.98	4.91	0.08
S	0.00	0.00	0.00	0.00	0.25	0.20	0.00
Si/K	4.57	2.26	5.45	1.78	2.05	2.54	5.38

In order to investigate the agglomeration during gasification of SFH, the morphology and surface elemental compositions of the selected agglomerates from gasification with an ER of 0 and a SFR of 2.3 are given in Figure 5-9. Consistent with the agglomerates formed in combustion, the bed particles are glued by a molten K silicates (Point 1), which probably result from the interaction between SFH ash and bed material.

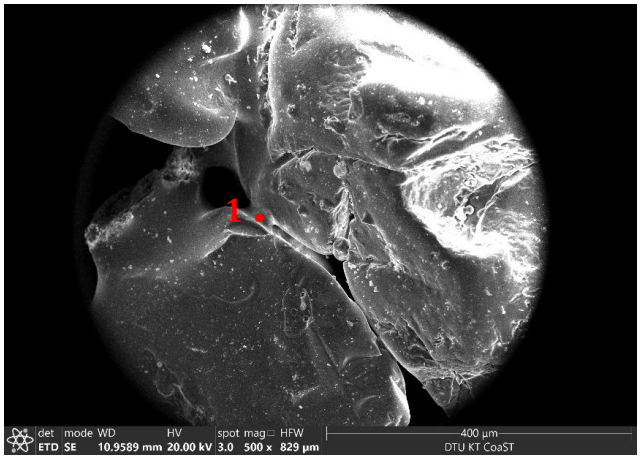

Element	K	Ca	Mg	Al
Atom%	20.53	0.45	0.45	0.29
Element	Si	P	S	
Atom%	78.15	0.12	0.00	

Data are in atom% (carbon and oxygen free basis).

Figure 5-9 Morphology (SEM: SE mode) (left) and EDX analysis of selected point (right) of agglomerates from SFH gasification with an ER of 0 and a SFR of 2.3.

5.3.6 K distribution predicted by thermodynamic equilibrium calculations

5.3.6.1 Predicted K-species distribution in the ash

As presented in the Table 5-1, the two wheat straws are Si-rich fuels with the Si/K molar ratios of 1.56 and 2.60, respectively, for WS-1 and WS-2, whilst the sunflower husk is a Si-lean fuel with a Si/K molar ratio of 0.04. Thermodynamic equilibrium calculations were performed to understand the possible ash transformation during combustion and gasification of the three biomasses at ER in a range of 0 - 1.4 at 850 °C, and the results are shown in Figure 5-10. For WS-1, a K and Si rich fuel with moderate Al, the thermodynamically favorable K-species under combustion condition are gas phase KCl, molten phase K containing slag, as well as solid phase $KAlSi_2O_6$ and K_2SO_4. The compositions of slag phase indicates that the slag phase is molten K-silicates and K-Al silicates, as shown in Figure C-2 in Appendix C. Solid phase $K_2Si_2O_5$ appears while K_2SO_4 disappears under a reducing atmosphere due to the fact that K_2SO_4 is unstable under reducing atmosphere. Since it is suggested that Si^{4+}, as a network former, increases the slag viscosity, and K^+, as a network modifier, could decrease the slag viscosity[13], the molar ratios of Si/K in the slag phase are plotted. As shown in Figure 5-11, the Si/K molar ratios of the slag formed under oxidizing atmosphere is higher than that of under reducing atmosphere, suggesting that the viscosity of slag phase produced under reducing atmosphere probably is lower than that formed under oxidizing atmosphere. For WS-2, a K and Si rich fuel with relatively high Al, the calculations predict that K-Al silicates ($KAlSi_2O_6$ and $KAlSi_3O_8$), are produced. However, the formation of K-Al silicates in the ash at 850 °C probably is a kinetics controlled process[14,15], resulting in the amount of K-Al silicates may be far below the equilibrium calculations[16,17]. Therefore, a slag phase still could be found in WS-2 ash. For SFH, K presents as gas phase KOH and KCl, as well as solid phase $K_2Ca(CO_3)_2$, K_2CO_3, and K_2SO_4 during combustion. During SFH gasification, the carbonates, such as $K_2Ca(CO_3)_2$ and K_2CO_3, are still the dominant K-species. However, $K_2Ca(CO_3)_2$ is unstable at the ER below 0.37. In general, the dominated K-species produced during conversion of WSs are K silicates. Potassium exists as K

carbonates during conversion of SFH. These results are in agreement with what has been found in thermodynamic equilibrium calculations calculated by Öhman[5]. The equilibrium calculations results generally are in agreement with the XRD analysis results.

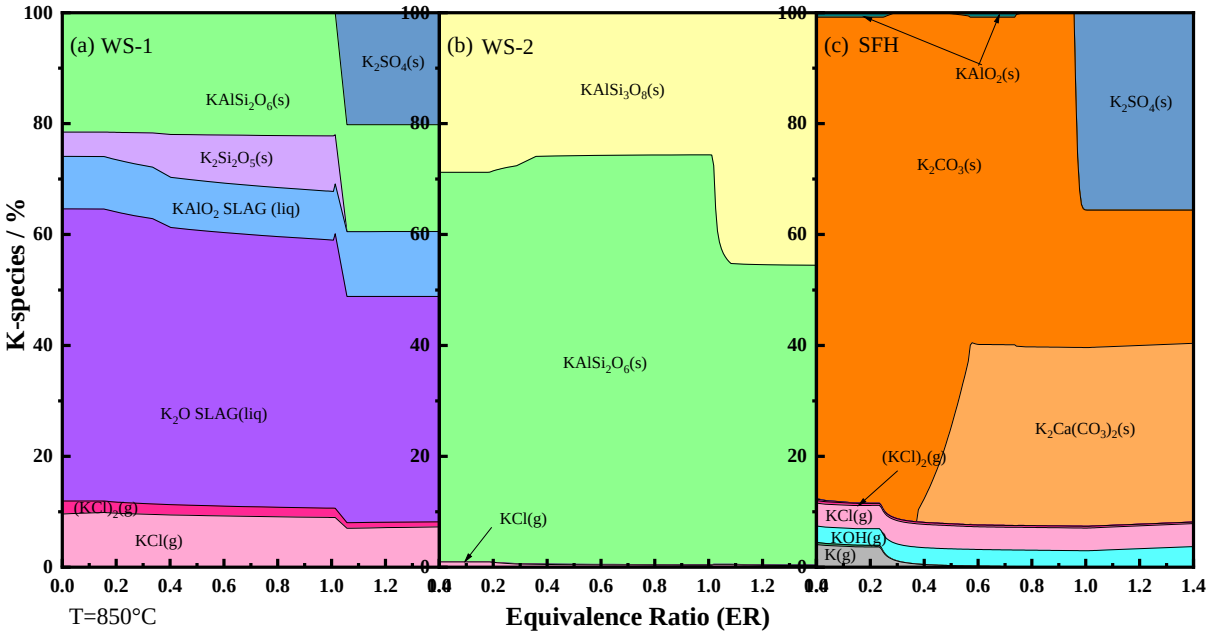

Figure 5-10 Predicated K-species in three ashes at various equivalence ratio by thermodynamic equilibrium calculations at 850 °C.

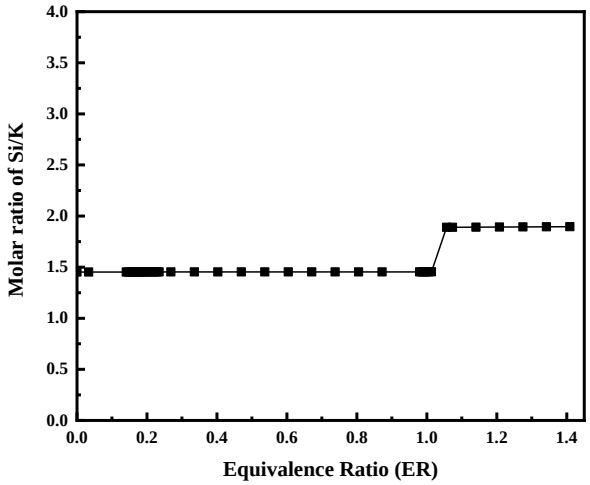

Figure 5-11 Predicated molar ratios of Si to K in the slag phase during WS-1 conversion at various equivalence ratio by thermodynamic equilibrium calculations at 850 °C.

5.3.6.2 Predicted K-species distribution with bed material

Figure 5-12 shows the predicted K-species distribution during WS-1 and SFH conversion at various ERs when the bed material are included. The addition of SiO_2 in the calculations slightly increases the amount of slag phase during WS-1 conversion. For SFH, significant amount of slag phase, which is composed of K_2O and SiO_2 (Figure C-3 in Appendix C), and/or K silicate ($K_2Si_4O_9$) are formed during gasification, probably resulting from the interaction between K carbonates and bed material (SiO_2). This result is in agreement with the observation found in SEM analysis of agglomerates.

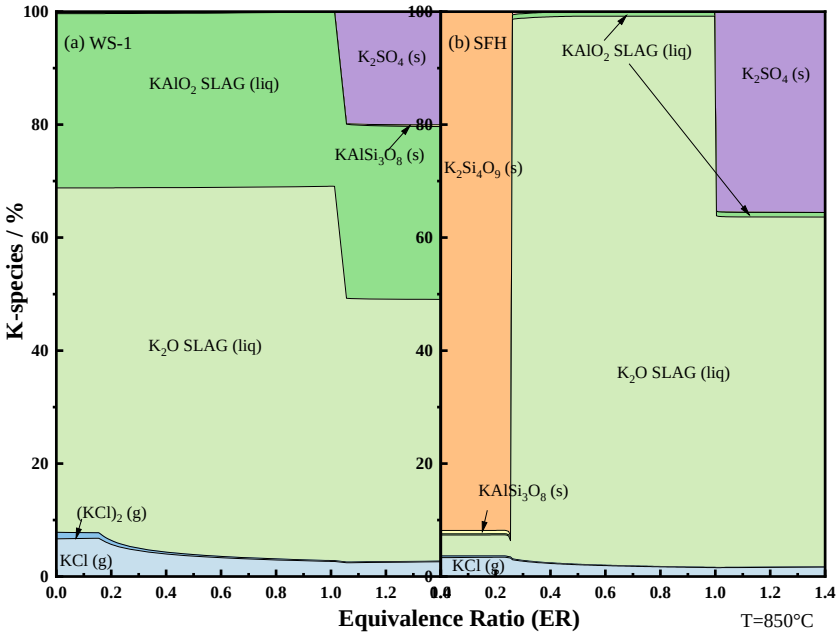

Figure 5-12 Predicted distribution of K-species during conversion of WS-1 and SFH in fluidized bed at 850 °C at various equivalence ratio by thermodynamic equilibrium calculations.

5.4 Discussion

5.4.1 Influence of Si/K on ash chemistry and agglomeration

The significantly different Si contents in WSs and SFH may result in the different distribution of K in their ashes, and thereby causing different agglomeration tendency and mechanism in combustion and gasification of WSs and SFH. SEM-EDX analyses of the ashes of WSs and SFH and the equilibrium calculations results suggest that the dominated K-species probably are K silicates and K carbonates, respectively, for WSs and SFH under both combustion and gasification conditions. Although K carbonates are not detected by XRD in the HTA of SFH, which probably due to a long ashing time during preparation of ash, significant amount K carbonates may be produced during SFH conversion as indicated by the XRD analysis of LTA of SFH. The agglomeration of WSs may be induced by the attachment of the partially molten ash, which contains significant amount of K-rich silicates, on the bed material, subsequently forming a coating layer[3]. A higher Al content in the WS

ash may increase the melting temperature of ash[18], causing a decrease in the agglomeration tendency of WS ash. Therefore, WS-2 ash has a lower agglomeration tendency than WS-1 ash. Although SFH is a Si-lean fuel, the dominated compositions of agglomeration necks still are molten K silicates. Therefore, the agglomeration during conversion of SFH may be caused by the interaction between SFH ash, whose ash may contain significant amount of K carbonates, and SiO_2. It is has be shown that K_2CO_3 may induce agglomeration under air condition by forming molten K silicates though reaction between K_2CO_3 and silica sand[19].

A reducing atmosphere and a high concentration of steam in gasification accelerate the agglomeration of WS ashes and SFH ash (as shown in Figure 5-2 and 5-3). As discussed in Chapter 3 and Chapter 4, the reducing atmosphere promotes the melting of the WS ashes, and thereby accelerating the agglomeration of WSs. The presence of steam most likely to decrease the residual carbon amount in the bed and to lower the viscosity of WS ashes, resulting in an accelerated agglomeration. The SEM-EDX analyses of agglomerates from gasification (Figure5-9) indicates that the formation of K silicates via the interaction between SFH ash and bed material may be the dominant agglomeration mechanism during SFH gasification. It is speculated that the reactivity of K_2CO_3 towards SiO_2 is promoted by the reducing atmosphere[19]. In addition, it is suggested that K_2CO_3 can be converted into KOH by reacting with steam[19,21,22], resulting in the reactivity of K_2CO_3 towards SiO_2 is strongly enhanced by the presence of steam[22]. It also has been speculated that SiO_2 probably could be glued by a molten KOH, which has a melting temperature of 360 °C, in a K_2CO_3/SiO_2 system under a steam containing atmosphere[19]. The promoted agglomeration of SFH caused by a reducing atmosphere and a high concentration of steam in this study may be related to these speculations. The melting of SFH ash may be promoted by the reducing atmosphere, due to the fact that K_2SO_4 with a melting temperature of 1069 °C is unstable under reducing atmosphere (as shown in Figure 5-10). Meanwhile, the reducing atmosphere probably accelerate the interaction between SFH ash and bed material, thus promoting the agglomeration. Under the condition with a high concentration of steam, the accelerated agglomeration probably caused by an increased melting of ashes and a promoted interaction between SFH ash and bed material. In addition, the viscosity of the produced K silicates may also be lowered by the steam. However, the detailed mechanism of influence of reducing atmosphere and steam on agglomeration of SFH needs to be further studied.

5.4.2 Influence of char reactivity on agglomeration

During gasification of biomass, the inhibition effect of residual carbon caused by decreasing ER decreases with increasing char reactivity. A higher char reactivity will result in a low amount of residual carbon in the bed and thereby causes a less inhibition effect on agglomeration during gasification, thus may increase the agglomeration tendency of biomass. The char reactivity of the three biomasses is consistent with their agglomeration tendency observed in fluidized bed gasification experiments with a low ER. Therefore, the higher amount of residual carbon in the bed in LTCFB gasification of WS-2, caused by the lower char reactivity of WS-2, may be the dominate reason for

the different agglomeration behaviors of WS-1 and WS-2 in LTCFB gasifier described in Chapter 1, Section 1.1. In the air blown gasification system, the lower critical ER of SFH compared to the WSs may be partially attributed to the higher char reactivity of SFH.

5.5 Conclusions

The agglomeration of two types of biomass (two batches of wheat straws and one sunflower husk) in fluidized bed combustion and gasification are investigated in this chapter. The effects of char reactivity and molar ratio of Si/K on the agglomeration of biomass at various ERs and SFRs are studied. The following conclusions can be drawn:

(1) The difference in the molar ratios of Si/K in WSs and SFH may result in the different agglomeration tendency and mechanisms of WSs and SFH. During combustion and gasification of WSs, the agglomeration may be caused by the partially molten ashes adhere on the bed particles and subsequently form a coating layer. The SFH ash may lead to the agglomeration by forming K silicates via interacting with bed particles (SiO_2) during SFH conversion. For WSs, the higher Al content in WS-2 compared to WS-1 may result in a decrease in the melting of ash, and thereby causing a decrease in the agglomeration tendency during conversion.

(2) A reducing atmosphere, a high concentration of steam, and the residual carbon in the bed show consistent effect on the agglomeration of the three fuels. However, the reducing atmosphere and steam probably promote the agglomeration of Si-rich wheat straws and Si-lean sunflower husk by different routes due to their different agglomeration mechanisms. For SFH, the promoted agglomeration under a reducing atmosphere and a high concentration of steam probably results from an increased melting of ash and a promoted interaction between ash and bed particles. The detailed mechanism of influence of reducing atmosphere and steam on agglomeration of SFH needs to be further studied.

(3) During gasification of biomass, the inhibition effect of residual carbon caused by decreasing ER reduces with increasing char reactivity. The high char reactivity of SFH results in less residual carbon in the bed, thus causing a high agglomeration tendency of SFH during gasification with a low ER.

(4) The critical ER of SFH, which is 0.04, is lower than that of WSs, which are 0.36. The low critical ER of SFH is probably attributed to the high char reactivity of SFH and the different agglomeration mechanism of SFH from WSs caused by a low Si/K molar ratio.

Reference

(1) Scala, F. Particle Agglomeration during Fluidized Bed Combustion: Mechanisms, Early Detection and Possible Countermeasures. *Fuel Process. Technol.* **2018**, *171*, 31–38.

(2) Morris, J. D.; Sheraz, S.; Chilton, S.; Nimmo, W. Mechanisms and Mitigation of Agglomeration during Fluidize Bed Combustion of Biomass : A Review. *Fuel* **2018**, *230*, 452–473.

(3) Grimm, A.; Skoglund, N.; Boström, D.; Öhman, M.; Bostr, D.; Ohman, M.; Boström, D.; Öhman, M.; Bostr, D.; Ohman, M. Bed Agglomeration Characteristics in Fluidized Quartz Bed Combustion of Phosphorus-Rich Biomass Fuels. *Energy & Fuels* **2011**, *25* (3), 937–947.

(4) Brus, E.; Öhman, M.; Nordin, A. Mechanisms of Bed Agglomeration during Fluidized-Bed Combustion of Biomass Fuels. *Energy & Fuels* **2005**, *19* (3), 825–832.

(5) Öhman, M.; Pommer, L.; Nordin, A. Bed Agglomeration Characteristics and Mechanisms during Gasification and Combustion of Biomass Fuels. *Energy & Fuels* **2005**, *19* (4), 1742–1748.

(6) Gatternig, B.; Karl, J. Investigations on the Mechanisms of Ash-Induced Agglomeration in Fluidized-Bed Combustion of Biomass. *Energy & Fuels* **2015**, *29*, 931–941.

(7) Lin, W.; Dam-Johansen, K.; Frandsen, F. Agglomeration in Bio-Fuel Fired Fluidized Bed Combustors. *Chem. Eng. J.* **2003**, *96* (1–3), 171–185.

(8) Lin, W.; Jensen, A. D.; Johnsson, J. E.; Dam-Johansen, K. Combustion of Biomass in Fluidized Beds: Problems and Some Solutions Based on Danish Experiences. In *Proceedings of the 17th International Conference on Fluidized Bed Combustion*; American Society of Mechanical Engineers: Jacksonville, Florida USA, 2003; pp 945–953.

(9) Lin, W.; Krusholm, G.; Dam-Johansen, K.; Musahl, E.; Bank, L. Agglomeration Phenomena in Fluidized Bed Combustion of Straw. In *Proceedings of the 14h International Conference on Fluidized Bed Combustion*; American Society of Mechanical Engineers: Canada, 1997; Vol. 2, pp 831–837.

(10) George, J.; Arun, P.; Muraleedharan, C. Experimental Investigation on Co-Gasification of Coffee Husk and Sawdust in a Bubbling Fluidised Bed Gasifier. *J. Energy Inst.* **2019**, *92* (6), 1977–1986.

(11) Werther, J.; Saenger, M.; Hartge, E. U.; Ogada, T.; Siagi, Z. Combustion of Agricultural Residues. *Prog. Energy Combust. Sci.* **2000**, *26* (1), 1–27.

(12) Chaivatamaset, P.; Tia, S. The Characteristics of Bed Agglomeration during Fluidized Bed Combustion of Eucalyptus Bark. *Appl. Therm. Eng.* **2015**, *75*, 1134–1146.

(13) Gao, J.; Wen, G.; Huang, T.; Tang, P.; Liu, Q. Effects of the Composition on the Structure and Viscosity of the CaO–SiO2-Based Mold Flux. *J. Non. Cryst. Solids* **2016**, *435*, 33–39.

(14) Wang, G.; Jensen, P. A.; Wu, H.; Frandsen, F. J.; Sander, B.; Glarborg, P. Potassium Capture

by Kaolin, Part 1: KOH. *Energy & Fuels* **2018**, *32* (2), 1851–1862.

(15) Wang, G.; Jensen, P. A.; Wu, H.; Frandsen, F. J.; Sander, B.; Glarborg, P. Potassium Capture by Kaolin, Part 2: K_2CO_3, KCl, and K_2SO_4. *Energy & Fuels* **2018**, *32* (3), 3566–3578.

(16) Wang, G.; Jensen, P. A.; Wu, H.; Frandsen, F. J.; Laxminarayan, Y.; Sander, B.; Glarborg, P. KOH Capture by Coal Fly Ash. *Fuel* **2019**, *242*, 828–836.

(17) Wang, G.; Jensen, P. A.; Wu, H.; Frandsen, F. J.; Laxminarayan, Y.; Sander, B.; Glarborg, P. Potassium Capture by Coal Fly Ash: K_2CO_3, KCl and K_2SO_4. *Fuel Process. Technol.* **2019**, *194*.

(18) Olofsson, G.; Ye, Z.; Bjerle, I.; Andersson, A. Bed Agglomeration Problems in Fluidized-Bed Biomass Combustion. *Ind. Eng. Chem. Res.* **2002**, *41*, 2888–2894.

(19) Ma, T.; Fan, C.; Hao, L.; Li, S.; Jensen, P. A.; Song, W.; Lin, W.; Dam-Johansen, K. Biomass Ash Induced Agglomeration in Fluidized Bed. Part 2: Effect of Potassium Salts in Different Gas Composition. *Fuel Process. Technol.* **2018**, *180*, 130–139.

(20) Aničić, B. Agglomeration Mechanisms during Fluidized Bed Combustion of Biomass, Technical University of Denmark, 2018.

(21) Sevonius, C.; Yrjas, P.; Hupa, M. Defluidization of a Quartz Bed - Laboratory Experiments with Potassium Salts. *Fuel* **2014**, *127*, 161–168.

(22) Zhao, H.; Xu, W.; Song, Q.; Zhuo, J.; Yao, Q. Effect of Steam and SiO2 on the Release and Transformation of K_2CO_3 and KCl during Biomass Thermal Conversion. *Energy & Fuels* **2018**, *32* (9), 9633–9639.

6. Application of Pulse Flow to a Fluidized Bed for Combustion and Gasification of Wheat Straw

Abstract

Agglomeration may cause severe problems in operation of biomass combustion and gasification in fluidized beds. Improving fluidization quality by external forces may be one of the options as the potential countermeasure to mitigate the agglomeration problem. In this chapter, the pulsed flow is applied to the fluidized bed reactor to examine the possibility for mitigation of agglomeration in combustion and gasification of wheat straw. The effects of parameters related to pulsed flow, such as flow rate ratio of pulsation (defined as the flow rate of pulsed flow divided by the total flow rate of primary gas), pulsation frequency and pulsation duty cycle (defined as the time of "flow-ON" period divided by the "flow-OFF" period in a pulsation), on the agglomeration tendency were studied in a lab-scale bubbling fluidized bed reactor at 850 °C using silica sand as bed material. The results reveal that the introducing of a pulsed flow to the reactor mitigates the agglomeration in fluidized bed combustor and gasifier. Among the parameters studied, the pulsation duty cycle shows the most significant effect on reducing the agglomeration tendency, while the pulsation frequency shows the least impact. At the condition of pulsation flow rate ratio of 0.4, pulsation frequency of 1.5 Hz and pulsation duty cycle of 25/75, the amounts of straw fed for inducing defluidization is 151.7% and 137.5% of that under the condition with the continuous flow for in combustion and gasification, respectively. Moreover, the effect of application of the pulsed flow to the reaction process is negligible.

This chapter has been written in a manuscript format. A slightly modified version of this chapter will be submitted to a peer-reviewed journal.

6.1 Introduction

Fluidized beds are widely applied in biomass combustion and gasification due to their fuel flexibility and high efficiency[1–3]. However, the occurrence of agglomeration causes operational problems, and may lead to completely defluidization[4]. Extensive investigations have been carried out for understanding the agglomeration mechanisms and for mitigating the agglomeration, as have been discussed in a few review papers[5–8]. It is widely accepted that the presence of the molten phase, mainly the potassium containing compounds, responsible for the agglomeration in fluidized bed reactor[9].

Many countermeasures to agglomeration have been proposed based on the mechanism of increasing the melting temperature of the ash by altering the ash chemistry, including utilization of alternative bed materials, such as Al-[10,11], Ca-[12], Mg-[13], or Fe-containing[14] materials, application of additives, such as Al-Si-[15], Ca-[16] or P-based[17] additives, pretreating of biomass[18], and co-combustion of K-lean fuels[19,20]. Other countermeasures are proposed based on the mechanism of improving the fluidization quality by increasing the ratio of gas velocity to the minimum fluidization velocity, i.e. applying high gas velocity[21] and selecting small particles[22], which may limit the agglomerates accumulation by a high break rate to the agglomerates[21]. The introducing of a pulsed flow to a fluidized bed, as a kind of external assistance, could be a countermeasure for improving the fluidization quality in fluidized bed[23,24].

Pulsed fluidization is a method that using an on-and-off primary gas to fluidize the bed particles. It is well known that application of a pulsed flow can improve the fluidization quality for Geldart Group A/B/C particles by reducing the minimum fluidization velocities of the bed particles[25,26]. It is suggested that the pulsed flow shows positive effects on enhancing the heating transfer in fluidized bed[27–29], accelerating the drying of biomass[30,31], and improving the mixing of particles[32]. Therefore, the pulsed fluidized bed reactor may be a potential countermeasure for mitigating agglomeration tendency in biomass combustion and gasification.

The potential of pulsed flow on tackling defluidization of Group B particles has been indicated by discrete element method (DEM) simulations[33]. However, mostly of experimental work has been carried out focusing on the effect of pulsed flow on the formation and breakage of agglomerates of nanoparticles[34,35]. Limited studies have been reported on the application of pulsed flow in fluidized bed combustion and gasification, and these studies focus on the influence of pulsed flow on the heat transfer and combustion efficiency[36]. The influence of pulse flow on agglomeration in fluidized bed combustion/gasification has not been revealed from author's knowledge. In this chapter, the possibility of application of pulsed flow to fluidized bed combustion/gasification of biomass to mitigate agglomeration is experimentally studied in a lab-scale bubbling fluidized bed.

6.2 Experimental section

6.2.1 Fuel and bed material

Silica sand (SiO_2 > 97 wt.%) with a density of 2600 kg/m^3 and a size range of 355 - 500 μm was used as bed material in the experiments. Wheat straw used in Chapter 3 was used as fuel and its compositions are shown in Table 3-1, Chapter 3. In order to achieve a smooth feeding, wheat straw with a size range of 0.6-2 mm was used.

6.2.2 Experimental apparatus

Experiments were carried out in a lab-scale bubbling fluidized bed reactor system, schematically shown in Figure 6-1. The setup consists of a gas supplying system, a fuel feeding system, a fluidized bed reactor, a gas sampling and analysis system and a data acquisition system. The gas supplied at the bottom of the reactor (U_t), which is called as primary gas, is composed of a continuous flow (U_c) and a pulsed flow (U_p). The compressed air and the N_2 in the continuous flow were controlled by the precision mass flow controllers (MFCs). The steam in the continuous flow was produced by a steam generator (VEIT 2365), and the supplying pipe was heated by an electric heat tracing. The schematic of square wave of gas pulsation was illustrated in Figure 6-2. A two-way solenoid valve, which was controlled by a programmable logic controller (PLC), was used to generate a gas pulsation (Yantai Songling Chemical Equipment CO., LTD, China). The valve opened when energized and closed when de-energized, and the gas flow, therefore, was intermittently supplied at a desired frequency. Duration of the "flow-ON" and "flow-OFF" period were separately controlled, allowing variations in both pulsation frequency and duty cycle. The accuracy of the "flow-ON" and "flow-OFF" period for each pulsation cycle was 10 milliseconds, resulting a maximum frequency of 50 Hz. The flow rate of pulsation during combustion was controlled by a gas regulator and a needle valve. The primary gas, passed through a preheating section (air-plenum) and distributed by a gas distributor with an open area of 4%, was introduced to the bubbling fluidized bed reactor with an inner diameter of 62.5 mm. The freeboard, with an inner diameter of 100 mm, was designed 600 mm above the gas distributor to reduce the elutriation of fine particles. The reactor, including preheating section and the reactor body, was externally heated by four independently controlled heating elements. A twin screws feeder (K-ML-KT20, Coperion K-Tron) was installed in the middle of the gas distributor and the freeboard to continuously feed the fuel with the assistance of a secondary gas. The fine particles in flue gas was collected in a container after being removed by a cyclone. A small amount of flue gas, sampled at the downstream of the cyclone, was sent to a series of analyzers (Emerson, NGA 2000 Analyser, FLSmidth A/S) after removal of the water and other condensed impurities to continuously monitor the concentrations of CO_2, CO, O_2, NO and SO_2. The temperatures right below air distributor (T_1), right above air distributor (T_2), 5 cm above air distributor (T_3), 2.5 cm above air distributor (T_4) were measured by four thermocouples, and the gauge pressure at position that right below air distributor (P_1, pressure in the air-plenum) and the pressure drop over the bed (P_2) were monitored by two

pressure sensors (Noding P121-4B0-311, with a pressure range of 0-50 mbar having a response time of 200 ms; Honeywell ST-3000 with a response time of 478 ms). The profiles of temperatures, pressures and gas concentrations were recorded by a data acquisition system every 200 ms during experiments.

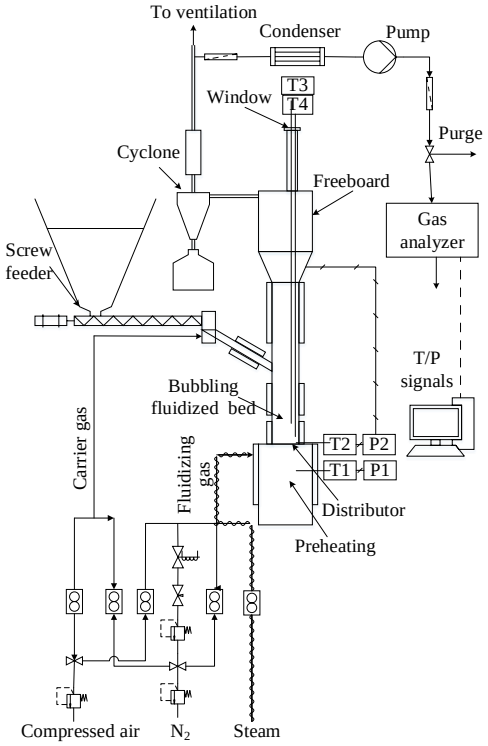

Figure 6-1 A schematic drawing of the lab-scale pulsed fluidized bed reactor

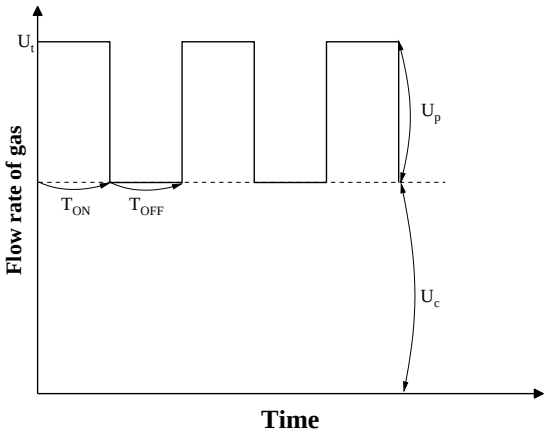

Figure 6-2 A schematic of square wave of gas pulsation. U_t: total flow rat of primary gas; U_p: flow rate of pulsed flow; U_c: flow rate of continuous flow; T_{ON}: time of "flow-ON" period; T_{OFF}: time of "flow-OFF" period

6.2.3 Experimental conditions and procedures

The primary gas was kept to a constant total flow rate of 11.5 Nl/min, with a composition of 100% air, and a mixture of 25 vol.% steam, 25 vol.% air, and 50 vol.% N_2 for combustion and gasification, respectively. The secondary gas, with a flow rate of 15.5 Nl/min, was 100% N_2 and a mixture of 55.5 vol.% air and 44.5 vol.% N_2, respectively, in combustion and gasification, to keep a constant total excess air ratio of 1.45 in the system. All experiments were conducted at a temperature of 850°C with a set fuel feeding rate of 0.11 kg/h.

The influence of vital parameters, including flow rate ratio of pulsation(U_p/U_t, defined as the flow rate of pulsed flow divided by the total flow rate of primary gas), pulsation frequency and pulsation duty cycle(T_{ON}/T_{OFF}, defined as the time of "flow-ON" period divided by the "flow-OFF" period in a pulsation), which show signification effects on the biomass drying[27,30] and the hydrodynamics[24,26] in fluidized bed, on agglomeration tendency were evaluated in combustion and gasification. In order

to maintain the fluidization of bed particles during the "flow-OFF" period, the flow rate ratio of pulsation was varied in the range from 0.2 to 0.4. Compressed air and N_2 was used as the pulsed flow in combustion and gasification, respectively. The fluidized bed can be considered analogous to a second-order mechanical vibration system and the undamped natural frequency of the system (f_N) can be calculated according to the equation that proposed by Bi *et al.*[37]:

$$f_N = \frac{1}{2\pi}\sqrt{\frac{g}{H_{mf}}}$$

where H_{mf} (m) is the static bed height. The pulsation frequency was varied in the range of 0.5 - 3 Hz, covering the f_N of this system, which is 1.57 Hz. Three typical pulsation duty cycles, namely 25/75, 50/50 and 75/25, were investigated. The experimental matrix is shown in Table 6-1. The repeatability of experiments are proved by the standard deviations of repeated experiments, which are within 2 g.

500 g of bed material (silica sand), corresponding to a static bed height of 0.1 m, was loaded and fluidized by the primary gas at the start-up of experiment. Afterwards, the reactor was heated at a heating rate of 10 °C/min to a designed temperature, which is 820 °C and 840 °C for combustion and gasification respectively, in order to keep the bed temperature stable at 850 °C after the straw was fed into the reactor. The fuel was continuously fed up to the occurrence of defluidization, which is indicated by a sudden decrease in pressure drop over the bed. The feeding was stopped once the defluidization is observed, and then the heating elements were turned off. The agglomeration tendency was evaluated by the amount of straw fed for causing defluidization in the experiments. The detailed procedures of experiments are described in Chapter 3, Section 3.2.3.

Table 6-1 Experiments matrix

Parameters	Exp. Name	U_p/U_t	f (Hz)	T_{ON}/T_{OFF}	Primary gas (Nl/min)			Secondary gas (Nl/min)	
					Air	Steam	N_2	Air	N_2
Combustion									
Reference	Ref-c	-	-	-	11.5	0	0	0	15.5
	Ref-c[a]		-	-	11.5	0	0	0	15.5
Flow rate	cR1	0.2	1.5	50/50	11.5	0	0	0	15.5
	cR2	0.25	1.5	50/50	11.5	0	0	0	15.5
	cR3	0.3	1.5	50/50	11.5	0	0	0	15.5
	cR3[a]	0.3	1.5	50/50	11.5	0	0	0	15.5
	cR4	0.35	1.5	50/50	11.5	0	0	0	15.5
	cR4[a]	0.35	1.5	50/50	11.5	0	0	0	15.5
	cR5	0.4	1.5	50/50	11.5	0	0	0	15.5
	cR5[a]	0.4	1.5	50/50	11.5	0	0	0	15.5
Frequency	cF1	0.3	0.5	50/50	11.5	0	0	0	15.5
	cF2	0.3	0.75	50/50	11.5	0	0	0	15.5
	cF3	0.3	1	50/50	11.5	0	0	0	15.5
	cF4	0.3	2	50/50	11.5	0	0	0	15.5
	cF5	0.3	3	50/50	11.5	0	0	0	15.5
	cF6	0.4	0.5	50/50	11.5	0	0	0	15.5
	cF7	0.4	0.75	50/50	11.5	0	0	0	15.5
	cF8	0.4	1	50/50	11.5	0	0	0	15.5
	cF9	0.4	2	50/50	11.5	0	0	0	15.5
	cF10	0.4	3	50/50	11.5	0	0	0	15.5
Duty cycle	cD1	0.4	1.5	25/75	11.5	0	0	0	15.5
	cD2	0.4	1.5	75/25	11.5	0	0	0	15.5
	cD2[a]	0.4	1.5	75/25	11.5	0	0	0	15.5
Gasification									
Reference	Ref-g	-	-	-	2.875	2.875	5.75	8.625	6.875
Flow rate	gR1	0.2	1.5	50/50	2.875	2.875	5.75	8.625	6.875
	gR2	0.3	1.5	50/50	2.875	2.875	5.75	8.625	6.875
	gR2[a]	0.3	1.5	50/50	2.875	2.875	5.75	8.625	6.875
	gR3	0.4	1.5	50/50	2.875	2.875	5.75	8.625	6.875
	gR3[a]	0.4	1.5	50/50	2.875	2.875	5.75	8.625	6.875
	gR3[b]	0.4	1.5	50/50	2.875	2.875	5.75	8.625	6.875
Frequency	gF1	0.2	0.75	50/50	2.875	2.875	5.75	8.625	6.875
	gF1[a]	0.2	0.75	50/50	2.875	2.875	5.75	8.625	6.875
	gF2	0.2	3	50/50	2.875	2.875	5.75	8.625	6.875
	gF3[a]	0.4	0.75	50/50	2.875	2.875	5.75	8.625	6.875
	gF3[a]	0.4	0.75	50/50	2.875	2.875	5.75	8.625	6.875
	gF4	0.4	3	50/50	2.875	2.875	5.75	8.625	6.875
Duty cycle	gD1	0.4	1.5	25/75	2.875	2.875	5.75	8.625	6.875
	gD1[a]	0.4	1.5	25/75	2.875	2.875	5.75	8.625	6.875
	gD2	0.4	1.5	75/25	2.875	2.875	5.75	8.625	6.875

[a], [b] Repetition experiments were performed.

The fluctuations of bed pressure drop could reflect the bubble size and fluidization quality[38]. A low-pressure fluctuation amplitude in the fluidized bed indicates the existence of small bubbles, and thus corresponding to a homogeneous fluidization[38]. Zhang *et al.*[39] found that the gauge pressure at air-plenum has the same fluctuations with the flow rate of gas through the air-plenum when the bed is empty. Sasic *et al*.[40] suggested that for a lab-scale fluidized bed that fed from pressurized air systems and has an air-distributor with a reasonably low pressure drop, the bed will interact with the air-plenum, and the trend of pressure fluctuations in the air-plenum is consistent with that of the flow fluctuations. Although the open area of air distributor in this work (4%) is a little lower than that used in their work (6.2%), the fluctuations of the flow still may be reflected by the fluctuations of pressure in the air-plenum. The fluctuation amplitudes and standard deviations of P_1 and P_2 during stable fluidization stage (without feeding of straw) were calculated to evaluate the fluidization behaviors in this work. In order to minimize the errors of the calculated values, the fluctuation amplitudes and the standard deviations for P_1 and P_2 in every 10 seconds were calculated, and then the averages of 60 calculated values in 10 consecutive minutes were used as the final fluctuation amplitudes and standard deviations of P_1 and P_2. The average values and standard deviation of the concentrations of CO, CO_2, O_2, SO_2 and NO in flue gas during steady combustion stage (10 - 20 minutes in the experiment) were calculated in the same method to evaluate the effects of pulsation on the combustion behaviors.

6.3 Results and discussion

6.3.1 Influence of pulsed flow on defluidization tendency during combustion

6.3.1.1 Flow rate ratio of pulsation

Firstly, the reference experiments were performed using a continuous flow as the primary gas, and the amounts of straw fed for leading to defluidization under combustion condition are 60 g and 62 g. As illustrated in Figure 6-3, the amounts of straw fed at the conditions with introducing of a pulsed flow in primary gas are higher than that fed at the condition with a continuous flow, indicating that the imposing of pulsed flow could decelerate the defluidization tendency in fluidized bed. This may be attributed to the reduced minimum fluidization velocity (U_{mf}) caused by the introducing of pulsed flow, and thereby the ratios of superficial gas velocity to minimum fluidization velocity (U_g/U_{mf}) are increased using the same total primary gas flow rate. A larger U_g/U_{mf} results in a better mixing of the bed particles, thus retarding the defluidization.

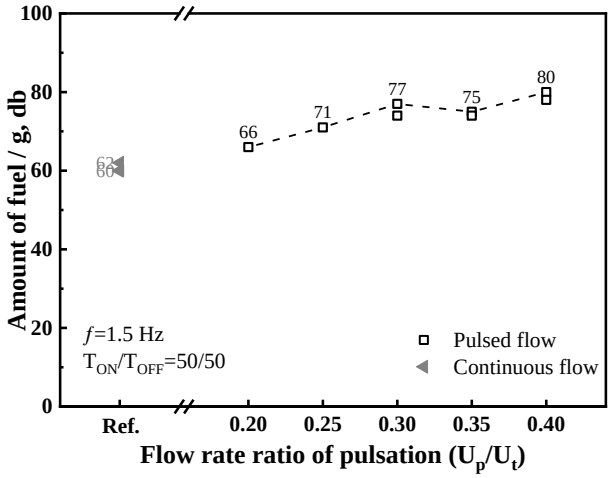

Figure 6-3 Influcence of flow rate ratio of pulsation (0.2-0.4) on amount of straw fed for inducing defluidization during combustion. Pulsation frequency = 1.5 Hz; pulsation duty cycle = 50/50.

The impact of flow rate ratio of pulsation (U_p/U_t), in the range of 0.2 - 0.4, on the defluidization tendency in combustion of wheat straw is investigated at a pulsation frequency of 1.5 Hz and a pulsation duty cycle of 50/50. When the U_p/U_t increases from 0.2 to 0.3, the amount of straw fed for inducing defluidization increases from 66 g to 77 g, suggesting that a higher U_p/U_t shows a more pronounced effect on mitigating defluidization (Figure 6-3). This may be partially attributed to a more intense fluctuation of pulsation at a higher U_p/U_t, suggested by the larger fluctuation amplitude and standard deviation of pressure in the air-plenum (P_1), as illustrated in Figure 6-4-a. It is suggested that the agglomerates are easier to be broken when falling from a greater height attained at higher velocity during the "flow-OFF" period bed collapse[35]. With an increase of U_p/U_t, the pulsed flow may give a higher moving velocity to the particles and lead to a higher particle displacement in the bed during the "flow-ON" period. Meanwhile, the lower continuous flow rate at the "flow-OFF" period may cause a higher falling speed. These two reasons result in a higher broken rate of agglomerates, thus slowing down the defluidization. As shown in Figure 6-4-b, the fluctuation amplitude and standard deviation of bed pressure drop (P_2) decrease with increasing U_p/U_t, suggesting that a more homogenous fluidization in the bed at a larger U_p/U_t. This may be another possible explanation for the better performance of pulsed flow at U_p/U_t of 0.3 than at U_p/U_t of 0.2. However, the increase in the amount of straw fed for causing defluidization becomes less pronounced when U_p/U_t is further increased from 0.3 to 0.4. This may be explained by the reason that the decrease in continuous flow rate will cause a low U_g/U_{mf} during the "flow-OFF" period of pulsation, although an increased fluctuation amplitude is achieved at a higher U_p/U_t. In addition, the fluctuation amplitude and standard deviation of P_2 maintains stable when U_p/U_t is in the range of 0.3 - 0.4, implying the fluidization quality is not further improved by increasing the U_p/U_t.

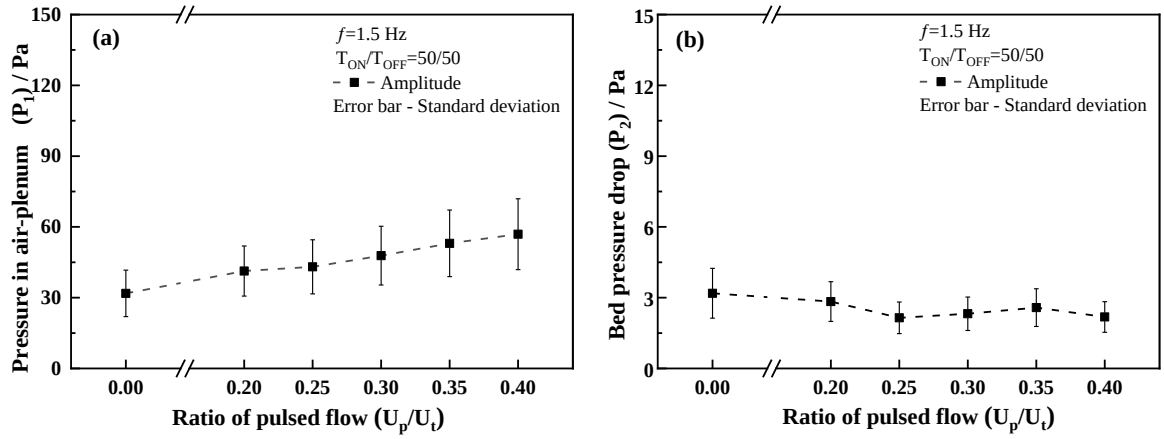

Figure 6-4 Fluctuation amplitudes and standard deviations of (a) pressure in the air-plenum (P_1) and (b) bed pressure drop (P_2) in the pulsed fluidized bed without feeding at different flow rate ratios of pulsation (0.2-0.4). Pulsation frequency =1.5 Hz; pulsation duty cycle = 50/50.

6.3.1.2 Pulsation frequency

The pulsation frequency shows a minor effect on the defluidization tendency in combustion of wheat straw, as shown in Figure 6-5. When the U_p/U_t and the T_{ON}/T_{OFF} maintain constants, the trend of straw amount fed for inducing defluidization during combustion is characterized by an initial slightly increase followed by an decrease as pulsation frequency increases in the range of 0.5 Hz - 3 Hz. The best performance is obtained at the pulsation frequency of 1.5Hz, which is close to the natural frequency of system calculated according to equation proposed by Hao and Bi[37]. Similar results are observed by Jia *et al*. in biomass drying in a pulsed fluidized bed[30,31]. They attribute this to the occurrence of resonance effect at the pulsation frequency that close to the natural frequency of system, and thus increasing the particle motion and mass transfer[30].

As shown in Figure 6-6, both the fluctuation amplitudes and standard deviations of P_1 and P_2 decrease with the increasing pulsation frequency in the range of 0.5 Hz - 2 Hz. It has been found both in experimental work and numerical simulation that an increase in the pulsation frequency will lead to a smoother and more homogenous bed behavior in pulsed fluidized bed[39,41]. This may be ascribed to the smaller amount of air entering the bed during each "flow-ON" period and the bed collapses to a less extent during the shorter "flow-OFF" periods at the higher frequency[39]. However, the short "flow-ON" and "flow-OFF" period may also result in a small particle displacement in the bed due to the small pressure build-up[39]. The impact of pulsation frequency on the defluidization tendency becomes unpronounced because the decrease in particle displacement and the increase in fluidization quality may neutralize each other as the pulsation frequency increases. An outlier is observed at the pulsation frequency of 3 Hz, and it may be imputed to the long response time of the pressure sensors. At a pulsation frequency of 3 Hz, the "flow-ON" and "flow-OFF" periods within a pulsation are 170 ms, which is smaller than the response time of the pressure sensors.

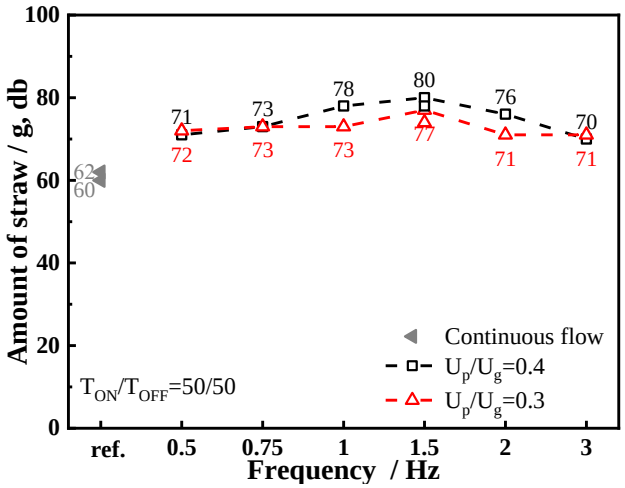

Figure 6-5 Influence of pulsation frequency (0.5-3 Hz) on amount of straw fed for inducing defluidization during combustion. Flow rate ratio of pulsaiton = 0.3 and 0.4; pulsation duty cycle = 50/50.

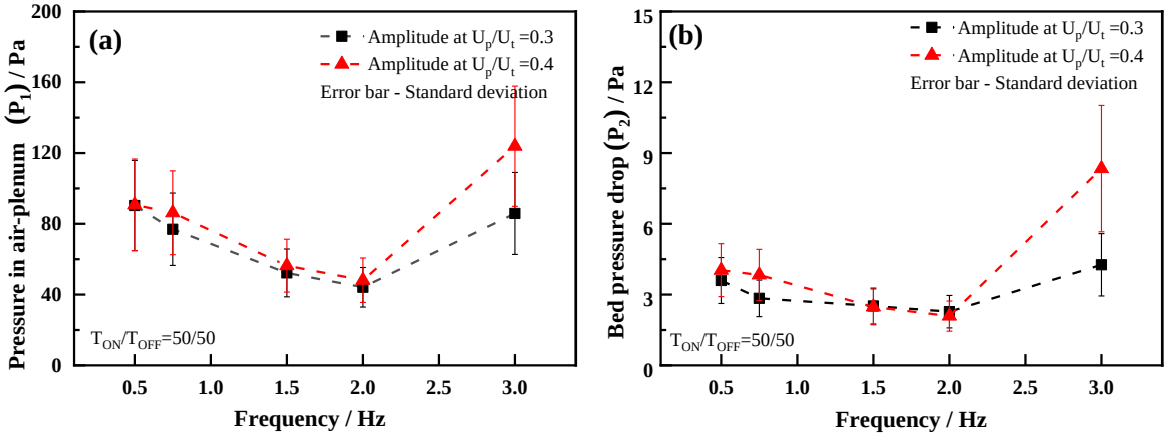

Figure 6-6 Fluctuation amplitudes and standard deviations of (a) pressure in the air-plenum (P_1) and (b) bed pressure drop (P_2) in the pulsed fluidized bed without feeding at different pulsation frequencies (0.5-3Hz). Flow rate ratio of pulsaiton = 0.3 and 0.4; pulsation duty cycle = 50/50.

6.3.1.3 Pulsation duty cycle

The pulsation duty cycle is an important parameter for the performance of pulsed fluidized bed. With a constant pulsation frequency of 1.5 Hz and a constant U_p/U_t of 0.4, the "flow-ON" period of pulsation within each cycle was set as 170 ms, 330 ms and 500 ms, resulting in a pulsation duty cycle of 25/75, 50/50, and 75/25, respectively. As shown in Figure 6-7, the pulsation duty cycle has the most significant effect on the defluidization tendency among the parameters that have been investigated in this work. The defluidization tendency decreases with the shorting "flow-ON" period of pulsation within each cycle. The amount of straw fed for causing defluidization is 91 g at the T_{ON}/T_{OFF} of 25/75, which is 151.7% of that fed at continuous flow. Similar results are observed by other researchers on the heat transfer in pulsed fluidized bed. Kobayashi *et al.*[42] investigated the heat transfer of the glass beads bed with a static bed height of 300 mm. They found that for the glass beads with an average diameter of 301 μm, the optimum pulsation duty cycle is 25/75 (a combination of

"flow-ON" and "flow-OFF" period of 0.25 s and 0.75 s). Nishimura *et al*.[43] studied the heat transfer of the glass beads bed having an average diameter of 340 μm with a static bed height of 700 mm. The optimum heat transfer is observed at the combination of the "flow-ON" period of 1 s and the "flow-OFF" period of 3 s, namely the duty cycle of 25/75. However, the effect of pulsation becomes negligible at the T_{ON}/T_{OFF} of 75/25.

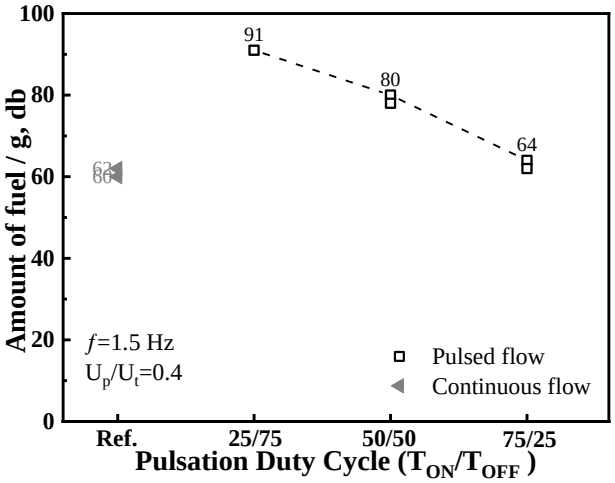

Figure 6-7 Influence of duty cycle of pulsation (25/75, 50/50, and 75/25) on amount of straw fed for inducing defluidization during combustion. Pulsation flow rate ratio U_p/U_t = 0.4; pulsation frequency = 1.5 Hz.

The good performance of pulsation at the T_{ON}/T_{OFF} of 25/75 may be ascribed to the large fluctuation amplitude of pulsation, which is also observed in the other work[30], caused by a high pressure build-up in a long "flow-OFF" period, as shown in Figure 6-8-a. As mentioned above, the agglomerates are likely broken by the large displacement of particles in the bed. Compared to the T_{ON}/T_{OFF} of 50/50, the higher pressure build-up at the T_{ON}/T_{OFF} of 25/75 may provide a higher instantaneous gas velocity to the particles, thus resulting in an increased displacement of particles. The instantaneous gas velocity is reduced by increasing duty cycle, since the same amount of gas enters in the bed over a longer "flow-ON" period[27]. Meanwhile, the longer "flow-OFF" period at the T_{ON}/T_{OFF} of 25/75, indicating a longer falling down period, may also promote the broken of agglomerates. For the T_{ON}/T_{OFF} of 75/25, the fluctuation amplitude and standard deviation of P_1 is larger than that at the T_{ON}/T_{OFF} of 50/50. However, the fluctuation amplitude and standard deviation of P_2 at the T_{ON}/T_{OFF} of 75/25 is significant larger than that at the T_{ON}/T_{OFF} of 50/50 (Figure 6-8-b), indicating a worse fluidization quality in the bed. This probably attributed to the behaviors of the pulsed fluidized bed with a T_{ON}/T_{OFF} of 75/25 may be similar to a conventional fluidized bed, and thereby the effect of pulsation becomes unpronounced at the T_{ON}/T_{OFF} of 75/25.

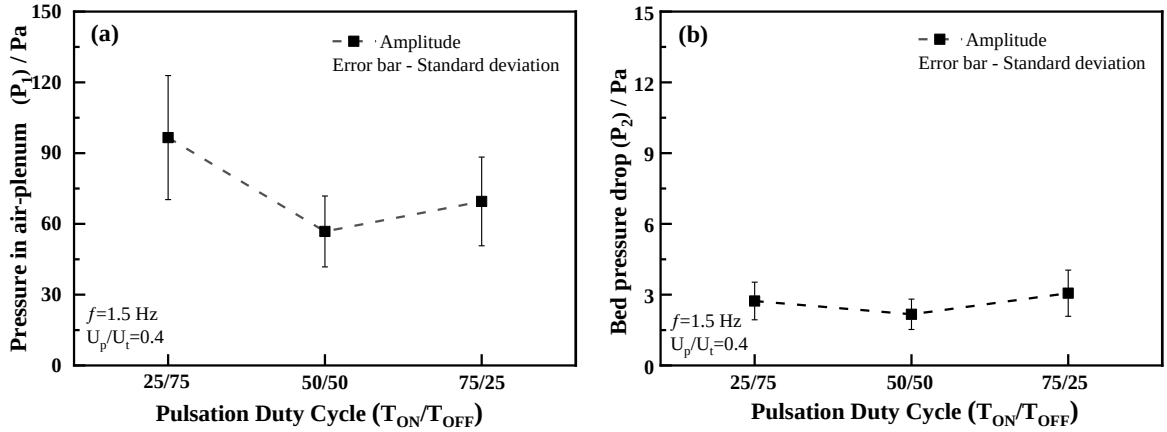

Figure 6-8 Fluctuation amplitudes and standard deviations of (a) pressure in the air-plenum (P_1) and (b) bed pressure drop (P_2) in a pulsed fluidized bed without feeding at different pulsation duty cycles. Flow rate ratio of pulsation U_p/U_t = 0.4; pulsation frequency = 1.5 Hz.

6.3.2 Application of pulsed flow on defluidization tendency during gasification

The influence of pulsed flow on the defluidization tendency during gasification of wheat straw is also investigated. Similarly, a reference experiment was performed using continuous primary gas, and the amount of straw fed for causing defluidization under steam/air gasification condition is 40 g. The impacts of flow rate, frequency, and duty cycle of pulsation are summarized in Figure 6-9. The results show that the pulsation shows a consistent influence on combustion and gasification of wheat straw. Compared to combustion condition, the effect of pulsed flow on the defluidization during steam/air gasification is less obvious. Besides the combination of U_p/U_t of 0.4, frequency of 1.5 Hz, and T_{ON}/T_{OFF} of 25/75, the amounts of straw fed for inducing defluidization at other conditions maintain in the range of 45 - 48 g. This may be attributed to the high defluidization tendency in gasification, and thereby the differences in defluidization at various conditions are within the uncertainties of the experiments. The best performance of pulsation under gasification condition is obtained at the combination of U_p/U_t of 0.4, frequency of 1.5 Hz, and T_{ON}/T_{OFF} of 25/75, which is consistent with the optimal condition under combustion condition. Under the optimum condition, the amount of straw fed for approaching defluidization is 55 g, which is 137.5% of that at continuous flow.

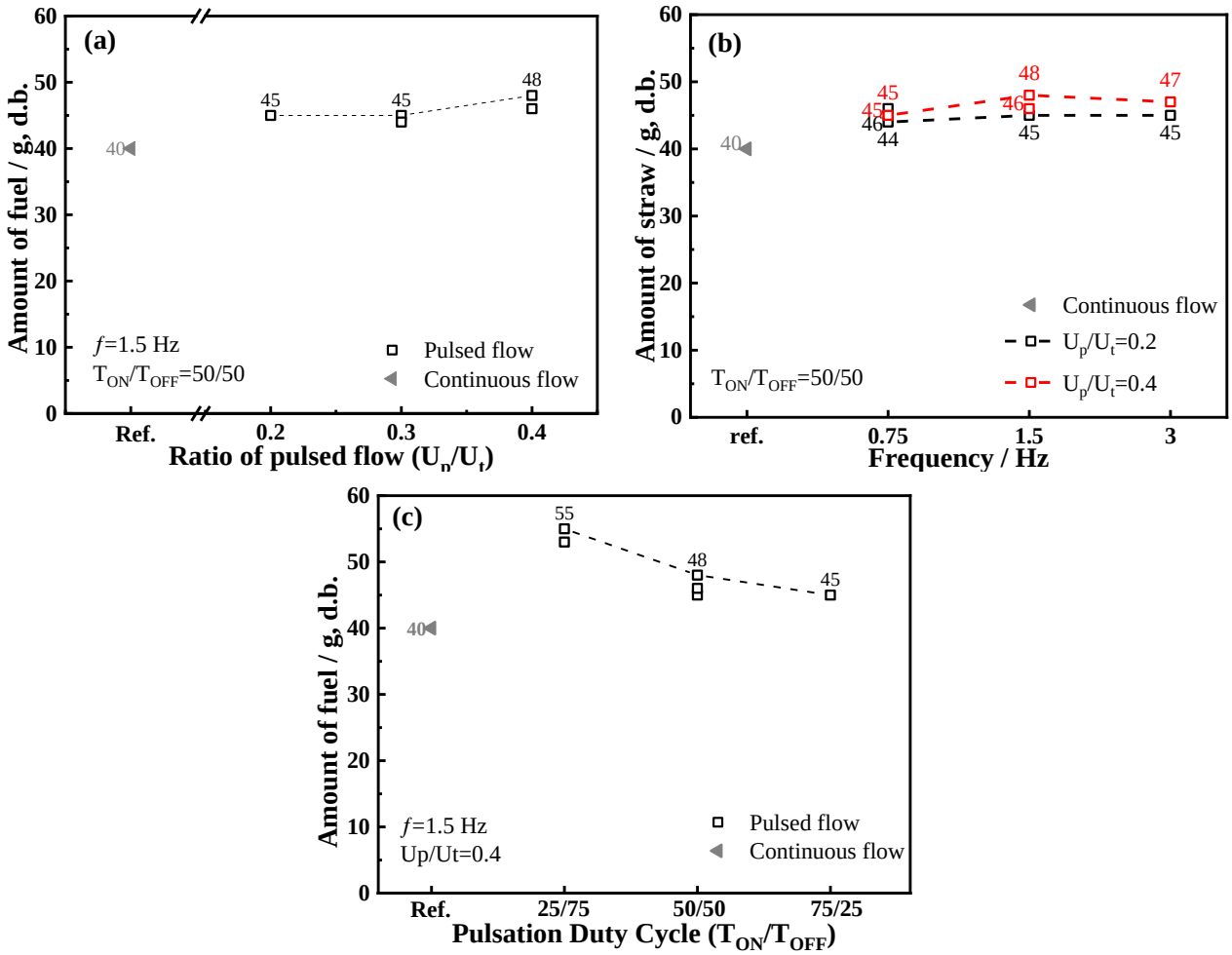

Figure 6-9 Influence of (a) flow rate of pulsation, (b) pulsation frequency and (c) pulsation duty cycle on amount of straw fed for inducing defluidization during gasification. (a) pulsation frequency = 1.5 Hz; pulsation duty cycle = 50/50; (b) pulsation flow rate ratio = 0.2 and 0.4; pulsation duty cycle =50/50; (c) pulsation flow rate ratio =0.4; pulsation frequency = 1.5 Hz.

The fluctuation amplitudes and standard deviations of P_1 and P_2 at all conditions are shown in Figure 6-10. Generally, the U_p/U_t, frequency, and T_{ON}/T_{OFF} shows consistent effects on the fluctuation amplitudes and standard deviations of P_1 and P_2 in gasification and combustion. An increase in U_p/U_t as well as a decrease in pulsation frequency and T_{ON}/T_{OFF} will result in an increasing fluctuations of P_1. An outlier is observed at the combination of U_p/U_t of 0.2, frequency of 3 Hz, and T_{ON}/T_{OFF} of 50/50, probably being attributed to the long response time of pressure sensors. The fluctuation amplitudes and standard deviations of P_2 in gasification are higher than that in combustion, indicating that the fluidization quality of bed particles in gasification is worse. This may be ascribed to an increased U_{mf} caused by the presence of steam in the primary gas. The larger fluctuation amplitudes of P_1 is probably caused by the fluctuated generation of steam.

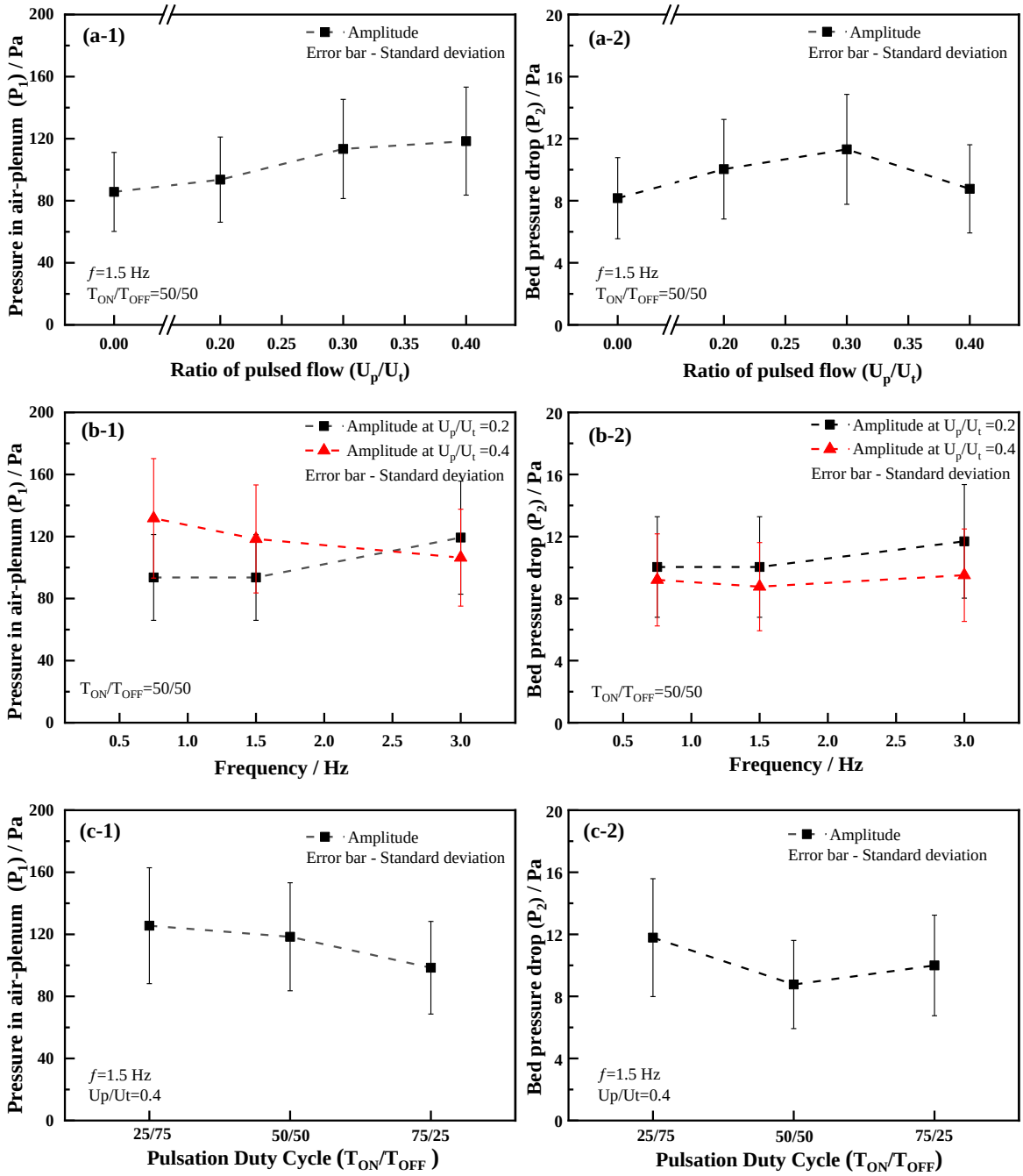

Figure 6-10 Fluctuation amplitudes and standard deviations of (a-1) pressure in the air-plenum (P_1) and (a-2) bed pressure drop (P_2) at different flow ratios of pulsaiton, (b-1) pressure in the air-plenum (P_1) and (b-2) bed pressure drop (P_2) at different pulsation frequencies, (c-1) pressure in the air-plenum (P_1) and (c-2) bed pressure drop (P_2) at different duty cycles in a pulsed fluidized bed without feeding during gasification. (a) pulsation frequency = 1.5 Hz; pulsation duty cycle = 50/50; (b) pulsation flow rate ratio = 0.2 and 0.4; pulsation duty cycle = 50/50; (c) pulsation flow rate ratio = 0.4; pulsation frequency = 1.5 Hz.

6.3.3 Influence of pulsed flow on combustion behaviors

The effects of pulsed flow on combustion behaviors are evaluated according to the concentrations of CO, CO_2, O_2, SO_2 and NO in flue gas during stable combustion period. As illustrated in Figure 6-11, the average O_2 concentrations in the flue gas are varied in the range of 2.3% - 3.3%. This range is in agreement with a stoichiometric ratio of 1.45 during combustion. The CO and CO_2 concentrations remain stable under all conditions, which are in the range of 0.23% - 0.69% and 5.1% - 6.6%, respectively. Since the feeding rate is slightly different in each experiment, the impact of pulsed flow gas on the combustion efficiency is difficult to evaluate. A larger feeding rate leads to a higher oxygen consumption and a higher incomplete conversion of carbon, and thereby causing a lower O_2 concentration and a higher CO concentration. An outlier is found at the combination of pulsation flow rate ratio of 0.4, pulsation frequency of 0.5 Hz, and pulsation duty cycle of 50/50 (Figure 6-11-c). Both O_2 and CO concentrations at pulsation frequency of 0.5 Hz are slightly higher than other frequencies. In addition to feeding rate, the CO concentration is related to the amount of air entering into the bed. The high CO concentration may be attributed to the less amount of air enters during the longer "OFF" period at a low frequency. The NO concentration has the opposite trend with CO concentration, while the concentration of SO_2 shows the same trend with CO concentration. These trends are consistent with the trends have been reported[44,45]. In addition to CO and CO_2 concentrations, the concentrations of NO and SO_2 in the flue gas also maintain stable. The results suggest that the pulsed flow shows negligible effect on the combustion behaviors in the bed.

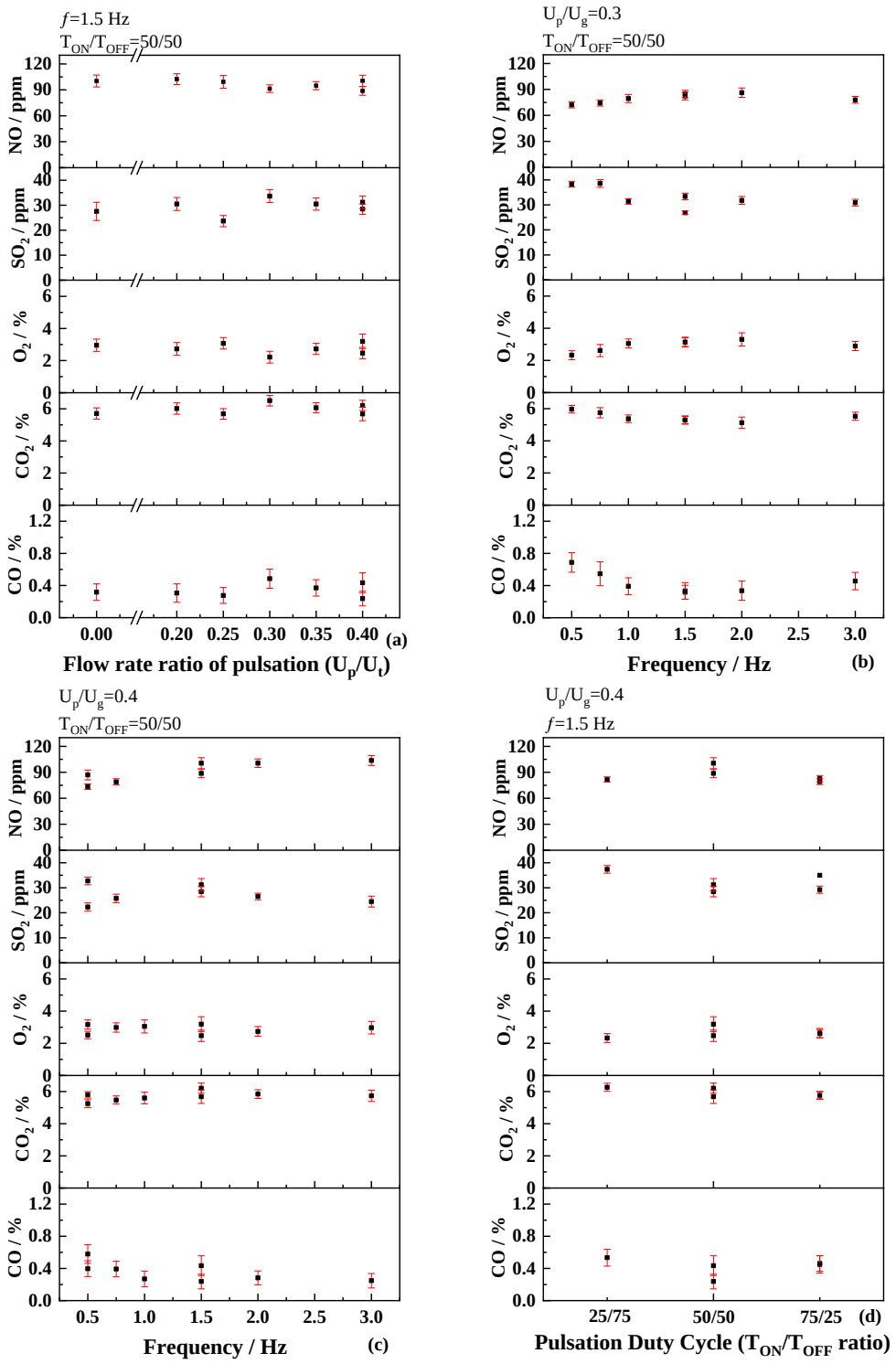

Figure 6-11 Influence of (a) flow rate of pulsation (b) & (c) pulsation frequency, and (d) pulsation duty cycle on flue gas (CO, CO_2, O_2, NO, and SO_2) compositions during stable combustion period. (a) pulsation frequency = 1.5 Hz; pulsation duty cycle = 50/50; (b) pulsation flow rate ratio = 0.3; pulsation duty cycle = 50/50; (c) pulsation flow rate ratio = 0.4; pulsation duty cycle = 50/50; (d) pulsation flow rate ratio = 0.4; pulsation frequency = 1.5 Hz.

6.4 Conclusions

A pulsed fluidized bed reactor could be a potential countermeasure for retarding the defluidization tendency during biomass combustion and gasification. The effects of operating parameters, including flow rate ratio of pulsation, pulsation frequency, and pulsation duty cycle, on defluidization tendency are investigated. Among the parameters have been investigated in this chapter, the pulsation duty cycle shows the most pronounced effect on the defluidization, whilst the pulsation frequency shows the least obvious influence. With imposing of a pulsed flow with pulsation flow rate ratio of 0.4, pulsation frequency of 1.5 Hz and pulsation duty cycle of 25/75, the amounts of straw fed for inducing defluidization are 151.6% and 137.5% of that during the conventional combustion and gasification, respectively. The good performance of pulsed flow on mitigating defluidization may be attributed to the large displacement of bed particles caused by a high moving velocity of particles during "flow-ON" period and/or a long falling down time during "flow-OFF" period, as well as the homogeneous fluidization in the bed resulted from a reduced minimum fluidization velocity. The mechanism of mitigated effect of pulsed flow on defluidization needs to be further investigated. Introducing of pulsed flow in primary gas shows negligible effect on the combustion behaviors.

Reference

(1) Shukla, S.; Murty, P.; Sanjay. Combined Heat and Power through Biomass - An Overview. *Sae Technical Papers*. SAE International 2011.

(2) Khan, A. A.; de Jong, W.; Jansens, P. J.; Spliethoff, H. Biomass Combustion in Fluidized Bed Boilers: Potential Problems and Remedies. *Fuel Process. Technol.* **2009**, *90* (1), 21–50.

(3) Koornneef, J.; Junginger, M.; Faaij, A. Development of Fluidized Bed Combustion-An Overview of Trends, Performance and Cost. *Prog. Energy Combust. Sci.* **2007**, *33* (1), 19–55.

(4) Lin, W.; Jensen, A. D.; Johnsson, J. E.; Dam-Johansen, K. Combustion of Biomass in Fluidized Beds: Problems and Some Solutions Based on Danish Experiences. In *Proceedings of the 17th International Conference on Fluidized Bed Combustion*; American Society of Mechanical Engineers: Jacksonville, Florida USA, 2003; pp 945–953.

(5) Scala, F. Particle Agglomeration during Fluidized Bed Combustion: Mechanisms, Early Detection and Possible Countermeasures. *Fuel Process. Technol.* **2018**, *171*, 31–38.

(6) Bartels, M.; Lin, W.; Nijenhuis, J.; Kapteijn, F.; van Ommen, J. R. Agglomeration in Fluidized Beds at High Temperatures: Mechanisms, Detection and Prevention. *Prog. Energy Combust. Sci.* **2008**, *34* (5), 633–666.

(7) Morris, J. D.; Sheraz, S.; Chilton, S.; Nimmo, W. Mechanisms and Mitigation of Agglomeration during Fluidize Bed Combustion of Biomass : A Review. *Fuel* **2018**, *230*, 452–473.

(8) Mettanant, V.; Basu, P.; Butler, J. Agglomeration of Biomass Fired Fluidized Bed Gasifier and Combustor. *Can. J. Chem. Eng.* **2009**, *87* (5), 656–684.

(9) Öhman, M.; Nordin, A.; Skrifvars, B. J.; Backman, R.; Hupa, M. Bed Agglomeration Characteristics during Fluidized Bed Combustion of Biomass Fuels. *Energy & Fuels* **2000**, *14* (1), 169–178.

(10) Ergudenler, A.; Ghaly, A. E. Agglomeration of Alumina Sand in a Fluidized Bed Straw Gasifier at Elevated Temperatures. *Bioresour. Technol.* **1993**, *43* (3), 259–268.

(11) Ghaly, A. E.; Ergüdenler, A.; Laufer, E. Agglomeration Characteristics of Alumina Sand-Straw Ash Mixtures at Elevated Temperatures. *Biomass and Bioenergy* **1993**, *5* (6), 467–480.

(12) Fernández Llorente, M. J.; Escalada Cuadrado, R.; Murillo Laplaza, J. M.; Carrasco García, J. E. Combustion in Bubbling Fluidised Bed with Bed Material of Limestone to Reduce the Biomass Ash Agglomeration and Sintering. *Fuel* **2006**, *85* (14–15), 2081–2092.

(13) Vuthaluru, H. B.; Zhang, D. K. Effect of Ca- and Mg-Bearing Minerals on Particle Agglomeration Defluidization during Fluidized-Bed Combustion of a South Australian Lignite. *Fuel Process. Technol.* **2001**, *69* (1), 13–27.

(14) Grubor, B.D.; Oka, S.N.; Ilic, M.S.; Dakic, D.V.; Arsic, B. .; Grubor, B. D.; Oka, S. N.; Ilic, M. S.; Dakic, D. V.; Arsic, B. T. Biomass FBC Combustion - Bed Agglomeration Problems.

In *Proceedings of the 13th International Conference on Fluidized Bed Combustion*; American Society of Mechanical Engineers: United States, 1995; Vol. 1, pp 515–522.

(15) Öhman, M.; Nordin, A.; Lundholm, K.; Boström, D.; Hedman, H.; Lundberg, M. Ash Transformations during Combustion of Meat-, Bonemeal, and RDF in a (Bench-Scale) Fluidized Bed Combustor. *Energy & Fuels* **2003**, *17* (5), 1153–1159.

(16) Chou, J. D.; Lin, C. L. Inhibition of Agglomeration/Defluidization by Different Calcium Species during Fluidized Bed Incineration under Different Operating Conditions. *Powder Technol.* **2012**, *219*, 165–172.

(17) Grimm, A.; Skoglund, N.; Boström, D.; Boman, C.; Öhman, M. Influence of Phosphorus on Alkali Distribution during Combustion of Logging Residues and Wheat Straw in a Bench-Scale Fluidized Bed. *Energy & Fuels* **2012**, *26* (5), 3012–3023.

(18) Arvelakis, S.; Gehrmann, H.; Beckmann, M.; Koukios, E. G. Preliminary Results on the Ash Behavior of Peach Stones during Fluidized Bed Gasification : Evaluation of Fractionation and Leaching as Pre-Treatments. *Biomass and Bioenergy* **2005**, *28*, 331–338.

(19) Skoglund, N.; Grimm, A.; Öhman, M.; Boström, D. Effects on Ash Chemistry When Co-Firing Municipal Sewage Sludge and Wheat Straw in a Fluidized Bed: Influence on the Ash Chemistry by Fuel Mixing. *Energy & Fuels* **2013**, *27* (10), 5725–5732.

(20) Nordgren, D.; Hedman, H.; Padban, N.; Boström, D.; Öhman, M. Ash Transformations in Pulverised Fuel Co-Combustion of Straw and Woody Biomass. *Fuel Process. Technol.* **2013**, *105*, 52–58.

(21) Lin, W.; Dam-Johansen, K.; Frandsen, F. Agglomeration in Bio-Fuel Fired Fluidized Bed Combustors. *Chem. Eng. J.* **2003**, *96* (1–3), 171–185.

(22) Ryabov, G.; Litoun, D.; Dik, E. Agglomeration of Bed Material: Influence on Efficiency of Biofuel Fluidized Bed Boiler. *Therm. Sci.* **2003**, *7* (1), 5–16.

(23) Saidi, M.; Basirat Tabrizi, H.; Grace, J. R. A Review on Pulsed Flow in Gas-Solid Fluidized Beds and Spouted Beds: Recent Work and Future Outlook. *Adv. Powder Technol.* **2019**, *30* (6), 1121–1130.

(24) Ireland, E.; Pitt, K.; Smith, R. A Review of Pulsed Flow Fluidisation; the Effects of Intermittent Gas Flow on Fluidised Gas-Solid Bed Behaviour. *Powder Technol.* **2016**, *292*, 108–121.

(25) Khosravi Bizhaem, H.; Basirat Tabrizi, H. Investigating Effect of Pulsed Flow on Hydrodynamics of Gas-Solid Fluidized Bed Using Two-Fluid Model Simulation and Experiment. *Powder Technol.* **2017**, *311*, 328–340.

(26) Khosravi Bizhaem, H.; Basirat Tabrizi, H. Experimental Study on Hydrodynamic Characteristics of Gas-Solid Pulsed Fluidized Bed. *Powder Technol.* **2013**, *237*, 14–23.

(27) Jia, D.; Bi, X.; Lim, C. J.; Sokhansanj, S.; Tsutsumi, A. Heat Transfer in a Tapered Fluidized Bed of Biomass Particles with Pulsed Gas Flow. *Particuology* **2019**, *42*, 2–14.

(28) Jia, D.; Bi, X.; Lim, C. J.; Sokhansanj, S.; Tsutsumi, A. Heat Transfer in a Pulsed Fluidized Bed of Biomass Particles. *Ind. Eng. Chem. Res.* **2017**, *56* (13), 3740–3756.

(29) Liu, Y.; Liu, Z.; Ohara, H. Heat Transfer and Fluidization Characteristics of Lignite in a Pulsation-Assisted Fluidized Bed. *Ind. Eng. Chem. Res.* **2017**, *56* (31), 8995–9005.

(30) Jia, D.; Bi, X.; Lim, C. J.; Sokhansanj, S.; Tsutsumi, A. Biomass Drying in a Pulsed Fluidized Bed without Inert Bed Particles. *Fuel* **2016**, *186*, 270–284.

(31) Jia, D.; Cathary, O.; Peng, J.; Bi, X.; Lim, C. J.; Sokhansanj, S.; Liu, Y.; Wang, R.; Tsutsumi, A. Fluidization and Drying of Biomass Particles in a Vibrating Fluidized Bed with Pulsed Gas Flow. *Fuel Process. Technol.* **2015**, *138*, 471–482.

(32) Hadi, B.; Van Ommen, J. R.; Coppens, M. O. Enhanced Particle Mixing in Pulsed Fluidized Beds and the Effect of Internals. *Ind. Eng. Chem. Res.* **2012**, *51* (4), 1713–1720.

(33) Wang, X. S.; Rhodes, M. J. Using Pulsed Flow to Overcome Defluidization. *Chem. Eng. Sci.* **2005**, *60* (18), 5177–5181.

(34) Ali, S. S.; Asif, M. Fluidization of Nano-Powders: Effect of Flow Pulsation. *Powder Technol.* **2012**, *225*, 86–92.

(35) Ali, S. S.; Asif, M.; Ajbar, A. Bed Collapse Behavior of Pulsed Fluidized Beds of Nano-Powder. *Adv. Powder Technol.* **2014**, *25* (1), 331–337.

(36) Yan, J.; Cen, K.; Kang, Q. Mechanism of Pulsating Fluidized Bed and Its Application in Combustion of Coal (in Chinese). *J. Zhejinag Univ.* **1986**, *20* (6), 123–131.

(37) Hao, B.; Bi, H. T. Forced Bed Mass Oscillations in Gas-Solid Fluidized Beds. *Powder Technol.* **2005**, *149* (2–3), 51–60.

(38) Bi, H. T. A Critical Review of the Complex Pressure Fluctuation Phenomenon in Gas-Solids Fluidized Beds. *Chem. Eng. Sci.* **2007**, *62* (13), 3473–3493.

(39) Zhang, D.; Koksal, M. Heat Transfer in a Pulsed Bubbling Fluidized Bed. *Powder Technol.* **2006**, *168* (1), 21–31.

(40) Sasic, S.; Leckner, B.; Johnsson, F. Fluctuations and Waves in Fluidized Bed Systems: The Influence of the Air-Supply System. *Powder Technol.* **2005**, *153* (3), 176–195.

(41) Gui, N.; Fan, J. R. Numerical Simulation of Pulsed Fluidized Bed with Immersed Tubes Using DEM-LES Coupling Method. *Chem. Eng. Sci.* **2009**, *64* (11), 2590–2598.

(42) Kobayashi, M.; Ramaswasi, D.; Brazelton, W. T. HEAT TRANSFER FROM AN INTERNAL SURFACE TO A PULSED BED. *Chem. Eng. Prog. Symp. Ser.* **1970**, *66* (105), 58–67.

(43) Nishimura, A.; Deguchi, S.; Matsuda, H.; Hasatani, M.; Mujumdar, A. S. Heat Transfer Characteristics in a Pulsating Fluidized Bed in Relation to Bubble Characteristics. *Heat Transf. - Asian Res.* **2002**, *31* (4), 307–319.

(44) Courtemanche, B.; Levendis, Y. A. A Laboratory Study on the NO, NO_2, SO_2, CO and CO_2 Emissions from the Combustion of Pulverized Coal, Municipal Waste Plastics and Tires. *Fuel* **1998**, *77* (3), 183–196.

(45) Kazanc, F.; Khatami, R.; Manoel Crnkovic, P.; Levendis, Y. A. Emissions of NO_x and SO_2 from Coals of Various Ranks, Bagasse, and Coal-Bagasse Blends Burning in O_2/N_2 and O_2/CO_2 Environments. *Energy & Fuels* **2011**, *25* (7), 2850–2861.

7. Conclusions and suggestions for future work

This chapter provides a summary of main conclusions, as well as the suggestions for the future work.

7.1 Conclusions

In this work, the agglomeration during combustion and gasification of biomass was investigated in a lab-scale bubbling fluidized bed reactor at 850 °C using silica sand as bed material. The influences of equivalence ratio (ER) and gasification agent (air, steam and carbon dioxide) on agglomeration of wheat straw were systematically studied. In addition, the agglomeration of sunflower husk and another batch of wheat straw was investigated to study the influences of type and property of biomass on agglomeration in combustion and gasification. The fusion behaviors of wheat straw ash were investigated a fixed bed reactor under combustion and gasification conditions to further understand the influence of gas atmosphere on agglomeration. Different techniques, such as scanning electron microscopy with energy-dispersive X-ray spectroscopy (SEM-EDX), X-ray diffraction (XRD), and thermogravimetric analysis (TGA), were applied to characterize the selected agglomerates, biomass ash, and char. The thermodynamic equilibrium calculations were carried out to shed light upon the distribution of potassium in the biomass ashes under the experimental conditions. A pulsed flow was applied to the fluidized bed to explore the possibility of mitigating the agglomeration in combustion/gasification of biomass and its effect on the conversion process. The main conclusions from this work are summarized as bellows.

The agglomeration in fluidized bed combustion and gasification of wheat straw is strongly influenced by the ER and gasification agent in primary gas. In an air blown fluidized bed, the agglomeration tendency of wheat straw first increases with decreasing ER, and then decreases as ER further decreases. By shifting ER from combustion region (ER > 1) gradually to gasification region (ER < 1), the enhanced reducing atmosphere could accelerate the agglomeration, possibly resulting from an increased melting of wheat straw ash. However, the increased amount of residual carbon caused by decreasing ER mitigates the agglomeration in the bed. The residual carbon may reduce the fusion tendency and melting flow behavior of ash, thus mitigating the agglomeration. In addition, the carbon attached on the sand surface may inhibit the agglomeration by preventing the interaction between ash and bed material. The competition between an enhanced reducing atmosphere and a higher amount of residual carbon by lowering ER results in the occurrence of a maximal agglomeration tendency at a critical ER. The critical ER would be lowered by adding steam to the primary gas, due to an increased carbon conversion. In addition, the presence of steam in primary gas may significantly

lower the viscosity of wheat straw ash, and thereby promoting the agglomeration. The addition of CO_2 in primary gas slightly mitigates the agglomeration.

The appearances of the ashes from wheat straw under combustion conditions (100% air and a mixture of 50 vol.% steam and 50 vol.% air) and gasification condition (a mixture of 50 vol.% steam and 50 vol.% N_2) are significantly different. The ash from normal combustion is friable and less cohesive, while the ashes from combustion with presence of steam and the ash from gasification with steam are tight and compact. The visual observation and SEM-EDX results indicate that the ash obtained from gasification with steam has the highest fusion tendency followed by the ash from combustion with presence of steam and lastly the ash from normal combustion, indicating that a high concentration of steam and a reducing atmosphere could promote the fusion behaviors of straw ashes. The fusion tendency of the ashes from a mixture of wheat straw and silica sand under the three conditions is consistent with the ashes from wheat straw. Although the formation of the agglomerates under all conditions are caused by the molten K-Ca silicates, a severer agglomeration is observed for the mixture that contains the ash with a higher fusion tendency. The fusion tendency of the ashes is consistent with the agglomeration tendency in fluidized bed experiments.

Sunflower husk ash has a higher agglomeration than wheat straw ash in both combustion and gasification. The different agglomeration tendency of two types of biomass probably result from the significantly different Si/K molar ratios for wheat straw and sunflower husk, which may result in different distribution of potassium in their ashes, thus causing different agglomeration mechanisms. The agglomeration mechanism of the Si-rich wheat straw probably is that the partially molten ashes adhere on the bed particles and subsequently form a coating layer, leading to agglomeration. The agglomeration of the Si-lean sunflower husk may be caused by the formation of K silicates via the interaction between sunflower husk ash and bed particles (SiO_2). The influence of ER on agglomeration tendency of sunflower husk follows the same trend as wheat straw, indicating that a reducing atmosphere and the residual carbon in the bed show consistent effects on the agglomeration of two types of biomass. In the air blown gasification, the critical ER of sunflower husk, which is 0.04, is lower than that of wheat straw, which is 0.36. Different from wheat straw, the accelerated agglomeration of sunflower husk under a reducing atmosphere possibly is attributed to a promoted reactivity of sunflower husk ash towards SiO_2. During gasification of biomass, a higher char reactivity results in a less amount of residual carbon in the bed. The inhibition effect of residual carbon caused by decreasing ER decreases with increasing char reactivity. Compared to wheat straw, the char reactivity of sunflower husk is higher, leading to a reduced inhibition effect of residual carbon. The low critical ER of sunflower husk may be ascribed to its high char reactivity and the different agglomeration mechanism from wheat straw caused by a low Si/K molar ratio of sunflower husk. The agglomeration of two types of biomass is promoted by adding a high concentration of steam to the primary gas. The accelerated agglomeration of sunflower husk under the condition with presence of steam may be attributed to an increased melting of sunflower husk ash and a promoted interaction

between sunflower husk ash and bed particles. For different batches of wheat straw, the straw with a higher Al content may has a slightly lower agglomeration tendency, probably due to a reduced melting of ash. In addition, the straw with a lower char reactivity shows a significantly lower agglomeration tendency during gasification, probably due to a more pronounced inhibition effect of residual carbon.

The application of pulsed fluidized bed reactor is a potential countermeasure for retarding the defluidization tendency during biomass combustion and gasification. Introducing of pulsed flow in the primary gas shows minor effect on the combustion behaviors. Among the parameters that have been studied, the pulsation duty cycle shows the most significant influence on the agglomeration, while the pulsation frequency has the smallest influence. The most pronounced effect of pulsed flow on defluidization tendency is observed at the condition of pulsation flow rate ratio of 0.4, pulsation frequency of 1.5 Hz, and pulsation duty cycle of 25/75. Under the optimum condition, the amounts of straw fed for inducing defluidization are 151.6% and 137.5% of that under the conventional combustion and gasification, respectively. The good performance of pulsed fluidized bed on reducing agglomeration may be attributed to an improved fluidization quality in the bed and an increased displacement of bed particles.

7.2 Suggestion for future work

The results of this PhD project provide an improved understanding of agglomeration in fluidized bed gasification of biomass, with a special emphasis on the influence of gasification agents, ER, and biomass type. In addition, a potential countermeasure for reducing agglomeration, application of pulsed fluidized bed, is preliminarily investigated. However, a few questions, such as the influence of concentrations of reducing agents on the fusion behaviors of wheat straw ash, as well as the influences of reducing atmosphere and steam on the fusion behaviors of sunflower husk ash and the interaction between sunflower husk ash and silica sand, are still unclear. Some suggestions for future work are shown as follows:

Influence of concentrations of reducing agents on the fusion behaviors of wheat straw ash

The results of fluidized bed experiments show that when the ER is higher than the critical ER, a decrease in ER will result in a slightly increased agglomeration tendency. The gradually increased agglomeration may be attributed to an increased melting of ash caused by an enhanced reducing atmosphere. The results of fixed bed experiments indicate that the reducing atmosphere formed in gasification could promote the fusion behaviors of wheat straw ash. However, the fusion behaviors of wheat straw ash under a reducing atmosphere with different reducing agents, such as H_2 and CO, are still unknown, and could be further investigated in a fixed bed reactor. In addition, the influence of concentrations of the reducing agents on the fusion behavior of wheat straw also of interest to be studied to improve the understanding of agglomeration in gasification of wheat straw.

Influence of reducing atmosphere and steam on the fusion behaviors of sunflower husk ash and the interaction between sunflower husk ash and silica sand

During gasification of sunflower husk, the reducing atmosphere and steam could promote the agglomeration, probably due to their promotive effects on the interaction between sunflower husk ash and bed material. However, no experimental evidence to this are found in this work. Therefore, the influence of reducing atmosphere and steam on the interaction between sunflower husk ash and silica sand could be studied in a fixed bed reactor. In addition, the fusion behaviors of wheat straw is promoted by a reducing atmosphere and a high concentration of steam. However, whether such phenomena occur to sunflower husk ash is still unclear. The further investigations on the influence of reducing atmosphere and steam on the fusion behaviors of sunflower husk ash and the interaction between sunflower husk ash and silica sand could provide an improved understanding of the agglomeration in sunflower husk gasification.

Agglomeration behaviors in gasification of other types of biomass

The various molar ratios of Si/K in different types of biomass results in a different K distribution in the ashes, and thereby causing a different agglomeration tendency and mechanism. For example, the ash of P-rich biomass may be dominated by phosphates, which will behavior different under gasification condition. Therefore, the agglomeration behaviors of other types of biomass, such as the P-rich rapeseed meal, in gasification could be investigated to have a more comprehensive understanding of agglomeration in fluidized bed gasification of biomass.

Appendix A

Selection of bed particle size

The influence of bed particles size on agglomeration are summarized in Figure A-1. The results reveal that the agglomeration tendency is significantly promoted by increasing the size range of bed particles, which is consistent with the previous work[1,2].

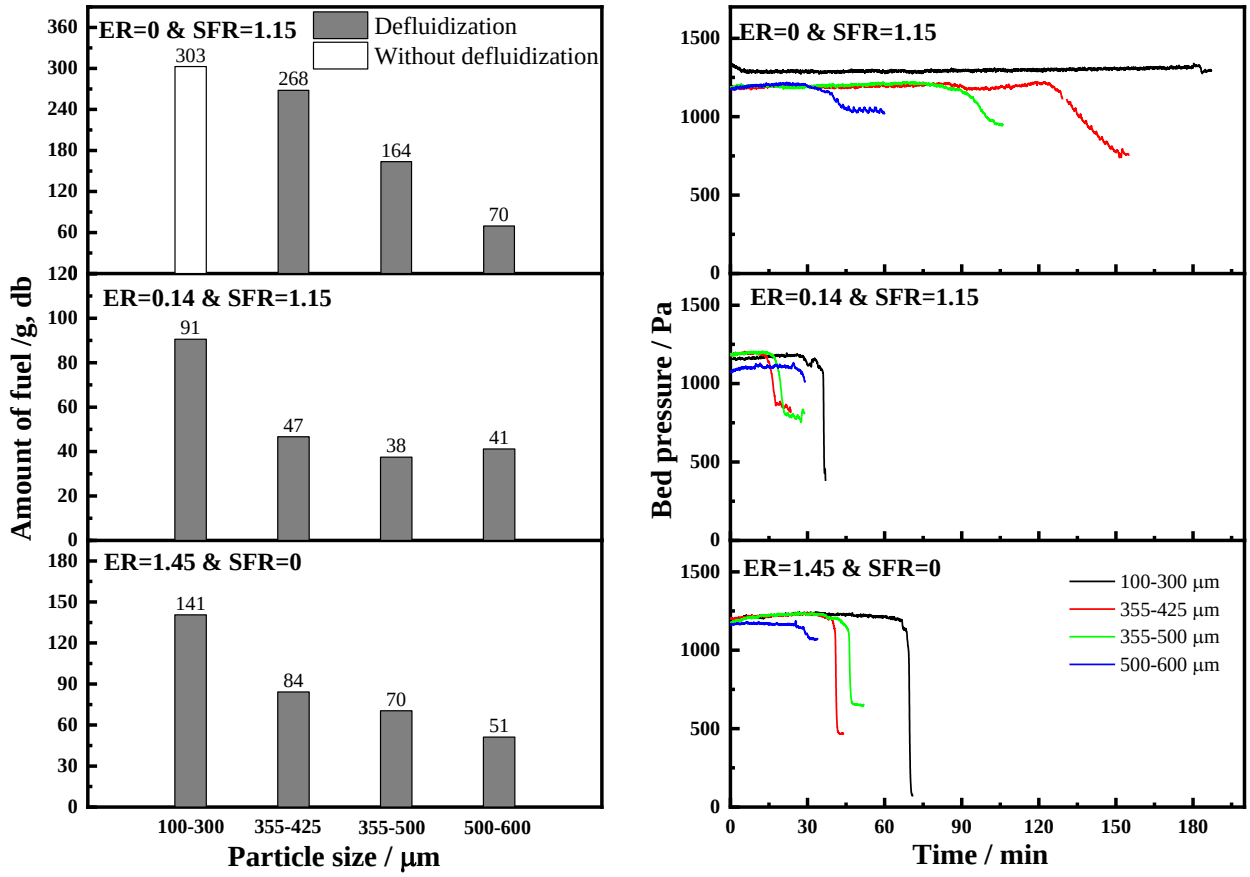

Figure A-1 Influence of bed particles size on straw amount fed for inducing defluidization under combustion with an ER of 1.45, gasification with an ER of 0.14 and a SFR of 1.15, and gasification with an ER of 0 and SFR of 1.15 using the fuel with a size range of 2 – 4 mm.

As given in Table A-1, the ratio between superficial gas velocity (U_g) and minimal fluidization velocity (U_{mf}) of coarse sand particles is much lower than the fine particles at 850 °C, resulting in a worse mixing of the particles in the bed. The temperatures profiles during stable reactions along the bed in the range from 5 to 10 cm are shown in Figure B-2 due to the static bed height in this work is 10 cm. For the sand with a size range of 500 – 600 μm, the difference in bed temperature at 5 cm and 10cm is as larger as 22 °C, indicating a worse mixing in the bed. In addition, it is found that the

pressure drop at defluidization point becomes less pronounced at larger particles size (as shown in Figure B-1).

Table A-1 Ratio between superficial gas velocity (U_g) and minimal fluidization velocity (U_{mf}) of sand particles at 850 °C

Size range	U_g/U_{mf}
100-300 µm	~5.4
355-425 µm	~3.1
355-500 µm	~2.2
500-600 µm	~1.5

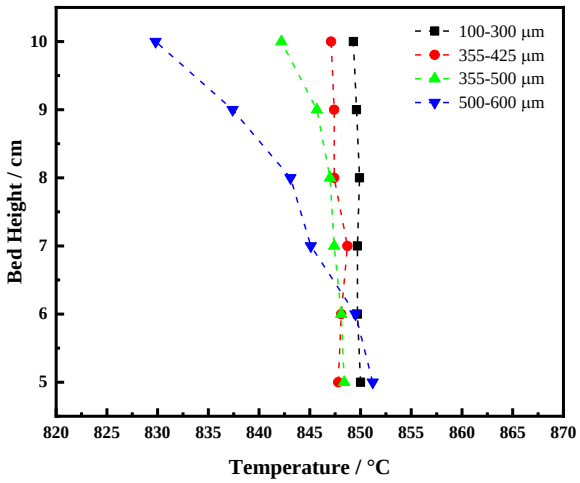

Figure A-2 Temperature profile during stable combustion of straw with a size range of 2 – 4 µm for different particle size.

Selection of fuel particle size

Compared with the bed particles size, the fuel size has relativity minor influence on the agglomeration tendency, as shown in Figure A-3. The agglomeration tendencies are stable for the fuels with the size ranges of 2 - 4 mm and 4 - 5.6 mm. However, by decreasing the fuel size range to 0.6 - 2mm, the agglomeration tendency is slightly promoted in combustion with an ER of 1.45 and gasification with an ER of 0.14 and a SFR of 1.15, whilst the agglomeration tendency is mitigated in gasification with an ER of 0 and a SFR of 1.15.

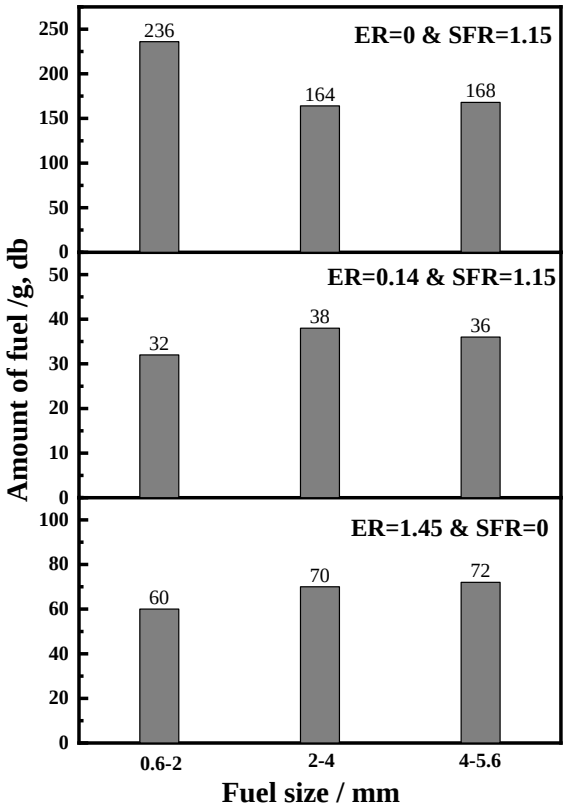

Figure A-3 Influence of fuel particles size on straw amount fed for inducing defluidization under combustion with an ER of 1.45, gasification with an ER of 0.14 and a SFR of 1.15, and gasification with an ER of 0 and SFR of 1.15 using silica sand with a size range of 355 – 500 µm.

Repeatability of experiments

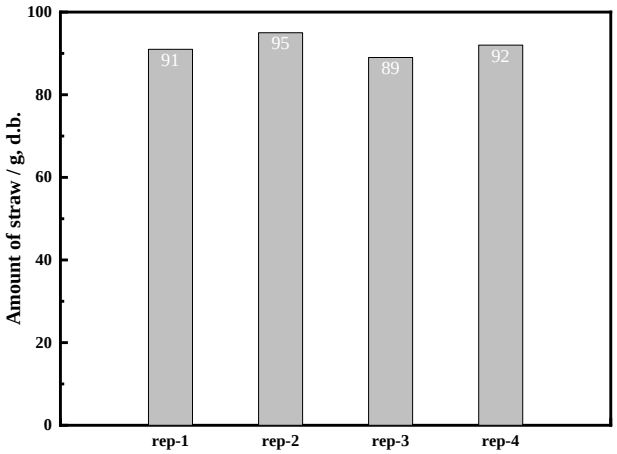

Figure A-4 Straw amount fed for inducing defluidization under combustion with an ER of 1.45 using silica sand with a size range of 355 – 500 µm.

Compositions of slag phase

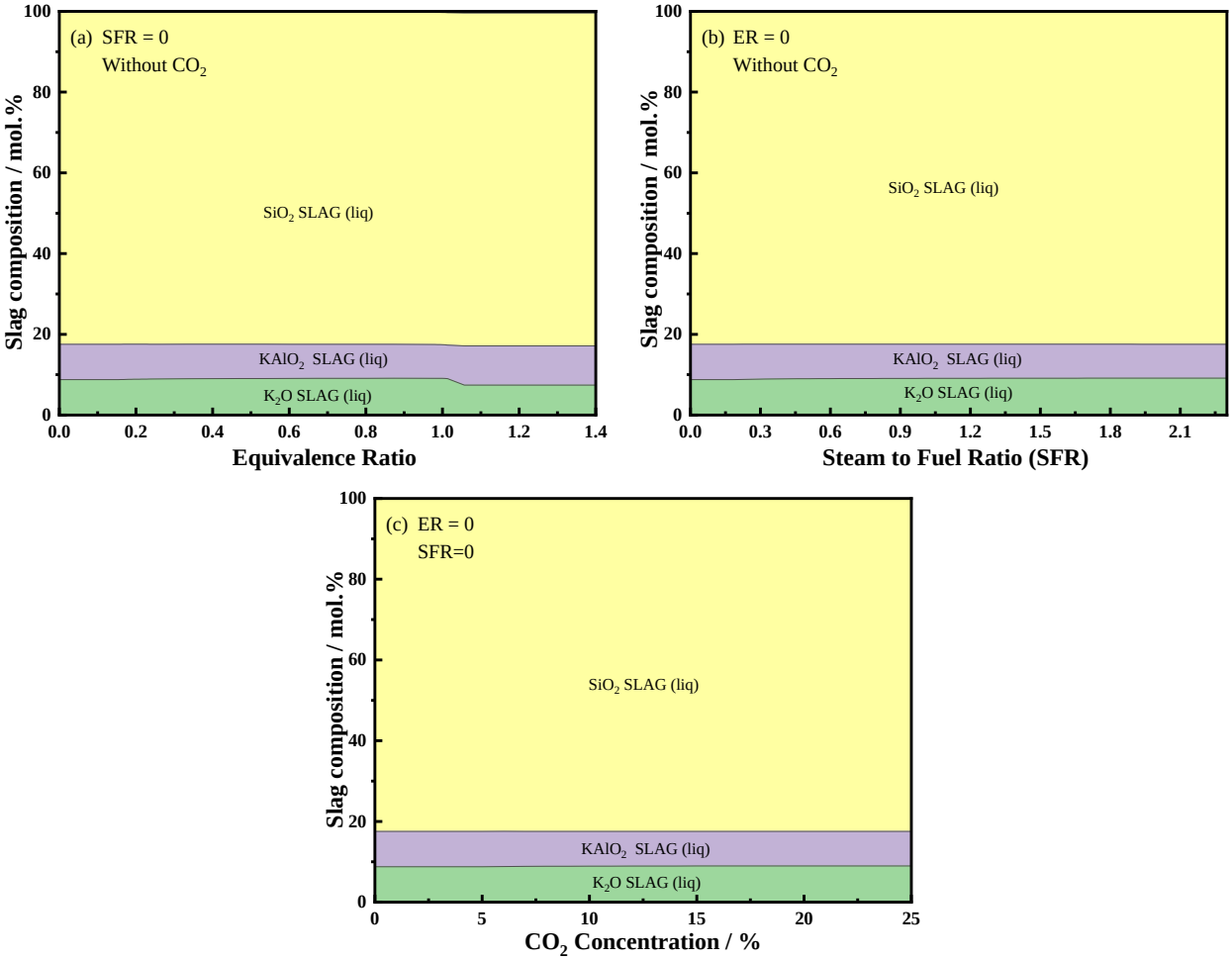

Figure A-5 Impact of (a) equivalence ratio, (b) steam to fuel ratio and (c) CO_2 concentration on the thermodynamic equilibrium calculation of slag phase compositions at 850 °C.

Reference

(1) Lin, W.; Dam-Johansen, K.; Frandsen, F. Agglomeration in Bio-Fuel Fired Fluidized Bed Combustors. *Chem. Eng. J.* **2003**, *96* (1–3), 171–185.

(2) Resjdues, C. Agglomeration of Turkish Lignites in Fluidised-Bed Combustion. *Jouof Inst. Energy* **1989**, *March*, 56–61.

Appendix B

Devolatilization period during wheat straw pyrolysis at 850 °C

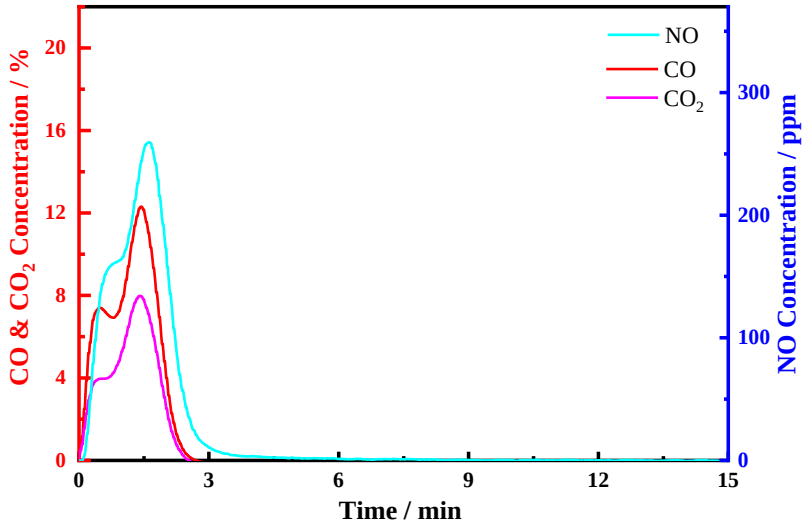

Figure B-1 CO, CO_2 and NO concentrations in flue gas during char samples formed at 850 °C

Appendix C

Agglomeration tendency of three fuels during gasification with steam

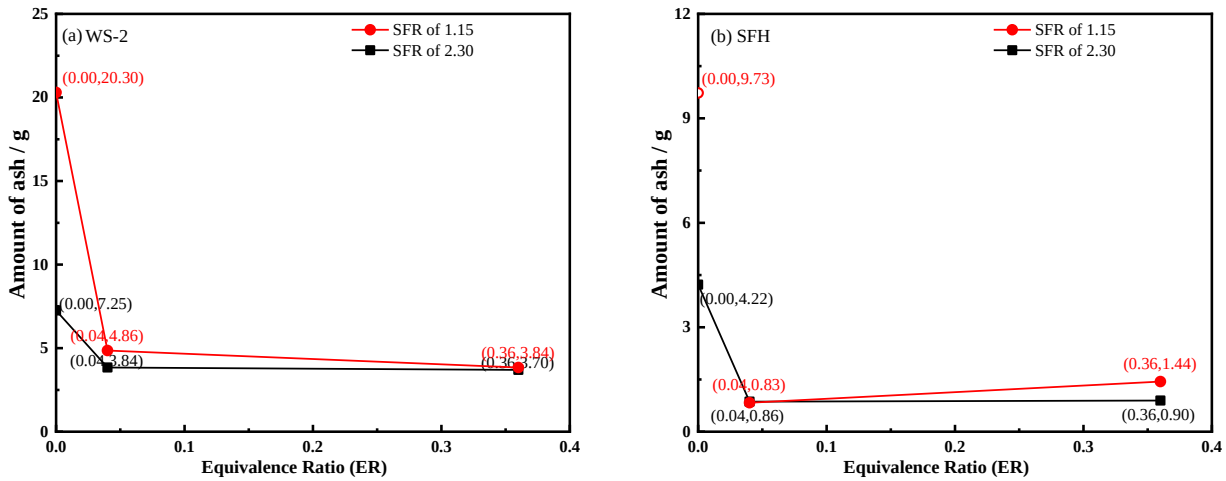

Figure C-1 Amount of ash in the fuel fed for inducing defluidization as functions of equivalence ratio in gasification with a SFR of 1.15 and 2.30 (solid symbols: defluidization occurred, open symbols: no defluidization occurred).

Raw EDX data

Table C-1 Raw EDX analysis of selected point of the residues shown in Figure 5-6 (atom%)

	WS-1 Point 1	WS-1 Point 2	WS-1 Point 3	WS-1 Point 4	WS-1 Point 5	WS-1 Point 6	SFH Point 1	SFH Point 2	SFH Point 3	SFH Point 4
C	64.53	69.34	9.14	54.17	75.98	85.65	12.63	8.46	7.18	6.84
O	24.05	20.93	55.00	29.84	11.60	7.43	50.66	53.52	60.26	55.74
K	2.97	3.23	5.47	4.25	5.89	3.52	10.19	8.71	3.44	4.03
Ca	3.09	1.15	0.20	0.11	1.62	0.54	5.35	9.38	17.11	19.78
Mg	0.90	0.48	0.04	0.14	0.72	0.43	16.55	15.50	0.21	0.46
Al	0.05	0.04	0.07	0.02	0.02	0.02	0.10	0.43	0.09	0.12
Si	2.10	2.93	29.15	10.52	0.74	0.54	0.31	0.69	9.73	10.71
P	1.00	0.54	0.18	0.11	0.88	0.27	1.20	1.20	0.76	1.10
S	0.48	0.41	0.00	0.15	1.23	0.85	2.01	1.60	0.34	0.42
Si/K	0.71	0.91	5.33	2.48	0.13	0.15	0.03	0.08	2.83	2.66

Predicted slag phase compositions based on the equilibrium calculations

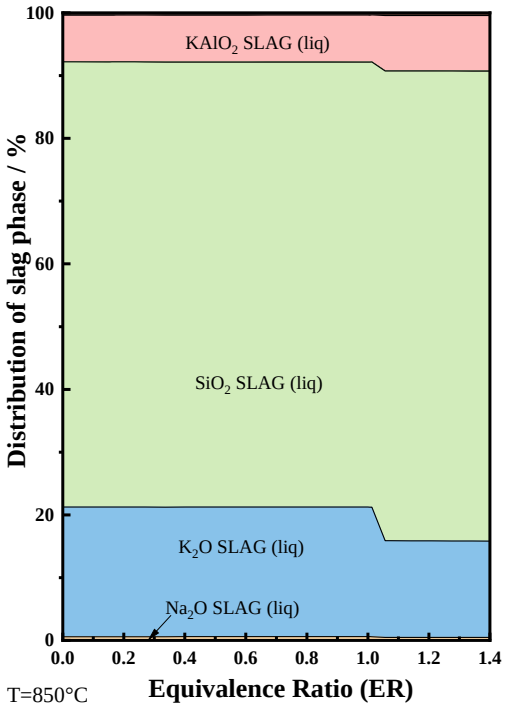

Figure C-2 Predicated slag phase compositions during conversion of WS-1 at various equivalence ratio by thermodynamic equilibrium calculations at 850 °C without bed material.

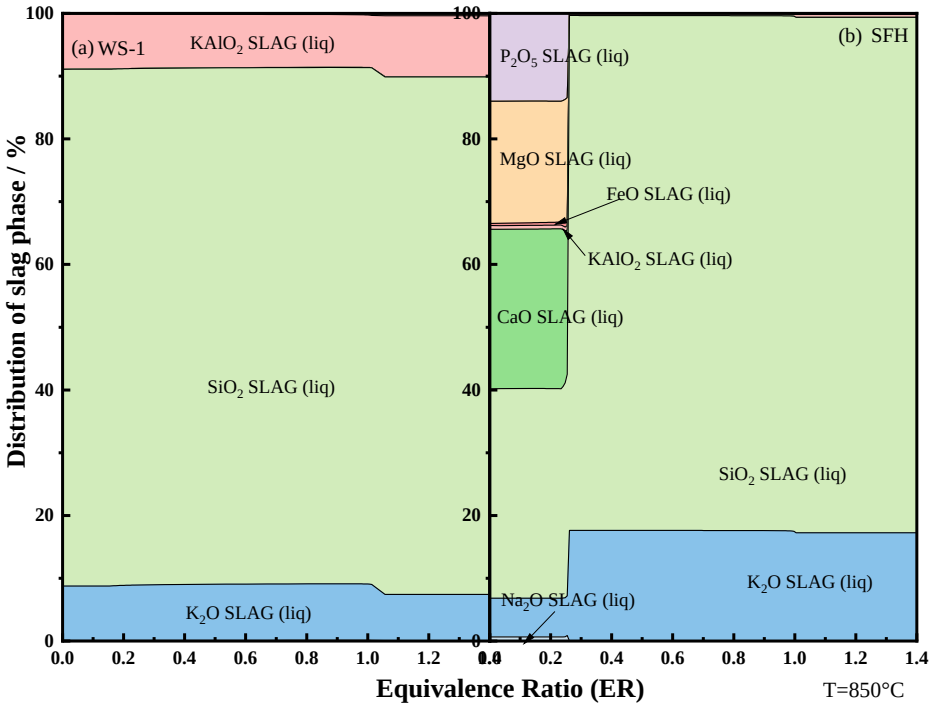

Figure C-3 Predicated slag phase compositions during conversion of (a) WS-1 and (b) SFH at various equivalence ratio by thermodynamic equilibrium calculations at 850 °C with bed material.